creative commons
COMMONS DEED

저작자표시-비영리-변경금지 2.0 대한민국

이용자는 아래의 조건을 따르는 경우에 한하여 자유롭게

- 이 저작물을 복제, 배포, 전송, 전시, 공연 및 방송할 수 있습니다.

다음과 같은 조건을 따라야 합니다:

저작자표시. 귀하는 원저작자를 표시하여야 합니다.

비영리. 귀하는 이 저작물을 영리 목적으로 이용할 수 없습니다.

변경금지. 귀하는 이 저작물을 개작, 변형 또는 가공할 수 없습니다.

- 귀하는, 이 저작물의 재이용이나 배포의 경우, 이 저작물에 적용된 이용허락조건을 명확하게 나타내어야 합니다.
- 저작권자로부터 별도의 허가를 받으면 이러한 조건들은 적용되지 않습니다.

저작권법에 따른 이용자의 권리는 위의 내용에 의하여 영향을 받지 않습니다.

이것은 이용허락규약(Legal Code)을 이해하기 쉽게 요약한 것입니다.

Disclaimer

dCollection

Thesis for the Degree of Doctor of Philosophy

Isolation and Structural Elucidation of Bioactive Secondary Metabolites of the Halophytes *Corydalis heterocarpa* and *Vitex rotundifolia*

You Ah Kim

Department of Marine Bioscience and Environment

The Graduate School

Korea Maritime University

August 2009

Isolation and Structural Elucidation of Bioactive Secondary Metabolites of the Halophytes *Corydalis heterocarpa* and *Vitex rotundifolia*

Advisor: Prof. Youngwan Seo

by

You Ah Kim

A dissertation submitted in partial fulfillment of the requirements

for the degree of

Doctor of Philosophy

In the Department of Marine Bioscience and Environment,

The Graduate School of Korea Maritime University

August 2009

Isolation and Structural Elucidation of Bioactive Secondary Metabolites of the Halophytes *Corydalis heterocarpa* and *Vitex rotundifolia*

A dissertation

by
You Ah Kim

Approved as to style and content by:

Certified by :

Youngwan Seo
Thesis Advisor

Accepted by :

Sun-Young Lim
Chairman

Jong-Woong Ahn
Member

Hyuncheol Oh
Member

Hee-Yeon Park
Member

August 2009

Contents

List of Tables

List of Figures

List of Schemes

염생식물 *Corydalis heterocarpa* 와 *Vitex rotundifolia* 로부터 생리활성물질의 분리 및 구조결정

김 유 아

한국해양대학교 대학원 해양생명환경학과

요 약

해양생물자원의 중요성에 대한 인식이 높아짐에 따라 해양생물을 이용한 새로운 생리활성물질의 개발에 관심이 증가되고 있으며, 그 중에서도 해수와 민물이 섞이는 독특한 환경에 서식하며 이에 적합한 적응기작을 발전시킨 염생식물이 새로운 신물질 자원으로서 주목 받고 있다.

염생식물의 일종인 염주괴불주머니 (*Corydalis heterocarpa*)와 순비기나무 (*Vitex rotundifolia*)는 한국의 각처 바닷가 모래 사장에서 자생하는 노란 꽃 및 자줏빛 꽃이 피는 식물로써, 조간대에서 매우 중요한 생태적 위치를 차지하고 있다. 또한 염주괴불주머니는 민간에서 오랫동안 산모의 진통이나 경련의 치료제로 사용되었으며, 순비기나무는 한방에서 그 열매를 만형자라 하여 두통, 안질, 귓병과 같은 질병의 치료에 사용되어 왔다. 염주괴불주머니의 경우, 같은 속의 다른 식물에서 다양한 이차 대사산물이 보고된 바 있으나, 지금까지 염주괴불주머니로부터 이차 대사산물의 분리나 유용한 생약학적 특성이 보고된 바 없다. 순비기나무는 다수의 연구에 의해 flavonoid 류 및

terpenoid 류의 화합물들이 분리된 바 있으며, 이들의 생리활성효과 또한 보고되었다.

따라서 본 연구에서는 염생식물 염주괴불주머니와 순비기나무에서 신규의 이차 대사물질을 분리하고, 분리된 화합물에 의한 항산화와 발암물질의 생성방지 및 생체방어 물질로서의 유용성을 검토하고자 하였다.

그 결과, 염주괴불주머니로부터 9 종의 알려진 화합물 (**1-3**, **5**, **7-11**)과 2 종의 신규 화합물 (**4**, **6**)을 분리하여 총 11 종의 순수한 화합물을 분리하였으며, 또한 순비기나무로부터 기지 화합물 14 종 (**12-19**, **21**, **22**, **27-30**)과 신규 화합물 5 종 (**20**, **23-26**)을 포함하여 총 19 종의 이차 대사물질을 분리하였다. 분리된 화합물의 구조는 분광학적 자료의 해석과 문헌치의 비교에 의해 결정되었으며, 특히, 염주괴불주머니의 2 종의 신규 화합물 **4** 와 **6** 은 각각 (2'*S*,7'*S*)-*O*-(2-methylbutanoyl)-columbianetin 과 (2'*S*)-columbianetin-3'-hydrogen sulfate 였으며, 순비기나무의 5 종의 신규 화합물 **20**, **23-26** 은 차례로 (5*S**,6*R**,8*R**,9*R**,10*S**)-6-acetoxy-9-hydroxy-16-hydroxy-13(14)-labden-16,15-olide, 3α-hydroxy pleuroziol, 9α*H*-manoyl oxide, abieta-11(12)-ene-9α,13α-endoperoxide 그리고 abieta-11(12)-ene-9β,13β-endoperoxide 로 결정되었다.

분리된 화합물의 암세포 증식 억제 효과를 탐색하기 위한 기초 연구로서 AGS 인체 위암세포, HT-29 인체 결장암세포, HT1080 인체 섬유육종 세포, MCF-7 인체 유방암세포 및 U-937 인체 구성 림프종 세포의 증식에 미치는 영향을 MTT assay 를 통해 관찰하였다. 그 결과, 전반적으로 다른 암세포에 비하여 AGS 인체 위암세포에서 화합물의 암세포 증식 억제 효과가 뛰어나 apoptosis 와 관련이 있는 여러 요소의 mRNA 발현 정도를 AGS 인체 위암세포에서 검토하였다.

분리된 모든 화합물에 대한 인체 암세포 증식 억제 효과를 검토한 결과, 염주괴불주머니의 신규화합물 **6** 과 순비기나무의 화합물 **14** 가 가장 활성이 뛰어났으며, 이들 화합물의 암세포 증식 억제 효과가 pro-/anti-apoptotic Bax/Bcl-2 유전자의 발현 조절 및 종양 억제 유전자 p53 및 p21 유전자의 up-regulation 에 의한 것으로 사료되었다.

화합물의 항산화 활성을 탐색하기 위한 일환으로 세포내 NO, ROS, GSH 및 산화적 스트레스와 관련된 iNOS 와 COX-2 유전자의 mRNA 발현 정도를 macrophage Raw 264.7 세포에서 확인하였다.

세포내 NO 의 함량은 Griess reaction 을 바탕으로 확인하였으며, 세포내 ROS 와 GSH 의 발생은 각각 형광물질인 2',7'-dichlorofluorescin diacetate (DCFH-DA)와 monobromobimane 을 이용하여 측정하였다. 또한, LPS 의 자극에 의하여 산화적 스트레스가 유도된 Raw 264.7 세포의 iNOS 와 COX-2 유전자의 발현은 RT-PCR 에 의하여 확인되었다.

산화적 스트레스가 유도된 Raw 264.7 세포에 염주괴불주머니와 순비기나무에서 분리된 화합물을 농도별로 처리한 결과, 농도의존적으로 다수의 화합물이 항산화 활성을 지님을 확인하였으며, 각각의 측정 방법에 따라 화합물의 활성을 나타내는 정도의 차이가 있었다. 특히, 염주괴불주머니에서 분리된 화합물 **2-4** 와 순비기나무에서 분리된 화합물 **16-18** 및 신규화합물 **23** 과 **24** 가 우수한 항산화 활성을 나타내는 것으로 확인되었다.

본 연구를 통해 염생식물의 일종인 염주괴불주머니와 순비기나무의 암세포 증식 억제 효과 및 다양한 항산화 활성 검색을 통해 암 예방 및 항산화 기능성 소재로써의 개발 가능성을 확인할 수 있었다. 특히, 각각의 연구에서

우수한 활성을 보인 화합물에 대한 집중적인 연구를 통해 새로운 생리활성물질의 개발이 기대된다.

1. Introduction

1.1. Halophytes (Salt Marsh Plants)

A marine system with a high variability in physical parameters such as temperature, salinity, or radiation can be considered to be an extreme environment. Tidal flats, salt marshes, mangrove swamps, and seashore ecosystems are subjected to these types of environmental extremes on a daily, seasonal, and annual basis. Salt marshes and tidal flats in particular undergo regular and intense changes in external parameters such as salinity, due to advancing and receding tidal salt water. Organisms that exist in these environments, especially plants that cannot avoid or seek shelter from adverse environmental changes, have to acclimatize by developing specific stress adaptation responses. In many plant species, this often includes the synthesis of unusual secondary metabolites.

In general, plants are classified as glycophytes or halophytes according to their capacity to grow in highly saline environments (Flowers *et al*., 1977). Halophytes naturally occur in ecosystems that have highly saline soils and have developed the ability to actively and efficiently exclude salts from their roots and leaves. A number of these plants can endure salt concentrations that are more than twice that of seawater. Therefore, halophytes can be viewed as salt-resistant plants that are well adapted to salinity stress (Min, 1998).

Halophytes have been classified into coastal salt marsh and estuarine salt marsh plants. According to their habitats, coastal salt marshes can be distinguished into three types: sandy salt marshes, sandy dune salt marshes, and clayey salt marshes.

Two forms of estuarine marshes are recognized: salt swamps and estuarine salt marshes (Ministry of Environment, 2006).

The Ministry of Environment (2006) recently researched fifty-seven plant families and 148 halophyte species in coastal and estuarine salt marshes from 59 sites on the western and the southern coasts of Korea. The distribution of halophytes was found to depend on the type of salt marsh. Among the species reported, *Suaeda maritima*, *Zoysia sinica*, *Artemisia fukudo,* and *Limonium tetragonum* communities dominated in sandy salt marshes, while *Vitex rotundifolia*, *Carex kobomugi*, *Elymus mollis,* and *Carex pumila* communities dominated in the sand dune salt marshes. In the clayey salt marshes, *Suaeda japonica*, *Phragmites communis*, *Carex scabrifolia,* and *Triglochin maritimum* communities were predominant. Salt swamps were dominated by *Phragmites communis*, *Triglochin maritimum*, *Suaeda maritima,* and *Carex scabrifolia* communities. In estuarine salt marshes, *Suaeda japonica*, *phragmites communis*, *Aster tripolium*, *Carex scabrifolia*, *Phacelurus latifolius,* and *Salicornia herbacea* communities predominated (Ministry of Environment, 2006).

These salt marsh plants are recognized environmentally as one of the most important ecosystems in tidal zones, since they play vital roles in all aspects of tidal ecology, serving as buffers that protect the shorelines from erosion by the force of waves and filtering contaminants that leach from the land. In addition, several species of halophytes, such as *Glehnia littoralis*, *Salicornia herbacea,* and *Limonium tetragonum,* are eaten as human food and are also important components

of Korean folk medicines (Masuda *et al*., 1998; Bang *et al*., 2002; Kong *et al*., 2008).

These salt marsh plants therefore have attracted the attention of researchers who are interested in their capacity to produce unusual bioactive secondary metabolites. However, the characterization and biological activities of these secondary metabolites have not as yet been fully elucidated (Jo *et al*., 2002; Bang *et al*., 2002; Han *et al*., 2003; Lee *et al*., 2004; Seo *et al*., 2005; Kong *et al*., 2008). The aim of the present study is to further the characterization and biological investigation of secondary metabolites from salt marsh plants.

1.2. Halophytes *Corydalis heterocarpa* and *Vitex rotundifolia*

In the search for novel bioactive secondary metabolites from salt marsh plants, a number of halophytes were collected in western Korea and screened for a series of biological activities. Among the collected halophytes, extracts from *Corydalis heterocarpa* and *Vitex rotundifolia*, salt-tolerant plants growing on sandy beaches, dunes, and rocky shorelines, showed significant cytotoxicities in a prescreening test that used a preliminary MTT assay (Table 1).

C. heterocarpa is found throughout Korea and Japan. It is a biennial herb that bears spikes of yellow flowers. The lanceolate leaves show an alternate phyllotaxis. The bead-like fruits ripen in July and contain black seeds lined with a projection. Flowering occurs in April-May singly at the ends of the branches. The plant grows 40-60 cm tall and stands upright and straight with the ridgeline. It has been

traditionally used as a folk medicine to treat a variety of symptoms including travails and spasms (Lee, 2002). *Corydalis* species have been extensively investigated and have yielded alkaloids, isoquinoline alkaloids, and cyanidin glycosides as some of their secondary metabolites (Ma *et al*., 1999; Tatsuzawa *et al*., 2005; Choi *et al*., 2007).

A number of *Corydalis* constituents have interesting biological activities. For example, the alkaloids from *Corydalis incise* and *Corydalis ambigua* showed antifungal activity against the growth of *Cladosporium herbarum* (Ma *et al*., 1999). The isoquinoline alkaloids from *Corydalis incisa* exhibited cytotoxicity against human A549, SK-OV-3, SK-MEL-2, and HCT15 tumor cells (Choi *et al*., 2007). Although many secondary metabolites of the genus *Corydalis* have been reported to date, full identification of the secondary metabolites of *C. heterocarpa* and their bioactivity have not yet been reported.

V. rotundifolia is distributed along the sandy beaches of Korea, China and Japan. It is a sprawling shrub, growing 20-80 cm in height, with gray-green to silvery round leaves that have a spicy fragrance. The bluish-purple flowers emerge in June-September as small clusters at the end of the branch. The round fruit are about 6mm in diameter and are bluish purple or black when ripe in September-October. The seeds and fruits of *V. rotundifolia* are used for treatment of various allergic diseases as well as for colds, headache, migraines, and eye pain (Lee, 2002). Several natural products, such as flavonoids, diterpenoids, and sesqiterpenoids have previously been reported in *V. rotundifolia* extracts (Kondo *et al*., 1986; Ono

et al., 1997; You *et al*., 1998; Ono *et al*., 1998; Kawazoe *et al*., 1999; Ono *et al*., 1999; Ono *et al*., 2000; Shin *et al*., 2000; Ko *et al*., 2000; Ko *et al*., 2001; Ono *et al*.[a,b], 2001; Wang *et al*., 2005).

All known secondary metabolites (V1 - V57) isolated from *V. rotundifolia* are illustrated in Fig. 1. Among these, flavonoids such as vitexicarpin and artemetin, and diterpenes such as rotundifuran and ferruginol, have shown antiproliferative and antioxidant effects *in vitro* (Ono *et al*., 1999; Ko *et al*., 2000; Ko *et al*., 2000; Wang *et al*., 2005). Therefore, these compounds present in *V. rotundifolia* might serve as potent preventative agents against chronic illnesses such as diabetes, heart disease, and cancer.

KOREA MARITIME UNIVERSITY 1945 한국해양대학교

Table 1. Cytotoxicity of solvent extracts from halophytes against an AGS cell line

Species	MeOH extracts (Inhibition %)	CH_2Cl_2 extracts (Inhibition %)
Rosa rugosa	-	++
Messerschmidia sibirica	-	++
Lathyrus japonicus	-	-
Carex scabrifolia	-	++
Sonchus brachyotus	-	++
Salsola komarvii lljin	-	+
Suaeda asparagoides	-	-
Suaeda japonica	-	-
Erigron annuus	-	+++
Ixeris tamagawaensis	-	-
Imperata cylindrica	-	-
Aster tripolium	-	++
Calystegia soldanella	-	+
Glehnia littoralis	-	++
Artemisia capillaris	-	++
Tetragonia tetragonoides	-	+++
Vitex rotundifolia	++	+++
Corydalis heterocarpa	++	+++
Aster spathulifolius	-	-
Salicornia herbacea	-	++
Carex kobomugi	-	+++
Polygonum bellardi	-	+

Species	MeOH extracts + CH_2Cl_2 extracts (Inhibition %)
Hypochoeris radicata	++
Erigron annuus	-
Suaeda maritima	-

+++: inhibition value > 90%, ++: 70% < inhibition value ≤ 90%, +: 50% < inhibition value ≤ 70%, -: inhibition value ≤ 50%. Final concentration of extracts were 100 μg/mL

Kondo *et al*., 1986; Ko *et al*., 2000

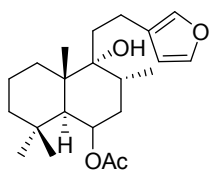

V1 rotundifuran

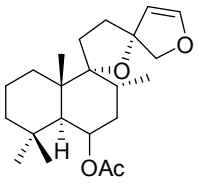

V2 prefotundifuran

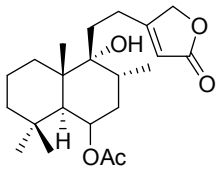

V3 vitexilactone

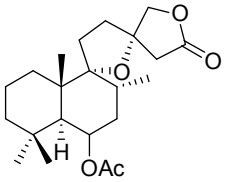

V4 previtexilactone

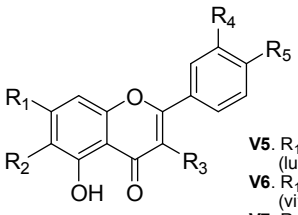

V5. R_1, R_4, R_5 = OH, R_2, R_3 = H
(luteolin)
V6. R_1 - R_3, R_5 = OMe, R_4 = OH
(vitexicarpin)
V7. R_1 - R_3 = OMe, R_4 - R_5 = OH
(2',3',5-trihydroxy-3,6,7-trimethoxyflavone)
V8. R_1 - R_5 = OMe
(artemetin)

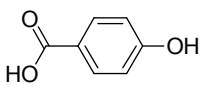

V9 p-hydroxybenzoic acid

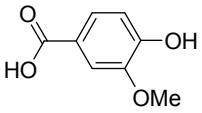

V10 vanillic acid

Ono *et al*., 1997

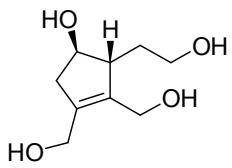

V11 eucommiol

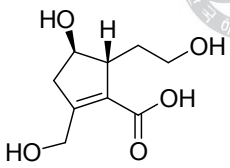

V12 1-oxo-eucommiol

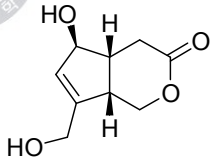

V13 iridolactone

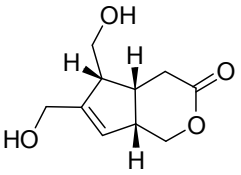

V14 pedicularis-lactone

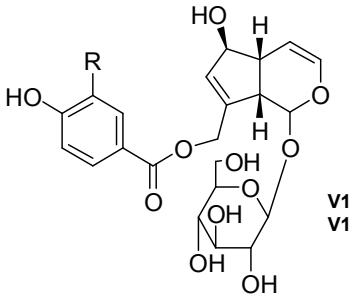

V15 R=H (agnuside)
V16 R=OCH_3
(10-*O*-vanilloyl aucubin)

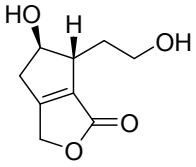

V17 viteoid I

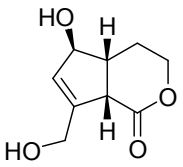

V18 viteoid II

Figure 1. Natural products isolated from *Vitex rotundifolia*.

Kawazoe *et al*., 1999

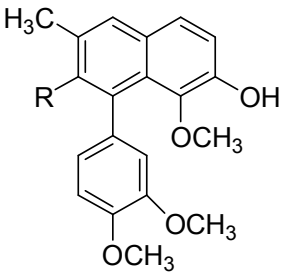

V19 R=H (vitrofolal A)
V20 R=OH (vitrofolal B)

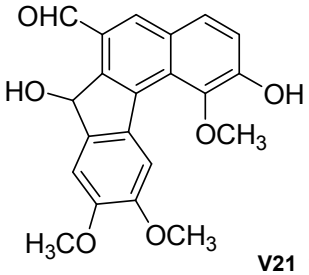

V21 vitrofolal C

Ono *et al*., 1998; Ono *et al*.,1999; Ono *et al*.[b], 2001

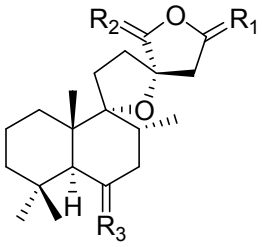

	R_1	R_2	R_3
V22	H, OCH_3	H, OCH_3	H
V23	OCH_3, H	OCH_3, H	H
V24	OCH_3, H	H, OCH_3	H
V25	H, OCH_3	H, OCH_3	OAc
V26	OCH_3, H	OCH_3, H	OAc

	R_1	R_2	R_3
V27	OCH_3, H	H, OCH_3	OAc
V28	H, OCH_3	OCH_3, H	OAc
V29	H, OCH_3	H_2	OAc
V30	OCH_3, H	H_2	OAc
V31	=O	OCH_3, H	OAc
V32	OCH_3, H	=O	OAc

Figure 1. (continued)

Ono *et al*., 1998; Ono *et al*.,1999; Ono *et al*.[b], 2001

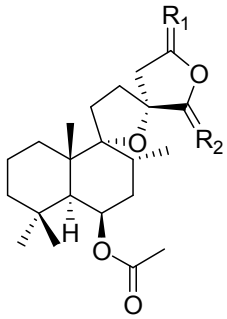

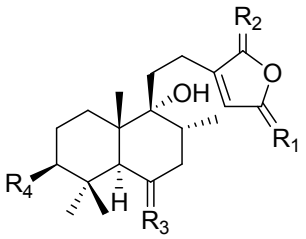

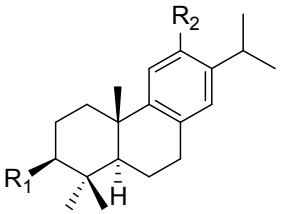

	R_1	R_2
V33	H, OCH_3	H_2
V34	OCH_3, H	H_2
V35	=O	H, OCH_3
V36	OCH_3, H	=O

	R_1	R_2	R_3	R_4
V37	$=H_2$	=O	OAc, H	H
V38	$=H_2$	=O	H, OAc	H
V39	OCH_3, H	=O	OAc, H	H

	R_1	R_2	
V40	H	OH	(ferruginol)
V41	OH	H	(abietatrien-3β-ol)

Ono *et al*.,2000

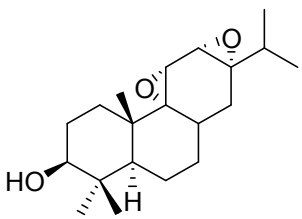

V42 vitetrifolin A

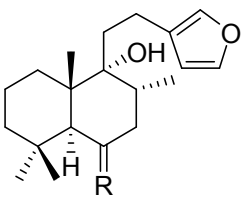

R

V43 H, OAc (vitetrifolin B)

V44 =O (dihydrosolidagenone)

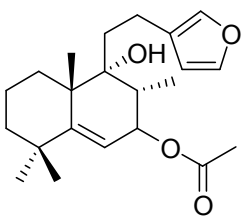

V45 vitetrifolin C

Figure 1. (continued)

Ono *et al*.[a],2001

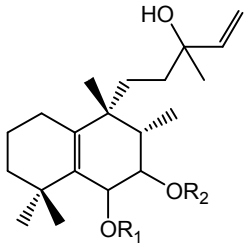

V46 R_1, R_2 = $COCH_3$ (vitetrifolin D)

V47 R_1 = $COCH_3$, R_2 = H (vitetrifolin E)

V48 R_1 = H, R_2 = $COCH_3$ (vitetrifolin F)

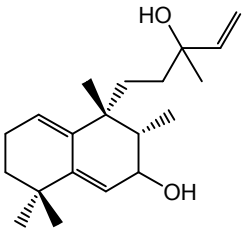

V49 vitetrifolin G

Ono *et al*.,2002

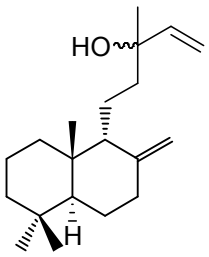

V50 vitexifolin A

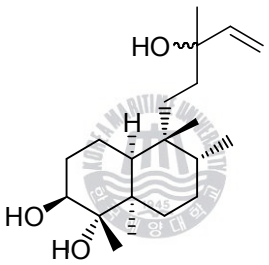

V51 vitexifolin B

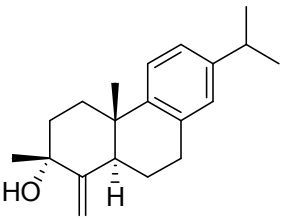

V52 vitexifolin C

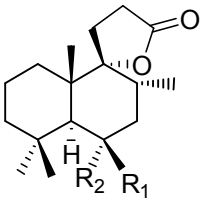

R_1 R_2

V53 H OAc (vitexifolin D)

V54 OAc H (trisnor-γ-lactone)

V55 H H (isoambreinolide)

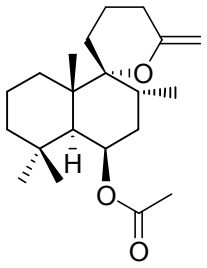

V56 vitexifolin E

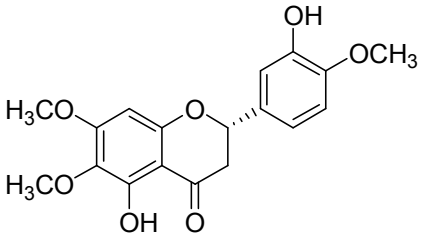

V57 5,3'-dihydroxy-6,7,4'-trimethoxyflavanone

Figure 1. (continued)

1.3. Oxidative/Nitrosative Stress

Reactive oxygen species (ROS) and reactive nitrogen species (RNS) are highly reactive molecules or molecular fragments that contain one or more unpaired oxygen/nitrogen atoms (Nordberg and Arnér, 2001; Pauly *et al*., 2006). It is well known that ROS/RNS include not only the free radicals such as superoxide anion ($O_2^{-}\cdot$), hydroperoxyl radical ($HO_2\cdot$), hydroxyl radical ($HO\cdot$), peroxyl radical ($ROO\cdot$), alkoxyl radical ($RO\cdot$), nitric oxide radical ($NO\cdot$), and nitrogen dioxide radical ($NO_2\cdot$), but also include non-radicals as hydrogen peroxide (H_2O_2) and peroxynitrite anion ($ONOO^-$) (Curtin *et al*., 2002; Gomes *et al*., 2005; Mangialasche *et al*., 2009) (Fig. 2).

ROS and RNS are continuously generated under normal conditions, as a consequence of normal aerobic metabolism. They have various physiological roles in the human body, but they are removed rapidly from the body for the reason that their persistence or over accumulation will cause cell damage and cell death. In general, living systems have developed defense mechanisms against the harmful effects of ROS/RNS. For example, a variety of antioxidant defense systems, such as enzyme and non-enzyme antioxidants, help to prevent and repair ROS/RNS induced damage. Thus, the balance between the formation of ROS/RNS and antioxidant defenses is maintained in the body (Nordberg and Arnér, 2001; Gomes *et al*., 2005). However, imbalances in biological systems occur when excessive production of ROS/RNS overwhelms the antioxidant defense system or when there is a significant decrease or lack of antioxidant defenses. The uncontrolled

ROS/RNS levels then initiate a series of harmful biochemical events that are associated with diverse pathological processes. The damage induced by overproduction of ROS/RNS is termed oxidative/nitrosative stress and these processes can lead to various diseases and characteristic types of cellular damage (Nordberg and Arnér, 2001; Gomes *et al*., 2005; Valko *et al*., 2007).

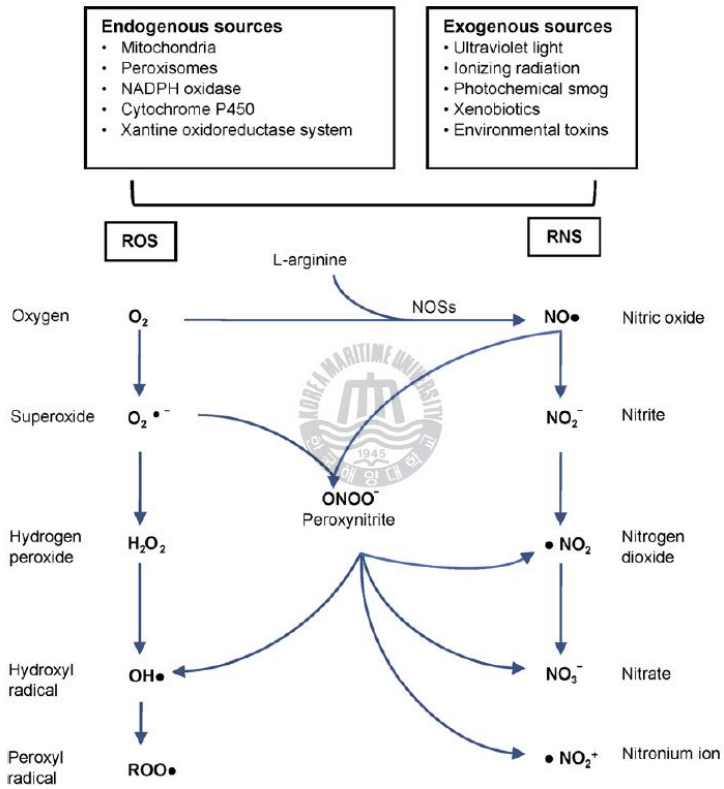

(Mangialasche *et al*., 2009)

Figure 2. The main ROS and RNS responsible for biomolecule damage in the human body, and their main sources. The most reactive ROSs are the superoxide anion and the hydroxyl radical. Peroxynitrite is the main RNS, but nitrogen dioxide and nitronium ion also exhibit significant oxidative properties. Peroxy radicals (ROO^-) also occur, with the simplest peroxyl radical being HOO^-, termed hydroperoxyl radical or perhydroxyl radical. Another important peroxyl radical is LOO^-, called lipid peroxyl radical. Enzymes such as nitric oxide synthases catalyze the formation of reactive nitrogen radicals.

1.4. Human Disease and Solution

As increasing wealth and industrialization has occurred on the planet, cancer has rapidly become one of the major unsolved public health problems in the world. Cancer still accounts for more deaths than does heart disease in humans, even though various treatment strategies have been developed (Jemal *et al*., 2008). In Korea specifically, the rate of cancer death has continuously increased since 1980 (Lee *et al*., 1996). The main reasons for the greater cancer burden are the earlier smoking, earlier alcohol use, and the adoption of Western nutrition and lifestyle. The Western lifestyle is characterized by a highly caloric diet, rich in fat, combined with low physical activity, resulting in an overall energy imbalance. It is associated with an imbalance of redox systems due to lack of nutrients known as antioxidants. The oxidative/nitrosative damage induced by a shortage of these nutrients is strongly correlated with diverse pathological processes, including aging, cardiovascular diseases, arterial hypertension, diabetes, and cancer. Among these diseases, the relationship between oxidative/nitrosative stress and cancer has been the subject of much speculation and controversy (Ames *et al*., 1993; Dröge, 2002; Valko *et al*., 2007; Aslan *et al*., 2008; Kirschvink *et al*., 2008; Liu *et al*., 2008). For these reasons, diet is now recognized as an important environmental factor in cancer induction and prevention, and much attention has been focused on finding chemopreventive or therapeutic agents from natural sources such as fruits, vegetables, terrestrial non-crop plants, and marine algae (Park and Pezzuto, 2002;

Jung *et al*., 2004; Lee *et al*., 2004; Seo *et al*., 2004; Lee and Seo, 2006; Stan *et al*., 2008).

The mechanisms of action of cancer chemopreventive agents can be classified into three types: inhibitors of carcinogen formation, 'blocking' (anti-initiating) agents, and 'suppressing' (anti-promotion/anti-progression) agents, according to the *in vivo* carcinogenesis model (Table 2) (Morse and Stoner, 1993). Among these mechanisms, an anti-initiating agent will suppress the mutation of DNA, RNA, or proteins by scavenging reactive species (ROS/RNS). Anti-promotion agents block the processes by which mutated cells are transformed into cancer cells.

Cancer is associated with decreased apoptosis and the development of apoptosis resistance in cancer cells is now viewed as a significant contributing factor to the failure of cancer therapies (Watson, 2004). Thus, the mechanisms of action of chemopreventive agents from natural products might be related to the modulation of relevant proteins or signal transduction cascades involved in the carcinogenesis process.

In the past, biomarkers have been used successfully as prognostic or diagnostic indicators for chemoprevention studies, and a number of these intermediate biomarkers are shown in table 3. Of the rest, mutations in the p53 gene are the most frequently observed genetic changes in tumor suppressor genes in human cancers (Moll *et al*., 2005; Garcea *et al*., 2005; Roos and Kaina, 2006). Expression of p53 induces a further transcriptional activation of the p21 gene, which inhibits cdk-mediated retinoblastoma protein phosphorylation, leading cells to arrest in G_1

(Garcea *et al*., 2005). In addition, p53 activates expression of Bax (a pro-apoptotic gene) and suppresses Bcl-2 (an anti-apoptotic gene), leading to cellular apoptosis. Briefly, several genes such as p53, p21, and Bax are believed to regulate cellular responses to DNA damage by inducing cell growth arrest or by promoting apoptosis in abnormal cells (Moll *et al*., 2005; Garcea *et al*., 2005; Roos and Kaina, 2006; Valko *et al*., 2007) (Fig. 3). Therefore, apoptosis-related factors (apoptotic index, Bcl-2, Bax, etc.), cell proliferation/cycle-related factors (p53, p21, etc.), and other factors are analyzed as part of the investigation presented in this thesis.

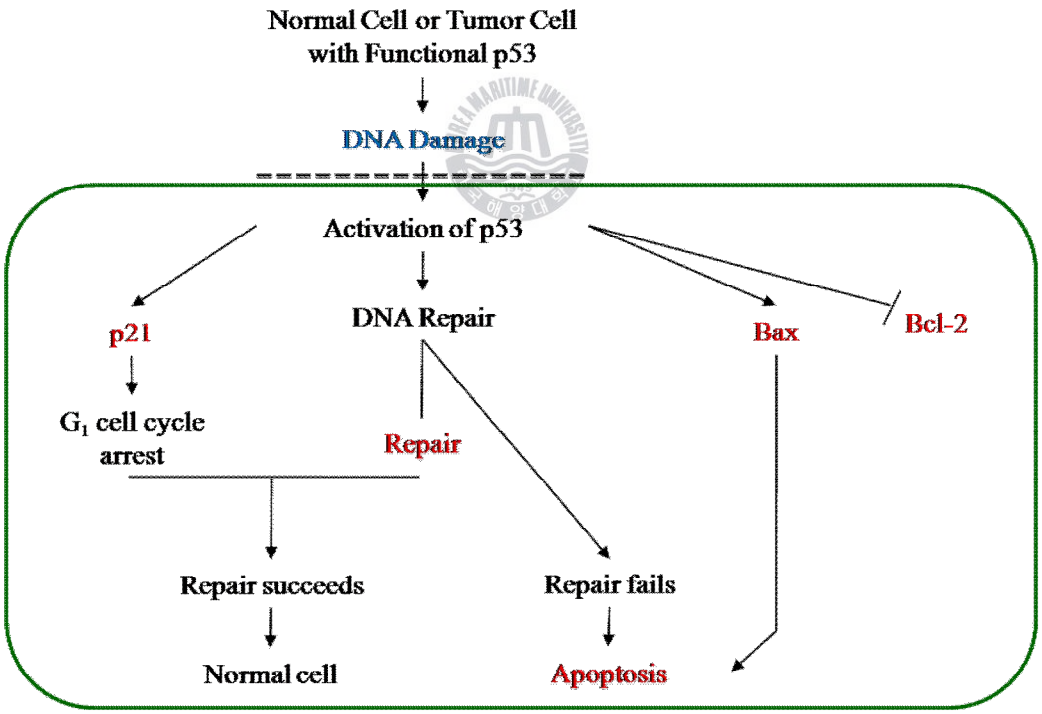

Figure 3. The p53 signaling pathway.

Table 2. Mechanisms of action of cancer chemopreventive agents

	Mechanism	Examples
blocking (anti-initiating)	Inhibition of cytochrome P450	dithiocarbamates isothiocyanates
	Induction of cytochrome P450	indole-3-carbinol β-naphthoflavone
	Induction of phase Ⅱ enzymes	isothiocyanates polyphenols
	Scavenging electrophiles	ellagic acid *N*-acetylcysteine sodium thiosulfate
	Induction of DNA repair	vanillin
suppressing (antipromotion/ antiprogression)	Inhibition of polyamine metabolism	α-ifluoromethylornithine substituted putrescines
	Inhibition of arachidonic acid metabolism	aspirin quercetin curcumin
	Protease inhibition	tosyl phenylalanine antipain
	Induction of differentiation	retinoids calcium vitamin D
	Inhibition of oncogene expression	lovastatin limonene antisense
	Inhibition of protein kinase C	staurosporine threo-dihydrosphingosine
	Inhibition of oxidative DNA damage	sarcophytol A epigallocatechin gallate selenium

Morse and Stoner, 1993

Table 3. Intermediate biomarkers

Class	Examples
Genomic biomarkers	oncogene activation tumor suppressor gene inactivation altered DNA methylation abnormal DNA content carcinogen-DNA adducts
Markers of proliferation	proliferating cell nuclear antigen thymidine labeling index bromodeoxyuridine incorporation Ki67 ornithine decarboxylase
Markers of differentiation	blood group antigens growth factors
Premalignant lesions	oral leukoplakia bronchial metaplasia sputum atypia aberrant crypts colonic adenomatous polyps dysplastic nevi

Morse and Stoner, 1993

1.5. Aims of the Research

The overall aim of this study was to pursue new bioactive secondary metabolites from halophytes collected in Korea, using a bioactivity-guided separation.

On the basis of a preliminary bioactivity screening test toward 25 species of halophytes, two halophytes, *C. heterocarpa* and *V. rotundifolia,* were ultimately selected for further scrutinizing of their secondary metabolite compositions (Table 1).

Halophytes were extracted and the crude extracts were separated on the basis of their chemical polarity and bioactivities, using a diverse array of chromatographic methods (C_{18} and silica gel column chromatography, preparative TLC, HPLC, etc.). Chemical structures of the isolated pure compounds were determined from the structure elucidation of pure compounds with the aid of MS, IR and NMR spectra, and their antiproliferative and antioxidant effects have been also evaluated.

The antiproliferative effects of pure compounds obtained from *C. heterocarpa* and *V. rotundifolia* were investigated using a MTT assay and mRNA expression of several factors (Bax, Bcl-2, p53, p21) related to apoptosis in human cancer cell lines. The antioxidant effects of the compounds were examined by measuring intracellular ROS (reactive oxygen species), NO (nitric oxide), GSH (glutathione). In addition, mRNA expression of iNOS, pro-oxidant and COX-2 in Raw 264.7 cells in the presence of the isolated secondary metabolites was evaluated by a RT-PCR method.

2. Materials and Methods

2.1. Plant Material

Whole plants of *Corydalis heterocarpa* and *Vitex rotundifolia* were collected in Muan-gun, Jeollanamdo, Korea in July, 2003 (Fig. 4). The plants were identified by Seong Gi Mun from their morphological characters. Voucher specimens are deposited in the laboratory of Jeom-Sook Lee (voucher No. 03H-7 and 03H-6, Department of Biology, Kunsan National University).

(a) ***Corydalis heterocarpa*** **(b)** ***Vitex rotundifolia***

Figure 4. Photographs of salt marsh plants (a) *Corydalis heterocarpa* and (b) *Vitex rotundifolia.*

2.2. General Experimental Procedures

Optical rotations were determined on a Perkin-Elmer polarimeter 341. NMR spectra were recorded in CD_3OD and $CDCl_3$ on a Varian Mercury 300 instrument at 300 MHz for ^1H and 75 MHz for ^{13}C using standard pulse sequence programs. All chemical shifts were recorded with respect to TMS as an internal standard. Mass spectroscopic data were obtained at the Korean Basic Science Institute, Seoul, Korea. Column chromatography was carried out on RP 18 (YMC-Pack ODS-A, 12nm, S-5 μm, 250×10mmI.D., YMC, USA) and silica gel (YMC-Pack SIL, 12nm, S-5 μm, 250×10mmI.D., YMC, USA). TLC plate (PLC Silica gel 60 F_{254}, 0.5mm, 20×20cm Merck, Germany) were used for TLC analysis. High performance liquid chromatography (HPLC) was performed on a Dionex P580 HPLC system equipped with a Varian 350 RI detector. All solvents used were spectral grade or were distilled from glass prior to use.

2.3. Extraction and Isolation of *Corydalis heterocarpa*

2.3.1. Extraction and Fractionation

The collected *C. heterocarpa* were air-dried and chopped into small pieces. The chopped plants were extracted with CH_2Cl_2 (3 L x 2) at room temperature for 2 days and filtered (No. 2, whatman). The residue was re-extracted with MeOH (3 L x 2) at room temperature for 2 days. The two extracts were combined, evaporated under reduced pressure (EYELA, N-N series, Japan), and the crude extracts (41.1 g) were partitioned between CH_2Cl_2 and water. The organic layer was further partitioned between *n*-hexane and 85% aq. MeOH, and the aqueous layer was partitioned with *n*-BuOH and H_2O, successively, to afford the *n*-hexane (7.3 g), 85% aq. MeOH (12.0 g), *n*-BuOH (4.3 g), and water (17.0 g) (Scheme 1).

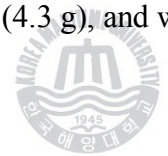

2.3.2. Isolation of Compounds

A portion of the 85% aq. MeOH fraction (7.0 g) was subjected to C_{18} reversed-phase vacuum flash chromatography using stepwise gradient mixtures of MeOH and water (50, 60, 70, 80, 90% aq. MeOH, and 100% MeOH) as eluents to give 6 subfractions (Fr. 1 – Fr. 6). Fr. 1 was separated by preparative TLC on a silica gel with the solvent system 10% MeOH in CH_2Cl_2 to yield **1** (329.1 mg). Reversed-phase HPLC (ODS-A, 65% aq. MeOH) of Fr. 3 and further purification using reversed-phase HPLC (ODS-A, 67% / 50% aq. CH_3CN) gave **2** (14.9 mg), **7** (13.6 mg), and **11** (6.4 mg). **3 (**63.8 mg) and **4** (146.9 mg) were obtained from Fr. 4 by

using reversed-phase HPLC (ODS-A, 75% aq. MeOH) followed by preparative TLC (silica, 100% CH_2Cl_2) (Scheme 2).

Half of the *n*-BuOH fraction (2.2 g) was chromatographed on C_{18} reversed-phase vacuum flash column by stepwise gradient elution of a mixture of MeOH and water (50, 60, 70, 80, 90% aq. MeOH, and 100% MeOH) to give 6 subfractions (Fr. 1 – Fr. 6). Fr. 1 was further separated on a silica gel column with stepwise gradient mixture (0, 5, 10, 20, 30, 40, 50, 70, and 100% MeOH in $CHCl_3$) to give 9 subfractions (Fr. 1-1 – Fr. 1-9). **5** (4.7 mg) was isolated from Fr. 1-3 by using reversed-phase HPLC (ODS-A, 45% aq. MeOH) followed by preparative TLC (silica, EtOAc : MeOH : H_2O (30 : 5 : 4)). Fr. 1-4 was separated by preparative TLC on a silica gel with EtOAc : MeOH : H_2O (23 : 4 : 3) to afford **8** (6.9 mg) and three mixtures (Mix. 2 – Mix. 4). Each mixture was analyzed with reversed-phase HPLC (ODS-A, 30 / 43 / 60% aq. MeOH) to yield **6** (5.7 mg), **9** (6.8 mg), and **10** (4.5 mg) (Scheme 3).

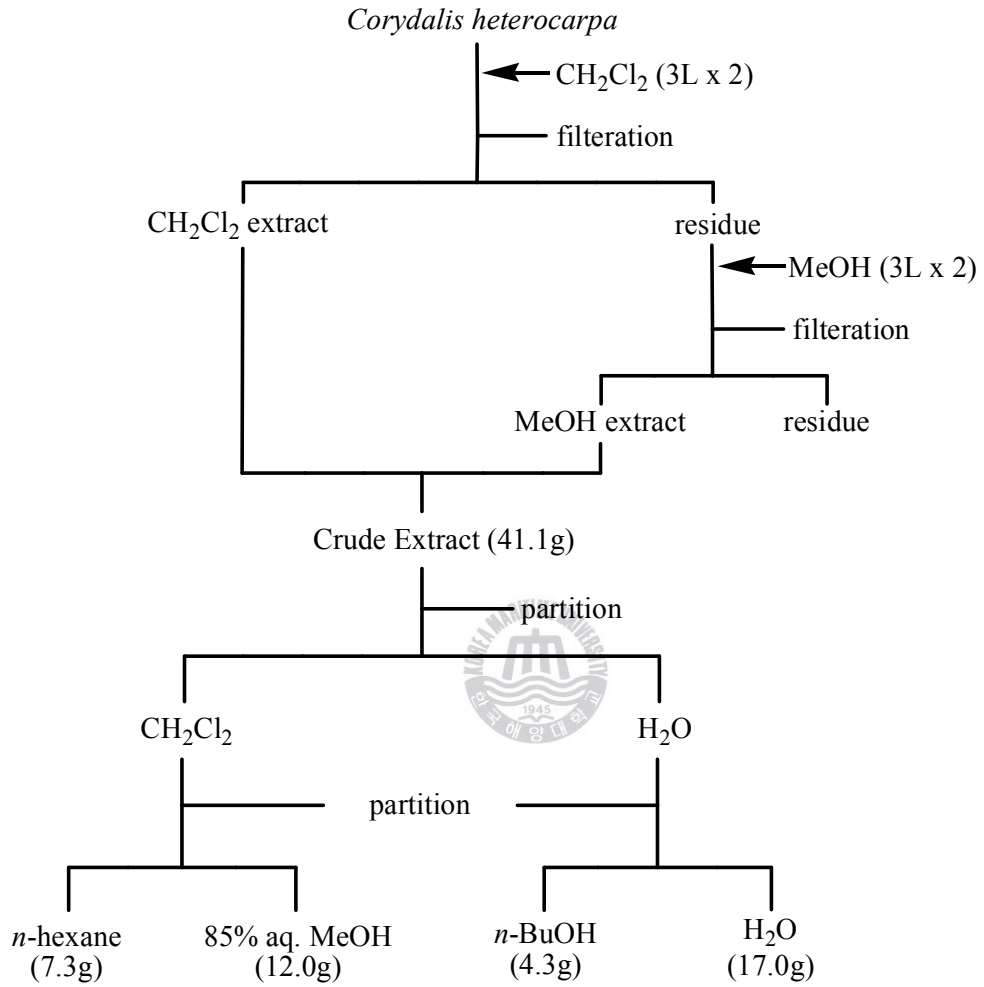

Scheme 1. Procedure of extraction and various fractions from *Corydalis heterocarpa.*

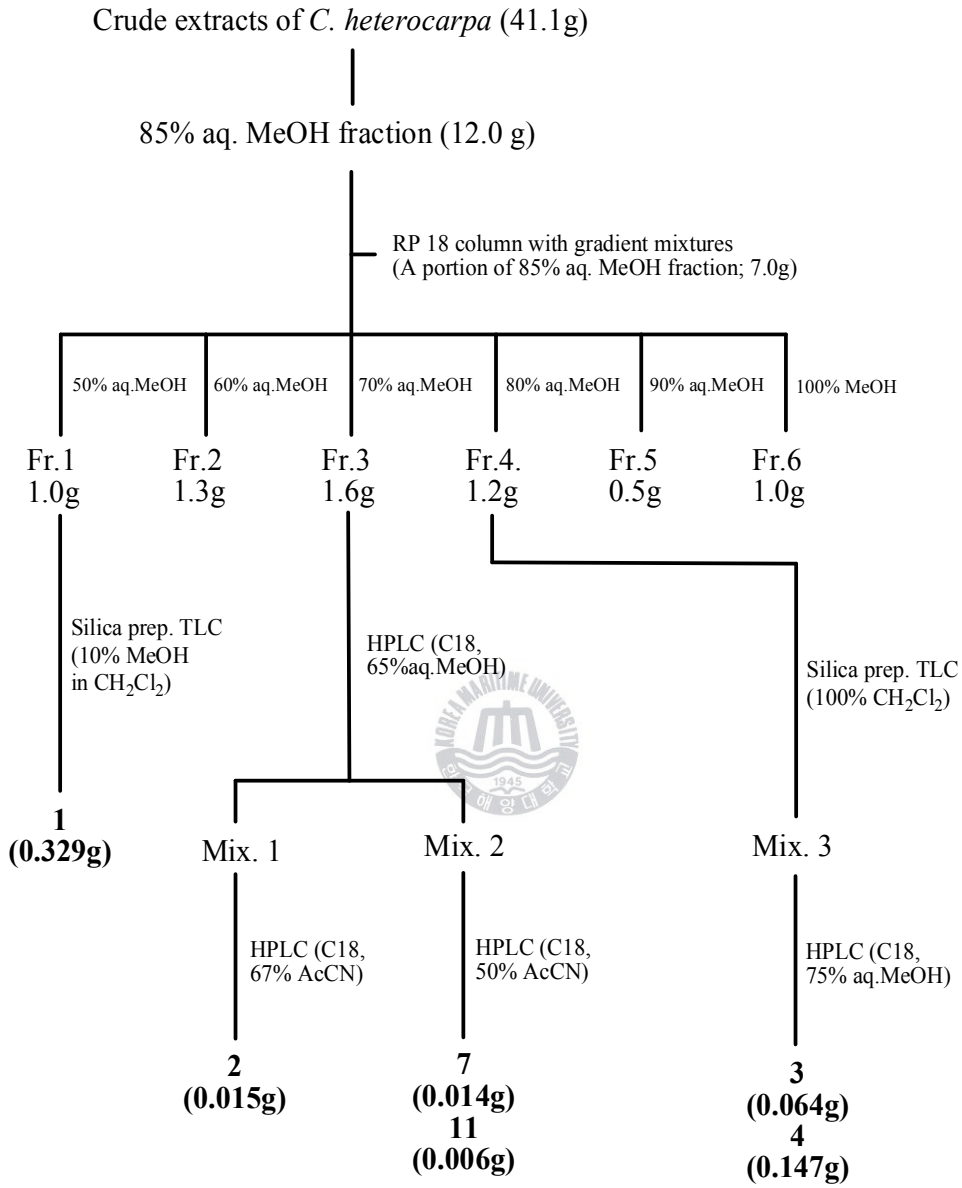

Scheme 2. Isolation procedure of compounds (**1-4**, **7**, **11**) from *Corydalis heterocarpa.*

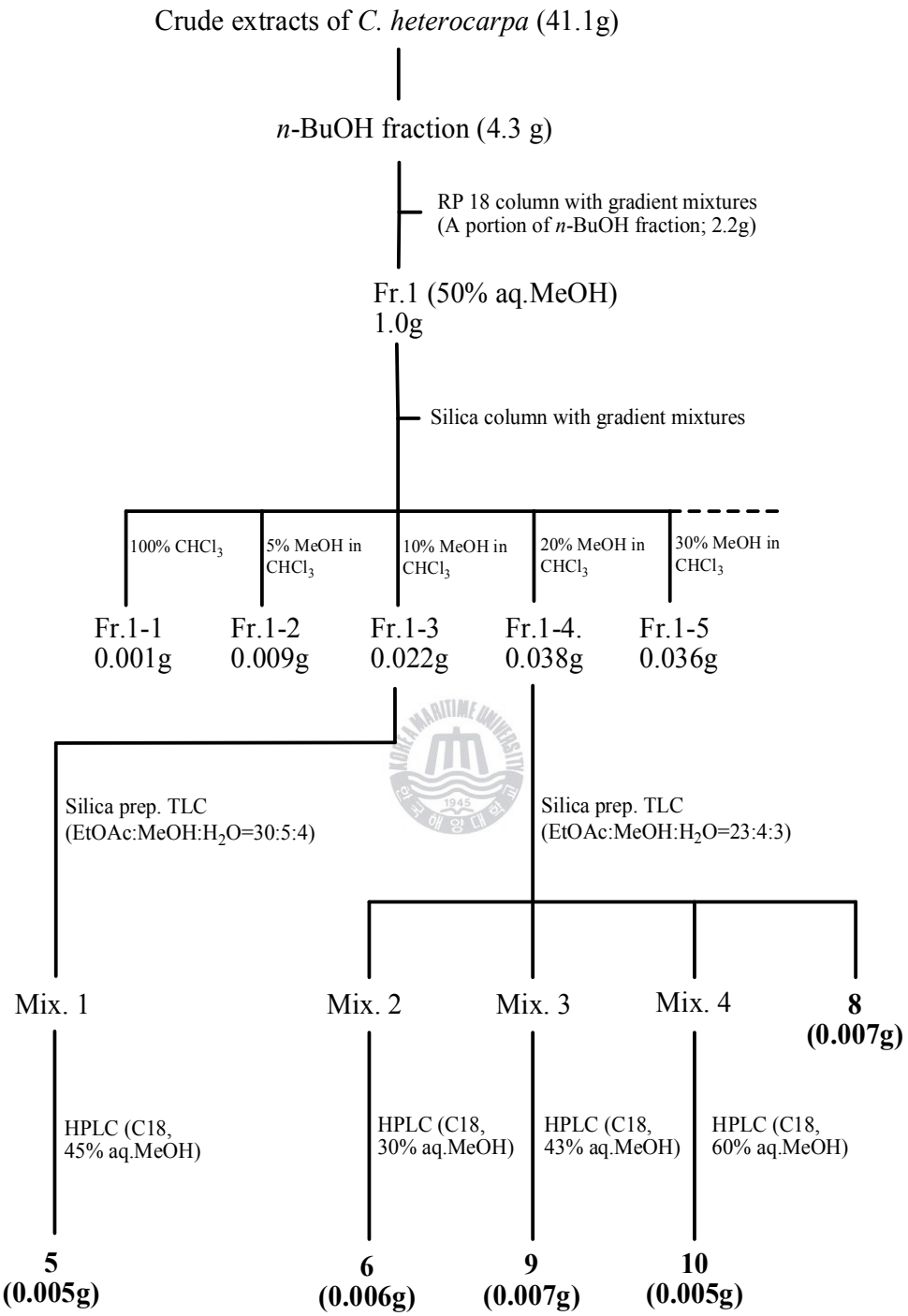

Scheme 3. Isolation procedure of compounds (**5-6**, **8-10**) from *Corydalis heterocarpa.*

2.3.3 Alkaline Hydrolysis of Compound **4**

A solution of **4** (5 mg) in MeOH (2 mL) was added 2 mL of 1.0 M KOH solution. The mixture was stirred overnight at room temperature and then evaporated to dryness. The residue was partitioned between EtOAc and water. After removal of solvent from the organic layer, (2'*S*)-columbianetin (**1**, 2.5 mg) was obtained (Scheme 4).

2.3.4. Synthesis of Compound **4**

(*S*)-(+)-2-methylbuanoic acid (0.51 g) in $SOCl_2$ (1 mL) was stirred under reflux for 1 h. The reaction mixture was concentrated under reduced pressure to give (*S*)-(+)-2-methylbutanoyl chloride. A solution of 9.7 mg of **1** in CH_2Cl_2 (2 mL) was added to a mixture of (*S*)-(+)-2-methylbutanoyl chloride and excessive 4-N,N-dimethylaminopyridine (50 mg) in CH_2Cl_2 (2 mL). After stirring overnight at room temperature, the crude ester was purified by silica gel thin layer chromatography with CH_2Cl_2 solvent system followed by reversed-phase HPLC (YMC-Pack ODS-A, 75% aq. MeOH) to afford the (2'*S*,7'*S*)-*O*-2-methylbutyryl-columbianetin (6.6 mg) (Scheme 5).

2.3.5. Acid Hydrolysis of Compound **6**

A solution of **6** (2 mg) in 0.05 N HCl (5 mL) was heated at 95 ^{o}C for 1.5 h. After hydrolysis the solution was extracted with EtOAc to give (2'*S*)-comlumbianetin (**1**). Sulfate ion (SO_4^{2-}) was detected from the concentrated aqueous layer (Scheme 6).

Scheme 4. Alkaline hydrolysis of compound **4** isolated from *Corydalis heterocarpa*.

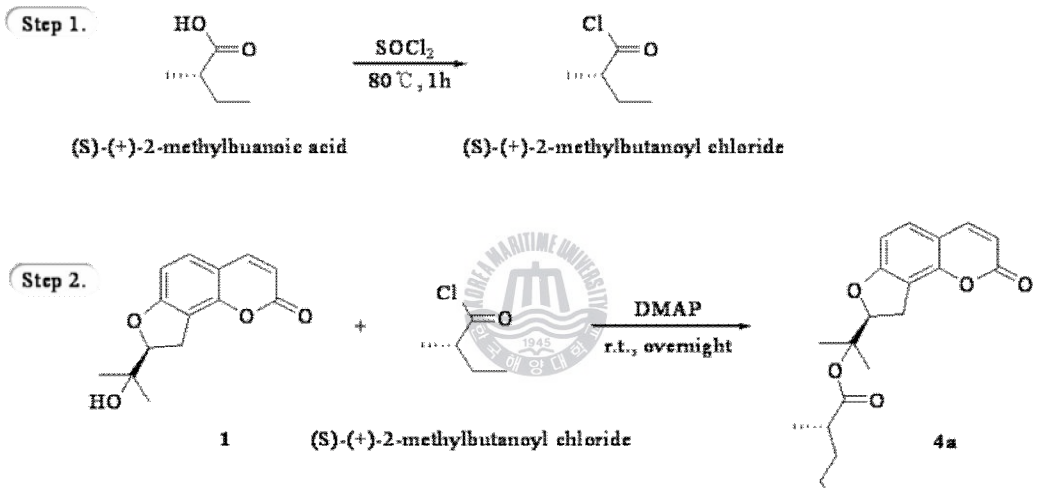

Scheme 5. Synthesize of compound **4** by esterification of compound **1** isolated from *Corydalis heterocarpa* with (*S*)-(+)-2-methylbutanoic acid.

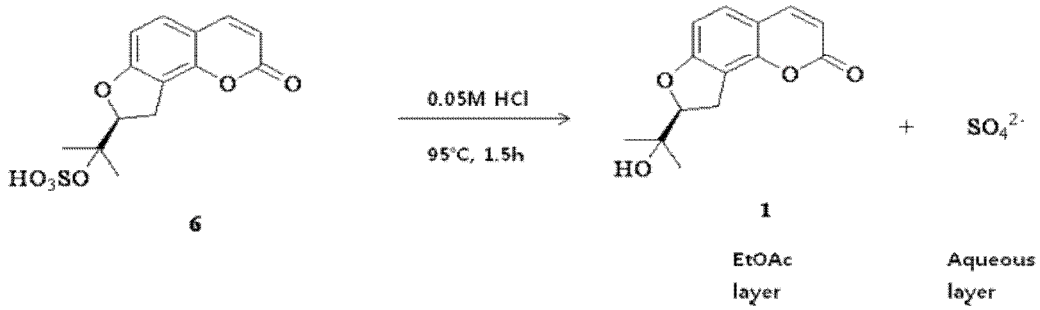

Scheme 6. Acid hydrolysis of compound **6** isolated from *Corydalis heterocarpa*.

2.4. Extraction and Isolation of *Vitex rotundifolia*

2.4.1. Extraction and Fractionation

The air-dried samples of *V. rotundifolia* were cut into small pieces and the pieces extracted for 2 days with MeOH (3 L x 2) and CH_2Cl_2 (3 L x 2), in turn. The two combined crude extracts (145.3 g) were filtered and concentrated under vacuum and partitioned between CH_2Cl_2 and water. Later, the organic layer was further partitioned between *n*-hexane (33.6 g) and 85% aq. MeOH (21.0 g), and the aqueous layer was fractionated with *n*-BuOH (39.0 g) and H_2O (47.8 g), successively (Scheme 7).

2.4.2. Isolation of Compounds

A portion of *n*-BuOH fraction (15.0 g) and 85% aq. MeOH fraction (21.0g) were subjected to C_{18} reversed-phase vacuum flash chromatography using stepwise gradient mixtures of MeOH and water (50, 60, 70, 80, 90% aq. MeOH, and 100% MeOH) as eluents to give 6 subfractions (Fr. 1 – Fr. 6), respectively. Fr. 3 obtained after C_{18} flash chromatography of *n*-BuOH fraction was purified by reversed-phase HPLC (ODS-A, 67% aq. MeOH) to give **12** (119.2 mg) (Scheme 8). Fr. 4 obtained from 85% aq. MeOH fraction was separated by reversed-phase HPLC (ODS-A, 78% aq. MeOH) to give **14** (71.4 mg) and six mixtures (Mix. 1 – Mix. 6), in order of elution. Mix. 1 / 2 / 3 were separately purified by reversed-phase HPLC with same solvent (ODS-A, 50% aq. CH_3CN) to give **13** (2.5 mg) and **22** (4.9 mg) / **20** (2.5 mg) and **23** (20.4 mg) / **15** (24.8 mg) and **16** (15.0 mg), respectively. Mix. 4 / 5

/ 6 was separated by reversed-phase HPLC (ODS-A, 63 / 68 / 60% aq. CH_3CN) to afford **19** (18.0 mg) / **17** (55.7 mg) / **18** (69.9 mg), respectively. **21** (2.9 mg) was isolated from Mix. 5 by using normal-phase HPLC (SIL, 25% EtOAc in hexane) followed by reversed-phase HPLC (ODS-A, 60% aq. CH_3CN) (Scheme 8).

A portion of the *n*-hexane (10 g) fraction was separated on a silica gel column chromatography with stepwise gradient mixtures of EtOAc and *n*-hexane (0, 10, 20, 30, 40, 50, 60, 70, and 100% EtOAc in hexane) as eluents to give 9 subfractions (Fr. 1 – Fr. 9). Fr. 2 was separated further by silica gel column chromatography with 0, 2, 4, 4, 6, 6, 8, and 10% EtOAc in hexane (Fr. 2-1 – Fr. 2-8). Fr. 2-3 was further purified by normal-phase HPLC (SIL, 100% hexane) to yield **24** (18.9 mg), **25** (31.4 mg), and **26** (30.8 mg). **29** (4.2 mg) and **30** (7.0 mg) were isolated from Fr. 2-3 by using reversed-phase HPLC (ODS-A, 90% CH_3CN in dioxane) followed by normal-phase HPLC (SIL, 100% hexane). Reversed-phase HPLC (ODS-A, 75% THF) of Fr. 2-4 afforded **28** (4.2 mg), and further purification of Fr. 2-4 using HPLC (SIL, 3% EtOAc in hexane, and ODS-A, 85% aq. CH_3CN, in turn) gave **27** (11.0 mg) (Scheme 9).

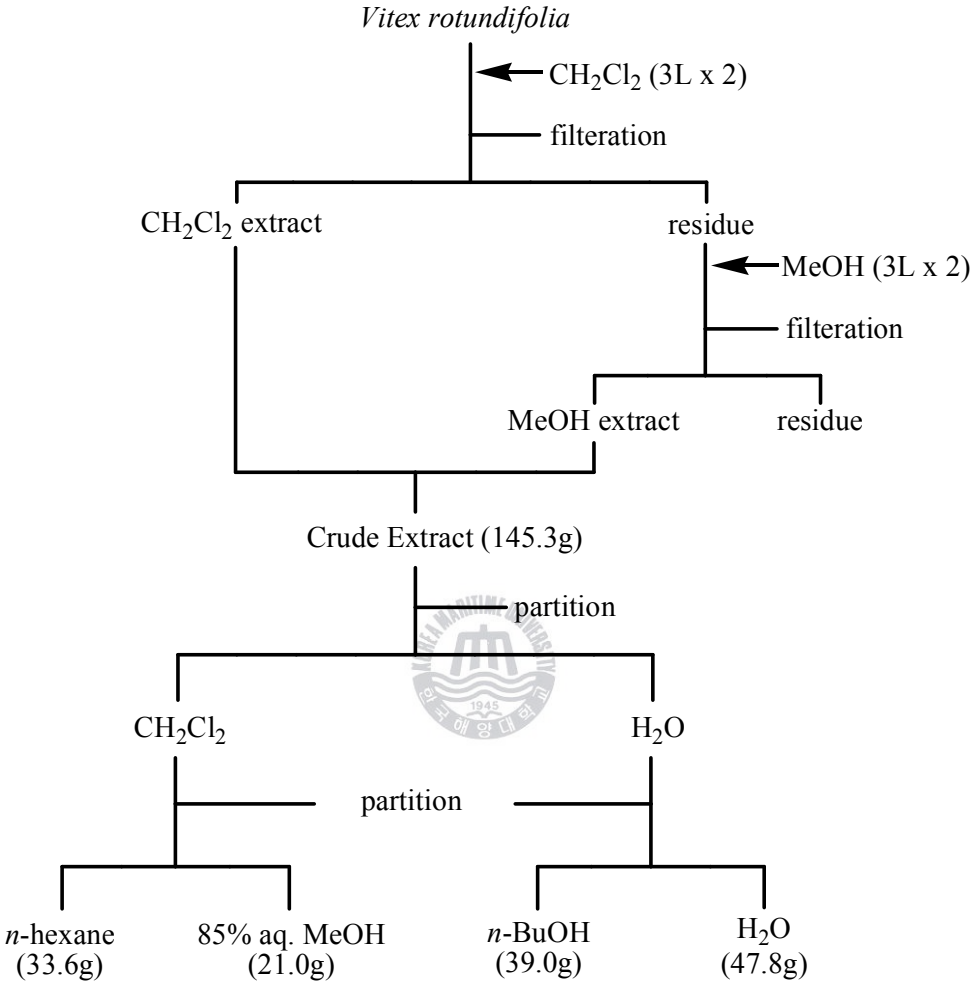

Scheme 7. Procedure of extraction and various fractions from *Vitex rotundifolia.*

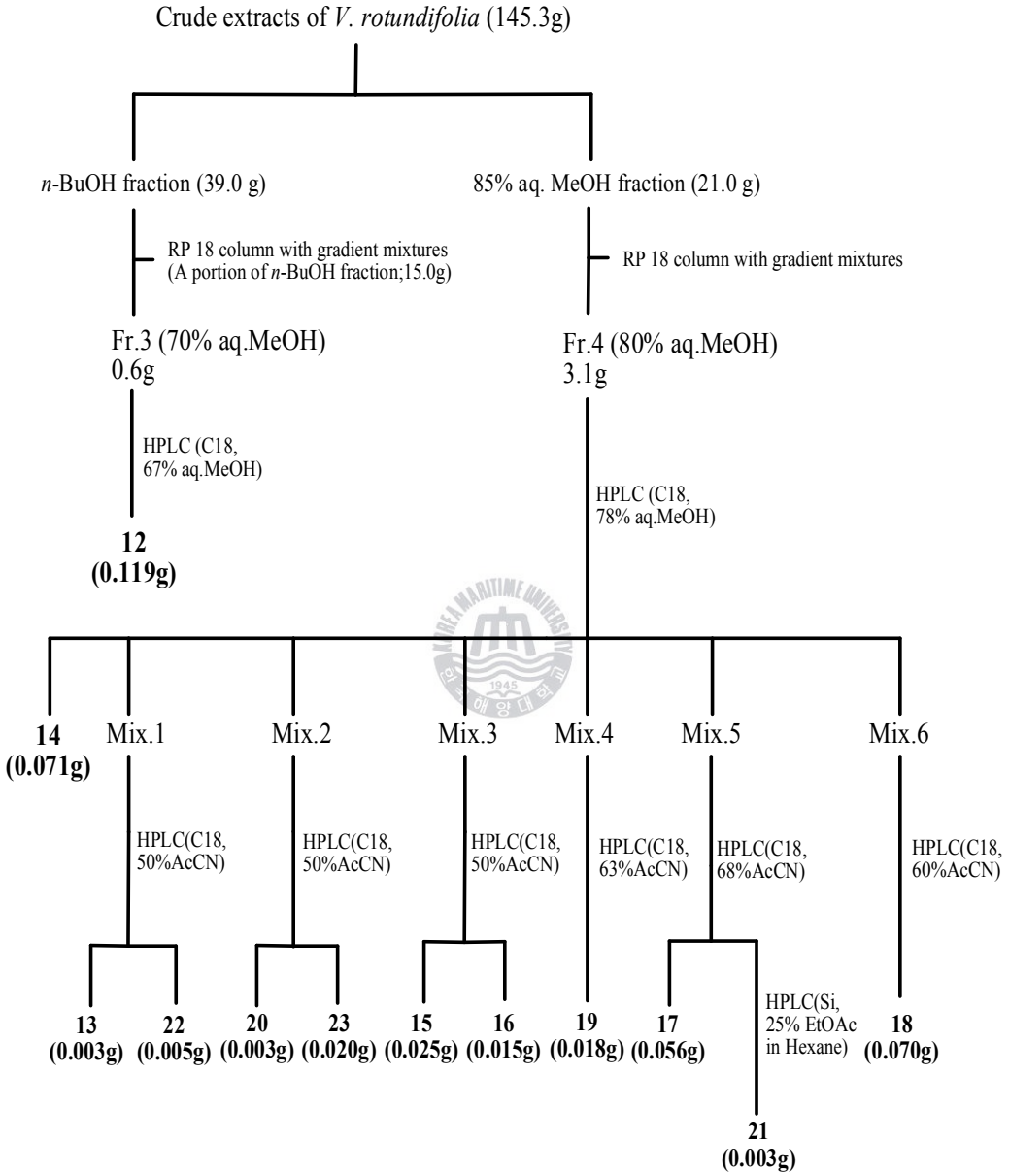

Scheme 8. Isolation procedure of the compounds (**12-23**) from *Vitex rotundifolia.*

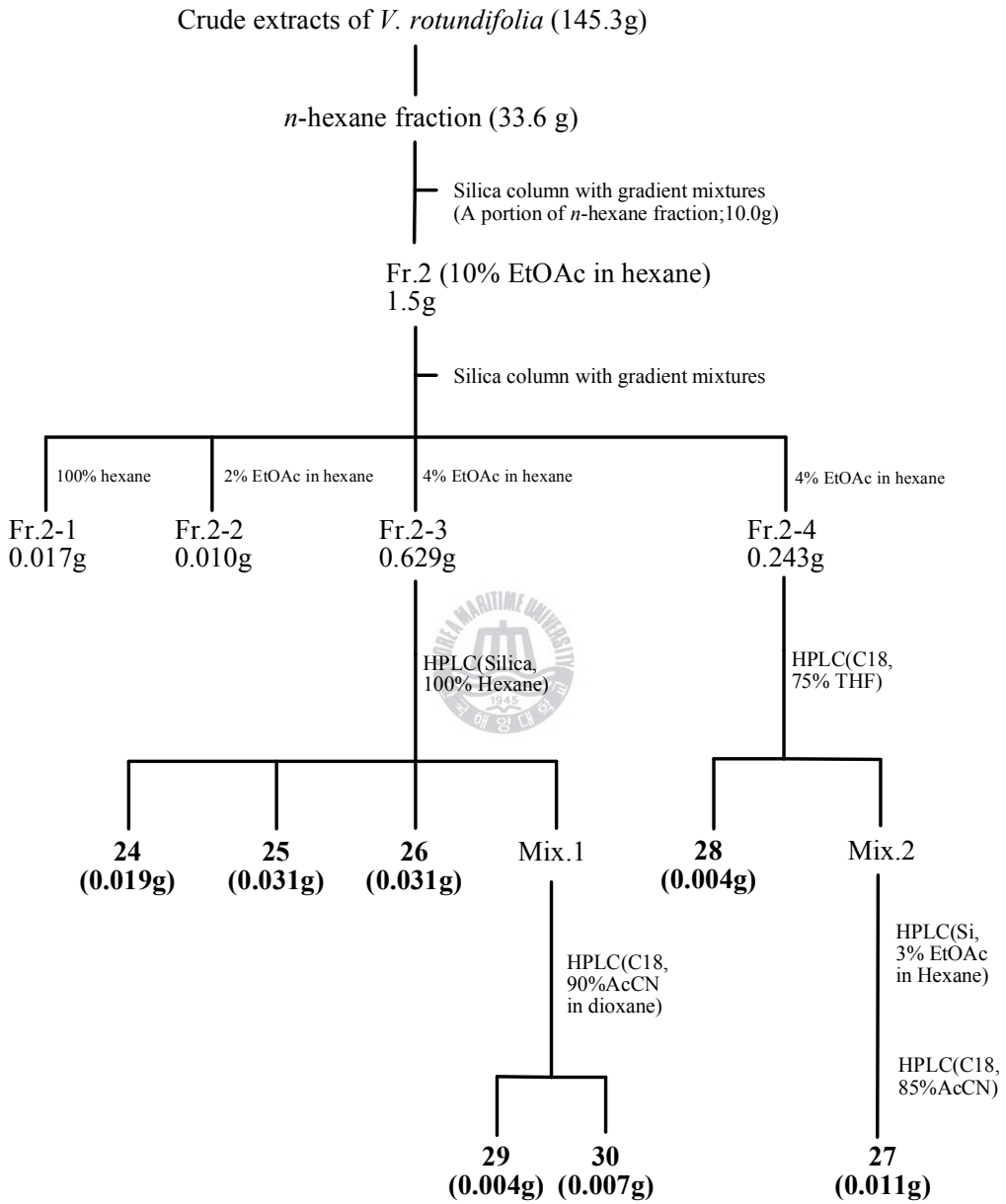

Scheme 9. Isolation procedure of the compounds (**24-30**) from *Vitex rotundifolia.*

2.5. Antiproliferative Effects

2.5.1. Cell Culture and Inhibition of Cancer Cell Proliferation

AGS (human gastric cancer), HT-29 (human colon cancer), HT-1080 (human fibrosarcoma), MCF-7 (human breast cancer) and U-937 (human leukemia) cell lines were separately grown as monolayers in T-75 tissue culture flasks (Nunc, Roskilde, Denmark) at 5% CO_2 and 37 ºC humidified atmosphere using appropriate media supplemented with 10% fetal bovine serum (FBS), 2 mM glutamine and 100 μg/mL penicillin-streptomycin. Dulbecco's modified eagle medium (DMEM, Gibco-BRL, Gaithersburg, MD, USA) and RPMI 1640 (Gibco-BRL, Gaithersburg, MD, USA) were used as the culture mediums and the medium was changed twice or three times each week. The antiproliferative effects of the isolated compounds on cultured cells were measured using MTT [3-(4,5-dimethylthiazol-2-yl)-2,5-diphenyltetrazolium bromide] assay, which is based on the conversion of MTT to MTT-formazan by mitochondrial enzyme (Hansen *et al*., 1989).

The cells were grown in 96-well plates at a density of 5×10^4 cells/well. After 24 h, cells were washed with fresh medium and treated with different concentrations of samples. After incubation for 24 h, the cells were rewashed and incubated with 100 μL of MTT (1 mg/mL) for 4 h. Finally, 150 μL of DMSO was added to solubilize the formed formazan crystals. The amount of formazan crystal was determined by measuring the absorbance at 540 nm using a multidetection microplate fluorescence spectrophotometer synergy HT (Bio-Tek instruments Inc., Winooski, VT, USA). Relative cell viability was determined by the amount of MTT converted into a formazan. Viability of cells was quantified as a percentage compared to the control.

2.5.2. Reverse Transcription-Polymerase Chain Reaction (RT-PCR)

Total RNA was isolated using a Trizol reagent (Invitrogen Co., CA, USA) following the manufacturer's recommendations. Total RNA was digested with RNase-free DNase (Roche, Penzberg, Germany) for 15 min at 37 ºC and repurified by the RNeasy kit according to the manufacturer's protocol (Promega, Madison, WI). The target cDNA was synthesized from 2 μg total RNA by incubation at 37 ºC for 1 h with AMV reverse transcriptase (Amersham) with random hexanucleotide according to the manufacturer's instructions.

Primers to specifically amplify the genes interested were as follows; forward 5'-CAG-CTG-CAC-CTG-ACG-3' and reverse 5'-GCT-GGG-TAG-GTG-CAT-3' for Bcl-2 gene; forward 5'-ATG-GAC-GGG-TCC-GGG-GAG-3' and reverse 5'-TGG-AAG-AAG-ATG-GGC-TGA-3' for Bax gene; forward 5'-GCT-CTG-ACT-GTA-CCA-CCA-TCC-3' and reverse 5'-CTC-TCG-GAA-CAT-CTC-GAA-GCG-3' for p53 gene; forward 5'-CTC-AGA-GGA-GGC-GCC-ATG-3' and reverse 5'-GGG-CGG-ATT-AGG-GCT-TCC-3' for p21 gene. For the internal control gene GAPDH, forward 5'-CGG-AGT-CAA-CGG-ATT-TGG-TCG-TAT-3' and reverse 5'-AGC-CTT-CTC-CAT-GGT-GGT-GAA-GAC-3' were used.

Amplification was performed in a master-cycler (Eppendorf, Hamburg, Germany) with cycles of denaturation at 94 ºC for 30 s, annealing at 58 ºC for 30 s, and extension at 72 ºC for 30 s, respectively. The amplified PCR products were run in 1.0% agarose gels and visualized by ethidium bromide (EtBr).

2.6. Antioxidant Effects

2.6.1. Cell Culture and Cytotoxicity Determination using MTT assay

Raw 264.7 macrophage cells were cultured in Dulbecco's modified eagle medium (DMEM, Gibco-BRL, Gaithersburg, MD, USA) containing 10% fetal bovine serum (FBS), 2 mM glutamine and 100 μg/mL penicillin-streptomycin (Gibco-BRL, Gaithersburg, MD, USA) and maintained at 37 ºC in humidified incubator containing 5% CO_2. The cell number was adjusted to 5×10^4 cells/well in 96-well plates. After cells were cultured in the presence of sample or not for 24 h, cell viability was determined by colorimetric measurement of the reduction product of MTT [3-(4,5-dimethylthiazol-2-yl)-2,5-diphenyltetrazolium bromide], which is based on the conversion of MTT to MTT-formazan by mitochondrial enzyme (Hansen *et al*., 1989). Briefly, the original medium was washed with fresh medium, then, 100 μL of MTT solution (1 mg/mL) was added to each well. After 4 h, 150 μL of DMSO was added to solubilize the formed formazan crystals, and the amount of formazan crystal was determined by measuring the absorbance at 540 nm using a multidetection microplate fluorescence spectrophotometer synergy HT (Bio-Tek instruments Inc., Winooski, VT, USA). Relative cell viability was determined by the amount of MTT converted into a formazan. Viability of cells was quantified as a percentage compared to the control.

2.6.2. Determination of Nitric Oxide (NO) Production

To determine the effects of compounds on the NO production in the cultured media, the Raw 264.7 cells were seeded at a density of 5×10^4 cells/well in 96-well plates using DMEM without phenol red. Following incubation for 24 h, the adherent cells were washed three times with PBS. The cells were then incubated in the medium with sample, with or without 1 μg/mL final concentration of LPS. After incubation for 48 h, the production of NO was determined based on the Griess reaction (Green *et al*., 1982). Each of the 50 μL of cultured medium was added onto a 96-well microtiter plate. The 50 μL of Griess reagent was added to each well and stand for 15 min at room temperature. The absorbance of the mixture at 550 nm was measured by using a multidetection microplate fluorescence spectrophotometer synergy HT (Bio-Tek instruments, USA). The concentrations of nitrite were calculated from regression analysis, using serial dilutions of sodium nitrite as a standard.

2.6.3. Measurement of Intracellular Reactive Oxygen Species (ROS) Levels

The extent of intracellular ROS formation was measured by using 2',7'-dichlorofluorescin diacetate (DCFH-DA) as the substrate (Okimoto *et al*., 2000). Raw 264.7 cells growing in fluorescence microtiter 96-well plates were loaded with 20 μM DCFH-DA in HBSS for 20 min in the dark. Nonfluorescent DCFH-DA dye, which freely penetrates into cells, gets hydrolyzed by intracellular esterases to 2',7'-dichlorodihydrofluororescein ($DCFH_2$), and traps inside the cells (Curtin *et al.*, 2002). After treatment with the different concentrations of sample, the Raw 264.7 cells were incubated for 1 h. The culture medium was removed, the cells were washed three times with PBS, and 500 μM H_2O_2 dissolved in HBSS was added to cells. The formation of 2',7'-dichlorofluorescein (DCF), a fluorescent compound ($\lambda_{excitation}$=485 nm; $\lambda_{emission}$ =528 nm) due to oxidation of $DCFH_2$ in the presence of various ROS, was read after every 30 min using a multidetection microplate fluorescence spectrophotometer synergy HT (Bio-Tek instruments, USA). Time-dependent effects of the compounds were plotted and compared with fluorescence intensity of control and blank groups.

2.6.4. Measurement of Intracellular Glutathione (GSH) Levels

Intracellular GSH concentration in intact cells was tested with monobromobimane as a thiol-staining reagent (Poot *et al*., 1986). Briefly, the Raw 264.7 cells were seeded into fluorescence microtiter 96-well plates at a density of 5×10^4 cells/mL and incubated with sample for 1h. The cells were washed three times with PBS, and monobromobimane (mBBr) in 1% DMSO was treated to cells at a final concentration of 40 μM for 30 min at 37 ℃ in the dark. The fluorescence intensity was measured ($\lambda_{excitation}$=360 nm; $\lambda_{emission}$=465 nm) after every 30 min using a multidetection microplate fluorescence spectrophotometer synergy HT (Bio-Tek instruments, USA). The averaged fluorescence values of cell populations were plotted and compared with control group.

2.6.5. Reverse Transcription-Polymerase Chain Reaction (RT-PCR)

The levels of iNOS and COX-2 mRNA were determined by RT-PCR. Total RNA was isolated with Trizol reagent (Invitrogen Co., CA, USA) according to manufacturer's recommendations. cDNA was synthesized from 2 μg total RNA by incubation at 37 ºC for 1 h with AMV reverse transcriptase (Amersham) with random hexanucleotide. The expression of a housekeeping gene, GAPDH, was used as an internal control.

Primers to specifically amplify the genes interested were as follows; forward 5'-AGA-GAG-ATC-CGG-TTC-ACA-3' and reverse 5'-CAC-AGA-ACT-GAG-GGT-ACA-3' for iNOS gene; forward 5'-TTC-AAA-TGA-GAT-TGT-GGG-AAA-ATT-GCT-3' and reverse 5'-AGA-TCA-TCT-CTG-CCT-GAG-TAT-CTT-3' for COX-2 gene. For the internal control gene GAPDH, forward 5'-CGG-AGT-CAA-CGG-ATT-TGG-TCG-TAT-3' and reverse 5'-AGC-CTT-CTC-CAT-GGT-GGT-GAA-GAC-3' were used.

Amplification was performed in a master-cycler (Eppendorf, Hamburg, Germany) with cycles of denaturation at 94 ºC for 30 s, annealing at 54 ºC for 30 s, and extension at 72 ºC for 60 s, respectively. The PCR products were visualized by electrophoresis through 1.0% agarose gel stained with ethidium bromide (EtBr).

2.7. Statistical Analysis

The data were presented as mean ± SD. Differences between the means of the individual groups were assessed by one-way ANOVA with Duncan's multiple range tests. Differences were considered significant at $p < 0.05$. The statistical software package, SAS v9.1 (SAS Institute Inc., NC, USA), was used for these analyses.

3. Results and Discussion

3.1. Secondary Metabolites Isolated from *Corydalis heterocarpa*

The crude extract of *C. heterocarpa* was partitioned with CH_2Cl_2 and H_2O. Each layer was further partitioned with *n*-hexane/85% aq. MeOH and *n*-BuOH/H_2O, respectively. The *n*-BuOH and 85% aq. MeOH fractions were then purified by various types of column chromatography, TLC, and HPLC using different solvent combinations, to yield nine compounds including two new compounds (**4** and **6**) (Fig. 5).

KOREA MARITIME UNIVERSITY 1945 한국해양대학교

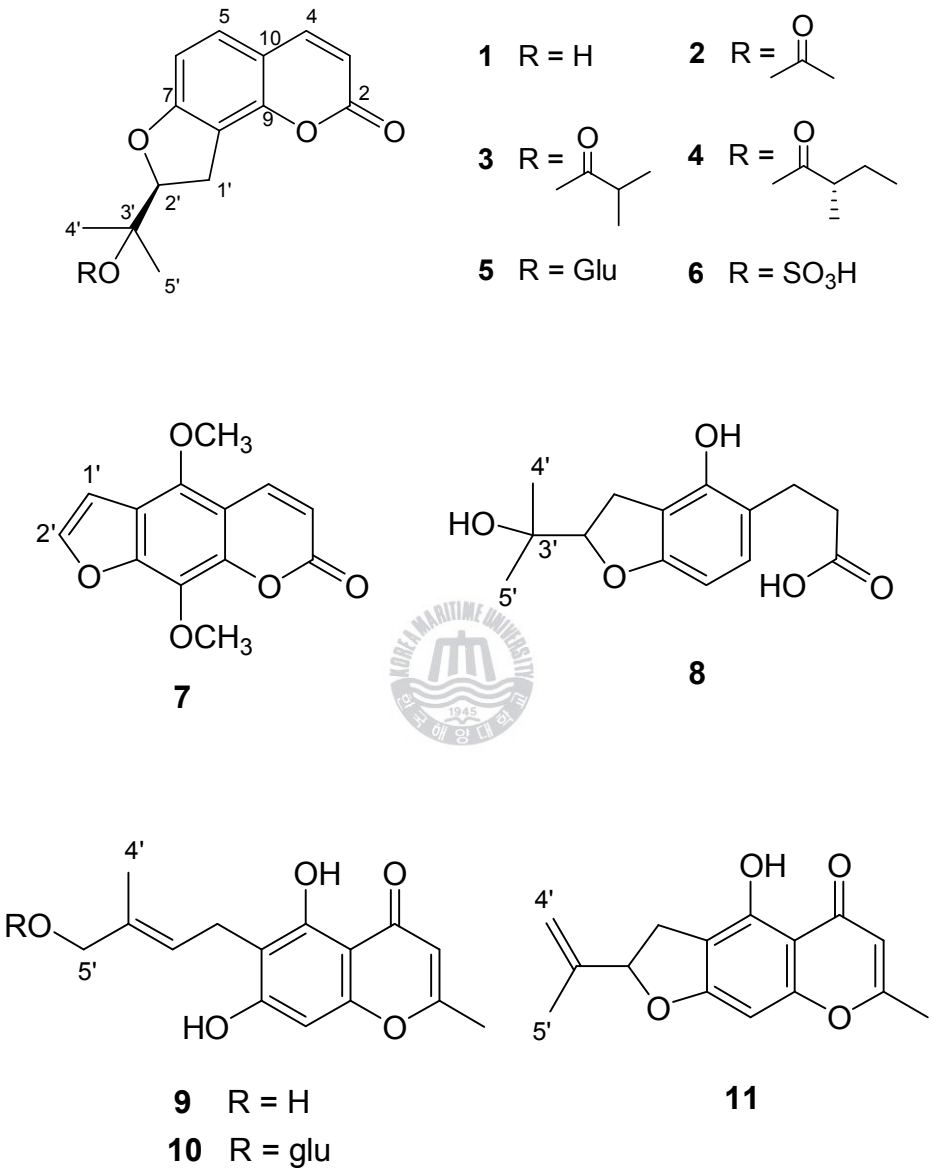

Figure 5. Chemical structure of compounds **1-11** isolated from *Corydalis heterocarpa*.

3.1.1. Structural Determination of Compounds **1-3** and **5**

Compound **1** was obtained as an amorphous white solid. The molecular formula of **1** was determined to be $C_{14}H_{14}O_4$ by a combination of EIMS and ^{13}C NMR spectrometry. The ^1H NMR spectrum of **1** contained signals for two tertiary methyls [δ 1.37, 1.24 (3H each, all s)], a methylene [δ 3.31 (2H, dd, *J* = 9.0, 4.8 Hz)], an oxygen-substituted methane [δ 4.79 (1H, t, *J* = 9.0 Hz)], and two sets of ortho-coupled aromatic protons [δ 6.20, 7.61 (1H each, all d, *J* = 9.5 Hz), δ 6.73, 7.26 (1H each, all d, *J* = 8.3 Hz)]. The ^{13}C NMR spectrum indicated the presence of 14 carbons, including one ester carbonyl carbon, two sp^2 and two oxygenated sp^3 carbons, one aliphatic carbon, and one phenyl group (Table 4). These data were typical furanocoumarin signals and a more detailed chemical structure was identified by extensive 2D NMR experiments, such as gDQCOSY, TOCSY, NOESY, gHMQC, and gHMBC. These spectral data established **1** to be the columbianetin, which has been previously reported in several plants, including *Peucedanum oreoselinum, Ligusticum seguieri, Cnidium japonicum, Xanthoxylum arnottianum, Lomatium dissectum*, and *Zanthoxylum punctatum* (Lemmich *et al*., 1970; Lemmich *et al*., 1971; Hata *et al*., 1972; Ishii *et al*., 1974; Van Wagenen *et al*., 1988; Stermitz and Sharifi, 1977). On the basis of comparison with published spectral data, the structure of compound **1** was established as (2'*S*)-columbianetin (Willette and Soine, 1964; Lemmich *et al*., 1970; Shipchandler *et al*., 1970; Lemmich *et al*., 1971; Steck, 1971; Hata *et al*., 1972; Bandopadhyay *et al*., 1974;

Ishii *et al*., 1974; Stermitz and Sharifi, 1977; Mchale *et al*., 1987; Van Wagenen *et al*., 1988; Awale *et al*., 2006).

Compound **2** was obtained as an amorphous white solid with an elemental composition of $C_{16}H_{16}O_5$, as determined from its EIMS and ^{13}C NMR data. The ^{1}H and ^{13}C NMR spectra of **2** were very similar to those of **1**, except for the acetyl groups [δ_C 170.0, 22.3; δ_H 1.97 (3H, s)]. Therefore, the structure of compound **2** was construed to be libanoridin by the analysis of 1D and 2D NMR experiments, as well as by comparison with the literature values (Lemmich *et al*., 1970; Lemmich *et al*., 1971; Hata *et al*., 1972).

Compound **3** was also similar to compound **1** and yielded molecular formula $C_{18}H_{20}O_5$ by EIMS and ^{13}C NMR spectral data. The ^{1}H and ^{13}C NMR spectra of **3** displayed typical features similar to those of **1**, except for the methylpropanoyl moiety [δ_C 176.0, 34.9, 19.0, 18.9; δ_H 2.40 (1H, m), 1.04 (3H, d, J = 7.2 Hz), 1.03 (3H, d, J = 7.2 Hz)]. Thus, the structure of compound **3** was identified as a cnidiadin by the analysis of 1D and 2D NMR experiments and by comparison of its spectral data with those reported in the literature (Hata *et al*., 1972).

Compound **5** was obtained as an amorphous white solid with an elemental composition of $C_{20}H_{24}O_9$, as determined from its FABMS. Comparison of the ^{1}H- and ^{13}C-NMR data of compound **5** with those of **1-3** revealed that **5** is also a coumarin. However, there were significant differences in the ^{13}C NMR spectrum as compared with **1**. The six carbon signals of the sugar moiety were at δ 98.8, 78.1, 77.5, 75.1, 71.4 and 62.3, suggesting that **5** was a coumarin glycoside. The carbon

resonances of **5** were in agreement with literature values for a β-D-glucopyranosyl residue. Therefore, the structure of the compound **5** was identified as (2'*S*)-columbianetin-*O*-β-D-glucopyranoside (Shipchandler *et al*., 1970; Mchale *et al*., 1987; Van Wagenen *et al*., 1988).

These compounds **1**-**3** and **5** are the first reported secondary metabolites from this halophyte.

KOREA MARITIME UNIVERSITY
1945
한국해양대학교

3.1.2. Structural Determination of Compound **4**

Compound **4**, which is a homologous series of compounds **1** - **3**, was obtained as an amorphous white powder with an elemental composition of $C_{19}H_{22}O_5$, as determined from its high-resolution EIMS ($[M]^+$ *m/z* 330.1467). The ^1H and ^{13}C NMR spectra of **4** were very similar to those of (2'*S*)-columbianetin (**1**) from *Cnidium japonicum* (Table 4) (Hata *et al*., 1972). However, there were significant differences in the ^1H NMR spectrum as compared with (2'*S*)-columbianetin (**1**). The signals for two methyls, one methylene, and one methine were observed at δ 1.01 (3H, d, *J* = 7.2 Hz), 0.85 (3H, t, *J* = 7.2 Hz), 1.50 (2H, m) and 2.20 (1H, m), respectively. Corresponding differences were found in the ^{13}C NMR spectrum, in which signals were observed of a quaternary carbon at δ 175.4, two methyl carbons at δ 16.7 and 11.7, a methylene at δ 26.7, and a methine carbon at δ 42.1, respectively. These differences were explained by the presence of additional signals due to a 2-methylbutanoyl group in **4**, which was confirmed by a HMBC experiment. Detailed analysis of the gDQCOSY, gHMQC, and gHMBC spectra indicated that **4** is *O*-(2-methylbutanoyl)-columbianetin.

The remaining problem was the determination of the relative configuration of **4**. This compound possesses asymmetric centers at C-2' and C-7'. The configuration at C-2' of **4** was determined as *S* by comparison of the optical rotation of **1** obtained after hydrolysis of **4** with that of the authentic compound (Scheme 4). To determine the configuration of C-7', **4** was synthesized by esterification of **1** with (*S*)-(+)-2-methylbutanoic acid. Spectroscopic data of the synthetic compound were identical

with those of **4** (Scheme 5). Thus, the structure of compound **4** was assigned as (2'*S*,7'*S*)-*O*-(2-methylbutanoyl)-columbianetin. This compound has not been previously reported in the literature.

KOREA MARITIME UNIVERSITY
1945
한국해양대학교

3.1.3. Structural Determination of Compound **6**

Compound **6** was isolated as an amorphous white powder that yielded $C_{14}H_{14}O_7S$ upon analysis by a combination of high-resolution ESIMS and ^{13}C NMR spectrometry. Strong absorption bands at 3415 and 1250 cm^{-1} in the IR spectrum indicated the presence of a hydrogen sulfate group. The ^{13}C NMR spectroscopic data of **6** were almost identical to those of **1** (Table 4). The only significant difference was the downfield shift of a quaternary carbon signal for **1** from δ 71.7 to 84.1. Its neighboring methyl carbon signals were also shifted upfield from δ 26.0 and 24.1 of **1** to δ 23.5 and 22.0 in **6**. In addition, corresponding differences were observed in the ^1H NMR spectra, in which two methyl proton signals at δ 1.37 (3H, s) and 1.24 (3H, s) in **1** were shifted downfield to δ 1.64 (3H, s) and 1.53 (3H, s) in **6**. These changes were accommodated by replacement of the hydroxy group with a hydrogen sulfate group, which naturally creates a stronger electron-withdrawing effect than the hydroxy group. This interpretation was also supported by **1** and sulfate obtained after acid hydrolysis of **6** (Scheme 6). Detection of the sulfate was done by precipitation with $BaCl_2$ and by a $BaCl_2$–$KMnO_4$ spray test (Mitchell and Waring, 1978). Thus, the structure of **6** was deduced as (2'*S*)-columbianetin-3'-hydrogen sulfate, and this compound has also not yet been reported before in the literature.

3.1.4. Structural Determination of Compounds **7-11**

Compound **7** was isolated as an amorphous white solid and its molecular formula was assigned as $C_{13}H_{10}O_5$ by EIMS and ^{13}C NMR spectrometry. The ^1H NMR spectrum of **7** exhibited signals arising from 5,8-dioxyfurocoumarin units at δ 8.11 (1H, d, *J* = 9.9 Hz), 6.28 (1H, d, *J* = 9.9 Hz), 7.62 (1H, d, *J* = 2.3 Hz) and 7.00 (1H, d, *J* = 2.3 Hz). The methoxy groups observed at δ 4.26 (3H, s) and 4.15 (3H, s) were found to be attached to C-5 and C-8, respectively, according to long-range C-H coupling in the HMBC experiment. On the basis of the above evidence, compound **7** was determined to be isopimpinellin, which was further confirmed by comparison with previously published NMR data (Hata *et al*., 1972; Elgmal *et al*., 1979).

Compound **8** was isolated as an amorphous white solid. The molecular formula $C_{14}H_{18}O_5$ of **8** was characterized from the FABMS and ^{13}C NMR spectrometric analysis. The ^1H NMR spectra of **8** indicated the presence of two methyls at δ 1.22 and 1.20 (3H each, both s), three methylenes at δ 3.03 (2H, dd, *J* = 2.3, 8.9 Hz), 2.74 (2H, t, *J* = 6.5 Hz) and 2.44 (2H, t, *J* = 6.5 Hz), an oxygenated methine at δ 4.53 (1H, t, *J* = 8.9 Hz) and two aromatic protons at δ 6.76 (1H, d, *J* = 8.1 Hz) and 6.17 (1H, d, *J* = 8.1 Hz). By extensive 2D NMR experiments, the structure of **8** was elucidated to be hyunganol Ⅱ, and this interpretation was further supported by comparison with spectroscopic data from the literature (Morikawa *et al*., 2004).

A homologous series of compounds **9-11** were characterized as follows. Compound **9** was obtained as an amorphous white powder with an elemental

composition of $C_{15}H_{16}O_5$, as determined from its ESIMS. The ^{13}C NMR spectra showed a carbonyl group (δ 184.3), the six carbons of a 1,3,5-oxygenated benzene system (δ 159.3, 157.6, 156.6, 116.6, 107.6, 99.8) and an enolic double bond (δ 169.9, 109.1). ^{1}H NMR signals corresponding to an aromatic ring and an enolic double bond were also observed at δ 7.21 (1H, s) and 6.12 (1H, s). Upon careful examination, these data were reminiscent of a benzopyran moiety. Detailed chemical structure was elucidated by 2D NMR experiments. In addition, the presence of 4-hydroxy-3-methylbut-2-enyl group was suggested by the ^{1}H and ^{13}C NMR spectra [δ_H 5.35 (1H, t, J = 7.7 Hz), 4.31 (2H, s), 3.46 (2H, d, J = 7.7 Hz), 1.74 (3H, s); δ_C 135.8, 125.4, 61.6, 22.5, 21.5] and confirmed by gDQCOSY and gHMBC. With the aid of the above results, a literature survey showed that the structure of **9** was cnidimol A. Its NMR spectral data were well matched with those reported previously (Baba et al., 1992; Baba et al., 1994).

Compound **10** was analyzed for $C_{21}H_{26}O_{10}$ by a combination of FABMS and ^{13}C NMR spectrometry. The ^{1}H NMR signals were closely related to those of **9**, except for the presence of a sugar moiety at δ 4.31-3.21 [anomeric H: δ 4.31 (1H, br.s)]. The ^{13}C NMR spectrum of **10** was also closely related to that of **9**, except for the presence of the signals assignable to a β-glucopyranosyl moiety (δ 102.3, 78.6, 77.7, 75.0, 71.6, 62.7). On the basis of the above evidence, and the comparison of data with that of the literature (Baba *et al*., 1994), compound **10** was determined to be cnidimoside A.

Compound **11** was isolated as an amorphous white powder that analyzed as $C_{15}H_{14}O_4$ by a combination of high resolution FABMS ($[M+H]^+$ *m/z* 259.0970) and ^{13}C NMR spectrometry. The ^1H and ^{13}C NMR spectra of **11** were strikingly similar with those of cnidimol A (**9**) and cnidimoside A (**10**) from *Cnidium japonicum* (Baba *et al*., 1992; Baba *et al*., 1994). However, there were significant differences in the ^1H NMR spectrum as compared with **10**. The ^1H NMR signals at δ 6.33 (1H, s) and 6.03 (1H, s) were characteristic for the compound of **11**. In addition, ^1H NMR spectrum showed the presence of a nonequivalent terminal methylene at δ 4.74 (1H, s) and 4.68 (1H, s), an adjacent benzyl methylene at δ 2.98 (1H, dd, *J* = 6.6, 13.5 Hz) and 2.85 (1H, dd, *J* = 6.6, 13.5 Hz), a methine linked to an oxygen atom at δ 4.38 (1H, t, *J* = 6.6 Hz) and two olefinic methyl groups at δ 2.34 (3H, s) and 1.81 (3H, s). A literature search showed that compound **11** reported as the artificial chromone of cnidimoside A (**10**) (Baba *et al*., 1994). The assignment of carbons and protons could be made through gDQCOSY, TOCSY, DEPT, gHMQC, gHMBC spectra and by comparison of the published data for related compounds. Thus, the structure of compound **11** was established to be 2,3-dihydro-4-hydroxy-7-methyl-2-isopropenyl-5H-furo[3,2g][1] benzopyran-5-one.

This is the first report of compounds **7-11** identified from *C. heterocarpa.*

Table 4. ^{1}H and ^{13}C NMR data for compounds **1, 4** and **6** isolated from *Corydalis heterocarpa*

Position	**4**[a]		**6**[b]		**1**[a]	
	δ_H	δ_C	δ_H	δ_C	δ_H	δ_C
1	-	-	-	-	-	-
2	-	160.8	-	163.0	-	160.9
3	6.18 (1H, d, J=9.4 Hz)	112.0	6.17 (1H, d, *J*=9.5 Hz)	112.2	6.20 (1H, d, *J*=9.5 Hz)	112.0
4	7.60 (1H, d, *J*=9.4 Hz)	143.8	7.84 (1H, d, *J*=9.5 Hz)	146.2	7.61 (1H, d, *J*=9.5 Hz)	143.8
5	7.23 (1H, d, *J*=8.3 Hz)	128.6	7.38 (1H, d, *J*=8.4 Hz)	130.2	7.26 (1H, d, *J*=8.3 Hz)	128.6
6	6.71 (1H, d, *J*=8.3 Hz)	106.5	6.75 (1H, d, *J*=8.4 Hz)	107.8	6.73 (1H, d, *J*=8.3 Hz)	106.6
7	-	163.7	-	165.4	-	163.5
8	-	112.8	-	114.3	-	113.0
9	-	151.0	-	152.3	-	151.1
10	-	113.4	-	114.8	-	113.9
1'	3.36 (1H, dd, *J*=16.5, 9.5 Hz) 3.28 (1H, dd, *J*=16.5, 7.7Hz)	27.6	3.42 (2H, m)	28.4	3.31 (2H,dd, *J*=9.0, 4.8 Hz)	27.6
2'	5.07 (1H,dd, *J*=9.5,7.7 Hz)	88.9	5.03 (1H, dd, *J*=9.6, 7.7Hz)	91.1	4.79 (1H, t, *J*=9.0 Hz)	91.3
3'	-	81.6	-	84.1	-	71.7
4'/5'	1.56 (3H, s) / 1.51 (3H, s)	22.3 /21.1	1.64 (3H ,s) / 1.53 (3H, s)	23.5 /22.0	1.37 (3H, s) / 1.24 (3H, s)	26.0 /24.1
6'	-	175.4				
7'	2.20 (1H, m)	42.1				
8'	1.50 (1H, m), 1.35 (1H, m)	26.7				
9'	0.85 (3H, t, *J*=7.2 Hz)	11.7				
10'	1.01 (3H, d, *J*=7.2 Hz)	16.7				

[a, b] Measured in $CDCl_3$ and CD_3OD at 300 and 75 MHz, respectively. Assignments were aided by ^{1}H gDQCOSY, TOCSY, DEPT, gHMQC, and gHMBC experiments.

3.1.5. Spectral Data

(2'*S*)-columbianetin (**1**): amorphous white solid; mp 160 - 163 ºC; $[\alpha]_D^{25}$ + 264 (*c* 1.1, MeOH); EIMS *m/z* 246 $[M]^+$; NMR data, see Table 4.

Libanoridin (**2**): amorphous white solid; mp 129 - 132 ºC; $[\alpha]_D^{25}$ + 252 (*c* 1.0, $CHCl_3$); EIMS *m/z* 288 $[M]^+$; ^1H NMR (300 MHz, $CDCl_3$) δ: 7.60 (1H, d, *J* = 9.6 Hz, H-4), 7.24 (1H, d, *J* = 8.3 Hz, H-5), 6.72 (1H, d, *J* = 8.3 Hz, H-6), 6.18 (1H, d, *J* = 9.6 Hz, H-3), 5.12 (1H, dd, *J* = 9.6, 7.8 Hz, H-2'), 3.35 (1H, dd, *J* = 16.5, 9.6 Hz, H-1'a), 3.26 (1H, dd, *J* = 16.5, 7.8 Hz, H-1'b), 1.97 (3H, s, H-7'), 1.55 (3H, s, H-4'/-5'), 1.50 (3H, s, H-4'/-5'); ^{13}C NMR (75 MHz, $CDCl_3$) δ: 170.0 (C, C-6'), 163.6 (C, C-7), 160.8 (C, C-2), 151.0 (C, C-9), 143.8 (CH, C-4), 128.7 (CH, C-5), 113.3 (C, C-10), 112.9 (C, C-8), 112.1 (CH, C-3), 106.6 (CH, C-6), 88.6 (CH, C-2'), 82.0 (C, C-3'), 27.6 (CH_2, C-1'), 22.3 (CH_3, C-7'), 22.0 (CH_3, C-4'/-5'), 21.0 (CH_3, C-4'/-5').

Cnidiadin (**3**): amorphous white solid; mp 138 - 142 ºC; $[\alpha]_D^{25}$ + 205 (*c* 1.0, $CHCl_3$); EIMS *m/z* 316 $[M]^+$; ^1H NMR (300 MHz, $CDCl_3$) δ: 7.60 (1H, d, *J* = 9.6 Hz, H-4), 7.24 (1H, d, *J* = 8.3 Hz, H-5), 6.71 (1H, d, *J* = 8.3 Hz, H-6), 6.18 (1H, d, *J* = 9.6 Hz, H-3), 5.08 (1H, dd, *J* = 9.5, 7.7 Hz, H-2'), 3.36 (1H, dd, *J* =16.4, 9.5 Hz, H-1'a), 3.28 (1H, dd, *J* = 16.4, 7.7 Hz, H-1'b), 2.40 (1H, m, H-7'), 1.56 (3H, s, H-5'), 1.50 (3H, s, H-4'), 1.04 (3H, d, *J* = 7.2 Hz, H-8'/-9'), 1.03 (3H, d, *J* = 7.2 Hz , H-8'/-9'); ^{13}C NMR (75MHz, $CDCl_3$) δ: 176.0 (C, C-6'), 163.8 (C, C-7), 160.9 (C, C-2),

151.0 (C, C-9), 143.9 (CH, C-4), 128.7 (CH, C-5), 113.4 (C, C-10), 112.9 (C, C-8), 112.0 (CH, C-3), 106.5 (CH, C-6), 88.9 (CH, C-2'), 81.6 (C, C-3'), 34.9 (CH, C-7'), 27.5 (CH_2, C-1'), 22.2 (CH_3, C-5'), 21.0 (CH_3, C-4'), 19.0 (CH_3, C-8'/-9'), 18.9 (CH_3, C-8'/-9').

(2'*S*,7'*S*)-*O*-(2-methylbutanoyl)-columbianetin (**4**): amorphous white solid; mp 88 - 91 ºC; $[\alpha]_D^{20}$ + 194 (*c* 0.67, $CHCl_3$); HREIMS *m/z* 330.1467 $[M]^+$ (calcd. for $C_{19}H_{22}O_5$, 330.1467); NMR data, see Table 4.

(2'*S*)-columbianetin-*O*-β-D-glucopyranoside (**5**): amorphous white solid; 116 – 119 ºC; $[\alpha]_D^{20}$ + 152 (*c* 0.32, MeOH); FABMS *m/z* 409 $[M+H]^+$; ^{1}H NMR (300 MHz, CD_3OD) δ: 7.85 (1H, d, *J* = 9.5 Hz, H-4), 7.38 (1H, d, *J* = 8.4 Hz, H-5), 6.75 (1H, d, *J* = 8.4 Hz, H-6), 6.18 (1H, d, *J* = 9.5 Hz, H-3), 4.92 (1H, t, *J* = 9.9 Hz, H-2'), 4.57 (1H, br.s, H-1''), 3.48 (2H, m, H-6''), 3.36 (1H, m, H-5''), 3.34 (2H, m, H-1'), 3.33 (1H, m, H-4''), 3.14 (1H, m, H-3''), 3.11 (1H, m, H-2''), 1.37 (3H, s, H-4'/-5'), 1.36 (3H, s, H-4'/-5'); ^{13}C NMR (75MHz, CD_3OD) δ: 165.4 (C, C-7), 163.1 (C, C-2), 152.4 (C, C-9), 146.2 (CH, C-4), 130.1 (CH, C-5), 115.4 (C, C-10), 114.4 (C, C-8), 112.2 (CH, C-3), 107.8 (CH, C-6), 98.8 (CH, C-1''), 91.8 (CH, C-2'), 79.1 (C, C-3'), 78.1 (CH, C-5''), 77.5 (CH, C-3''), 75.1 (CH, C-2''), 71.4 (CH, C-4''), 62.3 (CH_2, C-6''), 28.3 (CH_2, C-1'), 23.8 (CH_3, C-4'/-5'), 22.4 (CH_3, C-4'/-5').

(2'*S*)-columbianetin-3'-hydrogen sulfate (**6**): amorphous white solid; mp 160 - 163 ºC; $[\alpha]_D^{20}$ + 156 (*c* 0.17, MeOH); HRESIMS (negative-ion mode) *m/z* 325.0388 $[M-H]^-$ (calcd. for $C_{14}H_{13}O_7S$, 325.0382); NMR data, see Table 4.

Isopimpinellin (**7**): Amorphous white solid; $[\alpha]_D^{25}$: + 9.52 (*c* 0.21, MeOH); EIMS *m/z* 246 $[M]^+$; ^{1}H NMR (300 MHz, $CDCl_3$) δ: 8.11 (1H, d, *J* = 9.9 Hz, H-4), 7.62 (1H, d, *J* = 2.3 Hz, H-2'), 7.00 (1H, d, *J* = 2.3 Hz, H-1'), 6.28 (1H, d, *J* = 9.9 Hz, H-3), 4.26 (3H, s, H-5-OCH_3), 4.15 (3H, s, H-8-OCH_3); ^{13}C NMR (75MHz, $CDCl_3$) δ: 160.4 (C, C-2), 149.8 (C, C-7), 145.0 (CH, C-2'), 144.1 (C, C-5), 143.5 (C, C-9), 139.3 (CH, C-4), 128.0 (C, C-8), 114.7 (C, C-6), 112.7 (CH, C-3), 107.5 (C, C-10), 105.0 (CH, C-1'), 61.7 (C-8-OCH_3), 60.8 (C-5-OCH_3).

Hyunganol Ⅱ (**8**): Amorphous white solid; $[\alpha]_D^{20}$ + 22.33 (*c* 0.36, MeOH); FABMS *m/z* 267 $[M+H]^+$; ^{1}H NMR (300 MHz, CD_3OD) δ: 6.76 (1H, d, *J* = 8.1 Hz, H-9), 6.17 (1H, d, *J* = 8.1 Hz, H-8), 4.53(1H, t, *J* = 8.9 Hz, H-2'), 3.03 (2H, dd, *J* = 2.3, 8.9 Hz, H-1'), 2.74 (2H, t, *J* = 6.5 Hz, H-4), 2.44 (2H, t, *J* = 6.5 Hz, H-3), 1.22 (3H, s, H-5'), 1.20 (3H, s, H-4'); ^{13}C NMR (75 MHz, CD_3OD) δ: 182.5 (C, C-2), 160.8 (C, C-7), 152.8 (C, C-5), 130.5 (CH, C-9), 123.1 (C, C-10), 114.9 (C, C-6), 101.7 (CH, C-8), 90.7 (CH, C-2'), 72.6 (C, C-3'), 40.4 (CH_2, C-3), 29.5 (CH_2, C-1'), 27.5 (CH_2, C-4), 25.3 (CH_3, C-4'), 25.1 (CH_3, C-5').

Cnidimol A (**9**): Amorphous white solid; $[\alpha]_D^{20}$ – 18.00 (*c* 0.50, MeOH); ESIMS *m/z* 277 $[M+H]^+$; ^{1}H NMR (300 MHz, CD_3OD) δ: 7.21 (1H, s, H-8), 6.12 (1H, s, H-3), 5.35 (1H, t, *J* = 7.7 Hz, H-2'), 4.31 (2H, s, H-5'), 3.46 (2H, d, *J* = 7.7 Hz, H-1'), 2.31 (3H, s, 2-Me), 1.74 (3H, s, H-4'); ^{13}C NMR (75 MHz, CD_3OD) δ: 184.3 (C, C-4), 169.9 (C, C-2), 159.3 (C, C-7), 157.6 (C, C-5), 156.6 (C, C-9), 135.8 (C, C-3'), 125.4 (CH, C-2'), 116.6 (C, C-6), 109.1 (CH, C-3), 107.6 (C, C-10), 99.8 (CH, C-8), 61.6 (CH_2, C-5'), 22.5 (CH_2, C-1'), 21.5 (CH_3, C-4'), 20.4 (CH_3, 2-Me).

Cnidimoside A (**10**): Amorphous white solid; $[\alpha]_D^{20}$ – 3.16 (*c* 0.32, MeOH); FABMS *m/z* 439 $[M+H]^+$; ^{1}H NMR (300 MHz, CD_3OD) δ: 6.29 (1H, s, H-8), 5.98 (1H, s, H-3), 5.46 (1H, t, *J* = 7.0 Hz, H-2'), 4.65 (1H, d, *J* = 12.1 Hz, H-5'a), 4.32 (1H, d, *J* = 12.1 Hz, H-5'b), 4.31 (1H, br.s, H-1''), 3.89 (1H, dd, *J* = 1.9, 11.6 Hz, H-6''a), 3.72 (1H, dd, *J* = 4.5, 11.6 Hz, H-6''b), 3.37 (1H, m, H-4''), 3.35 (2H, d, *J* = 7.0 Hz, H-1'), 3.34 (1H, m, H-5''), 3.32 (1H, m, H-3''), 3.21 (1H, m, H-2''), 2.31 (3H, s, 2-Me), 1.76 (3H, s, H-4'); ^{13}C NMR (75 MHz, CD_3OD) δ: 183.6 (C, C-4), 168.6 (C, C-2), 164.0 (C, C-7), 159.6 (C, C-5), 157.6 (C, C-9), 132.3 (C, C-3'), 128.7 (CH, C-2'), 112.1 (C, C-6), 108.6 (CH, C-3), 104.5 (C, C-10), 102.3 (CH, C-1''), 94.3 (CH, C-8), 78.6 (CH, C-5''), 77.7 (CH, C-3''), 75.0 (CH, C-2''), 71.6 (CH, C-4''), 68.1 (CH_2, C-5'), 62.7 (CH_2, C-6''), 22.0 (CH_2, C-1'), 21.8 (CH_3, C-4'), 20.3 (CH_3, 2-Me).

2,3-dihydro-4-hydroxy-7-methyl-2-isopropenyl-5H-furo[3,2g][1] benzopyran-5-one (**11**): Amorphous white solid; mp 155 - 158 ºC; $[\alpha]_D^{20}$ + 20 (*c* 0.25, MeOH); HRFABMS *m/z* 259.0970 $[M+H]^+$ (calcd. for $C_{15}H_{14}O_4$, 259.0970); ^{1}H NMR (300 MHz, CD_3OD) δ: 6.33 (1H, s, H-8), 6.03 (1H, s, H-3), 4.74 (1H, s, H-4'a), 4.68 (1H, s, H-4'b), 4.38 (1H, t, *J* = 6.6 Hz, H-2'), 2.98 (1H, dd, *J* = 6.6, 13.48 Hz, H-1'a), 2.85 (1H, dd, *J* = 6.6, 13.48 Hz, H-1'b), 2.34 (3H, s, 2-Me), 1.81 (3H, s, H-5'); ^{13}C NMR (75 MHz, CD_3OD) δ: 183.8 (C, C-4), 164.2 (C, C-7), 168.8 (C, C-2), 160.5 (C, C-5), 157.9 (C, C-9), 148.5 (C, C-3'), 110.2 (C, C-6), 111.0 (CH_2, C-4'), 108.7 (CH, C-3), 104.7 (C, C-10), 94.4 (CH, C-8), 76.2 (CH, C-2'), 29.7 (CH_2, C-1'), 20.3 (CH_3, 2-Me), 17.8 (CH_3, C-5').

3.2. Secondary Metabolites Isolated from *Vitex rotundifolia*

The solvent extract of *V. rotundifolia* was partitioned with CH_2Cl_2 and H_2O. Each layer was further partitioned with *n*-hexane/85% aq. MeOH and *n*-BuOH/H_2O, respectively. The *n*-BuOH, 85% aq. MeOH and *n*-hexane fractions were purified by various types of column chromatography, TLC, and HPLC, using different solvent combinations, to yield nineteen compounds including five new compounds (**20** and **23**-**26**) (Fig. 6 and 7).

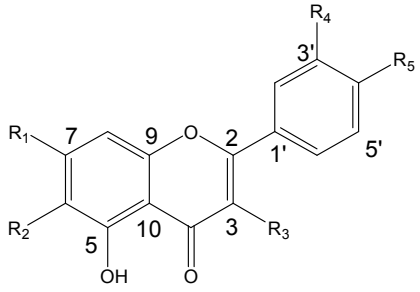

12. R_1, R_4, R_5 = OH, R_2, R_3 = H

13. R_1, R_3 =OMe, R_2 = H, R_4, R_5 = OH

14. R_1 - R_3, R_5 = OMe, R_4 = OH

15. R_1 - R_5 = OMe

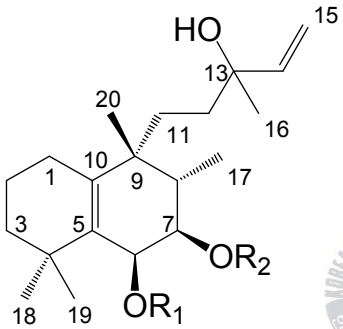

16. R_1 = H, R_2 = $COCH_3$

17. R_1 = $COCH_3$, R_2 = H

18. R_1, R_2 = $COCH_3$

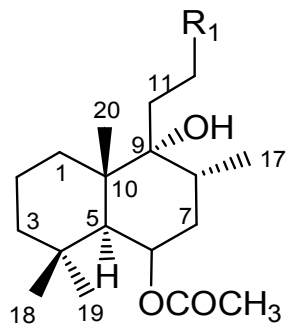

19. R_1 =

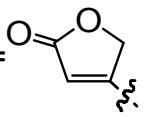

20. R_1 =

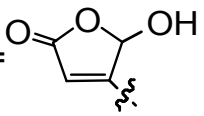

21. R_1 =

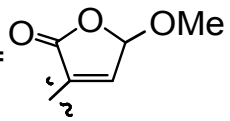

Figure 6. Chemical structure of compounds **12**-**21** isolated from *Vitex rotundifolia*.

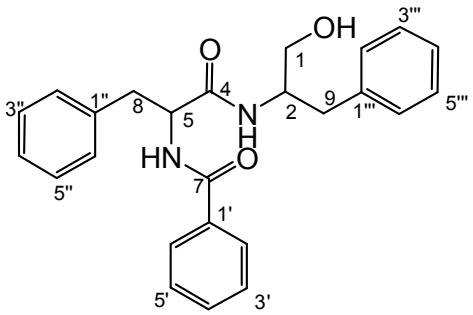

22

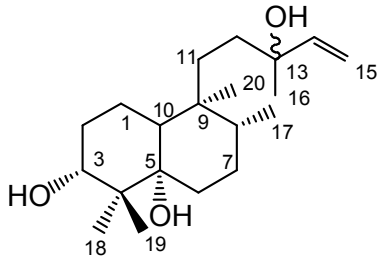

23

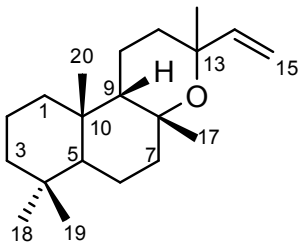

24

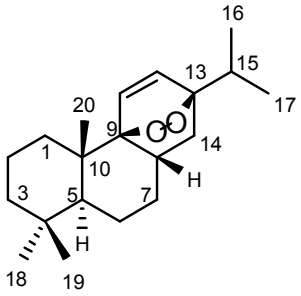

25

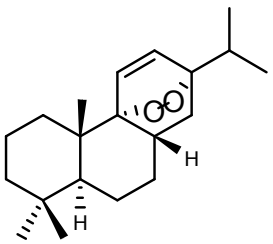

26

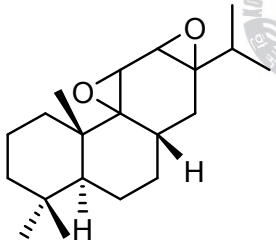

27

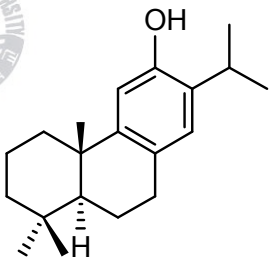

28

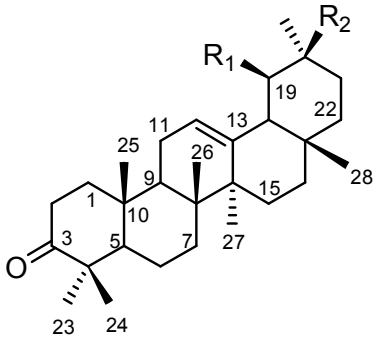

29. R_1 = H, R_2 = CH_3

30. R_1 = CH_3, R_2 = H

Figure 7. Chemical structure of compounds **22-30** isolated from *Vitex rotundifolia*.

3.2.1. Structural Determination of Compounds **12-15**

Compound **12** was isolated as a yellow solid. The molecular formula of **12** was established as $C_{15}H_{10}O_6$ on the basis of EIMS and ^{13}C NMR spectrometry. The IR spectrum of **12** showed a broad hydroxyl and α,β-unsaturated carbonyl absorption at 3,368 cm^{-1} and 1,655 cm^{-1}, respectively. The ^{1}H and ^{13}C NMR spectra revealed signals typical of a flavonoid. The ^{1}H NMR signals due to the flavonoid skeleton [δ 7.35 (1H, d, J = 8.3 Hz), 7.34 (1H, br s), 6.88 (1H, d, J = 8.3 Hz), 6.51 (1H, s), 6.41 (1H, br s), 6.18 (1H, br s)] showed the characteristic pattern of luteolin. Therefore, compound **12** was determined as luteolin and was further confirmed by assignment of NMR data previously reported (Yoshioka *et al*., 2004; Loizzo *et al*., 2007).

Compounds **13-15** were isolated as pale yellow solids and the ^{1}H and ^{13}C NMR signals of **13-15** were quite similar to those of **12**, except for the methoxy groups. Thus, compounds **13-15** were identified as quercetin 3,7-dimethyl ether (**13**) (Sadhu *et al*., 2006), vitexicarpin (**14**) (Yoshioka *et al*., 2004), and artemetin (**15**) (Iinuma *et al*., 1980; Rahman *et al*., 1988; Ahmad *et al*., 1995; Yoshioka *et al*., 2004), by the analysis of NMR data and by comparison with published data. Among these, this is the first report of compound **13** from *V. rotundifolia.*

3.2.2. Structural Determination of Compounds **16-18**

Compound **16** was obtained as a colorless syrup. In the EIMS, **16** did not show a molecular ion peak but showed a fragment ion peak at *m/z* 304 $[M\text{-}CH_3COOH]^+$. The molecular formula of **16** was determined to be $C_{22}H_{36}O_4$ by EIMS and ^{13}C NMR spectrometry. The ^1H NMR spectrum of **16** indicated signals due to four tertiary methyl groups [δ 1.21 (3H, s), 1.15 (3H, s), 1.05 (3H, s), 1.05 (3H, s)], one secondary methyl group [δ 0.94 (3H, d, *J* = 7.0 Hz)], one acetyl groups [δ 2.09 (3H, s)], one vinylic group [δ 5.84 (1H, dd, *J* = 17.4, 10.7 Hz), 5.15 (1H, dd, *J* = 17.4, 1.5 Hz), 5.01 (1H, dd, *J* = 10.7, 1.5 Hz)], and two oxygenated methylene protons [δ 4.80 (2H, dd, *J* = 12.5, 3.1 Hz), 4.18 (2H, d, *J* = 3.1 Hz)]. The ^{13}C NMR spectrum of **16** gave 22 carbon signals, including one carbonyl group (δ 172.8), one tetra-substituted olefinic bond (δ 139.6, 137.1), one vinylic group (δ 145.9, 112.3), one oxygenated quaternary carbon (δ 73.8), and two oxygenated methine carbons (δ 76.9, 65.2), suggesting **16** to be a diterpene with a 3-hydroxy-3-methyl-1-propenyl group and one acetyl group. These ^1H and ^{13}C NMR spectroscopic signals were assigned with the aid of 2D NMR techniques, and the structure of **16** was determined as vitetrifolin F, and was further supported by comparison of the obtained spectroscopic data with those reported in the literature (Ono *et al*., 2001).

Compounds **17** and **18** were obtained as colorless needles and a colorless syrup, respectively. The ^1H NMR spectra of **17** were similar to those of **16**, except that the signal due to an acetyl group moved and signals assignable to H-6 and H-7 in **17** were shifted down- and up-field by 1.38 ppm and 1.18 ppm, respectively, in

comparison with those of **16**. The ^{1}H NMR spectra of **18** was also similar to that of **16**, except that the signal due to another new acetyl group appeared and signals assignable to H-6 in **18** was shifted downfield by 1.49 ppm, in comparison with those of **16**. Therefore, **17** and **18** were recognized as vitetrifolin E (**17**) and vitetrifolin D (**18**), respectively, by comparison with structures reported in the literature (Ono *et al*., 2001).

3.2.3. Structural Determination of Compounds **19** and **21**

Compound **19** was isolated as a pale yellow solid. The molecular formula of **19** was determined to be $C_{22}H_{34}O_5$ by EIMS and ^{13}C NMR spectrometry. The IR spectrum of **19** exhibited the presence of hydroxy (3509 cm^{-1}), acetoxyl (1734 cm^{-1}), and α,β-unsaturated γ-lactone (1779 cm^{-1}) groups. The ^1H NMR spectrum of **19** contained signals for four tertiary methyls [δ 2.04, 1.23, 0.99, 0.95 (3H each, all s)], a methine [δ 5.35 (1H, q, J = 2.5 Hz)] on a carbon bearing an acetoxyl group [δ 2.04 (3H, s)], a methylene proton [δ 4.73 (2H, d, J = 1.7 Hz)] and an olefinic proton [δ 5.82 (1H, s)] of the α,β-unsaturated γ-lactone system (Table 5). On the basis of these results, it was concluded that **19** is vitexilactone, and this conclusion was further supported by comparison of the spectroscopic data with literature values (Kondo *et al*., 1986; Hoberg *et al*., 1999; Ono *et al*., 2001).

Compound **21** was obtained as an amorphous white solid, and its ESIMS afforded a $[M-H]^-$ peak at *m/z* 407, suggesting the molecular formula, $C_{23}H_{36}O_6$. The ^1H and ^{13}C NMR spectra of **21** were almost superimposable on those of **19**, apart from the chemical shifts of signals due to the olefinic group [δ_H 6.75 (1H, d, J = 1.2 Hz, H-14); δ_C 141.4 (C-14), 139.1 (C-13) in **21**; δ_H 5.82 (1H, s, H-14), δ_C 170.9 (C-13), 114.8 (C-14) in **19**], which exhibited the replacement of a β-substituted butenolide ring in **19** by an α-substituted butenolide ring. The signal due to a methoxyl group appeared at δ 3.57 (3H, s). Accordingly, by comparison to literature data, **21** was defined as (5*S**,6*R**,8*R**,9*R**,10*S**)-6-acetoxy-9-hydroxy-15-methoxy-13(14)-labden-16,15-olide (Ono *et al*., 2001).

3.2.4. Structural Determination of Compound **20**

Compound **20** was obtained as a pale yellow solid. The molecular formula of **20** was determined to be $C_{22}H_{34}O_6$ by a combination of high resolution ESIMS ([M-H]$^-$ *m/z* 393.2286) and ^{13}C NMR spectrometry. The ^{1}H NMR spectrum of **20** was similar to that of **19**, with the exception that a signal due to a hydroxyl group appeared at δ 5.98 (1H, s), while the signal at δ 4.73 (2H, d, J = 1.7 Hz) assignable to an H-16 disappeared. This suggestion was supported by the ^{13}C NMR spectral data. Comparing the ^{13}C NMR spectra of **20** with those of **19**, the signals of C-14 and C-16 in **19** were shifted downfield from δ 114.8 and 73.2 of **19** to δ 117.3 and 98.9 in **20**, respectively, whereas those of C-13 and C-15 were shifted upfield from δ 170.9 and 170.9 of **19** to δ 170.3 and 170.5 in **20**, respectively, and the other carbon signals were quite similar to those of **19** (Table 5).

The relative stereochemistry in **20** was examined from its NOESY spectral data. The NOE correlation between H-20/H-19, H-20/H-11a, and H-20/H-8 were observed in **20**. In addition, NOE correlations between H-18/H-19, H-18/H-6, and H-18/H-5 (Fig. 8) were observed. On the basis of these data, the configurations at C-5, C-6, C-8, C-9 and C-10 were determined to be S^*, R^*, R^*, R^* and S^*, respectively. Thus, **20** was determined as (5S^*,6R^*,8R^*,9R^*,10S^*)-6-acetoxy-9-hydroxy-16-hydroxy-13(14)-labden-16,15-olide. This compound has not been reported previously in the literature.

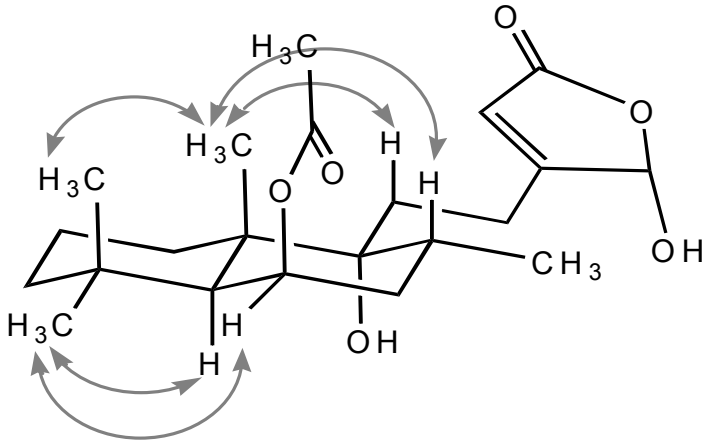

Figure 8. NOESY correlation of compound **20** isolated from *Vitex rotundifolia*.

3.2.5. Structural Determination of Compound **22**

Compound **22**, $C_{25}H_{26}N_2O_3$ (FABMS *m/z* 403 $[M+H]^+$), a neutral compound, did not exhibit any characteristic UV absorption. The ^1H NMR spectrum of **22** confirmed the presence of 15 aromatic protons incorporated in a benzoyl [δ 7.70 (2H, d, *J* = 11.3 Hz), 7.50 (1H, t, *J* = 11.3 Hz), 7.42 (2H, t, *J* = 11.3 Hz)] and two benzyl groups [δ 7.31 (2H, t, *J* = 11.3 Hz), 7.26 (2H, d, *J* = 11.3 Hz), 7.25 (1H, t, *J* = 11.3 Hz), 7.16 (2H, t, *J* = 11.3 Hz), 7.12 (1H, t, *J* = 11.3 Hz), 7.06 (2H, d, *J* = 11.3 Hz)]. The ^{13}C NMR spectrum of **22** showed the presence of two carbonyls (δ 170.6, 167.0) in addition to three methylenes (δ 63.6, 38.8, 36.9) and two aliphatic methines (δ 55.3, 52.9). It was apparent from their chemical shifts that the three lowfield aliphatic carbons were situated next to hetero-atoms. All of the signals in the ^1H and ^{13}C NMR spectrum could be unequivocally assigned only after the structure of aurantiamide had been established from its literature values (Banerji and Ray, 1981; Wahidulla *et al*., 1991; Ferreira *et al*., 1995; Lu *et al*., 1999; Isshiki *et al*., 2001). This is the first report of compound **22** identified from this halophyte.

3.2.6. Structural Determination of Compound **23**

Compound **23** was obtained as a pale yellow solid, and its high-resolution FABMS afforded a $[M+Na]^+$ peak at *m/z* 247.2993, suggesting the molecular formula, $C_{20}H_{36}O_3$. The ^1H NMR spectrum of **23** contained signals for four tertiary methyls [δ 1.25, 1.18, 1.16, 0.91 (3H each, all s)], one secondary methyl [δ 0.80 (d, *J* = 6.9 Hz)] and one vinylic group [δ 5.87 (dd, *J* = 17.4, 10.8 Hz), 5.16 (dd, *J* = 17.4, 1.5 Hz), 5.00 (dd, *J* = 10.8, 1.5 Hz)]. The ^{13}C NMR spectrum indicated the presence of 20 carbons including two quaternary carbons (δ 78.0, 74.4) and one secondary carbon (δ 76.9) bearing hydroxy group (Table 6). The above spectral data, coupled with the molecular formula, indicated that **23** was a bicyclic diterpenoid having two tertiary hydroxy groups, one secondary hydroxy group and one vinyl group. From the above observations, compound **23** was similar to characteristics of the known compound, pleuroziol, isolated from the liverwort *Pleurozia gigantean* (Asakawa *et al.*, 1990). The only difference was that H-3 in pleuroziol was replaced by a hydroxy group in **23**, resulting in the presence of a downfield carbon signal C-3 (δ 76.9) in **23**. Corresponding change in the ^1H NMR spectra was found at δ 3.46 (1H, t, *J* = 2.5 Hz) in **23**. Thus, the above data indicated that **23** is a 3-hydroxy derivative of pleuroziol.

In order to clarify the stereochemistry, the difference NOE was measured. The NOE correlations between H-6/H-8, H-10/H-19, H-10/H-2a, H-3/H-2, H-3/H-18, H-20/H-1a, H-20/H-17 and H-16/H-17 were observed in NOESY spectra of **23** (Fig. 9). The 3-hydroxy group was confirmed to be α orientation by the small

coupling constant (J = 2.5 Hz) of the H-3 this is due to H-2/H-3 coupling constant. Therefore, the structure of **23** was represented as 3α-hydroxy pleuroziol. This compound has never been reported in the literature prior to the present study.

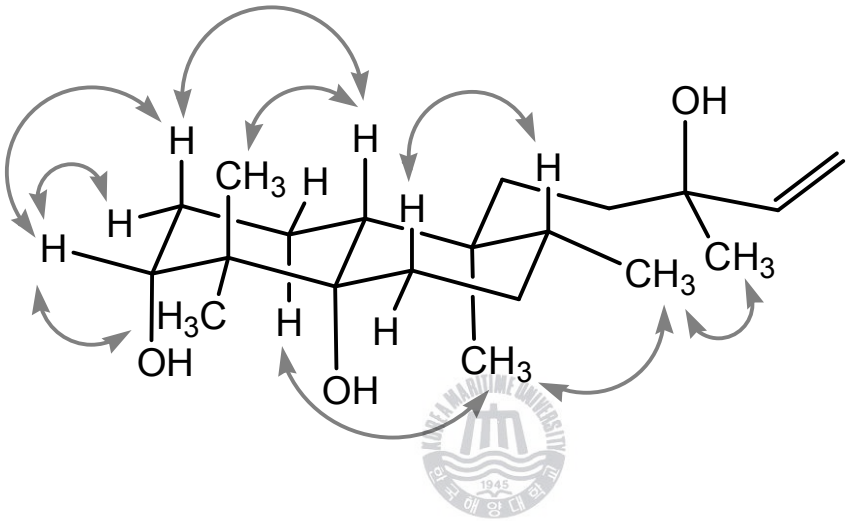

Figure 9. NOESY correlation of compound **23** isolated from *Vitex rotundifolia*.

3.2.7. Structural Determination of Compound **24**

Compound **24** was obtained as a colorless solid. The ^{13}C NMR and EIMS ($[M]^+$ *m/z* 290) data indicated that the molecular formula for **24** was $C_{20}H_{34}O$, with an unsaturation index of four. The ^1H NMR data of **24** showed the signals of five tertiary methyls [δ 1.34, 1.10, 1.07, 0.81, 0.75 (3H each, all s)], one vinylic group [δ 5.91 (1H, ddd, *J* = 17.9, 11.0, 1.8 Hz), 4.94 (1H, dd, *J* = 11.0, 1.0 Hz), 4.93 (1H, dd, *J* = 17.9, 1.0 Hz)]. The ^{13}C NMR and DEPT spectra showed the presence of five methyl carbons, night methylene carbons, two methine carbons and four quaternary carbons. The ^{13}C NMR spectra also indicated the presence of one vinylic group (δ 147.0, 109.8) and two carbons linked to oxygen (δ 77.5, 72.4). On the basis of the absence of triple bond signals in its spectra, an oxo-tricyclic structure was proposed for this compound. ^1H NMR and ^{13}C NMR assignments (Table 6) together with the results of the gDQCOSY, TOCSY, gHMQC, gHMBC and NOESY experiments led for **24** to a manoyl oxide (Bower and Rowe, 1967; Cheng and Rudloff[a,b], 1970; Anthonsen and Bergland 1973; Tabacchi *et al*., 1975; Almqvist *et al*., 1975; Zhou *et al*., 1995). The problematic aspect of the structure elucidation was the assignment at the five asymmetric centers, C-5, C-8, C-9, C-10 and C-13. The *cis*-stereochemistry at the junction of the rings B and C could be deduced from the chemical shift of C-17 (δ 32.5) when compared to that of manoyl oxide (δ 25.5). The NOESY experiment confirmed the proposed *cis*-configuration of the moiety, with correlation between H-14/H-7b, H-14/H-11b, H-14/H-12a, and H-15/H-16. In addition, correlations between H-20/H-19, H-20/H-17, and H-20/H-

6b were observed in NOESY spectra of **24** (Fig. 10). Thus, the structure of **24** was determined as 9α*H*-manoyl oxide, which is a stereoisomer of manoyl oxide at the C-9 position. This compound has not yet been reported in the literature.

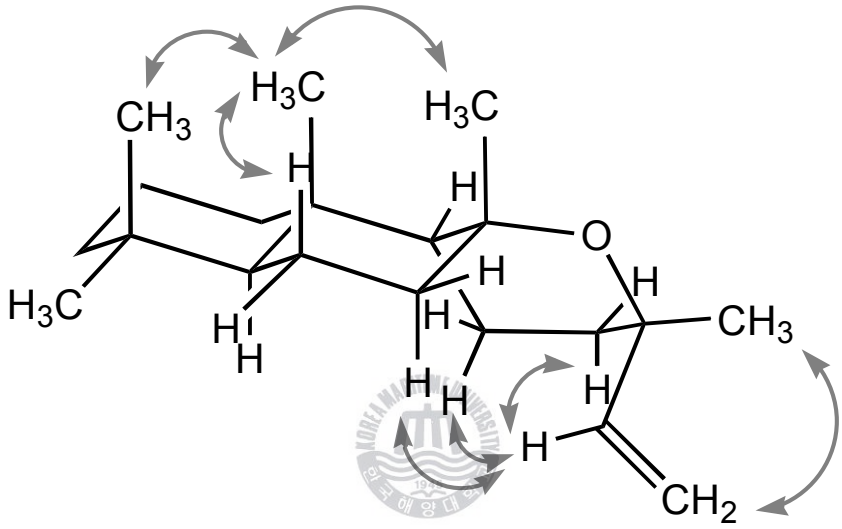

Figure 10. NOESY correlation of compound **24** isolated from *Vitex rotundifolia*.

3.2.8. Structural Determination of Compounds **25** and **26**

Compound **25** was isolated as a colorless solid. The molecular formula of **25** was established as $C_{20}H_{32}O_2$ on the basis of high-resolution ESIMS ($[M+Na]^+$ *m/z* 327.2299) data. The ^1H NMR and ^{13}C NMR data of **25** showed the presence of an isopropyl [δ_C 32.1, 17.4, 17.1; δ_H 1.86 (1H, m), 0.96 (3H, d, J = 6.9 Hz), 0.94 (3H, d, J = 6.9 Hz)], three tertiary methyls [δ_C 33.2, 22.2, 17.0; δ_H 1.05, 0.86, 0.82, (3H each, all s)], and a peroxy bridge between two fully substituted sp^3 carbon atoms (δ 81.3, 79.3). Two deshielded carbon resonances at δ 133.8 and 133.4 correlated with two deshielded proton resonances at δ 6.57 (1H, d, J = 8.8 Hz) and 6.45 (1H, d, J = 8.8 Hz), respectively, and were assigned to a *cis*-disubstituted double bond (Table 7). The lack of carbonyl resonances in the ^{13}C NMR spectrum indicated that four rings were required to account for the remaining degrees of unsaturation on the molecule. All of these data were very similar to those of methyl 2α-abieta-11(12)-ene-9α,13α-endoperoxyl malonate isolated from a *C. purpurea* except for the presence of an additional malonate moiety (Chamy *et al.*, 1993), and could be accommodated in the abietane carbon skelecton as depicted in **25**. The structure of **25** was thus established as abieta-11(12)-ene-9α,13α-endoperoxide.

Compound **26** was also isolated as a colorless solid and possessed the molecular formula $C_{20}H_{32}O_2$, as determined from its high-resolution ESIMS ($[M+Na]^+$ *m/z* 327.2292). Its ^1H NMR and ^{13}C NMR data were very similar to those of **25** (Table 7). The observed differences between the NMR spectroscopic data of **25** and **26** were consistent with a change in the orientation of the peroxide bridge. The largest

difference was shown at C-5, where a deshielding effect of $\Delta\delta_C$ + 3.5 was due to a γ-gauche effect. The shielding effect of $\Delta\delta_C$ – 2.2 on C-20 was due to the disappearance of the γ-gauche effect (Chamy *et al.*, 1993). Therefore, the structure of **26** was determined as abieta-11(12)-ene-9β,13β-endoperoxide.

These compounds **25** and **26** have not been reported in the literature before.

KOREA MARITIME UNIVERSITY 1945 한국해양대학교

3.2.9. Structural Determination of Compounds **27-30**

Compound **27** showed a $[M+Na]^+$ molecular peak at *m/z* 327.2297 (calcd. for $C_{20}H_{32}O_2Na$, 327.2300) in the HRESIMS. The ^1H NMR spectra indicated signals due to three tertiary methyl protons [δ 1.06, 0.86, 0.81 (3H each, all s)], two secondary methyl protons [δ 0.95 (3H, d, *J* = 6.8 Hz), 0.89 (3H, d, *J* = 6.8 Hz)] and two oxygenated methine protons [δ 3.32 (1H, d, *J* = 3.0 Hz), 2.99 (1H, d, *J* = 3.0 Hz)]. The ^{13}C NMR spectra showed 20 carbon signals, including two oxygenated methine carbons (δ 54.7, 49.4) and two oxygenated quaternary carbons (δ 68.0, 58.9). These ^1H and ^{13}C NMR spectroscopic signals were assigned with the aid of gDQCOSY, NOESY, gHMQC and gHMBC experiments. On the basis of above results, the structure of **27**, possessing two epoxy rings, was determined to be abieta-9(11):12(13)-di-α-epoxide, previously isolated from the *V. rotundifolia* (Sakurai *et al*., 1999).

Compound **28** was isolated as colorless needles. The molecular formula of **28** was determined to be $C_{20}H_{30}O$ by FABMS and ^{13}C NMR spectrometry. The ^1H NMR spectra contained signals for three tertiary methyls [δ 1.17, 0.93, 0.91 (3H each, all s)], two secondary methyls [δ 1.24 (3H, d, *J* = 6.9 Hz), 1.22 (3H, d, *J* = 6.9 Hz)], two methines [δ 3.10 (1H, sept, *J* = 6.9 Hz), 1.31 (1H, dd, *J* = 12.4, 2.3 Hz)], and two olefinic methines [δ 6.81 (1H, s), 6.61 (1H, s)]. The ^{13}C NMR spectra showed 20 carbon signals, including one phenyl group. These ^1H and ^{13}C NMR spectroscopic signals were assigned with the aid of 2D NMR experiments, and the

structure of **28** was determined as ferruginol, and was further supported by literature survey (Ulubelen, 1990; Chang *et al*., 2001).

Compounds **29** and **30** were isolated as colorless solids and possessed the same molecular formula, $C_{30}H_{48}O$. Compounds **29** and **30** were identified as β-amyrenone (**29**) and α-amyrenone (**30**), respectively, by a combination of 1D/2D NMR experiments and comparison with the literature data (Seo *et al*., 1975; Seo *et al*., 1981; Yan *et al*., 1989; Shiojima *et al*., 1995; Humberto *et al*., 2004). These compounds **29** and **30** are the first report of these substances from halophytes such as *V. rotundifolia*.

KOREA MARITIME UNIVERSITY 1945 한국해양대학교

Table 5. ^{1}H and ^{13}C NMR data for compounds **19** and **20** isolated from *Vitex rotundifolia*

Position	**20**		**19**	
	δ_H	δ_C	δ_H	δ_C
1	1.45 (2H, m)	33.7	1.43 (2H, m)	33.7
2	1.48 (2H, m)	18.6	1.47 (2H, m)	18.7
3	1.35 (2H, m)	43.6	1.25 (2H, m)	43.6
4	-	34.1	-	34.1
5	1.51 (1H, m)	47.8	1.55 (1H, d, *J*=2.5 Hz)	47.7
6	5.37 (1H, q, *J*=2.5, 2.5 Hz)	69.7	5.35 (1H, q, *J*=2.5 Hz)	69.8
7	1.58 (2H, m)	36.1	1.61 (2H, m)	36.1
8	2.13 (1H, m)	32.2	2.11 (1H, m)	32.1
9	-	77.6	-	76.4
10	-	43.7	-	43.8
11	2.13 (1H, m) 1.79 (1H, m)	31.5	1.95 (1H, ddd, *J*=14.3, 9.4, 7.2 Hz) 1.72 (1H, ddd, *J*=14.3, 9.4, 7.2 Hz)	31.7
12	2.53 (2H, m)	24.3	2.48 (2H, dd, *J*=9.4, 7.2 Hz)	25.5
13	-	170.3	-	170.9
14	5.86 (1H, s)	117.3	5.82 (1H, s)	114.8
15	-	170.5	-	170.9
16	5.98 (1H, s)	98.9	4.73 (2H, d, *J*=1.7 Hz)	73.2
17	0.91 (3H, d, *J*=6.6 Hz)	16.2	0.88 (3H, d, *J*=6.6 Hz)	16.2
18	0.96 (3H, s)	33.7	0.95 (3H, s)	33.7
19	1.01 (3H, s)	23.7	0.99 (3H, s)	23.8
20	1.26 (3H, s)	19.0	1.23 (3H, s)	19.1
6-$CO\underline{C}H_3$	2.05(3H, s)	22.0	2.04(3H, s)	22.0
6-$\underline{C}OCH_3$	-	169.6	-	170.3

Measured in $CDCl_3$ at 300 and 75 MHz, respectively. Assignments were aided by ^{1}H gDQCOSY, TOCSY, DEPT, gHMQC, and gHMBC experiments.

Table 6. ^{1}H and ^{13}C NMR data for compounds **23** and **24** isolated from *Vitex rotundifolia*

Position	**23**[a]		**24**[b]	
	δ_H	δ_C	δ_H	δ_C
1	1.79 (1H, m) , 1.25 (1H, m)	19.4	1.50 (1H, m), 1.01 (1H, m)	37.1
2	1.98 (1H, tt, *J*=13.7, 3.4 Hz) 1.57 (1H, m)	29.8	1.65 (1H, m), 1.39 (1H, m)	19.0
3	3.46 (1H, t, *J*=2.5 Hz)	76.9	1.32 (1H, m), 1.07 (1H, m)	42.5
4	-	43.7	-	33.4
5	-	78.0	1.00 (2H, m)	47.4
6	2.28 (2H, m)	30.4	1.51 (1H, m), 1.21 (1H, m)	21.4
7	1.45 (2H, m)	29.3	2.06 (1H, m), 1.30 (1H, m)	35.6
8	1.64 (1H, m)	38.4	-	77.5
9	-	39.8	1.09 (1H, m)	55.5
10	1.69 (1H, m)	43.5	-	38.2
11	1.76 (1H, m), 1.20 (1H, m)	31.0	1.69 (1H, m), 1.53 (1H, m)	18.7
12	1.72 (1H,m), 1.43 (1H,m)	37.9	2.03 (1H, ddd, *J*=13.5, 7.2, 6.3 Hz) 1.31 (1H, m)	33.5
13	-	74.4	-	72.4
14	5.87 (1H, dd, *J*=17.4, 10.8 Hz)	146.0	5.91 (1H, ddd, *J*=17.9, 11.0, 1.8 Hz)	147.0
15	5.16 (1H, dd, *J*=17.4, 1.5 Hz) 5.00 (1H, dd, *J*=10.8, 1.5 Hz)	111.8	4.94 (1H, dd, *J*=11.0, 1.0 Hz) 4.93 (1H, dd, *J*=17.9, 1.0 Hz)	109.8
16	1.25 (3H, s)	28.2	1.10 (3H, s)	32.9
17	0.80 (3H, d, *J*=6.9 Hz)	16.5	1.34 (3H, s)	32.5
18	1.18 (3H, s)	22.0	0.81 (3H, s)	33.3
19	1.16 (3H, s)	21.9	0.75 (3H, s)	21.8
20	0.91 (3H, s)	30.0	1.07 (3H, s)	25.0

[a]Measured in CD_3OD at 800 and 75 MHz. [b]Measured in $CDCl_3$ at 900 and 600 MHz. Assignments were aided by ^{1}H gDQCOSY, TOCSY, DEPT, gHMQC, and gHMBC experiments.

Table 7. ^{1}H and ^{13}C NMR data for compounds **25** and **26** isolated from *Vitex rotundifolia*

Position	**25**		**26**	
	δ_H	δ_C	δ_H	δ_C
1	1.61 (1H, m) 1.41 (1H, m)	32.3	1.66 (1H, m) 1.61 (1H, m)	33.9
2	1.42 (2H, m)	18.4	1.46 (2H, m)	18.3
3	1.33 (1H, m) 1.11 (1H, m)	41.6	1.44 (1H, m) 1.18 (1H, m)	42.0
4	-	33.3	-	33.3
5	1.66 (1H, m)	45.6	1.22 (1H, m)	49.1
6	1.73 (2H, m)	21.2	1.49 (2H, m)	21.4
7	1.63 (1H, m) 1.29 (1H, m)	31.5	1.58 (1H, m) 0.69 (1H, m)	32.7
8	1.73 (1H, m)	30.9	2.40 (1H, m)	31.5
9	-	81.3	-	82.6
10	-	39.3	-	39.9
11	6.57 (1H, d, *J*=8.8 Hz)	133.8	6.66 (1H, d, *J*=8.9 Hz)	133.0
12	6.45 (1H, d, *J*=8.8 Hz)	133.4	6.44 (1H, d, *J*=8.9 Hz)	131.8
13	-	79.3	-	79.5
14	1.71 (1H, m) 1.30 (1H, m)	34.3	2.09 (1H, m) 1.44 (1H, m)	32.7
15	1.86 (1H, m)	32.1	1.87 (1H, m)	32.2
16	0.96 (3H, d, *J*=6.9 Hz)	17.4	0.96 (3H, d, *J*=6.9 Hz)	17.2
17	0.94 (3H, d, *J*=6.9 Hz)	17.1	0.96 (3H, d, *J*=6.9 Hz)	17.4
18	0.86 (3H, s)	33.2	0.88 (3H, s)	33.8
19	0.82 (3H, s)	22.2	0.87 (3H, s)	21.9
20	1.05 (3H, s)	17.0	1.13 (3H, s)	14.8

Measured in $CDCl_3$ at 300 and 75 MHz, respectively. Assignments were aided by ^{1}H gDQCOSY, TOCSY, DEPT, gHMQC, and gHMBC experiments.

3.2.10. Spectral Data

Luteolin (**12**): a yellow solid; $[\alpha]_D^{20}$ – 22 (*c* 0.58, MeOH); EIMS *m/z* 286 $[M]^+$; ^{1}H NMR (300 MHz, CD_3OD) δ: 7.35 (1H, d, *J* = 8.3 Hz, H-6'), 7.34 (1H, br s, H-2'), 6.88 (1H, d, *J* = 8.3 Hz, H-5'), 6.51 (1H, s, H-3), 6.41 (1H, br s, H-8), 6.18 (1H, br s, H-6); ^{13}C NMR (75 MHz, CD_3OD) δ: 183.6 (C, C-4), 166.1 (C, C-2), 165.8 (C, C-7), 163.0 (C, C-5), 159.2 (C, C-9), 150.8 (C, C-4'), 146.8 (C, C-3'), 123.5 (C, C-1'), 120.2 (CH, C-6'), 116.6 (CH, C-5'), 114.0 (CH, C-2'), 105.2 (C, C-10), 103.8 (CH, C-3), 100.0 (CH, C-6), 94.9 (CH, C-8).

Quercetin 3,7-dimethyl ether (**13**): a pale yellow solid; $[\alpha]_D^{20}$ – 30 (*c* 0.03, MeOH); EIMS *m/z* 330 $[M]^+$; ^{1}H NMR (300 MHz, CD_3OD) δ: 7.63 (1H, s, H-2'), 7.54 (1H, d, *J* = 8.4 Hz, H-6'), 6.89 (1H, d, *J* = 8.4 Hz, H-5'), 6.58 (1H, s, H-8), 6.32 (1H, s, H-6), 3.88 (3H, s, 7-OMe), 3.79 (3H, s, 3-OMe); ^{13}C NMR (75 MHz, CD_3OD) δ: 179.9 (C, C-4), 167.1 (C, C-7), 162.7 (C, C-5), 158.2 (C, C-2), 158.2 (C, C-9), 149.9 (C, C-4'), 146.3 (C, C-3'), 139.6 (C, C-3), 122.7 (C, C-1'), 122.3 (CH, C-6'), 116.4 (CH, C-2'), 116.3 (CH, C-5'), 106.6 (C, C-10), 98.8 (C, C-6), 93.0 (CH, C-8), 60.5 (CH_3, 3-OMe), 56.5 (CH_3, 7-OMe)

Vitexicarpin (**14**): a pale yellow solid; $[\alpha]_D^{20}$ + 10 (*c* 0.10, MeOH); EIMS *m/z* 374 $[M]^+$; ^{1}H NMR (300 MHz, $CDCl_3$) δ: 12.6 (1H, s, 5-OH), 7.67 (1H, dd, *J* = 8.4, 2.0 Hz, H-6'), 7.65 (1H, d, *J* = 2.0 Hz, H-2'), 6.92 (1H, d, *J* = 8.4 Hz, H-5'), 6.47 (1H, s, H-8), 5.83 (1H, s, 3'-OH), 3.96 (3H, s, 4'-OMe), 3.93 (3H, s, 7-OMe), 3.90

(3H, s, 5-OMe), 3.84 (3H, s, 3-OMe); ^{13}C NMR (75 MHz, $CDCl_3$) δ: 178.7 (C, C-4), 158.6 (C, C-7), 155.5 (C, C-2), 152.5 (C, C-5), 152.1 (C-9), 148.7 (C, C-4'), 145.4 (C, C-3'), 138.8 (C, C-3), 132.1 (C, C-6), 123.4 (C, C-1'), 121.4 (CH, C-6'), 114.2 (CH, C-2'), 110.3 (CH, C-5'), 106.5 (C, C-10), 90.3 (CH, C-8), 60.9 (CH_3, 6-OMe), 60.1 (CH_3, 3-OMe), 56.3 (CH_3, 7-OMe), 56.0 (CH_3, 4'-OMe).

Artemetin (**15**): a pale yellow solid; EIMS *m/z* 388 $[M]^+$; ^{1}H NMR (300 MHz, $CDCl_3$) δ: 12.6 (1H, s, 5-OH), 7.70 (1H, dd, *J* = 8.6, 2.0 Hz, H-6'), 7.65 (1H, d, *J* = 2.0 Hz, H-5'), 6.97 (1H, d, *J* = 8.6 Hz, H-2'), 6.49 (1H, s, H-8), 3.97(3H, s, 7-OMe), 3.96 (3H, s, 4'-OMe), 3.95 (3H, s, 3'-OMe), 3.91 (3H, s, 6-OMe), 3.86 (3H, s, 3-OMe); ^{13}C NMR (75 MHz, $CDCl_3$) δ: 178.7 (C, C-4), 158.6 (C, C-7), 155.7 (C, C-2), 152.6 (C, C-9), 152.2 (C-5), 151.3 (C, C-4'), 148.7 (C, C-3'), 138.7 (C, C-3), 132.2 (C, C-6), 122.8 (C, C-1'), 122.1 (CH, C-6'), 111.2 (CH, C-5'), 110.8 (CH, C-2'), 106.5 (C, C-10), 90.3 (CH, C-8), 60.9 (CH_3, 6-OMe), 60.2 (CH_3, 3-OMe), 56.4 (CH_3, 7-OMe), 56.1 (CH_3, 4'-OMe), 56.0 (CH_3, 3'-OMe).

Vitetrifolin F (**16**): a colorless syrup; $[\alpha]_D^{20}$ + 83 (*c* 0.22, MeOH); EIMS *m/z* 304 $[M\text{-}CH_3COOH]^+$; ^{1}H NMR (300 MHz, CD_3OD) δ: 5.84 (1H, dd, *J* = 17.4, 10.7 Hz, H-14), 5.15 (1H, dd, *J* = 17.4, 1.5 Hz, H-15a), 5.01 (1H, dd, *J* = 10.7, 1.5 Hz, H-15b), 4.80 (2H, dd, *J* = 12.5, 3.1 Hz, H-7), 4.18 (2H, d, *J* = 3.1 Hz, H-6), 2.18 (1H, dq, 12.6, 6.5 Hz, H-8), 2.03 (2H, m, H-1), 1.65 (2H, m, H-2), 1.50 (2H, m, H-3), 1.48 (2H, m, H-11), 1.22 (2H, m, H-12), 1.21 (3H, s, H-16), 2.09 (3H, s, 7-

CO$\underline{CH_3}$), 1.15 (3H, s, H-18), 1.05 (3H, s, H-19), 1.05 (3H, s, H-20), 0.94 (3H, d, *J* = 7.0 Hz, H-17); ^{13}C NMR (75 MHz, CD_3OD) δ: 172.8 (C, 7-$\underline{CO}CH_3$), 145.9 (CH, C-14), 139.6 (C, C-10), 137.1 (C, C-5), 112.3 (CH_2, C-15), 76.9 (CH, C-7), 73.8 (C, C-13), 65.2 (CH, C-6), 44.1 (C, C-9), 40.8 (CH_2, C-3), 40.2 (CH_2, C-12), 37.0 (CH, C-8), 35.6 (C, C-4), 30.8 (CH_2, C-11), 30.0 (CH_3 C-18), 29.7 (CH_3, C-19), 28.4 (CH_3, C-20), 27.3 (CH_3, C-16), 26.8 (CH_2, C-1), 21.2 (CH_3, 7-CO$\underline{CH_3}$), 20.8 (CH_2, C-2), 11.6 (CH_3, C-17).

Vitetrifolin E (**17**): a colorless needles, $[\alpha]_D^{20}$ + 60 (*c* 0.38, MeOH); EIMS *m/z* 304 $[M\text{-}CH_3COOH]^+$; ^{1}H NMR (300 MHz, CD_3OD) δ: 5.83 (1H, dd, *J* = 17.3, 10.7 Hz, H-14), 5.56 (1H, d, *J* = 3.3 Hz, H-6), 5.15 (1H, dd, *J* = 17.3, 1.5 Hz, H-15a), 5.02 (1H, dd, *J* = 10.7, 1.5 Hz, H-15b), 3.62 (1H, dd, *J* = 12.4, 3.3 Hz, H-7), 2.02 (2H, m, H-1), 2.01(3H, s, 6-CO$\underline{CH_3}$), 1.87 (1H, dq, *J* = 12.4, 6.9 Hz, H-8), 1.62 (2H, m, H-2), 1.47 (2H, m, H-3), 1.44 (2H, m, H-11), 1.21 (3H, s, H-16), 1.14 (2H, m, H-12), 1.08 (3H, s, H-18), 1.04 (3H, s, H-20), 1.01 (3H, d, *J* = 6.9 Hz, H-17), 0.94 (3H, s, H-19); ^{13}C NMR (75 MHz, CD_3OD) δ: 173.1 (C, 6-$\underline{CO}CH_3$), 145.9 (CH, C-14), 142.8 (C, C-10), 134.0 (C, C-5), 112.4 (CH_2, C-15), 73.8 (C, C-13), 71.9 (CH, C-6), 70.7 (CH, C-7), 44.0 (C, C-9), 41.0 (CH_2, C-3), 40.3 (CH_2, C-12), 40.1 (CH, C-8), 35.5 (C, C-4), 30.9 (CH_2, C-11), 29.7 (CH_3 C-18), 29.1 (CH_3, C-20), 28.5 (CH_3, C-19), 27.2 (CH_2, C-1), 27.2 (CH_3, C-16), 20.7 (CH_2, C-2), 21.8 (CH_3, 6-CO$\underline{CH_3}$), 11.9 (CH_3, C-17).

Vitetrifolin D (**18**): a colorless syrup; $[\alpha]_D^{20}$ + 104 (*c* 1.28, MeOH); EIMS *m/z* 346 $[M\text{-}CH_3COOH]^+$, 286 $[M\text{-}CH_3COOH\times2]^+$; ^1H NMR (300 MHz, CD_3OD) δ: 5.84 (1H, dd, *J* = 17.4, 10.7 Hz, H-14), 5.67 (1H, d, *J* = 3.3 Hz, H-6), 5.15 (1H, dd, *J* = 17.4, 1.4 Hz, H-15a), 5.02 (1H, dd, *J* = 10.7, 1.4 Hz, H-15b), 4.85 (1H, dd, *J* = 12.7, 3.3 Hz, H-7), 2.08 (1H, m, H-8), 2.06 (2H, m, H-1) 2.01(3H, s, 7-CO$\underline{CH_3}$), 1.95(3H, s, 6-CO$\underline{CH_3}$), 1.66 (1H, m, H-2a), 1.56 (1H, m, H-2b), 1.50 (2H, m, H-3), 1.48 (2H, m, H-12), 1.45 (1H, m, H-11a), 1.21 (3H, s, H-16), 1.20 (1H, m, H-11b), 1.08 (3H, s, H-20), 1.07 (3H, s, H-18), 0.95 (3H, d, *J* = 6.9 Hz, H-17), 0.91 (3H, s, H-19); ^{13}C NMR (75 MHz, CD_3OD) δ: 172.6 (C, 7-$\underline{CO}CH_3$), 172.5 (C, 6-$\underline{CO}CH_3$), 145.8 (CH, C-14), 143.3 (C, C-10), 133.4 (C, C-5), 112.4 (CH_2, C-15), 74.4 (CH, C-7), 73.7 (C, C-13), 67.5 (CH, C-6), 44.2 (C, C-9), 40.6 (CH_2, C-3), 40.2 (CH_2, C-12), 37.8 (CH, C-8), 35.7 (C, C-4), 30.7 (CH_2, C-11), 29.6 (CH_3 C-18), 28.7 (CH_3, C-20), 28.5 (CH_3, C-19), 27.3 (CH_3, C-16), 27.1 (CH_2, C-1), 21.4 (CH_3, 7-CO$\underline{CH_3}$), 21.0 (CH_3, 6-CO$\underline{CH_3}$), 20.6 (CH_2, C-2), 11.5 (CH_3, C-17).

Vitexilactone (**19**): a pale yellow solid; $[\alpha]_D^{20}$ – 3 (*c* 0.37, MeOH); EIMS *m/z* 318 $[M\text{-}CH_3COOH]^+$; NMR data, see Table 5.

(5*S,6*R**,8*R**,9*R**,10*S**)-6-acetoxy-9-hydroxy-16-hydroxy-13(14)-labden-16,15-olide** (**20**): a pale yellow solid; $[\alpha]_D^{20}$ + 17 (*c* 0.42, MeOH); HRESIMS (negative-ion mode) *m/z* 393.2286 $[M\text{-}H]^-$ (calcd. for $C_{22}H_{33}O_6$, 393.2277); NMR data, see Table 5.

(5*S,6*R**,8*R**,9*R**,10*S**)-6-acetoxy-9-hydroxy-15-methoxy-13(14)-labden-16,15-olide** (**21**): Amorphous white solid; ESIMS (negative-ion mode) *m/z* 407 $[M-H]^-$, EIMS *m*/z 348 $[M-CH_3COOH]^+$; ^{1}H NMR (300 MHz, $CDCl_3$) δ: 6.75 (1H, d, *J* = 1.2 Hz, H-14), 5.71 (1H, d, *J* = 1.2 Hz, H-15), 5.37 (1H, q, *J* = 2.7 Hz, H-6), 3.57 (3H, s, 15-OCH_3), 2.42 (2H, dd, *J* = 8.5, 8.0 Hz, H-12), 2.10 (1H, m, H-8), 2.04 (3H, s, 6-OCO$\underline{CH_3}$), 1.80 (2H, m, H-11), 1.63 (1H, d, *J* = 2.7 Hz, H-5), 1.58 (2H, m, H-7), 1.51 (2H, m, H-2), 1.46 (2H, m, H-1), 1.25 (2H, m, H-3), 1.23 (3H, s, H-20), 0.99 (3H, s, H-19), 0.96 (3H, s, H-18), 0.92 (3H, d, *J* = 6.9 Hz, H-17); ^{13}C NMR (75 MHz, $CDCl_3$) δ: 171.4 (C, C-16), 170.3 (CH_3 6-O$\underline{CO}CH_3$), 141.4 (CH, C-14), 139.1 (C, C-13), 102.6 (CH, C-15), 77.2 (C, C-9), 70.1 (CH, C-6), 57.2 (CH_3, 15-OCH_3), 47.6 (CH, C-5), 43.8 (C, C-10), 43.7 (CH_2, C-3), 36.2 (CH_2, C-7), 34.0 (C, C-4), 33.7 (CH_2, C-1), 33.7 (CH_3 C-18), 32.1 (CH_2, C-11), 31.9 (CH, C-8), 23.8 (CH_3, C-19), 22.1 (CH_2, C-12), 22.0 (CH_3, 6-OCO$\underline{CH_3}$), 19.1 (CH_3, C-20), 18.7 (CH_2, C-2), 16.2 (CH_3, C-17).

Aurantiamide (**22**): amorphous white solid, FABMS *m/z* 403 $[M+H]^+$; ^{1}H NMR (900 MHz, $CDCl_3$) δ: 7.70 (2H, d, *J* = 11.3 Hz, H-2'/6'), 7.50 (1H, t, *J* = 11.3 Hz, H-4'), 7.42 (2H, t, *J* = 11.3 Hz, H-3'/5'), 7.31 (2H, t, *J* = 11.3 Hz, H-3"/5"), 7.26 (2H, d, *J* = 11.3 Hz, H-2"/6"), 7.25 (1H, t, *J* = 11.3 Hz, H-4"), 7.16 (2H, t, *J* = 11.3 Hz, H-3"'/5"'), 7.12 (1H, t, *J* = 11.3 Hz, H-4"'), 7.06 (2H, d, *J* = 11.3 Hz, H-2"'/6"'), 4.74 (1H, m, H-5), 4.07 (1H, m, H-2), 3.44 (1H, dd, *J* = 11.1, 3.5 Hz, H-1a), 3.39 (1H, dd, *J* = 11.1, 4.5 Hz, H-1b), 3.26 (1H, dd, *J* = 13.7, 6.0 Hz, H-8a), 3.02 (1H,

dd, *J* = 13.7, 8.8 Hz, H-8b), 2.77 (1H, dd, *J* = 13.8, 7.5 Hz, H-9a), 2.67 (1H, dd, *J* = 13.8, 7.3 Hz, H-9b); ^{13}C NMR (75 MHz, $CDCl_3$) δ: 170.6 (C, C-4), 167.0 (C, C-7), 133.5 (C, C-1'), 137.1 (C, C-1'''), 136.7 (C, C-1''), 131.9 (CH, C-4'), 129.3 (CH, C-2''/6''), 129.0 (CH, C-2'''/6'''), 128.8 (CH, C-3''/5''), 128.6 (CH, C-3'/5'), 128.5 (CH, C-3'''/5'''), 127.1 (CH, C-4''), 127.0 (CH, C-2'/6'), 126.5 (CH, C-4'''), 63.6 (CH_2, C-1), 55.3 (CH, C-5), 52.9 (CH, C-2), 38.8 (CH_2, C-8), 36.9 (CH_2, C-9).

3α-hydroxy pleuroziol (**23**): a pale yellow solid; $[\alpha]_D^{20}$ + 15 (*c* 0.13, MeOH); HRFABMS *m/z* 347.2563 $[M+Na]^+$ (calcd. for $C_{20}H_{36}O_3Na$, 347.2562); NMR data, see Table 6.

9α*H*-manoyl oxide (**24**): a colorless solid, EIMS *m/z* 290 $[M]^+$; NMR data, see Table 6.

Abieta-11(12)-ene-9α,13α-endoperoxide (**25**): a colorless solid, $[\alpha]_D^{20}$ – 37 (*c* 0.60, $CHCl_3$); HRESIMS *m/z* 327.2299 $[M+Na]^+$ (calcd. for $C_{20}H_{32}O_2Na$, 327.2300); NMR data, see Table 7.

Abieta-11(12)-ene-9β,13β-endoperoxide (**26**): a colorless solid, $[\alpha]_D^{20}$ + 8 (*c* 0.27, $CHCl_3$); HRESIMS *m/z* 327.2292 $[M+Na]^+$ (calcd. for $C_{20}H_{32}O_2Na$, 327.2300); NMR data, see Table 7.

Abieta-9(11):12(13)-di-α-epoxide (**27**): a colorless needles, $[\alpha]_D^{20}$ - 27 (*c* 0.15, $CHCl_3$); HRESIMS *m/z* 327.2297 $[M+Na]^+$ (calcd. for $C_{20}H_{32}O_2Na$, 327.2300); ^1H NMR (300 MHz, $CDCl_3$) δ: 3.32 (1H, d, *J* = 3.0 Hz, H-11), 2.99 (1H, d, *J* = 3.0 Hz, H-12), 1.94 (1H, m, H-8), 1.73 (2H, m, H-7), 1.65 (2H, m, H-6), 1.63 (1H, m, H-14a), 1.45 (1H, m, H-15), 1.38 (2H, m, H-2), 1.32 (1H, m, H-3a), 1.21 (1H, m, H-14b), 1.20 (1H, m, H-5), 1.12 (1H, m, H-3b), 1.11 (2H, m, H-1), 1.06 (3H, s, H-20), 0.95 (3H, d, *J* = 6.8 Hz, H-16), 0.89 (3H, d, *J* = 6.8 Hz, H-17), 0.86 (3H, s, H-18), 0.81 (3H, s, H-19); ^{13}C NMR (75 MHz, $CDCl_3$) δ: 68.0 (C, C-9), 58.9 (C, C-13), 54.7 (CH, C-12), 50.6 (CH, C-5), 49.4 (CH, C-11), 41.4 (CH_2, C-3), 37.6 (C, C-10), 34.5 (CH, C-15), 33.5 (C, C-4), 32.9 (CH_3 C-18), 32.8 (CH_2, C-7), 32.0 (CH, C-8), 30.6 (CH_2, C-1), 29.1 (CH_2, C-14), 21.9 (CH_3, C-19), 21.5 (CH_2, C-6), 19.6 (CH_3, C-20), 18.1 (CH_3, C-16), 18.0 (CH_2, C-2), 17.2 (CH_3, C-17).

Ferruginol (**28**): a colorless needles, $[\alpha]_D^{20}$ + 22.5 (*c* 0.13, $CHCl_3$); FABMS *m/z* 286 $[M]^+$; ^1H NMR (300 MHz, $CDCl_3$) δ: 6.81 (1H, s, H-14), 6.61 (1H, s, H-11), 3.10 (1H, sept, *J* = 6.9 Hz, H-15), 2.81 (2H, m, H-7), 2.16 (2H, m, H-1), 1.71 (2H, m, H-2), 1.44 (1H, m, H-3a), 1.31 (1H, dd, *J* = 12.4, 2.3 Hz, H-5), 1.24 (3H, d, *J* = 6.9 Hz, H-17), 1.22 (3H, d, *J* = 6.9 Hz, H-16), 1.19 (1H, m, H-3b), 1.17 (3H, s, H-20), 1.84 (2H, m, H-6), 0.93 (3H, s, H-18), 0.91 (3H, s, H-19); ^{13}C NMR (75 MHz, $CDCl_3$) δ: 150.5 (C, C-12), 148.5 (CH, C-9), 131.2 (C, C-13), 127.2 (C, C-8), 126.5 (CH, C-14), 110.4 (CH, C-11), 50.4 (CH, C-5), 41.7 (CH_2, C-3), 38.9 (CH_2, C-1), 37.6 (C, C-10), 33.5 (C, C-4), 33.4 (CH_3 C-18), 29.8 (CH_2, C-7), 26.9 (CH,

C-15), 24.9 (CH_3, C-20), 22.6 (CH_3, C-16), 22.8 (CH_3, C-17), 21.7 (CH_3, C-19), 19.4 (CH_2, C-6), 19.3 (CH_2, C-2).

β-amyrenone (**29**): a colorless solid, $[\alpha]_D^{20}$ + 75 (*c* 0.13, $CHCl_3$); FABMS *m/z* 425 $[M+H]^+$; ^1H NMR (300 MHz, $CDCl_3$) δ: 5.20 (1H, t, *J* = 3.6 Hz, H-12), 2.54 (1H, m, H-2a), 2.36 (1H, m, H-2b), 1.96 (1H, m, H-18), 1.93 (2H, m, H-11), 1.90 (1H, m, H-1a), 1.66 (1H, m, H-19a), 1.66 (1H, m, H-9), 1.56 (1H, m, H-7a),1.53 (2H, m, H-6), 1.47 (1H, m, H-22a), 1.39 (1H, m, H-1b), 1.37 (1H, m, H-7b), 1.36 (1H, m, H-21a), 1.32 (1H, m, H-5), 1.22 (1H, m, H-22b), 1.14 (3H, s, H-27), 1.11 (1H, m, H-21b), 1.09 (2H, m, H-15), 1.09 (1H, m, H-23), 1.07 (1H, m, H-25), 1.05 (1H, m, H-24), 1.04 (1H, s, H-19b), 1.02 (3H, s, H-26), 1.00 (2H, m, H-16), 0.87 (3H, s, H-29), 0.87 (3H, s, H-30), 0.84 (3H, s, H-28); ^{13}C NMR (75 MHz, $CDCl_3$) δ: 217.6 (C, C-3), 145.1 (C, C-13), 121.4 (CH, C-12), 55.3 (CH, C-5), 47.5 (C, C-4), 47.4 (CH C-18), 46.9 (CH, C-9), 46.8 (CH_2, C-19), 41.9 (C, C-14), 39.9 (C, C-8), 39.4 (CH_2, C-1), 37.2 (CH_2, C-22), 36.7 (C, C-10), 34.8 (CH_2, C-21), 34.3 (CH_2, C-2), 33.4 (CH_3, C-29), 32.6 (C, C-17), 32.3 (CH_2, C-7), 31.2 (C, C-20), 28.5 (CH_3 C-28), 27.0 (CH_2, C-15), 26.6 (CH_3, C-23), 26.2 (CH_2, C-16), 26.0 (CH_3, C-27), 23.8 (CH_2, C-11), 23.8 (CH_3, C-30), 21.6 (CH_3, C-24), 19.8 (CH_2, C-6), 16.8 (CH_3, C-26), 15.3 (CH_3, C-25).

α-amyrenone (**30**): a colorless solid, $[\alpha]_D^{20}$ + 94 (*c* 0.12, $CHCl_3$); ESIMS *m/z* 447 $[M+Na]^+$; ^1H NMR (300 MHz, $CDCl_3$) δ: 5.13 (1H, t, *J* = 3.6 Hz, H-12), 2.54

(1H, m, H-2a), 2.38 (1H, m, H-2b), 2.01 (1H, m, H-15a), 1.96 (2H, m, H-11), 1.95 (1H, m, H-19), 1.93 (1H, m, H-16a), 1.89 (1H, m, H-15b), 1.86 (1H, m, H-1a), 1.84 (1H, m, H-16b), 1.61 (1H, m, H-9), 1.59 (1H, m, H-7a), 1.49 (2H, m, H-6), 1.46 (1H, m, H-22a), 1.41 (1H, m, H-21a), 1.38 (1H, m, H-1b), 1.38 (1H, m, H-7b), 1.34 (1H, m, H-5), 1.33 (1H, m, H-20), 1.32 (1H, m, H-18), 1.26 (1H, m, H-21b), 1.26 (1H, m, H-22b), 1.09 (1H, m, H-23), 1.08 (3H, s, H-27), 1.07 (1H, m, H-25), 1.05 (1H, m, H-24), 1.05 (3H, s, H-26), 0.91 (3H, s, H-30), 0.81 (3H, s, H-28), 0.78 (3H, s, H-29); ^{13}C NMR (75 MHz, $CDCl_3$) δ: 217.6 (C, C-3), 139.6 (C, C-13), 124.1 (CH, C-12), 59.2 (CH C-18), 55.3 (CH, C-5), 47.5 (C, C-4), 47.0 (CH, C-9), 42.3 (C, C-14), 41.6 (CH_2, C-22), 40.1 (C, C-8), 39.7 (CH, C-19), 39.7 (CH, C-20), 39.5 (CH_2, C-1), 36.7 (C, C-10), 34.3 (CH_2, C-2), 33.9 (C, C-17), 32.5 (CH_2, C-7), 31.3 (CH_2, C-21), 28.9 (CH_3 C-28), 28.2 (CH_2, C-15), 26.7 (CH_3, C-23), 26.6 (CH_2, C-16), 23.6 (CH_2, C-11), 23.3 (CH_3, C-27), 21.6 (CH_3, C-24), 21.5 (CH_3, C-30), 19.8 (CH_2, C-6), 17.6 (CH_3, C-29), 16.9 (CH_3, C-26), 15.6 (CH_3, C-25).

3.3. Antiproliferative Effects of *Corydalis heterocarpa* Secondary Metabolites

3.3.1. Effects of Compounds **1-6** on Cancer Cell Growth

Antiproliferative effects of the isolated compounds **1-6** against AGS, HT-29, HT-1080, MCF-7, and U-937 cancer cells were compared with the control at the concentrations of 10, 50, and 100 μM (Fig. 11).

In comparative analysis, compounds **2**, **5**, and **6** showed high growth inhibitory effects on all five cell lines in a dose-dependent manner ($p < 0.05$). AGS human cancer cells were the most sensitive cell line to the antiproliferative effects of all compounds, while U-937 human leukemia cells were the least sensitive. However, all compounds still exhibited dose-dependent inhibitory effects, even on proliferation of U-937 cells ($p < 0.05$).

New compound **6** in particular exerted the highest antiproliferative activity among all compounds tested. It was capable of inhibiting the proliferation of the AGS, HT-29, HT-1080, MCF-7, and U-937 cells, at rates of 54, 43, 51, 50 and 17 %, respectively, at a concentration of 100 μM.

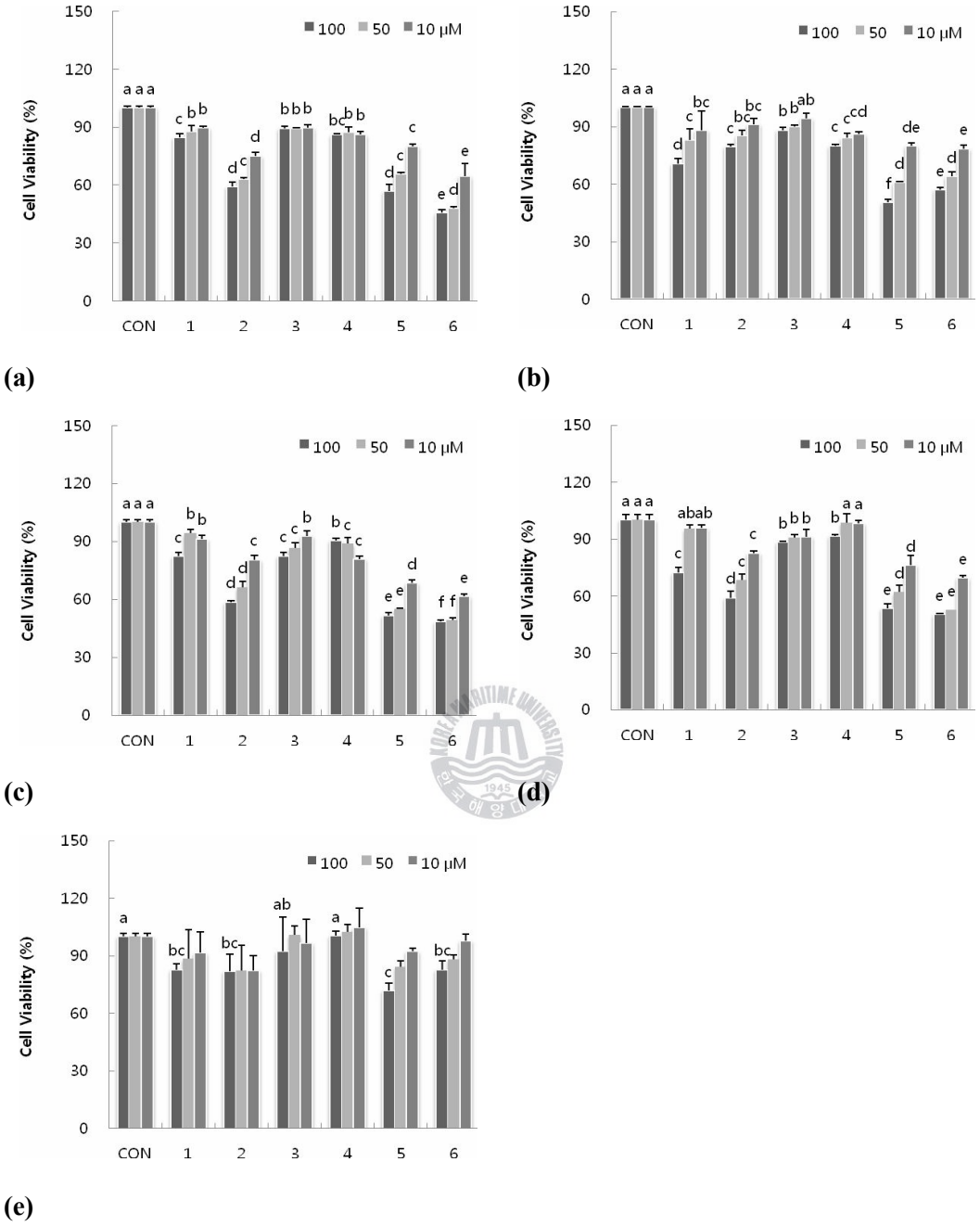

Figure 11. Antiproliferative effects of compounds **1-6** isolated from *Corydalis heterocarpa* in AGS (a), HT-29 (b), HT-1080 (c), MCF-7 (d), and U-937 (e) cells.

[a-f] Means with the different letters at the same concentration are significantly different ($p < 0.05$) by Duncan's multiple range test. Values are means ± SD (n=3).

3.3.2. Apoptosis Induction by Compounds **1**-**6** in AGS Cancer Cells

To further characterize whether the inhibitory activity of the compounds **1**-**6** against proliferation of cells was related to the induction of apoptosis, activations of Bax and Bcl-2 genes were examined by RNA extraction and RT-PCR (Antonsson, 2001; Zornig *et al*., 2002). Since these compounds exhibited the highest antiproliferative effect in AGS human gastric cancer cells, their effect on expression of Bax and Bcl-2 genes were also examined using AGS human gastric adenocarcinoma cells (Fig. 12).

In the presence of any of the compounds, expression of the anti-apoptotic Bcl-2 at a concentration of 10 μM decreased, while expression of the pro-apoptotic Bax at a concentration of 100 μM increased. The change in rate of Bax expression levels was more noticeable with compounds **1**, **4**, **5**, and **6** for the others, at a concentration of 100 μM (Fig. 12b). The presence of compound **2** led to significant down-regulation of an anti-apoptotic Bcl-2 level (Fig. 12a). Activation of pro-apoptotic Bax was also observed in the presence of compound **2**, but the activation level was not high. Among these compounds, **5** most remarkably induced the down-regulation of the anti-apoptotic primer Bcl-2 level as well as the up-regulation of the pro-apoptotic primer Bax level, both in a dose-dependent manner ($p < 0.05$). However, new compound **6** induced simultaneous expression of level of both the Bcl-2 and Bax to the highest up-regulation at 100 μM. Members of the Bcl-2 subfamily are the most important regulators for characterization of apoptosis and can be divided into an anti-apoptotic subfamily including Bcl-2 and a pro-

apoptotic subfamily including Bax (Miyashita *et al*., 1994; Roy *et al*., 1997; Deveraux and Reed, 1999). Therefore, the changed rate of Bcl-2 subfamily expression levels has been examined to determine apoptotic mechanisms.

Almost all of the compounds significantly activated p53 and p21 levels in a dose-dependent manner (Fig. 13). However, compound **5** up-regulated p53 levels even at a concentration of 10 μM but had no effect on p21 levels. Compounds **4** and **6** caused a dose-dependent activation of both p53 and p21 levels. Compounds **1** and **2** induced activation of p53 and p21 levels, and p21 levels were activated even at 10 μM.

The correct balance of pro-apoptotic and anti-apoptotic proteins can determine whether apoptosis occurs. p53 is a tumor suppressor gene that plays an essential role in many types of cell death and apoptosis. p53 can up- and down-regulate the pro-apoptotic Bax and anti-apoptotic primer Bcl-2, which can in turn lead to disruption of the mitochondrial membrane. Induction of p21 can alter the progression of cell cycles, arrest cell growth, and promote the occurrence of apoptosis (Gartel and Tyner, 2002). Since p53 is located at upstream of p21, the induction of p21 is primarily mediated through a p53-dependent pathway.

Therefore, these data suggest that part of the antiproliferative activity of these compounds is related to up-regulation of p53 and p21, and that apoptosis can be induced through a Bax and a Bcl-2 dependent pathway.

Accordingly, the present work demonstrates that the halophyte *Corydalis heterocarpa* has potent inhibitory effects on proliferation of human cancer cells.

The compounds **2**, **5** and **6** exhibited higher antiproliferative effects than did the other compounds. The antiproliferative effect of **2** was brought about by apoptosis induction through the Bax and Bcl-2 dependent pathway and was related to significant up-regulation of p53 and p21. Compound **5** suppressed proliferation of AGS human adenocarcinoma cells by induction of apoptosis, which was associated with a significant decrease in Bcl-2 expression and increase in Bax expression through a p53-dependent pathway. In addition, the antiproliferative effect of **6** may have been induced by apoptosis through activation of pro-apoptotic Bax expression and may also have been related to the significant p53 and p21 expression observed.

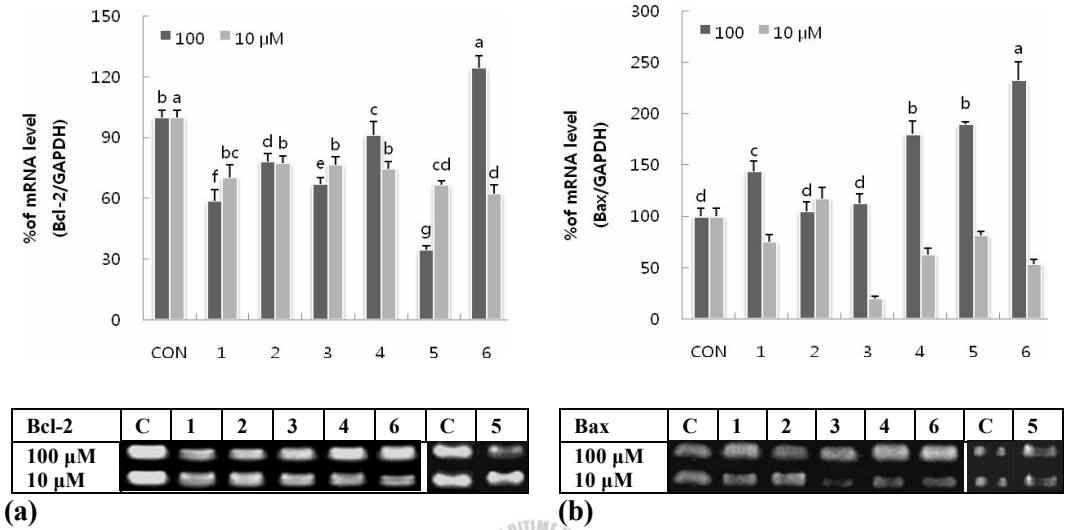

Figure 12. Effects of compounds **1-6** isolated from *Corydalis heterocarpa* on mRNA levels of Bcl-2 (a) and Bax (b) in AGS human gastric cancer cells. Cells were incubated with compounds for 24 h, then total RNA was isolated and RT-PCR was performed using the indicated primers. The amplified PCR products were run in 1% agarose gel and visualized by EtBr staining. GAPDH was used as a housekeeping control gene.

[a-g] Means with the different letters at the same concentration are significantly different ($p < 0.05$) by Duncan's multiple range test. Values are means ± SD (n=3).

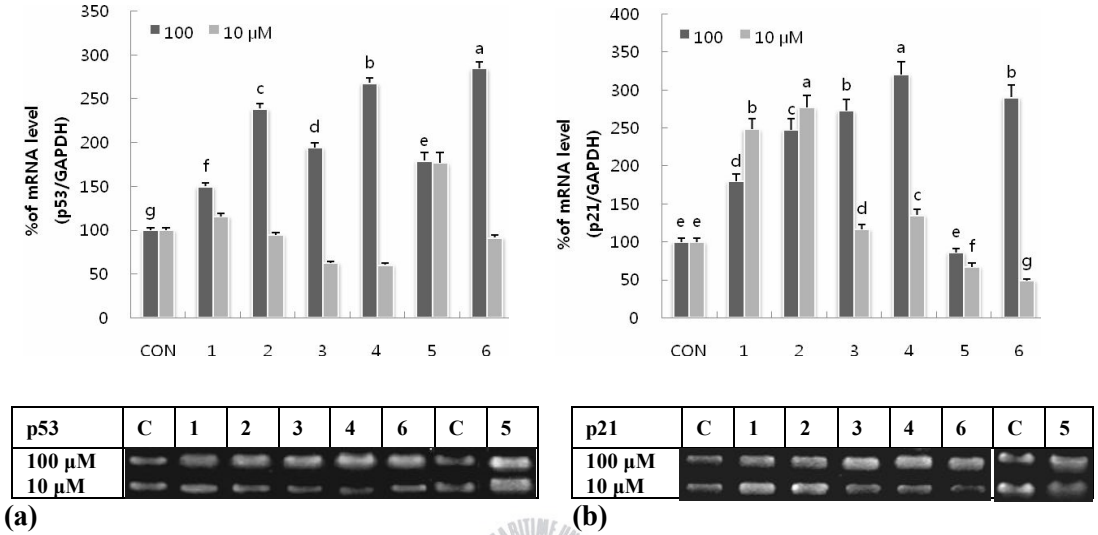

(a) **(b)**

Figure 13. Effects of compounds **1-6** isolated from *Corydalis heterocarpa* on mRNA levels of p53 (a) and p21 (b) in AGS human gastric cancer cells. Cells were incubated with compounds for 24 h, then total RNA was isolated and RT-PCR was performed using the indicated primers. The amplified PCR products were run in 1% agarose gel and visualized by EtBr staining. GAPDH was used as a housekeeping control gene.

[a-g] Means with the different letters at the same concentration are significantly different ($p < 0.05$) by Duncan's multiple range test. Values are means ± SD (n=3).

3.3.3. Effects of Compounds **7-11** on Cancer Cell Growth

To test whether treatment with compounds **7-11** alters proliferation of cancer cells, we incubated the four human cancer cell lines (AGS, HT-29, HT-1080, MCF-7 cancer cells) with various concentrations of compounds **7-11** for 24 h and assessed cell viability with a MTT assay (Fig. 14).

Treatment with compounds **7-11** resulted in a dose-dependent cytotoxic response on all cancer cell lines and most cancer cells were sensitive to sample treatment. Among the compounds tested, compound **10** and **11** had a comparatively high antiproliferative effect on human cancer cell lines ($p < 0.05$). Compound **10** showed growth inhibitory rates of 44% against HT-1080 cancer cells at a concentration of 100 μM. Compound **11** inhibited the proliferation of the AGS, HT-1080, and MCF-7 at rates of 43%, 29%, and 39%, respectively, at a concentration of 100 μM. AGS human gastric cancer cells were slightly more sensitive to treatment with these compounds than were the other cell lines.

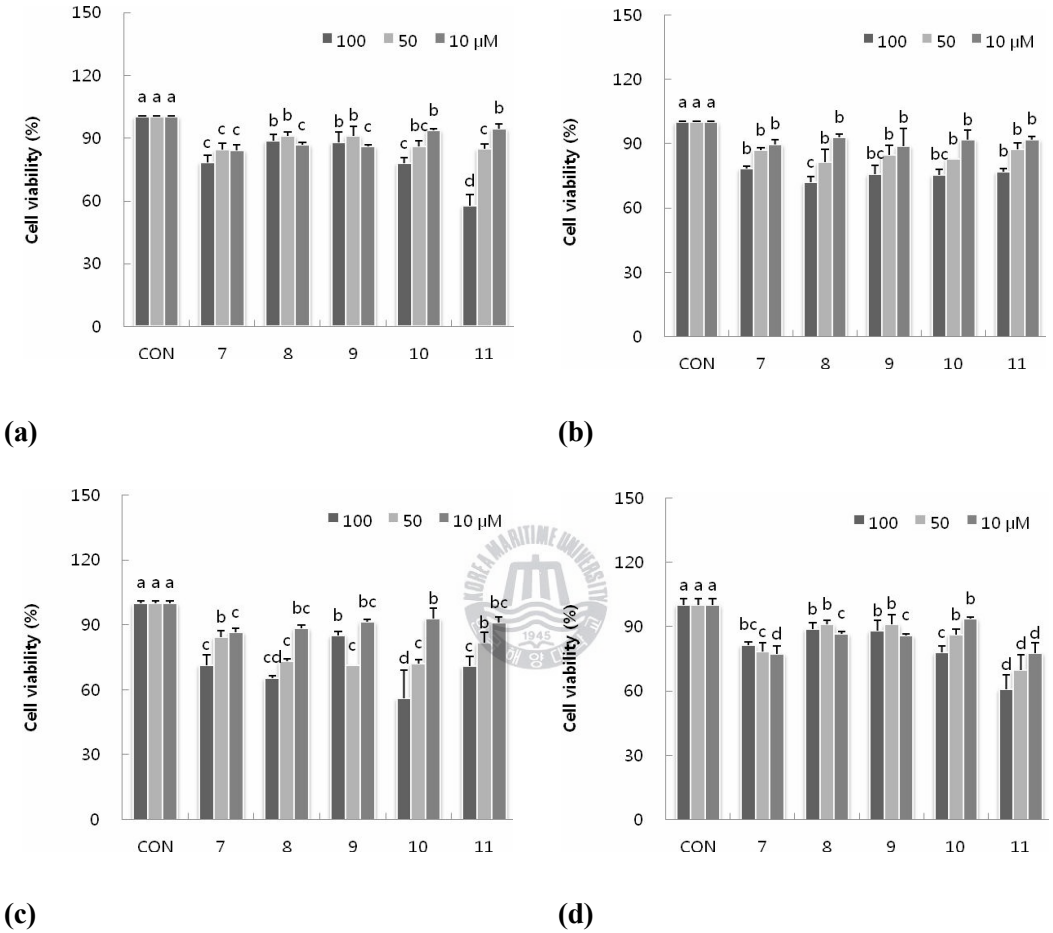

Figure 14. Antiproliferative effects of compounds **7-11** isolated from *Corydalis heterocarpa* in AGS (a), HT-29 (b), HT-1080 (c), and MCF-7 (d) cells.

[a-d] Means with the different letters at the same concentration are significantly different ($p < 0.05$) by Duncan's multiple range test. Values are means ± SD (n=3).

3.3.4. Apoptosis Induction by Compounds **7-11** in AGS Cancer Cells

To confirm and to further characterize whether the inhibitory activity of the compounds **7-11** against proliferation of cells was related to the induction of apoptosis, we examined the activations of regulator genes by RT-PCR analysis.

As shown in Fig. 15, the expression levels of anti-apoptotic Bcl-2 substantially decreased, whereas that of pro-apoptotic Bax markedly increased in AGS cells treated with the compounds **7-11** compared with control cells. Among them, the mRNA expression levels of Bax were more noticeable in compounds **7**, **10** and **11** than others at a concentration of 100 μM. In addition, treatment of compound **7** most remarkably reduced the level of Bcl-2 to ~30% of control, and compounds **9**, **10** and **11** also similarly down-regulated Bcl-2 levels in a dose-dependent manner ($p < 0.05$).

The mRNA levels of p53 and p21 were also observed using RT-PCR on the AGS cells. The results described in Fig. 16 showed that there was an obviously increased expression of p53 and p21 compared with control cells. Particularly, compound **11** extremely up-regulated p53 and p21 levels at a concentration of 100 μM. In case of compound **10**, there is no significant difference between the mRNA expression levels of p53 and p21 on the control cells, but the expression level of p21 at a concentration of 10 μM was higher than other compounds at the same concentration.

To summarize, compounds **10** and **11** exhibited higher antiproliferative effects than did the other compounds. These effects may have been induced by apoptosis

through activating pro-apoptotic Bax and anti-apoptotic Bcl-2 expressions. In addition, the strong antiproliferative effect of compound **11** may be closely related to significant up-regulation of p53 and p21.

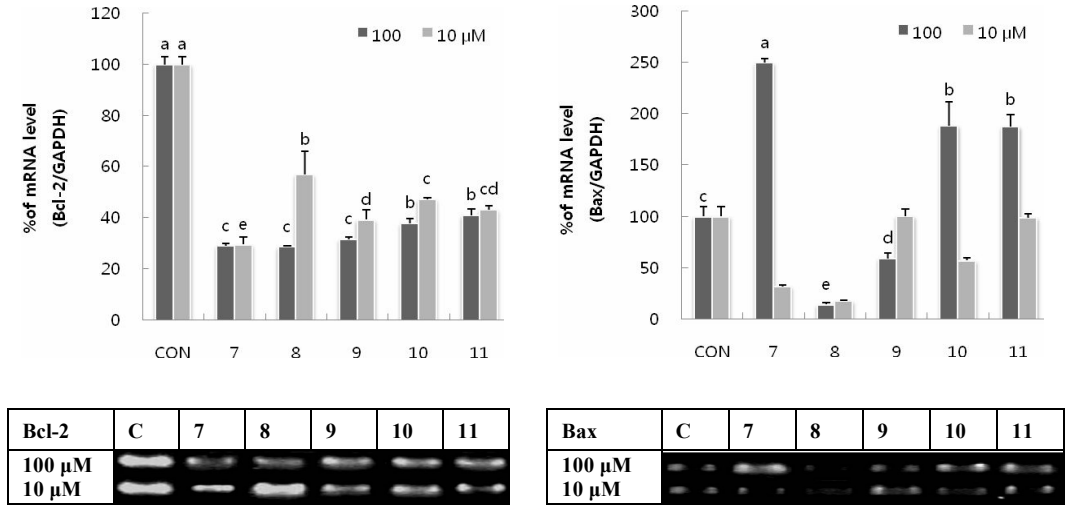

Figure 15. Effects of compounds **7-11** isolated from *Corydalis heterocarpa* on mRNA levels of Bcl-2 (a) and Bax (b) in AGS human gastric cancer cells. Cells were incubated with compounds for 24 h, then total RNA was isolated and RT-PCR was performed using the indicated primers. The amplified PCR products were run in 1% agarose gel and visualized by EtBr staining. GAPDH was used as a housekeeping control gene.

[a-e] Means with the different letters at the same concentration are significantly different ($p < 0.05$) by Duncan's multiple range test. Values are means ± SD (n=3).

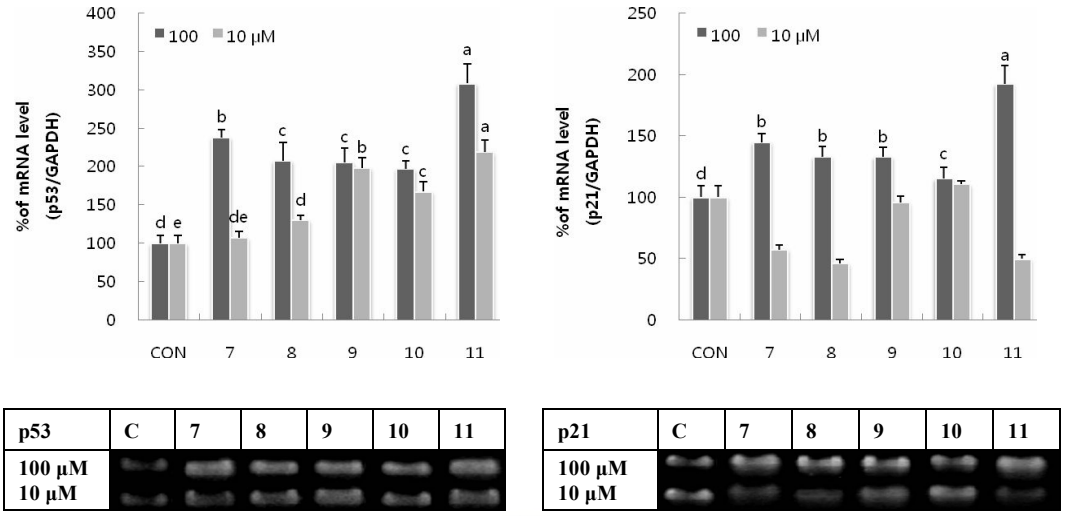

Figure 16. Effects of compounds **7-11** isolated from *Corydalis heterocarpa* on mRNA levels of p53 (a) and p21 (b) in AGS human gastric cancer cells. Cells were incubated with compounds for 24 h, then total RNA was isolated and RT-PCR was performed using the indicated primers. The amplified PCR products were run in 1% agarose gel and visualized by EtBr staining. GAPDH was used as a housekeeping control gene.

[a-e] Means with the different letters at the same concentration are significantly different ($p < 0.05$) by Duncan's multiple range test. Values are means ± SD (n=3).

3.4. Antiproliferative Effects of *Vitex rotundifolia* Secondary Metabolites

3.4.1. Effects of Compounds **12**, **14** and **15** on Cancer Cell Growth

Antiproliferative effects of compounds **12**, **14** and **15** against AGS, HT-29, HT-1080 and MCF-7 cancer cells were compared with the control at the concentrations of 50, 25, 10, 5 and 1 μM by using a MTT assay (Fig. 17). AGS human cancer cells showed the greatest sensitivity to the antiproliferative effect of all compounds in a dose-dependent manner ($p < 0.05$), while MCF-7 human breast cancer cells were the least sensitive. In a comparative analysis, compound **14** exhibited the strongest antiproliferative effects, at 58% in AGS, 68% in HT-29, 49% in HT-1080 and 32 % in MCF-7 cells at a concentration of 50 μM. Compound **14**, in particular, greatly inhibited the proliferation of the AGS cells, even at a concentration of 1 μM, at rate of 43%, which is similar and comparable activity to that of doxorubicin and paclitaxel (taxol), a well characterized and widely used anti-tumor agent (Table 8).

Table 8. Antiproliferative effects of paclitaxel (taxol) and doxorubicin

Cell lines	Taxol (IC_{50})	Doxorubicin (IC_{50})
AGS	7.61±0.48	0.68±0.02
HT-29	0.61±0.07	6.38±0.40
HT1080	33.18±3.48	9.68±2.46
MCF-7	18.28±1.43	40.83±2.86

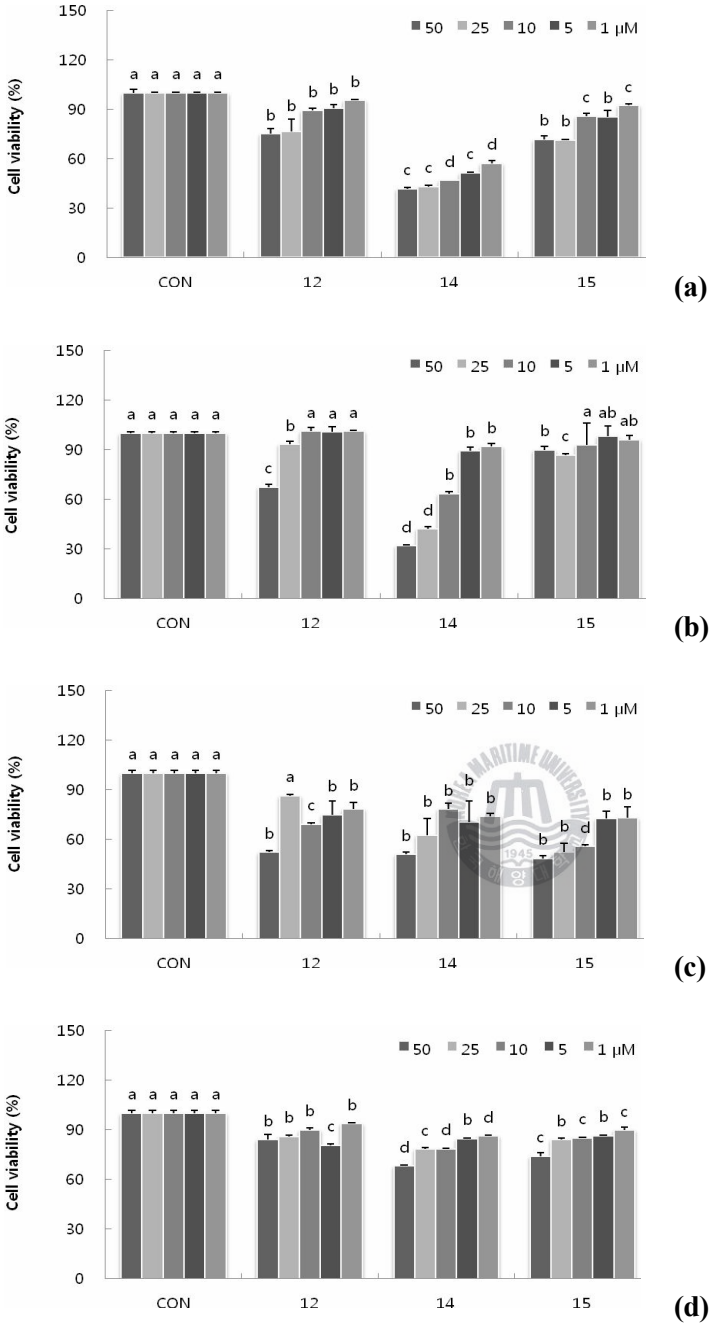

Figure 17. Antiproliferative effects of compounds **12**, **14** and **15** isolated from *Vitex rotundifolia* in AGS (a), HT-29 (b), HT-1080 (c), and MCF-7 (d) cells.

[a-d] Means with the different letters at the same concentration are significantly different ($p < 0.05$) by Duncan's multiple range test. Values are means ± SD (n=3).

3.4.2. Apoptosis Induction by Compounds **12**, **14** and **15** in AGS Cancer Cells

Changes in gene expression of anti-apoptotic Bcl-2 and pro-apoptotic Bax, by treatment of compounds **12**, **14** and **15**, are shown in Fig. 18.

Whereas no effects on Bax expression were observed, compounds **12**, **14** and **15** showed a strong stimulating effect on Bcl-2 gene expression. Of the three compounds, compound **14** exhibited the strongest down-regulation of Bcl-2 level to 20% at a concentration of 25 μM.

As shown in Fig. 19, treatment with compounds **12**, **14** and **15** resulted in a change in mRNA levels of the p53 tumor suppressor gene and its downstream effector p21 in the AGS cells. In the cases of compounds **12** and **15**, there was no significant effect, but compound **14** remarkably up-regulated p53 and p21 levels at a concentration of 25 μM. Therefore, the antiproliferative effect of **14** may have been induced by apoptosis through down-regulation of Bcl-2 expression and therefore may have been related with the significant up-regulation of p53 and p21 expressions observed.

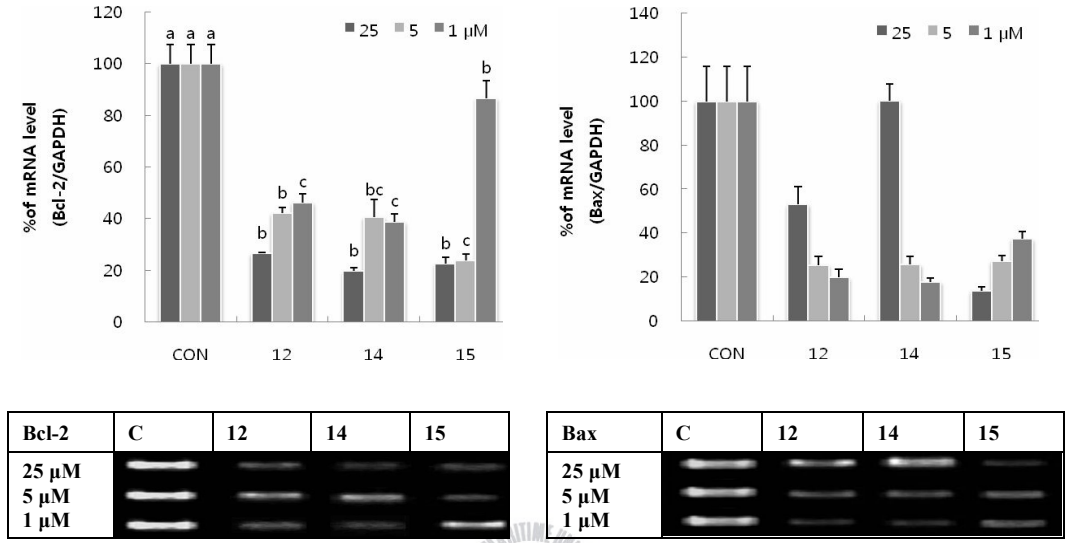

Figure 18. Effects of compounds **12**, **14** and **15** isolated from *Vitex rotundifolia* on mRNA levels of Bcl-2 (a) and Bax (b) in AGS human gastric cancer cells. Cells were incubated with compounds for 24 h, then total RNA was isolated and RT-PCR was performed using the indicated primers. The amplified PCR products were run in 1% agarose gel and visualized by EtBr staining. GAPDH was used as a housekeeping control gene.

[a-c] Means with the different letters at the same concentration are significantly different ($p < 0.05$) by Duncan's multiple range test. Values are means ± SD (n=3).

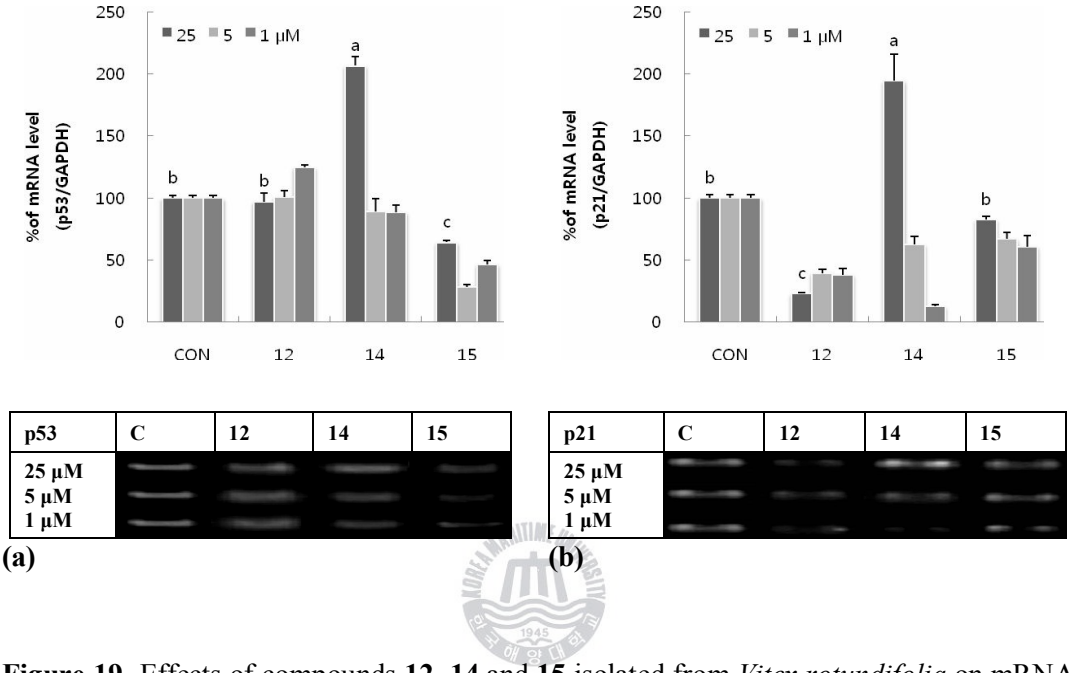

Figure 19. Effects of compounds **12**, **14** and **15** isolated from *Vitex rotundifolia* on mRNA levels of p53 (a) and p21 (b) in AGS human gastric cancer cells. Cells were incubated with compounds for 24 h, then total RNA was isolated and RT-PCR was performed using the indicated primers. The amplified PCR products were run in 1% agarose gel and visualized by EtBr staining. GAPDH was used as a housekeeping control gene.

[a-c] Means with the different letters at the same concentration are significantly different ($p < 0.05$) by Duncan's multiple range test. Values are means ± SD (n=3).

3.5. Antioxidant Effects of *Corydalis heterocarpa* Secondary Metabolites

3.5.1. Cellular Nitric Oxide (NO) Production by Compounds **1-6**

There is a close connection between the murine macrophage cell line (Raw 264.7) and ROS/RNS-mediated cellular events, because these cells can produce high amounts of reactive species after stimulation (Arató *et al*., 2006). For this reason, we examined changes in intracellular NO levels induced by compounds **1-6** isolated from *C. heterocarpa* in Raw 264.7 cells that were abundantly producing NO due to stimulation with lipopolysaccharide (LPS). Reactive NO can combine with $O_2 \cdot^-$ to generate peroxynitrite ($ONOO^-$), which can then act as a powerful oxidant by the chemical reaction with superoxide (Patel *et al*., 1999; Reiter *et al*., 2002; Virag *et al*., 2003; Lee *et al*., 2004; Seo *et al*., 2004; Chen *et al*., 2005; Tsao *et al*., 2005; Lee and Seo, 2006). Therefore, NO production is an important step in the regulation of NO-mediated diseases. Prior to the analysis of intracellular NO levels, the cytotoxic effects of the compounds were examined using a MTT assay, in order to determine non-toxic concentrations for the antioxidant activity test (Fig. 20a). Compared to the control, all compounds (100 and 50 μM) except compounds **5** and **6** at a concentration of 100 μM showed no significant cytotoxicity ($p < 0.05$) toward Raw 264.7 cells. Therefore, the effects of compounds **1-6** on LPS-induced NO production were examined at concentrations of less than 100 μM. The nitrite in the cultured medium was detected by the Griess reagent, an indirect method for measuring the release of NO (Fig. 20b). In Raw 264.7 cells treated with 1 μg/mL LPS for 48hr, the nitrite concentration was 55.9 ± 1.6 μM, which was much higher

than that of untreated Raw 264.7 cells (10.3 ± 0.1). In cultures pretreated with 100 μM of compounds **1**-**6**, the NO production was changed significantly (34.9 ± 1.9, 16.2 ± 0.2, 35.9 ± 0.5, 47.9 ± 0.6, 63.9 ± 2.2 and 47.3 ± 1.6 μM). Among these, compound **2** showed the highest suppression of NO production in a dose-dependent manner (100, 50 and 10 μM, respectively, corresponding to a NO production of 16.2 ± 0.2, 19.9 ± 0.3, 44.5 ± 4.4 μM). The level of NO production at a concentration of 100 μM was comparable to that seen in the untreated Raw 264.7 cells.

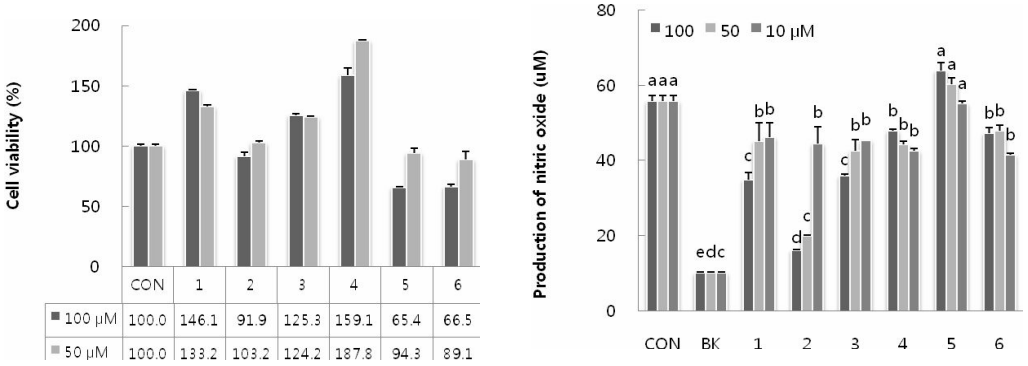

(a) **(b)**

Figure 20. Effects of compounds **1-6** isolated from *Corydalis heterocarpa* on cell viability as determined by MTT assay (a) and effects of compounds **1-6** on nitric oxide production (expressed as nitrite) (b) in LPS-induced Raw 264.7 cells.

[a-e] Means with the different letters at the same concentration are significantly different ($p < 0.05$) by Duncan's multiple range test. Values are means ± SD (n=3).

3.5.2. Scavenging Effects of Compounds **1-6** on Reactive Oxygen Species (ROS)

Chemiluminescence of DCFH-DA has been most widely used to detect several ROS and RNS in biological media (Okimoto *et al*., 2000; Curtin *et al*., 2002). Cellular esterases first hydrolyze 2',7'-dichlorodihydrofluororescein diacetate (DCFH-DA) to non-fluorescent 2',7'-dichlorodihydrofluororescein ($DCFH_2$). In turn, peroxidases such as cytochrome *c* and Fe^{2+} can convert $DCFH_2$ to highly fluorescent 2',7'-dichlorofluorescein (DCF) in the presence of H_2O_2 (Curtin *et al*., 2002; Gomes *et al*., 2005). DCF fluorescence of each compound was described only as the result after incubation for 2h. As shown in Fig. 21, DCF fluorescence intensity that was increased by H_2O_2 was significantly decreased, time-dependently, in the presence of 10 or 100 μM levels of each compound. Among the compounds tested, compounds **1** and **2** generated a more than 50% decrease in intracellular ROS levels compared to control, which was treated with an equal volume of PBS instead of the compounds. Compound **4** presented the highest ROS-scavenging activity at 50 μM concentration.

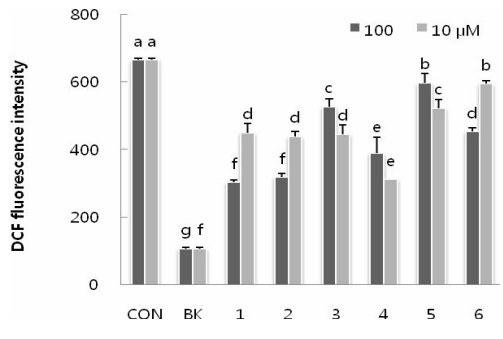

(a)

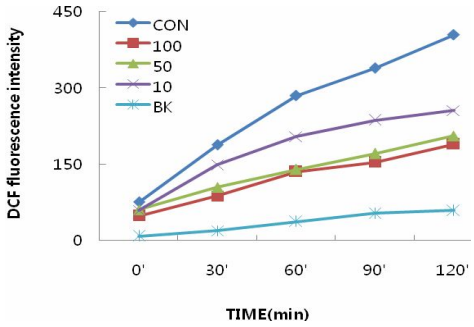

(b) compound 1

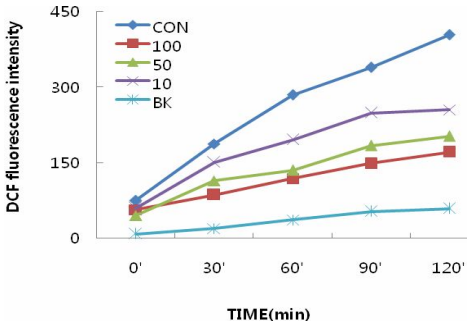

(c) compound 2

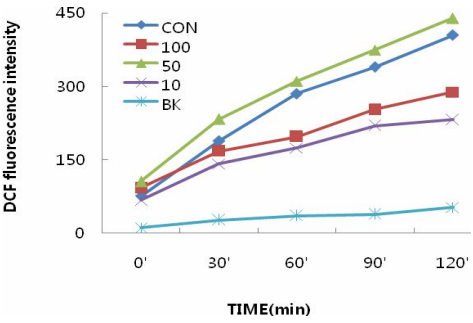

(d) compound 3

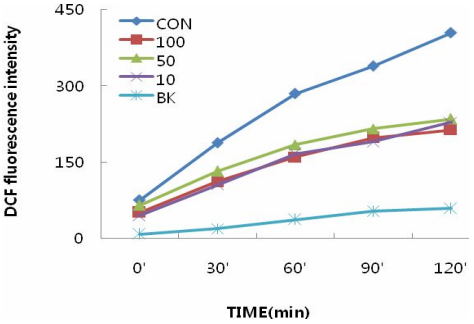

(e) compound 4

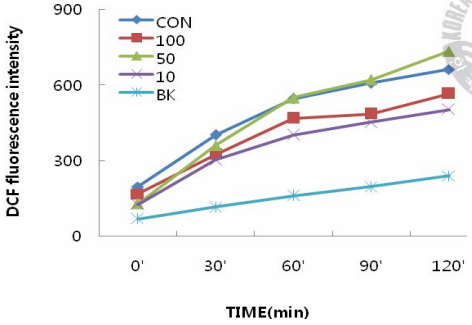

(f) compound 5

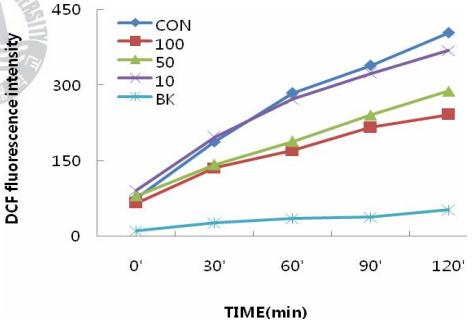

(g) compound 6

Figure 21. Effects of compounds **1-6** isolated from *Corydalis heterocarpa* on intracellular ROS levels induced by hydrogen peroxide in Raw 264.7 cells. The cells were incubated with different concentrations (100 and 10 μM) of the compounds **1-6** for 120 min (a) and with compounds **1-6** for the indicated times (b-g), respectively. DCF fluorescence was measured at $\lambda_{excitation}$=485 nm and $\lambda_{emission}$=528 nm.

[a-g] Means with the different letters at the same concentration are significantly different ($p < 0.05$) by Duncan's multiple range test. Values are means ± SD (n=3).

3.5.3. Measurement of Intracellular Glutathione (GSH) Levels in the Presence of Compounds **1-6**

Glutathione (γ-Glu-Cys-Gly or GSH), a naturally occurring tripeptide, is a most important antioxidant that acts as an ROS scavenger and functions in the regulation of the intracellular redox state (Sies, 1999; Curtin *et al*., 2002; Watson and Jones, 2003). For this reason, intracellular GSH levels in compound-treated cells were measured using a monobromobimane assay. There were no significant differences in the GSH levels between cultures pretreated with compounds **1**-**6** and the control group (Fig. 22). However, compound **2** significantly increased GSH level at a concentration of 100 μM, yielding an activity 2.8-fold higher than the control activity. Thus, compound **2** was highlighted as a potential positive regulator of intracellular GSH content and antioxidant enzyme activity in Raw 264.7 cells.

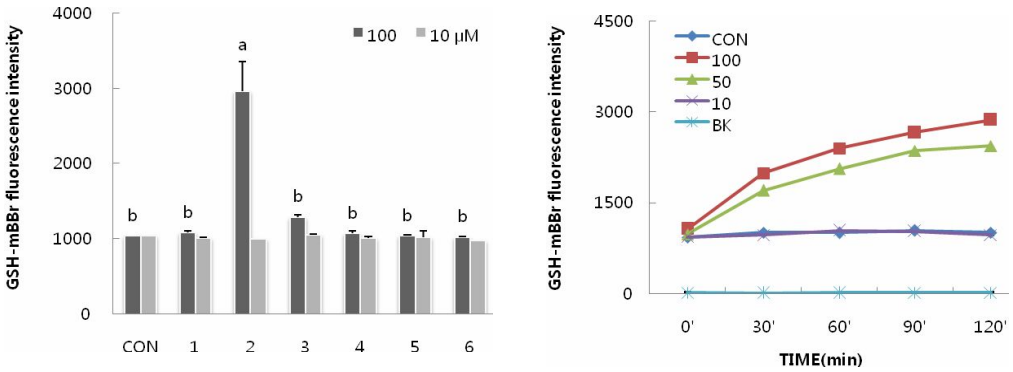

(a) **(b) compound 2**

Figure 22. Effects of compounds **1-6** isolated from *Corydalis heterocarpa* on regulation of GSH levels in Raw 264.7 cells. The cells were incubated with different concentrations (100 and 10 μM) of the compounds **1-6** for 120 min (a) and with compound **2** for the indicated times (b). Cellular GSH levels were determined using mBBr as a thiol-staining reagent according to the method described in the text measuring mBBr-GSH fluorescence intensity at λexcitation=360 nm and λemission =465 nm.

[a-b] Means with the different letters at the same concentration are significantly different ($p < 0.05$) by Duncan's multiple range test. Values are means ± SD (n=3).

3.5.4. Anti-inflammatory Effects of Compounds **1-6**

iNOS and COX-2 genes are closely related to inflammation caused by oxidation reactions in cells. Therefore, expression of iNOS and COX-2 genes in activated Raw 264.7 cells was further analyzed by means of RNA extraction and RT-PCR analysis. As shown in Fig. 23, compounds **1-6** at the concentrations of 100 and 10 μM decreased mRNA expression levels of iNOS and COX-2 in the presence of LPS in a concentration-dependent manner ($p < 0.05$).

The rate of change in iNOS expression levels was more noticeable for compounds **1-4** than for others at a concentration of 100 μM. In particular, compounds **2** and **3** induced strong down-regulation of iNOS levels to 9% and 4% of the control level, respectively. The down-regulation of iNOS level by compound **3** was substantial even at 10 μM (Fig. 23a). On the other hand, in the case of COX-2, compounds **5** and **6** at 100 μM showed strong inhibition of mRNA expression levels (13% and 8%) (Fig. 23b). However, if we consider the cytotoxic effects of compounds **5** and **6** mentioned before, we can conclude that compound **2** most significantly down-regulated the COX-2 expression levels to 24% and 39% at the concentrations of 100 and 10 μM, respectively. Compounds **3** and **4** also decreased mRNA expression levels of COX-2 compared with control. It is apparent that all of the compounds showed inhibitory effects on the expression of iNOS and COX-2 in stimulated Raw 264.7 cells. These data implied that the inhibitory effects of the *C. heterocarpa* compounds on expression of iNOS and COX-2 genes could be partly

attributed to inhibition of nitric oxide and ROS production in stimulated macrophages.

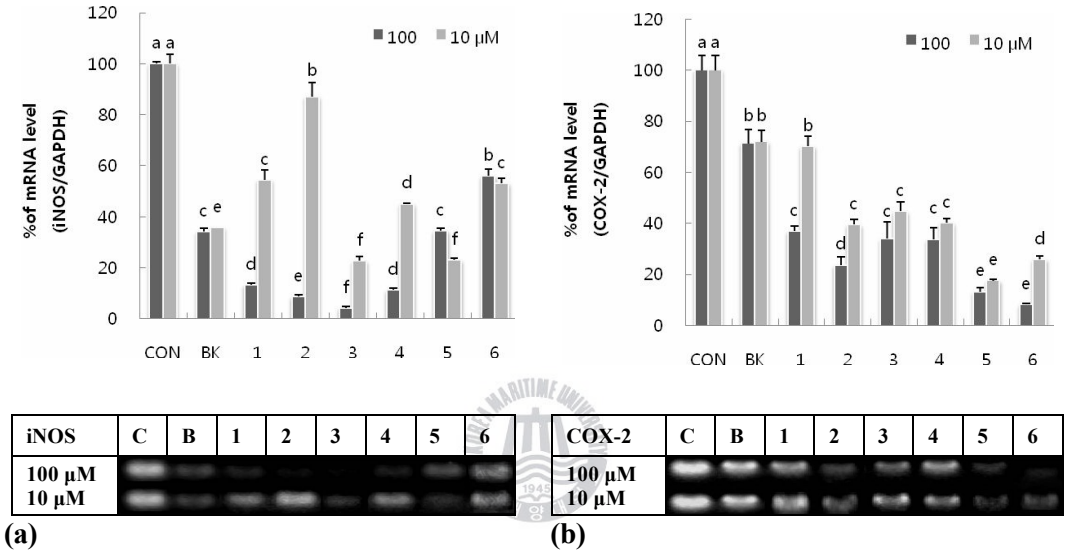

Figure 23. Effects of compounds **1-6** isolated from *Corydalis heterocarpa* on mRNA levels of iNOS (a) and COX-2 (b) in LPS-stimulated Raw 264.7 cells. Cells were incubated with compounds for 48 h, then total RNA was isolated and RT-PCR was performed using the indicated primers. The amplified PCR products were run in 1% agarose gel and visualized by EtBr staining. GAPDH was used as a housekeeping control gene.

[a-f] Means with the different letters at the same concentration are significantly different ($p < 0.05$) by Duncan's multiple range test. Values are means ± SD (n=3).

3.6. Antioxidant Effects of *Vitex rotundifolia* Secondary Metabolites

3.6.1. Cellular Nitric Oxide (NO) Production by Compounds **16-19** and **23-26**

The cytotoxic effects of compounds **12**, **14-19** and **23-26** were examined using the MTT assay in order to determine non-toxic concentrations for the antioxidant activity test (Fig. 24a). At a concentration of 50 μM, most compounds except compounds **14** and **15** showed no significant toxic effects ($p < 0.05$) on the growth of cells. On the basis of these results, compounds **16-19** and **23-26** were used for the antioxidant experiments. To measure inhibition of cellular NO production by these compounds, Raw 264.7 cells were treated with compounds at concentrations of 50 and 10 μM for 1 h, and then stimulated with 1 μg/mL LPS for another 48 h. At a concentration of 50 μM, compounds **16-19** exhibited potent inhibitory activities on NO production (corresponding to 13.0 ± 0.6, 12.9 ± 1.1, 8.3 ± 0.0, 10.6 ± 0.1 μM, respectively) compared to the control (20.5 ± 0.1 μM) (Fig. 24b). Among the compounds tested, compound **18** exhibited the strongest inhibition in a dose-dependent manner.

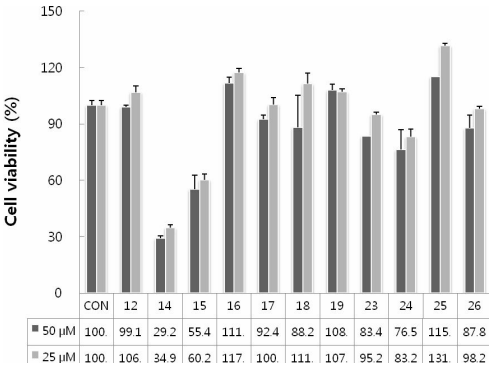

(a)

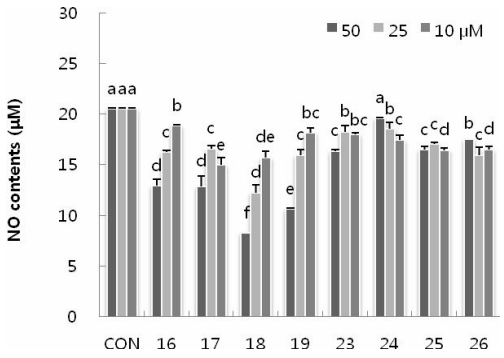

(b)

Figure 24. Effects of compounds **12**, **14-19** and **23-26** isolated from *Vitex rotundifolia* on cell viability as determined by MTT assay (a) and effects of compounds **16-19** and **23-26** on nitric oxide production (expressed as nitrite) (b) in LPS-induced Raw 264.7 cells.

[a-f] Means with the different letters at the same concentration are significantly different ($p < 0.05$) by Duncan's multiple range test. Values are means ± SD (n=3).

3.6.2. Scavenging Effects of Compounds **16-19** and **23-26** on Reactive Oxygen Species (ROS)

ROS-scavenging effects of compounds **16-19** and **23-26** were examined using DCFH-DA. DCF fluorescence intensity was found to decrease in dose- and time-dependent manners in the presence of these compounds, as shown in Fig. 25. Most of the compounds were significantly effective at a concentration of 50 μM. In particular, compounds **16-18** and **23** showed stronger ROS-scavenging activity than did the others.

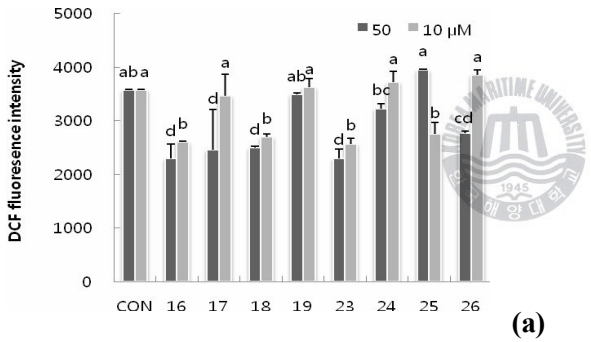

(a)

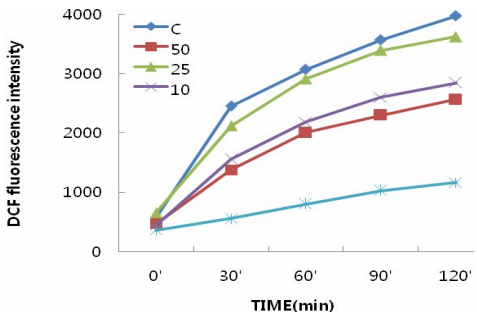

(b) compound 16

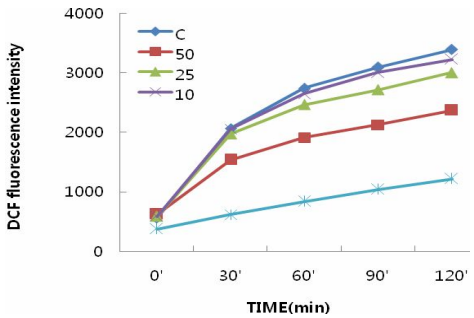

(c) compound 17

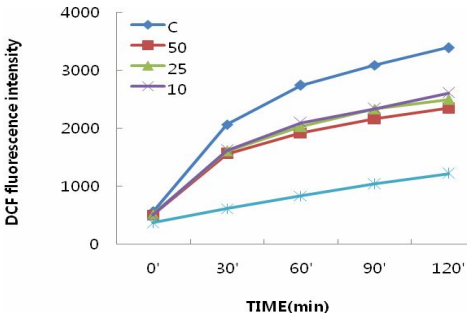

(d) compound 18

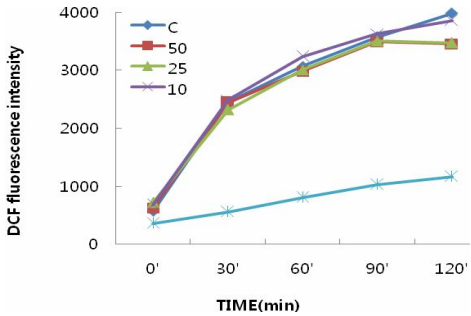

(e) compound 19

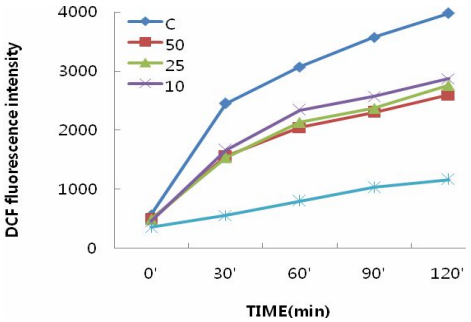

(f) compound 23

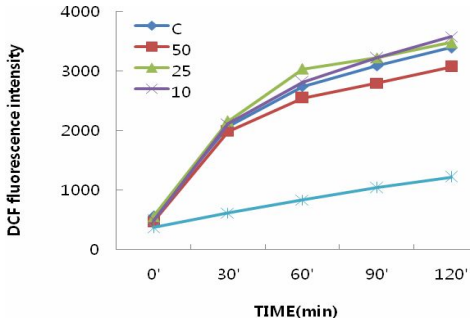

(g) compound 24

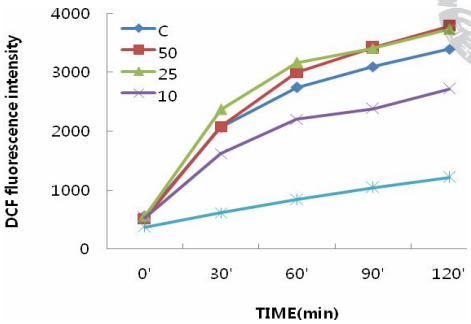

(h) compound 25

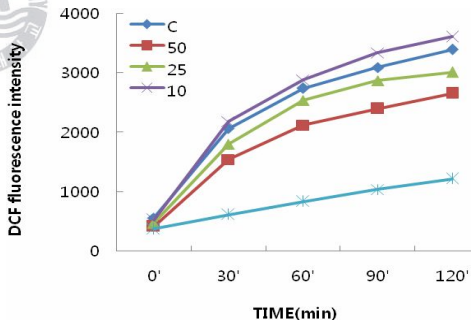

(i) compound 26

Figure 25. Effects of compounds **16-19** and **23-26** isolated from *Vitex rotundifolia* on intracellular ROS levels induced by hydrogen peroxide in Raw 264.7 cells. The cells were incubated with different concentrations (50 and 10 μM) of the compounds **16-19** and **23-26** for 90 min (a) and with compounds **16-19** and **23-26** for the indicated times (b-i), respectively. DCF fluorescence was measured at $\lambda_{excitation}$=485 nm and $\lambda_{emission}$=528 nm.

[a-d] Means with the different letters at the same concentration are significantly different (p < 0.05) by Duncan's multiple range test. Values are means ± SD (n=3).

3.6.3. Measurement of Intracellular Glutathione (GSH) Levels in the Presence of Compounds **16-19** and **23-26**

Intracellular GSH levels of compounds **16-19** and **23-26** were investigated using the monobromobimane assay. At a concentration of 50 μM, GSH levels increased in cells treated with compound **19**, but the magnitude of increase of GSH level was not particularly great. There were no other significant differences in the GSH levels in cells pretreated with the other compounds (Fig. 26).

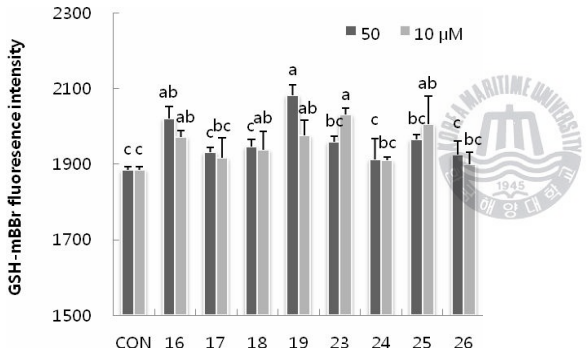

Figure 26. Effects of compounds **16-19** and **23-26** isolated from *Vitex rotundifolia* on regulation of GSH levels in Raw 264.7 cells. The cells were incubated with different concentrations (100 and 10 μM) of the compounds **16-19** and **23-26** for 90 min. Cellular GSH levels were determined using mBBr as a thiol-staining reagent according to the method described in the text measuring mBBr-GSH fluorescence intensity at λexcitation=360 nm and λemission =465 nm.

[a-c] Means with the different letters at the same concentration are significantly different ($p < 0.05$) by Duncan's multiple range test. Values are means ± SD (n=3).

3.6.4. Anti-inflammatory Effects of Compounds **16-19** and **23-26**

Effects of compounds **16-19** and **23-26** on the expression of iNOS and COX-2 genes were further examined by RNA extraction and RT-PCR analysis. Upon exposure to 1 μg/mL LPS, the expression levels of iNOS and COX-2 mRNA increased in comparison with untreated cells (blank) as shown in Fig. 27. Pretreatment with compounds **16-19** and **23-26** for 1hr before LPS treatment significantly inhibited the expression of iNOS and COX-2 genes ($p < 0.05$). Among these, mRNA expression levels of iNOS were more noticeably decreased in response to compounds **17**, **19**, **23** and **24** at rates of 41%, 33%, 42% and 32%, respectively, compared to the others, even at a concentration of 10 μM (Fig. 27a). On the other hand, compounds **16**, **18**, **19** and **24** at a concentration of 50 μM showed strong down-regulation of COX-2 expression to 7%, 14%, 20% and 15% mRNA levels, respectively (Fig. 27b). These data implied that the inhibitory effects of compounds on iNOS and COX-2 genes could be closely related with inhibition of nitric oxide and ROS in stimulated macrophages.

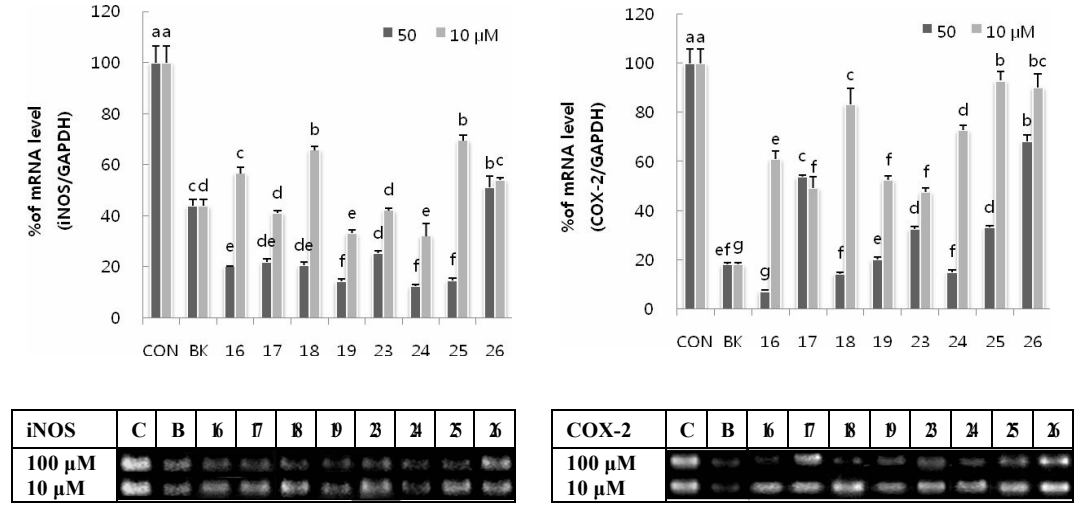

Figure 27. Effects of compounds **16-19** and **23-26** isolated from *Vitex rotundifolia* on mRNA levels of iNOS (a) and COX-2 (b) in LPS-stimulated Raw 264.7 cells. Cells were incubated with compounds for 48 h, then total RNA was isolated and RT-PCR was performed using the indicated primers. The amplified PCR products were run in 1% agarose gel and visualized by EtBr staining. GAPDH was used as a housekeeping control gene.

[a-g] Means with the different letters at the same concentration are significantly different ($p < 0.05$) by Duncan's multiple range test. Values are means ± SD (n=3).

Conclusions

In recent years, there has been much interest and research into the influence of natural products on several diseases, including aging-related illness, cancer, neurodegenerative disease, and cardiovascular disease. Recent epidemiological studies have suggested that dietary pattern is commonly associated with the risk of chronic diseases (Hu, 2002). This association may be attributed to the presence of natural chemo-preventers, such as vitamins, polyphenols, and flavonoids, which prevent free radical damage (Park and Pezzuto, 2002; Jung *et al*., 2004; Lee *et al*., 2004; Seo *et al*., 2004; Lee and Seo, 2006; Stan *et al*., 2008). Oxygen free radicals, or reactive oxygen species (ROS) and reactive nitrogen species (RNS), are products of normal cellular metabolism. ROS and RNS are well recognized for playing a dual role as both deleterious and beneficial species (Valko *et al*., 2007). Usually, antioxidants defend against the harmful effects of these naturally occurring free radicals. However, excessive production of ROS/RNS may lead to oxidative stress, which damages normal cellular function and ultimately induces apoptosis or necrosis (Nordberg and Arnér, 2001; Gomes *et al*., 2005). Therefore, oxidative stress by ROS/RNS may be the direct or indirect cause of many human diseases such as aging, cancer, atherosclerosis, and inflammation.

For these reasons, interest has considerably increased in searching for naturally occurring chemopreventive agents to replace synthetic materials, many of which are prohibited due to their carcinogenicity (Sasaki *et al*., 2002). Therefore, natural chemopreventive agents isolated from plants and marine algae represent the most

useful and as yet unmined source of material for disease prevention (Park and Pezzuto, 2002; Jung *et al*., 2004; Lee *et al*., 2004; Seo *et al*., 2004; Lee and Seo, 2006; Stan *et al*., 2008).

In the present study, *Corydalis heterocarpa* and *Vitex rotundifolia*, which are salt-tolerant plants and which have been used traditionally as a folk medicine, were investigated for their bioactive constituents.

The investigation of these two salt marsh plants provided eleven compounds, including two new compounds, from *C. heterocarpa* and nineteen compounds, including five new compounds, from *V. rotundifolia*. The chemical structures of the two new compounds **4** and **6** from *C. heterocarpa* were established as (2'*S*,7'*S*)-*O*-(2-methylbutanoyl)-columbianetin and (2'*S*)-columbianetin-3'-hydrogen sulfate. Five new compounds **20** and **23**-**26** from *V. rotundifolia* were determined as (5*S**,6*R**,8*R**,9*R**,10*S**)-6-acetoxy-9-hydroxy-16-hydroxy-13(14)-labden-16,15-olide, 3α-hydroxy pleuroziol, 9α*H*-manoyl oxide, abieta-11(12)-ene-9α,13α-endoperoxide, and abieta-11(12)-ene-9β,13β-endoperoxide. The NMR spectral data of the new compounds were completely assigned by a combination of 1D/2D NMR experiments including ^{1}H–^{1}H gDQCOSY, TOCSY, DEPT, gHMQC and gHMBC correlations.

The nine known compounds from *C. heterocarpa* were identified as (2'*S*)-columbianetin (**1**), libanoridin (**2**), cnidiadin (**3**), (2'*S*)-columbianetin-*O*-β-D-glucopyranoside (**5**), isopimpinellin (**7**), hyunganol Ⅱ (**8**), cnidimol A (**9**),

cnidimoside A (**10**) and 2,3-dihydro-4-hydroxy-7-methyl-2-isopropenyl-5H-furo[3,2g][1] benzopyran-5-one (**11**).

The fourteen known compounds from *V. rotundifolia* were identified as luteolin (**12**), quercetin 3,7-dimethyl ether (**13**), vitexicarpin (**14**), artemetin (**15**), vitetrifolin F (**16**), vitetrifolin E (**17**), vitetrifolin D (**18**), vitexilactone (**19**), (5*S**,6*R**,8*R**,9*R**,10*S**)-6-acetoxy-9-hydroxy-15-methoxy-13(14)-labden-16,15-olide (**21**), aurantiamide (**22**), abieta-9(11):12(13)-di-α-epoxide (**27**), ferruginol (**28**), β-amyrenone (**29**) and α-amyrenone (**30**) by a combination of spectroscopic analysis and by comparison with the data reported in the literature.

Potential inhibitory activity of the isolated compounds against human cancer cells was evaluated by MTT assay and mRNA expression of several factors related to apoptosis. In comparative analysis, the AGS human cancer cell line was the most sensitive to the antiproliferative effect of all of the isolated compounds.

Among compounds isolated from *C. heterocarpa*, compounds **2**, **5**, **6** and **11** showed strong growth inhibitory effects against human cancer cells in a dose-dependent manner ($p < 0.05$). The antiproliferative effect of new compound **6** was the highest among all compounds tested. These effects may be caused by modulation of apoptosis through the Bax and Bcl-2 dependent pathway and may also be related to the significant up-regulation of p53 and p21 seen in response to treatment with salt marsh plant secondary metabolites.

The antiproliferative effects of compounds **12**, **14** and **15** isolated from *V. rotundifolia* were compared with the control by MTT assay. Among the tested

compounds, **14** exhibited the highest inhibitory activity in the AGS cells. At the gene expression levels, it strongly down-regulated Bcl-2 level and up-regulated p53 and p21 levels.

The antioxidant activity of the compounds was evaluated by four different activity tests, including measurement of intracellular NO, ROS, GSH, and mRNA expression of iNOS and COX-2. Compounds **1-6** isolated from *C. heterocarpa* obviously decreased production of NO and ROS, increased production of GSH, and inhibited both iNOS and COX-2 expressions under LPS-stimulated condition. Compounds **2-4** in particular consistently exhibited higher antioxidant effects compared to the other compounds.

In the cases of compounds **12**, **14-19** and **23-26** isolated from *V. rotundifolia*, compounds **16-19** remarkably suppressed NO production while compounds **16-18** and **23** showed strong ROS-scavenging effects. However, there were no significant effects on GSH levels. The expression levels of iNOS and COX-2 were down-regulated by compounds **16-19**, **23** and **24**. On the basis of these above results, these compounds may be useful candidates as antioxidant sources for treatment of oxidative damage caused by reactive species in macrophage cells.

Although further studies are needed to confirm these observations, the current study suggests that compounds isolated from *C. heterocarpa* and *V. rotundifolia* may be used to reduce human cancer risk, and that their antiproliferative effects are partly related to induction of several genes related to apoptosis, including Bax, Bcl-2, p53, and p21. In addition, these compounds may be used to retard oxidative

destruction by reactive species and thus reduce the risk of many diseases that involve oxidative stress, such as aging, cancer, diabetes mellitus, neurological disorders, renal disorders, and hypertension.

Therefore, the two salt marsh plants examined here, *C. heterocarpa* and *V. rotundifolia,* may be beneficial natural sources of valuable chemopreventive agents and may also contribute to the reduction of risks of cancer and other oxidation-related diseases.

Acknowledgement (감사의 글)

나는 8 월의 한 그루 나무입니다
비옥한 땅에 깊게 뿌리를 박은 강한 나무입니다
한아름 큰 둘레의 기둥을 가진 곧은 나무입니다
푸른 하늘을 향해 가지를 뻗은 밝은 나무입니다
강한 햇살을 듬뿍 받은 푸른 잎의 나무입니다
다가올 계절에 단 열매를 맺을...
나는 나무입니다.

한 여름의 나무 한 그루가 홀로서기를 하려 합니다. 갚진 열매를 맺기 위해 한 발 나아가고자 합니다. 나무가 열매를 맺는 건 혼자만의 힘이 아니란 것을 압니다. 푸른 잎처럼 많은 가르침과 앎을 주셨기에 가능한 것입니다. 무수히 뻗은 가지처럼 저에게 손 내밀어 준 고마운 벗들이 있었기에 세찬 비바람도 견딜 수 있었습니다. 한국해양대학교 해양환경생명과학부라는 든든한 기둥이 버팀목이 되어주었기에 우뚝 자리할 수 있었습니다. 그리고 무엇보다 기름진 땅에 마음의 뿌리를 두도록 해주신 가족이 있었기에 제가 이 땅에 서 있는 것입니다. 첫 앓이를 하기 전 나무의 주위를 둘러보며 인사 드립니다.
누구보다 크고 넓은 마음으로 부족한 저 끝까지 이끌어 주신 서영완 교수님.. 마지막까지 꼼꼼히 많은 가르침 주신 안종웅, 임선영, 박희연, 오현철 선생님께 진심으로 고개 숙여 감사 드립니다.
한국해양대학교는 10 년간 저의 집이였습니다. 가족과 같은 사랑으로 만났던 많은 분들이 생각납니다. 해양환경생명과학부의 든든한 교수님들, 부족한 선배를 믿고 따라준 착하고 믿음직한 후배들.. 특히 생유기신소재연구실 우리 동생들.. 그리고 선배가 없는 저에게 누구보다 큰 선배가 되어주신 공창숙 박사님.. 지칠 때마다 많은 힘이 되었고 큰 사랑 가지고 갑니다. 고맙습니다.
내가 살아가는 이유이자 희망인 우리 가족. 큰 딸 항상 믿어주시는 그 마음에 보답하겠습니다. 그 누구보다 존경하고 사랑합니다.
마지막으로 내 곁을 지켜주는 우리 님에게 고맙다는 말을 전합니다.
해마다 피고 지며 인생을 반복하겠지만 처음이 되기까지의 모습들을 잊지 않겠습니다. 나무가 마지막 열매를 맺는 그날까지 언제나처럼 저의 힘이 되어 주십시오.

References

Ahmad, V.U., Khan, M.A., Baqai, F.T. and Tareen, R.B. (1995) Santoflavone, a 5-Deoxyflavonoid from *Achillea santolina*. *Phytochemistry* **38**, 1305-1307.

Almqvist, S.O., Enzell, C.R. and Wehrli, F.W. (1975) Carbon-13 NMR Studies of Labdane Diterpenoids. *Acta. Chem. Scand*. **29**, 695-702.

Ames, B.N., Shigenaga, M.K. and Hagen, T.M. (1993) Oxidants, Antioxidants, and the Degenerative Diseases of Aging. *Proc. Natl. Acad. Sci.* **90**, 7915-7922.

Anthonsen, T. and Bergland, G. (1973) Constituents of Solidago Species. III. The Constitution and Stereochemistry of Diterpenoids from *Solidago missouriensis* Nutt. **27**, 1073-1082.

Antonsson, B. (2001) Bax and Other Pro-apoptotic Bcl-2 Family "killer-proteins" and Their Victim the Mitochondrion. *Cell Tissue Res*. **306**, 347-361.

Arató, E., Kürthy, M., Jancsó, G., Sínay, L., Kasza, G., Verzár, Z., Benko, L., Cserepes, B., Kollár, L. and Roth, E. (2006) Oxidative Stress and Leukocyte Activation after Lower Limb Revascularization Surgery. *Magy. Seb*. **59**, 50-57.

Asakawa, Y., Lin, X., Tori, M. and Kondo, K. (1990) Fusicoccane-, Dolabellane- and Rearranged Labdane-type Diterpenoids from the Liverwort *Pleurozia gigantean*. *Phytochemistry* **29**, 2597-2603.

Aslan, M., Cort, A. and Yucel, I. (2008) Oxidative and Nitrative Stress Markers in Glaucoma. *Free Radical Bio. Med.* **45**, 367-376.

Awale, S., Nakashima, E.M.N., Kalauni, S.K., Tezuka, Y., Kurashima, Y., Lu, J., Esumi, H. and Kadota, S. (2006) Angelmarin, a Novel Anti-cancer Agent able

to Elimiate the Tolerance of Cancer Cells to Nutrient Starvation. *Bioorg. Med. Chem. Lett*. **16**, 581-583.

Baba, K., Kawanishi, H., Taniguchi, M. and Kozawa, M., (1992) Chromones from *Cnidium monnieri*. *Phytochemistry* **31**, 1367-1370.

Baba, K., Kawanishi, H., Taniguchi, M. and Kozawa, M., (1994) Chromone Glucosides from *Cnidium japonicum*. *Phytochemistry* **35**, 221-225.

Bandopadhyay, M., Pardeshi, M.P. and Seshadri, T.R. (1974) Synthesis of Some Naturally Occurring Coumarins. *Indian J. Chem*. **12**, 23-25.

Banerji, A. and Ray, R. (1981) Aurantiamides: A New Class of Modified Dipeptides from *Piper aurantiacum*. *Phytochemistry* **20**, 2217-2220.

Bang, M.A., Kim, H.A. and Cho, Y.J. (2002) Hypoglycemic and Antioxidant Effect of Dietary Hamcho Powder in Streptozotocin-induced Diabetic Rats. *J. Korean Soc. Food Sci. Nutr.* **31**, 840-846.

Bower, C.L. and Rowe, J.W. (1967) Extractives of Jack Pine Bark: Occurrence of (+)-13-Epimanoyl Oxide and Related Labdanes Diterpenes. *Phytochemistry* **6**, 151-153.

Chamy, M.C., Piovano, M., Garbarino, J.A., Pascard, C. and Cesario, M. (1993) Endoperoxide Diterpenes from *Calceolaria purpurea*. *Phytochemistry* **34**, 1103-1106.

Chang, S.T., Cheng, S.S. and Wang, S.Y. (2001) Antitermitic Activity of Essential Oils and Components from Taiwania (*Taiwania cryptomerioides*). *J. chem.. ecol.* **27**, 717-724.

Chen, Y., Hsu, K., Tsai, J., Hung, C., Kuo, T. and Chen, Y. (2005) Involvement of Protein Kinase C in the Inhibition of Lipopolysaccharide-induced Nitric Oxide Production by Thapsigargin in RAW 264.7 Macrophages. *Int. J. Biochem. Cell B.* **37**, 2574-2585.

[a]Cheng, Y.S. and Rudloff, E. (1970) Two New Diterpenoid Oxides from the Leaf Oil of Chamaecyparis Nootkatensis. *Tetrahedron Lett*. **14**, 1131-1132.

[b]Cheng, Y.S. and Rudloff, E. (1970) The Volatile Oil of the Leaves of *Chamaecyparis nootkatensis*. *Phytochemistry* **9**, 2517-2527.

Choi, S.U., Baek, N.I., Kim, S.H., Yang, J.H., Eun, J.S., Shin, T.Y., Lim, J.P., Lee, J.H., Jeon, H., Yun, M.Y., Leem, K.H., Park, H.W. and Kim, D.K. (2007) Cytotoxic Isoquinoline Alkaloids from the Aerial Parts of *Corydalis incise*. *Arch. Pharm. Res.* **30**, 151-154.

Curtin, J.F., Donovan, M. and Cotter, T.G. (2002) Regulation and Measurement of Oxidative Stress in Apoptosis. *J. Immunol. Methods* **265**, 49-72.

Deveraux, Q.L. and Reed, J.C. (1999) IAP Family Proteins Suppressors of Apoptosis. *Genes Dev.* **13**, 239-252.

Dröge, W. (2002) Free Radicals in the Physiological Control of Cell Function. *Physiol. Rev.* **82**, 47-95.

Elgmal, M.H.A., Elewa, N.H., Elkhrisy, E.A.M. and Duddck, H. (1979) ^{13}C NMR Chemical Shift and Carbon Proton Coupling Constants of Some Furocoumarins and Furochromones. *Phytochemistry* **18**, 139-143.

Ferreira, D.T., Silva, R.B., Oliveira, A.B., Isobe, M. and Braz-Filho, R. (1995) Dipeptide from the Roots of *Zeyhera digitalis*. *J. Braz. Chem. Soc*. **6**, 323-326.

Flowers, T.J., Troke, P.F. and Yeo, A.R. (1977) The Mechanism of Salt Tolerance in Halophytes. *Annu. Rev. Plant Physiol*. **28**, 89-121.

Garcea, G., Neal, C.P., Pattenden, C.J., Steward, W.P. and Berry D.P. (2005) Molecular Prognostic Markers in Pancreatic Cancer: A systematic review. *Eur. J. Cancer* **41**, 2213-2236.

Gartel, A.L. and Tyner, A.L. (2002) The Role of the Cyclin-dependent Kinase Inhibitor p21 in Apoptosis. *Mol. Cancer Ther.* **1**, 639-649.

Gomes, A., Fernandes, E. and Lima, J. (2005) Fluorescence Probes Used for Detection of Reactive Oxygen Species. *J. Biochem. Bioph. Meth*. **65**, 45-80.

Green, L.C., Wagner, D.A., Logowski, G.J., Skipper, P.L., Wishnok, J.S. and Tannenbaum, S.R. (1982) Analysis of Nitrate, Nitrite, and [15N] Nitrate in Biological Fluids. *Anal.l Biochem.* **126**, 131-138.

Han, S.K., Kim, S.M. and Pyo, B.S. (2003) Antioxidative Effect of Glasswort (*Salicornia herbacea* L.) on the Lipid Oxidation of Pork. *Korean J. Food Sci. Ani. Resour.* **23**, 46-49.

Hansen, M.B., Nielsen, S.E. and Berg, K. (1989) Re-examination and Further Development of a Precise and Rapid Dye Method for Measuring Cell Growth/ Cell Kill. *J. Immunol. Meth.* **119**, 203-210.

Hao, X.J., Yang, X.S., Zhang, Z. and Shang, L.J. (1995) Clerodane Diterpenes from *Polyalthia cheliensis*. *Phytochemistry* **39**, 447-448.

Hata, K., Kozawa, M. and Baba, K. (1972) Coumarins from Chinese Crude Drug "She Huangzi," the Fruits of *Cnidium* sp. and *from Cnidium japonicum* Mrq. *Yakugaku Zasshi* **92**, 1289-1294.

Hoberg, E., Orjala, J., Meier, B. and Sticher, O. (1999) Diterpenoids from the Fruits of *Vitex agnus-castus*. *Phytochemistry* **52**, 1555-1558.

Humberto, M.M.S., Nascimento, M.C.B.S. and Sant'Ana, A.E.G. (2004) Pentacyclic Triterpene 5-Phenylpenta-2,4-dienoyl Esters from *Peltastes peltatus* (Vell.) Woodson. *Phytochem. Anal*. **15**, 339-344.

Hu, F.B. (2002) Dietary Pattern Analysis: A New Direction in Nutritional Epidemiology. *Current Opinion in Lipidology* **13**, 3-9.

Iinuma, M., Matsuura, S. and Kusuda, K. (1980) ^{13}C-Nuclear Magnetic Resonance (NMR) Spectral Studies on Polysubstituted Flavonoids. I. ^{13}C-NMR Spectra of Flavones. *Chem. Pharm. Bull.* **28**, 708-716.

Ishii, H., Hosoya, K., Ishikawa, T. and Haginiwa, J. (1974) Studies on the Chemical Constituents of Rutaceous Plants. ⅩⅩ. The Chemical Constituents of *Xanthoxylum arnottianum* Maxim (1). Isolation of the Chemical Constituents of the Xylem of Roots. *Yakugaku Zasshi* **94**, 309-321.

Isshiki, K., Asai, Y., Tanaka, S., Nishio, M., Uchida, T., Okuda, T., Kamatsubara, S. and Sakurai, N. (2001) Aurantiamide Acetate, a Selective Cathepsin Inhibitor, produced by *Aspergillus penicilloides*. *Biosci. Biotechnol. Biochem.* **65**, 1195-1197.

Jemal, A., Siegel, R., Ward, E., Hao, Y., Xu, J., Murray, T. and Thun, M.J. (2008) Cancer Statistics. *CA Cancer J Clin.* **58**, 71-96.

Jo, Y.C., Ahn, J.H., Chon, S.M., Lee, K.S., Bae, T.J. and Kang, D.S. (2002) Studies on Pharmacological Effects of Glasswort (*Salicornia herbacea* L.). *Korean J. Medicinal Crop Sci.* **10**, 93-99.

Jung, H.A., Lee, H.J., Kim, Y.A., Park, K.E., Ahn, J.W., Lee, B.J., Moon, S.G. and Seo. Y. (2004) Antioxidant Activity of *Artemisia capillaries* Thunberg. *Food sci. Biotechnol*. **13**, 328-331.

Kawazoe, K., Yutani, A. and Takaishi, Y. (1999) Aryl Naphthalenes Norlignans from *Vitex rotundifolia*. *Phytochemistry* **52**, 1657-1659.

Key, T.J., Allen, N.E., Spencer, E.A. and Travis, R.C. (2002) The Effect of Diet on Risk of Cancer. *Lancet* **360**, 861-868.

Kirschvink, N., Moffarts, B. and Lekeux P. (2008) The Oxidant/Antioxidant Equilibrium in Horses. *The Veterinary Journal* **177**, 178-191.

Ko, W.G., Kang, T.H., Lee, S.J., Kim, N.Y., Kim, Y.C., Sohn, D.H. and Lee, B.H. (2000) Polymethoxy-avonoids from *Vitex rotundifolia* Inhibit Proliferation by Inducing Apoptosis in Human Myeloid Leukemia Cells. *Food Chem. Toxicol*. **38**, 861-865.

Ko, W.G., Kang, T.H., Lee, S.J., Kim, Y.C. and Lee, B.H. (2001) Rotundifuran, A Labdane Type Diterpene from *Vitex rotundifolia*, Induces Apoptosis in Human Myeloid Leukaemia Cells. *Phytother. Res*. **15**, 535-537.

Kondo, Y., Sugiyama, K. and Nozoe, S. (1986) Studies on the Constituents of *Vitex rotundifolia* L. fil. *Chem. Pharm. Bull.* **34**, 4829-4832.

Kong, C.-S., Um, Y.R., Lee, J.I., Kim, Y.A., Lee, J.-S. and Seo, Y. (2008) Inhibition Effects of Extracts and Its Solvent Fractions Isolated from *Limonium tetragonum* on Growth of Human Cancer Cells. *Korean J. Biotechnol. Bioeng.* **23**, 177-182.

La Vecchia, C. and Bossetti, C. (2006) Diet and Cancer Risk in Mediterranean Countries: Open Issues. *Public Health Nutr* **9**, 1077-1082.

Lee, H.J., Kim, Y.A., Ahn, J.W., Lee, B.J., Moon, S.G. and Seo. Y. (2004) Screening of Peroxynitrite and DPPH Radical Scavenging Activities from Salt Marsh Plants. *Korean J. Biotechnol. Bioeng*. **19**, 57-61.

Lee, H.J. and Seo, Y. (2006) Antioxidant Properties of *Erigeron annuus* Extract and Its Three Phenolic Constituents. *Biotechnol. Bioprocess Eng*. **11**,13-18.

Lee, J.O., Choi, S.Y., Park, N.S., Shim, Y.S., Yoo, S.Y., Lee, J.I., Lee, E.D. and Chin, S.Y. (1996) Statistical Analysis on Cancer Patients of Korea Cancer Center Hospital. *J Korean Cancer* **28**, 336-349.

Lee, Y.N. (2002) Flora of Korea, Kyo-Hak Publishing Co. Ltd., p 241(711), 666(2100).

Lemmich, E., Lemmich, J. and Nielsen, B.E. (1970) Constituents of Umbelliferous Plants. ⅩⅣ. Coumarins of *Peucedanum oreoselinum* (L.) Moench. *Acta Chem. Scand*. **24**, 2893-2900.

Lemmich, J., Peersen, P.A. and Nielsen, B.E. (1971) Constituents of Umbelliferous Plants. ⅩⅧ. Terpenoids and Coumarins of the Root of *Ligusticum seguieri* Koch. *Acta Chem. Scand*. **25**, 344-346.

Lenis, L.A., Ferreiro, M.J., Debitus, C., Jiménez, C., Quiñoá, E. and Riguera, R. (1998) The Unusual Presence of Hydroxylated Furanosesquiterpenes in the Deep Ocean Tunicate *Ritterella rete*. Chemical Interconversions and Absolute Stereochemistry. *Tetrahedron* **54**, 5385-5406.

Liu, Y.H., Lin, S.Y., Lee, C.C. and Hou, W.C. (2008) Antioxidant and Nitric Oxide Production Inhibitory Activities of Galacturonyl Hydroxamic Acid. *Food Chem.* **109**, 159-166.

Loizzo, M.R., Said, A., Tundis, R., Rashed, K., Statti, G.A., Hufner. A. and Menichini1, F. (2007) Inhibition of Angiotensin Converting Enzyme (ACE) by Flavonoids Isolated from *Ailanthus excelsa* (Roxb) (Simaroubaceae). *Phytother. Res.* **21**, 32-36.

Lu, H., Hu, J., Zhang, L.X. and Tan R.X. (1999) Bioactive Constituents from *Pteris multifida*. *Planta Med.* **65**, 586-587.

Ma, W.G., Fukushi, Y. and Tahara, S. (1999) Fungitoxic Alkaloids from Hokkaido *Corydalis* species. *Fitoterapia* **70**, 258-265.

Mangialasche, F., Polidori, M.C., Monastero, R., Ercolani, S., Camarda, C., Cecchetti, R. and Mecocci, P. (2009) Biomarkers of Oxidative and Nitrosative Damage in Alzheimer's Disease and Mild Cognitive Impairment. *Ageing Res. Rev.* **xxx**, xxx-xxx.

Masuda, T., Takasugi, M. and Anetai, M. (1998) Psoralen and Other Linear Furanocoumarins as Phytoalexins in *Glehnia littoralis*, *Phytochemistry* **47**, 13-16.

Mchale, D., Khopkar, P.P. and Sheridan, J.B. (1987) Coumarin Glycosides from *Citurs* Flavedo. *Phytochemistry* **26**, 2547-2549.

Min, B.M. (1998) Vegetation on the West Coast of Korea, *Ocean Reserch* **20**, 167-178.

Ministry of Environment (2006) Development of Ecological Conservation and Management Techniques of Halophye Communities on Salt Marshes of Southwestern coast in Korea. *Ministry of Environment* GOVP1200710847.

Mitchell, S.C. and Waring, R.H. (1978) Detection of Inorganic Sulphate and Other Anions on Paper and Thin-layer Chromatograms. *J. Chroma.* **166**, 341-343.

Miyashita, T., Krajewki, S., Kragewska, M., Wang, H.G., Lin, H.K., Liebermann, D.A., Hoffman, B. and Reed, J.C. (1994) Tumor Suppressor p53 is a Regulator of Bcl-2 and Bax Gene Expression *in vitro* and *in vivo*. *Oncogene* **9**, 1799-1805.

Moll, U.M., Wolff, S., Speidel, D. and Deppert, W. (2005) Transcription-independent Pro-apoptotic Functions of p53. *Curr. Opin. Cell Biol.* **17**, 631-636.

Morikawa, T., Matsuda, H., Nishida, N., Qugushi, T. and Yoshikawa, M. (2004) Structures of New Aromatics Glycosides from a Japanese Folk Medicine, the Roots of *Angelica furcijuga*. *Chem. Pharm. Bull.* **52**, 1387-1390.

Morse, M.A. and Stoner, G.D. (1993) Cancer Chemoprevention: Principles and Prospects. *carcinogenesis* **14**, 1737-1746.

Nordberg, J. and Arnér, E.S.J. (2001) Reactive Oxygen Species, Antioxidants, and the Mammalian Thioredoxin System. *Free Radical Bio. Med.* **31**, 1287-1312.

Okimoto, Y., Watanabe, A., Niki, E., Yamashita, T. and Noguchi, N. (2000) A Novel Fluorescent Probe Diphenyl-1-pyrenylphosphine to Follow Lipid Peroxidation in Cell Membranes. *FEBS Lett*. **474**, 137-140.

Ono, M., Ito, Y., Kubo, S. and Nohara, T. (1997) Two New Iridoids from Viticis trifoliae Fructus (Fruit of *Vitex rotundifolia* L.) *Chem. Pharm. Bull.* **45**, 1094-1096.

Ono, M., Ito, Y. and Nohara, T. (1998) A Labdane Diterpene Glycoside from Fruit of *Vitex rotundifolia*. *Phytochemistry* **48**, 207-209.

[a]Ono, M., Ito, Y. and Nohara, T. (2001) Four New Halimane-Type Diterpenes, Vitetrifolins D–G, from the Fruit of *Vitex trifolia*. *Chem. Pharm. Bull.* **49**, 1220-1222.

Ono, M., Sawamura, H., Ito, Y., Mizuki, K. and Nohara, T. (2000) Diterpenoids from the Fruits of *Vitex trifolia*. *Phytochemistry* **55**, 873-877.

Ono, M., Yamamoto, M., Masuoka, C., Ito, Y., Yamashita, M. and Nohara, T. (1999) Diterpenes from the Fruits of *Vitex rotundifolia*. *J. Nat. Prod.* **62**, 1532-1537.

[b]Ono, M., Yamamoto, M., Yanaka, T. Ito, Y. and Nohara, T. (2001) Ten New Labdane-Type Diterpenes from the Fruit of *Vitex rotundifolia*. *Chem. Pharm. Bull.* **49**, 82-86.

Ono, M., Yanaka, T., Yamamoto, M., Ito, Y. and Nohara, T. (2002) New Diterpenes and Norditerpenes from the Fruits of *Vitex rotundifolia*. *J. Nat. Prod.* **65**, 537-541.

Park, E.J. and Pezzuto, J.M. (2002) Botanicals in Cancer Chemoprevention. *Cancer Metas. Rev.* **21**, 231-255.

Patel, R.P., McAndrew, J., Sellak, H., White, C.R., Jo, H., Freeman, B.A. and Darley-Usmar, V.M. (1999) Biological Aspects of Reactive Nitrogen Species. *Biochim. Biophys. Acta*. **1411**, 385-400.

Pauly, N., Pucciariello, C., Mandon, K., Innocenti, G., Jamet, A., Baudouin, E., Herouart, D., Frendo, P. and Puppo, A. (2006) Reactive Oxygen and Nitrogen Species and Glutathione: Key Players in the Legume–*Rhizobium* Symbiosis. *J. Exp. Bot.* **57**, 1769-1776.

Poot, M., Verkerk, A., Koster, J.F. and Jongkind, J.F. (1986) De Novo Synthesis of Glutathione in Human Fibroblasts During in vitro Ageing and in Some Metabolic Diseases as Measured by a Flow Cytometric Method. *Biochim. Biophys. Acta*. **883**, 580-584.

Rahman, A.U., Ahmed, D., Choudhary, M.I., Turkoz, S. and Sener, B. (1988) Chemical Constituents of *Buxus sempervirens*. *Planta med*. **54**, 173-174.

Reiter, R.J., Tan D.X. and Burkhardt, S. (2002) Reactive Oxygen and Nitrogen Species and Cellular and Organismal Decline: Amelioration with Melatonin. *Mech. of ageing Dev.* **123**, 1007-1019.

Rock, C.L. (2003) Diet and Breast Cancer: Can Dietary Factors Influence Survival? *J. Mammary Gland Biol.* **8**, 119-132.

Roos, W.P. and Kaina, B. (2006) DNA Damage-induced Cell Death by Apoptosis. *Trends Mol. Med.* **12**, 440-450.

Roy, N., Deveraux, O.L., Takahashi, R., Salvesen, G.S. and Reed, J.C. (1997) The c-IAP-1 and c-IAP-2 Proteins are Direct Inhibitors of Specific Caspases. *EMBO J.* **16**, 6914-6925.

Sadhu, S.K., Okuyama, E. Fujimoto, H., Ishibashi, M. and Yesilada, E. (2006) Prostaglandin Inhibitory and Antioxidant Components of *Cistus laurifolius*, a Turkish Medicinal Plant. *J. Ethnopharmacol*. **108**, 371-378.

Sakurai, A., Okamoto, Y., Kokubo, S. and Chida, A. (1999) Abietane-type Diterpenoids from the Fruit of *Vitex Rotundifolia* L. fil. *Nippon Kagaku Kaishi* **3**, 207-211.

Sasaki, Y.F., Kawaguchi, S., Kamaya, A., Ohshita, M., Kabasawa, K., Iwama, K., Taniguchi, K. and Tsuda, S. (2002) The Comet Assay with 8 Mouse Organs: Results with 39 Currently Used Food Additives. *Mutat. Res*. **519**, 103-109.

Seo, S., Tomita, Y. and Tori, K. (1975) Carbon-13 NMR Spectra of Urs-12-enes and Application to Structural Assignments of Components of *Isodon japonicus* Hara Tissue Cultures. *Tetrahedron Letters* **1**, 7-10.

Seo, S., Tomita, Y. and Tori, K. (1981) Biosynthesis of Oleanene- and Ursene-Type Triterpenes from [4-^{13}C] Mevalonolactone and [1,2-$^{13}C_2$] Acetate in Tissue Cultures of *Zsodon japonicus* Hara. *J. Am. Chem. Soc*. **103**, 2075-2080.

Seo, Y., Lee, H.J., Kim, Y.A., Youn, H.J. and Lee, B.-J. (2005) Effects of Several Salt Marsh Plants on Mouse Spleen and Thymus Cell Proliferation using MTT Assay. *Ocean Science Journal* **40**, 209-212.

Seo, Y., Lee, H.J., Park, K.E., Kim, Y.A., Ahn, J.W., Yoo, J.S. and Lee, B.J. (2004) Peroxynitrite Scavenging Constituents from the Brown Alga *Sargassum thunbergii*. *Biotechnol. Bioprocess Eng*. **9**, 212-216.

Shin, T.Y., Kim, S.H., Lim, J.P., Suh, E.S., Jeong, H.J., Kim, B.D., Park, E.J., Hwang, W.J., Rye, D.G., Baek, S.H., An, N.H. and Kim, H.M. (2000) Effect of *Vitex rotundifolia* on Immediate-type Allergic Reaction. *J. Ethnopharmacol.* **72**, 443-450.

Shiojima, K., Masuda, K., Suzuki, H., Lin, T., Ooishi, Y. and Ageta, H. (1995) Composite Constituents : Forty-Two Triterpenoids Including Eight Novel Compounds Isolated from *Picris hieracioides* subsp. *Japonica*. *Chem. Pharm. Bull.* **43**, 1634-1639.

Shipchandler, M., Soine, T.O. and Gupta, P.K. (1970) Coumarins. XI. A Total Synthesis of (±)-Columbianetin. *J. Pharm. Sci*. **59**, 67-71.

Sies, H. (1999) Glutathione and Its Role in Cellular Function. *Free Radic. Biol. Med.* **27**, 916-921.

Stan, S.D., Kar, S., Stoner, G.D. and Singh, S.V. (2008) Bioactive Food Components and Cancer Risk Reduction. *J. Cell Biochem.* **104**, 339-356.

Steck, W. (1971) New Synthesis of Columbianetin and Related Coumarins. *Can. J. Chem*. **49**, 1197-1201.

Stella, C. and Photis, D (2009) Detection and Quantification of Phenolic Compounds in Olive Oil by High Resolution ^{1}H Nuclear Magnetic Resonance Spectroscopy. *Analytica. Chimica. Acta.* **633**, 283-292.

Stermitz, F.R. and Sharifi, I.A. (1977) Alkaloids of *Zanthoxylum monophyllum* and *Z. punctatum. Phytochemistry* **16**, 2003-2006.

Tabacchi, R., Garnero, J. and Buil, P. (1975) Sur la Présence d'un Ester du Décadiénol-2(*E*), 4(*Z*) et de Diterpènes dans l'huile Essentielle de Cyprès (*Cupressus sempervirens* L.). *Helv. Chim. Acta*. **58**, 1184-1187.

Tatsuzawa, F., Mikanagi, Y., Saito, N., Shinoda, K., Shigihara, A. and Honda, T. (2005) Cyanidin Glycosides in Flowers of Genus *Corydalis* (Fumariaceae). *Biochemical Systematics and Ecology*. **33**, 789-798.

Tsao, L., Tsai, P., Lin, R., Huang, L., Kuo, S. and Wang, J. (2005) Inhibition of Lipopolysaccharide-induced Expression of Inducible Nitric Oxide Synthase by Phenolic (3E)-4-(2-hydroxyphenyl)but-3-en-2-one in RAW 264.7 Macrophages. *Biochem. Pharmacol.* **70**, 618-626.

Ulubelen, A. (1990) New Diterpenoids from the Roots of *Salvia triloba*. *Planta med*. **56**, 82-83.

Valko, M., Leibfritz, D., Moncol, J., Cronin, M.T.D., Mazur, M. and Telser, J. (2007) Free Radicals and Antioxidants in Normal Physiological Functions and Human Disease. *Int. J. Biochem. Cell. B*. **39**, 44-84.

Van Wagenen, B.C., Huddleston, J. and Cardellina, J.H. (1988) Native American Food and Medicinal Plants, 8. Water-soluble Constituents of *Lomatium Dissectum*. *J. Nat. Prod*. **51**, 136-141.

Virag, L., Szabo, E., Gergely, P. and Szabo, C. (2003) Peroxynitrite-induced Cytotoxicity: Mechanism and Opportunities for Intervention. *Toxicol. Lett.* **140**, 113-124.

Wahidulla, S., D'Souza, L. and Kamat, S.Y. (1991) Dipeptides from the Red Alga *Acantophora spicifera*. *Phytochemistry* **30**, 3323-3325.

Wang, H.Y., Cai, B., Cui, C.B., Zhang, D.Y. and Yang, B.F. (2005) Vitexicarpin, a Flavonoid from *Vitex trifolia* L., Induces Apoptosis in K562 Cells via Mitochondria-controlled Apoptotic Pathway. *Yao Xue Xue Bao.* **40**, 27-31.

Watson, A.J.M. (2004) Apoptosis and Colorectal Cancer. *Gut* **53**, 1701-1709.

Watson, W.H. and Jones, D.P. (2003) Oxidation of Nuclear Thioredoxin during Oxidative Stress. *FEBS Lett.* **543**, 144-147.

Willette, R.E. and Soine, T.O. (1964) Coumarins. II. Structures of Columbianandin and Columbianin. *J. Pharm. Sci*. **53**, 275-279.

Yan, X.Z., Kuo, Y.H., Lee, T.J., Shih, T.S., Chen, C.H., McPhail, D.R., McPhail, A.T. and Lee, K.H. (1989) Cytotoxic Components of *Dzospyros morrisiana*. *Phytochemistry* **28**, 1541-1543.

Yoshioka, T., Inokuchi, T., Fujioka, S. and Kimura, Y. (2004) Phenolic Compounds and Flavonoids as Plant Growth Regulators from Fruit and Leaf of *Vitex rotundifolia*. *Z. Naturforsch.* **59**, 509-514.

You, K.M., Son, K.H., Chang, H.W., Kang, S.S. and Kim, H.P. (1998) Vitexicarpin, a Flavonoid from the Fruits of *Vitex rotundifolia*, Inhibits Mouse Lymphocyte Proliferation and Growth of Cell Lines *in vitro*. *Planta med*. **64**, 546-550.

Zhou, L., Fuentes, E.R., Hoffmann, J.J. and Timmermann, B.N. (1995) Diterpenoids from *Grindelia tarapacana*. *Phytochemistry* **40**, 1201-1207.

Zornig, M., Hueber, A., Baum, W. and Evan, G. (2002) Apoptosis Regulators and Their Role in Tumorigenesis. *Biochem. Biophys. Acta.* **1551**, 1-37.

Appendix

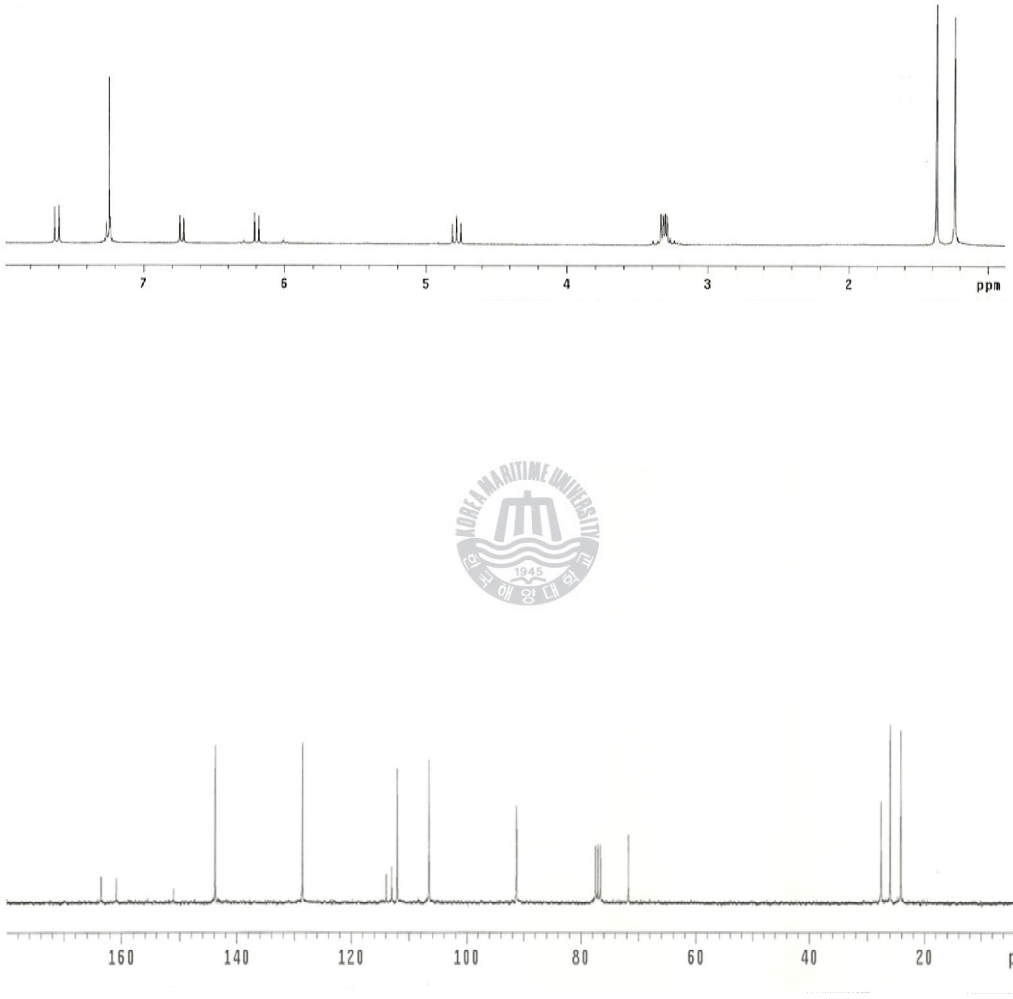

Figure 28. ^{1}H and ^{13}C NMR spectrum of compound **1** isolated from *Corydalis heterocarpa* in $CDCl_3$.

Figure 29. ^{1}H and ^{13}C NMR spectrum of compound **2** isolated from *Corydalis heterocarpa* in $CDCl_3$.

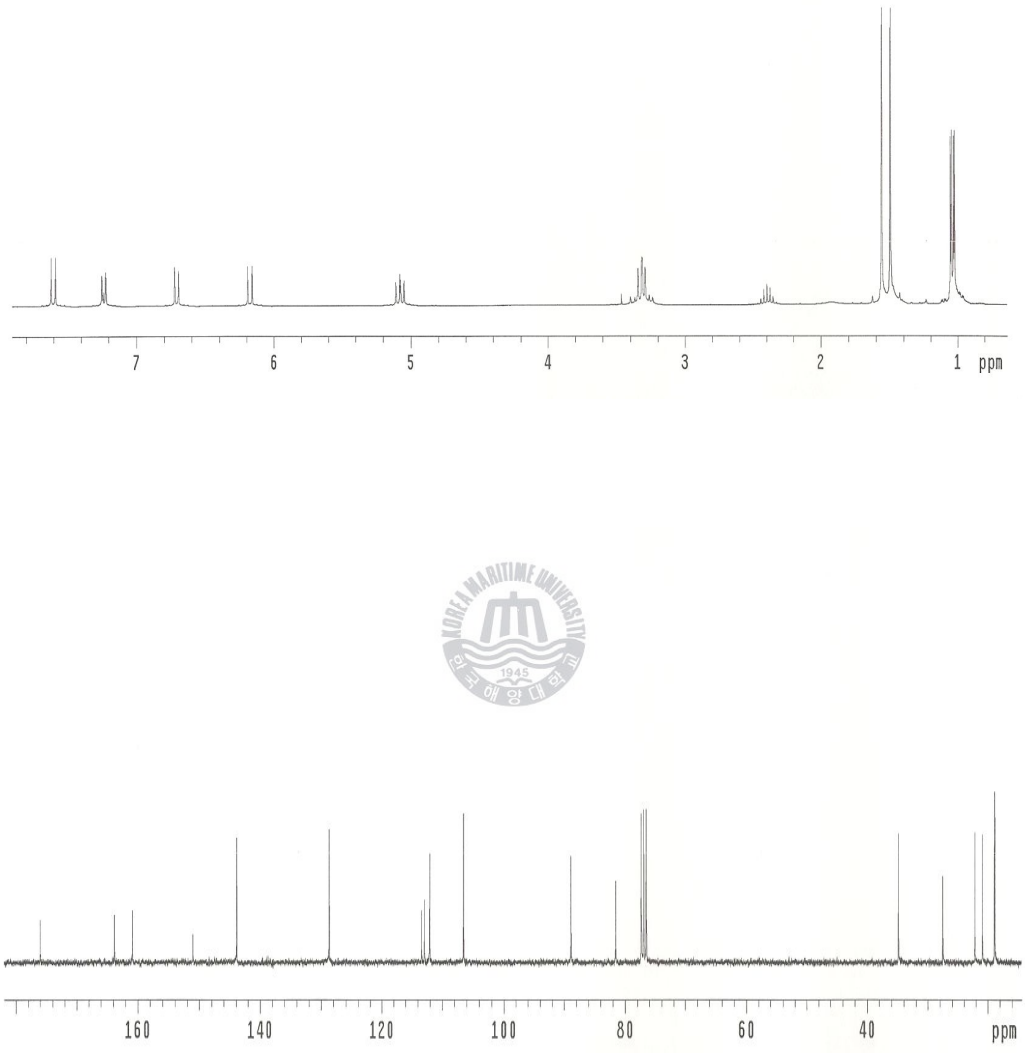

Figure 30. ^{1}H and ^{13}C NMR spectrum of compound **3** isolated from *Corydalis heterocarpa* in $CDCl_3$.

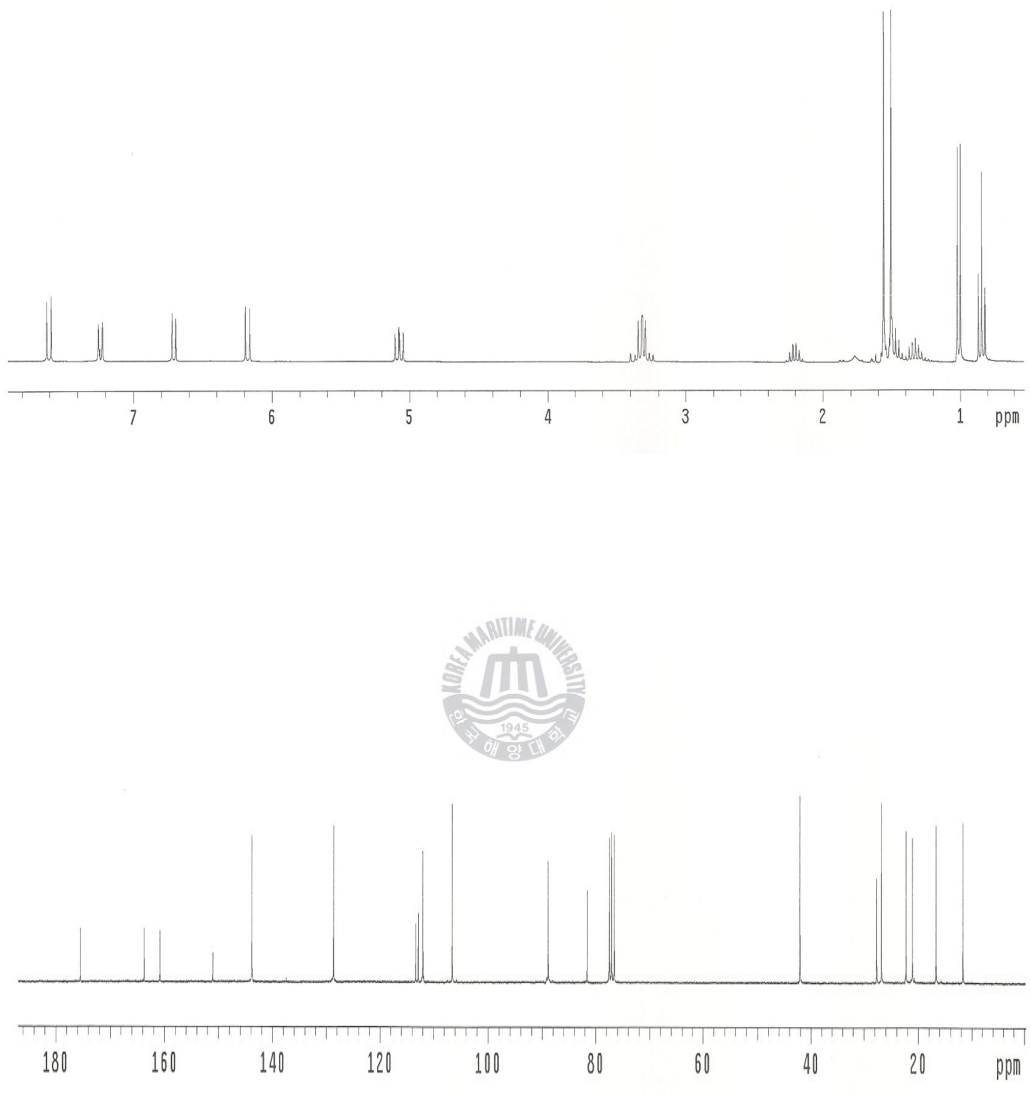

Figure 31. ^{1}H and ^{13}C NMR spectrum of compound **4** isolated from *Corydalis heterocarpa* in $CDCl_3$.

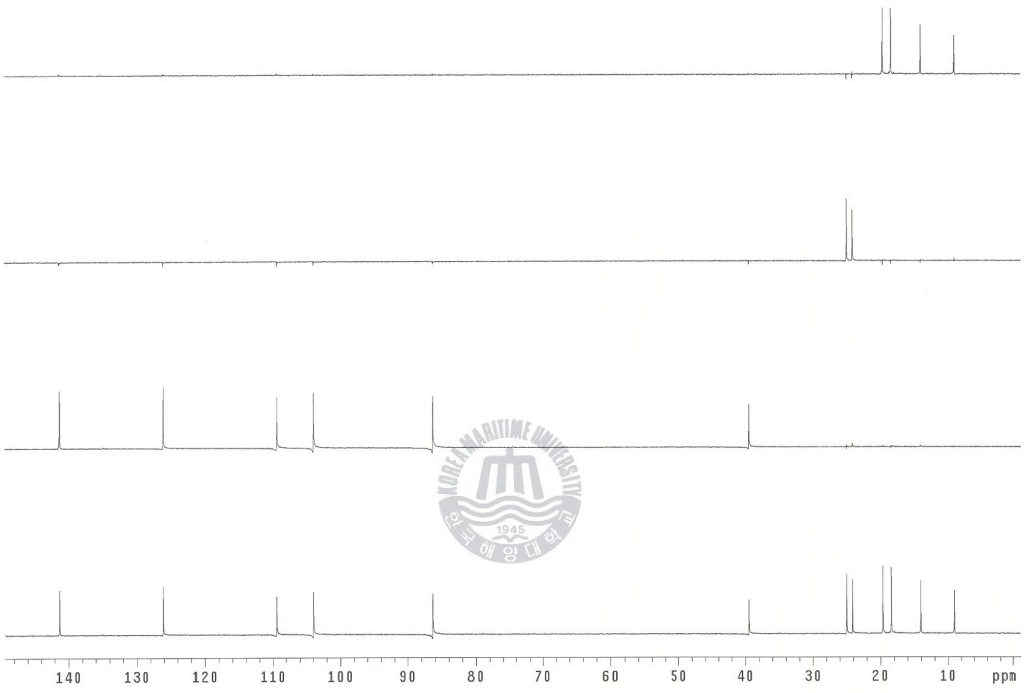

Figure 32. DEPT spectrum of compound **4** isolated from *Corydalis heterocarpa* in $CDCl_3$.

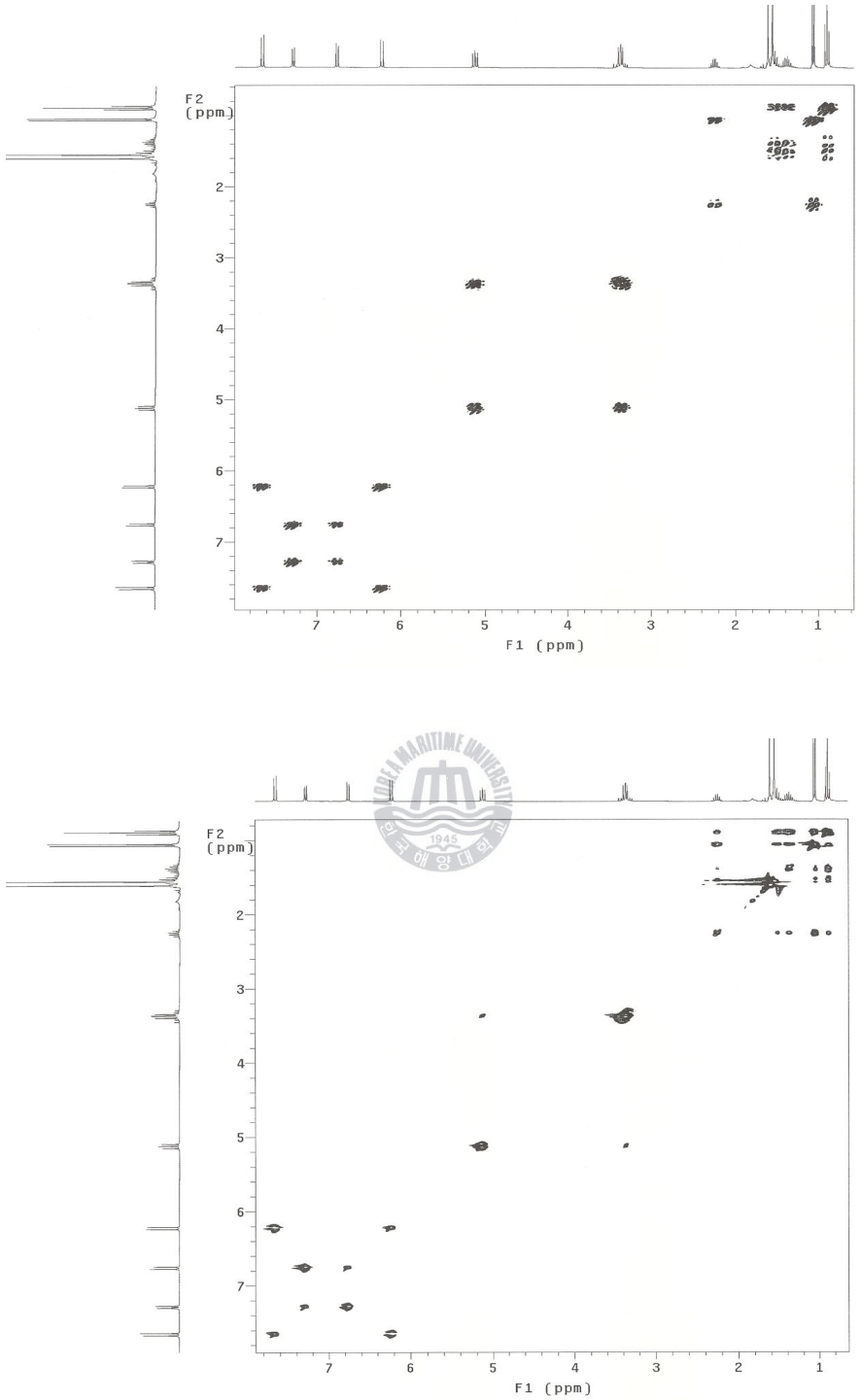

Figure 33. gDQCOSY and TOCSY spectrum of compound **4** isolated from *Corydalis heterocarpa* in $CDCl_3$.

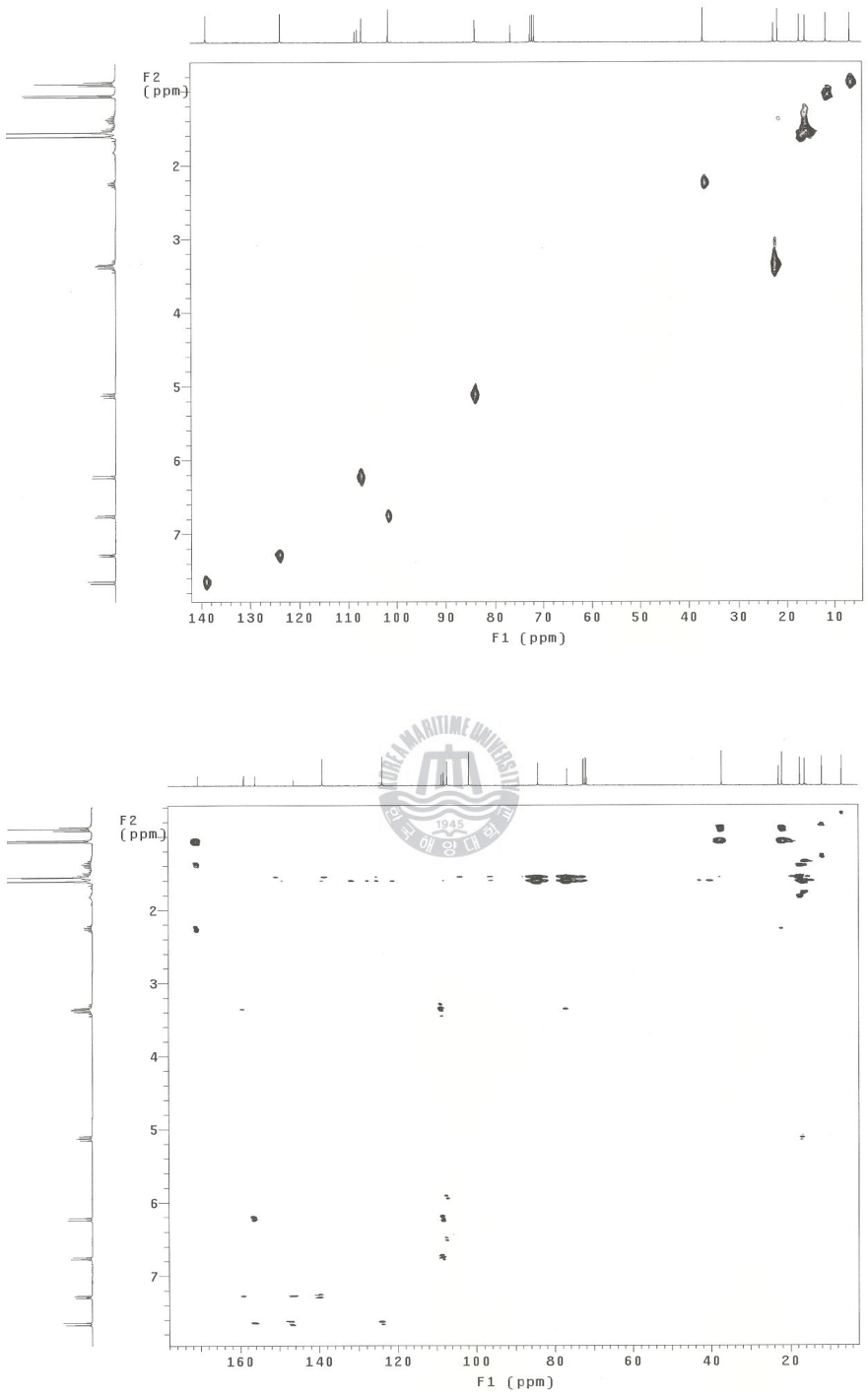

Figure 34. gHMQC and gHMBC spectrum of compound **4** isolated from *Corydalis heterocarpa* in $CDCl_3$.

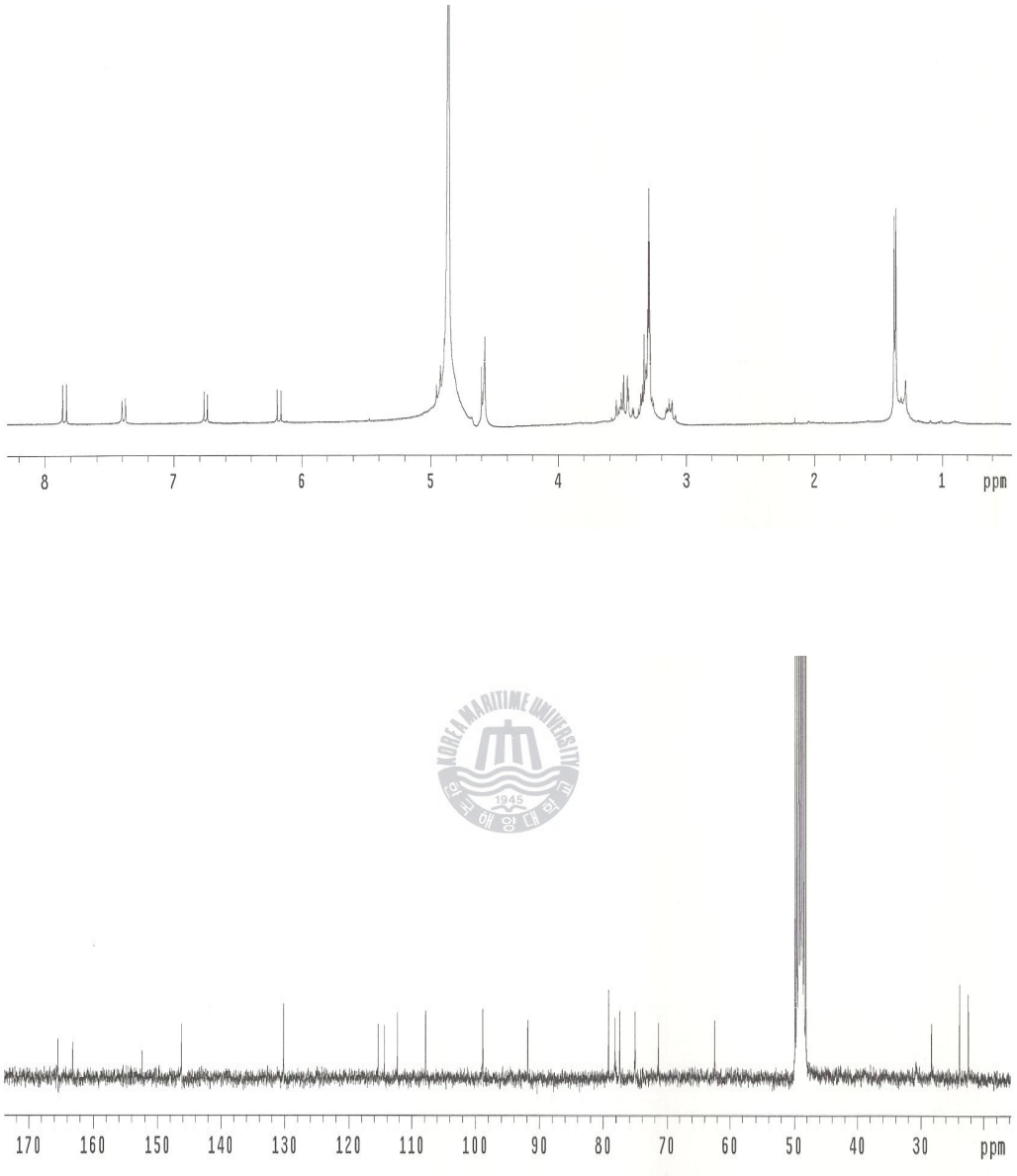

Figure 35. ^{1}H and ^{13}C NMR spectrum of compound **5** isolated from *Corydalis heterocarpa* in CD_3OD.

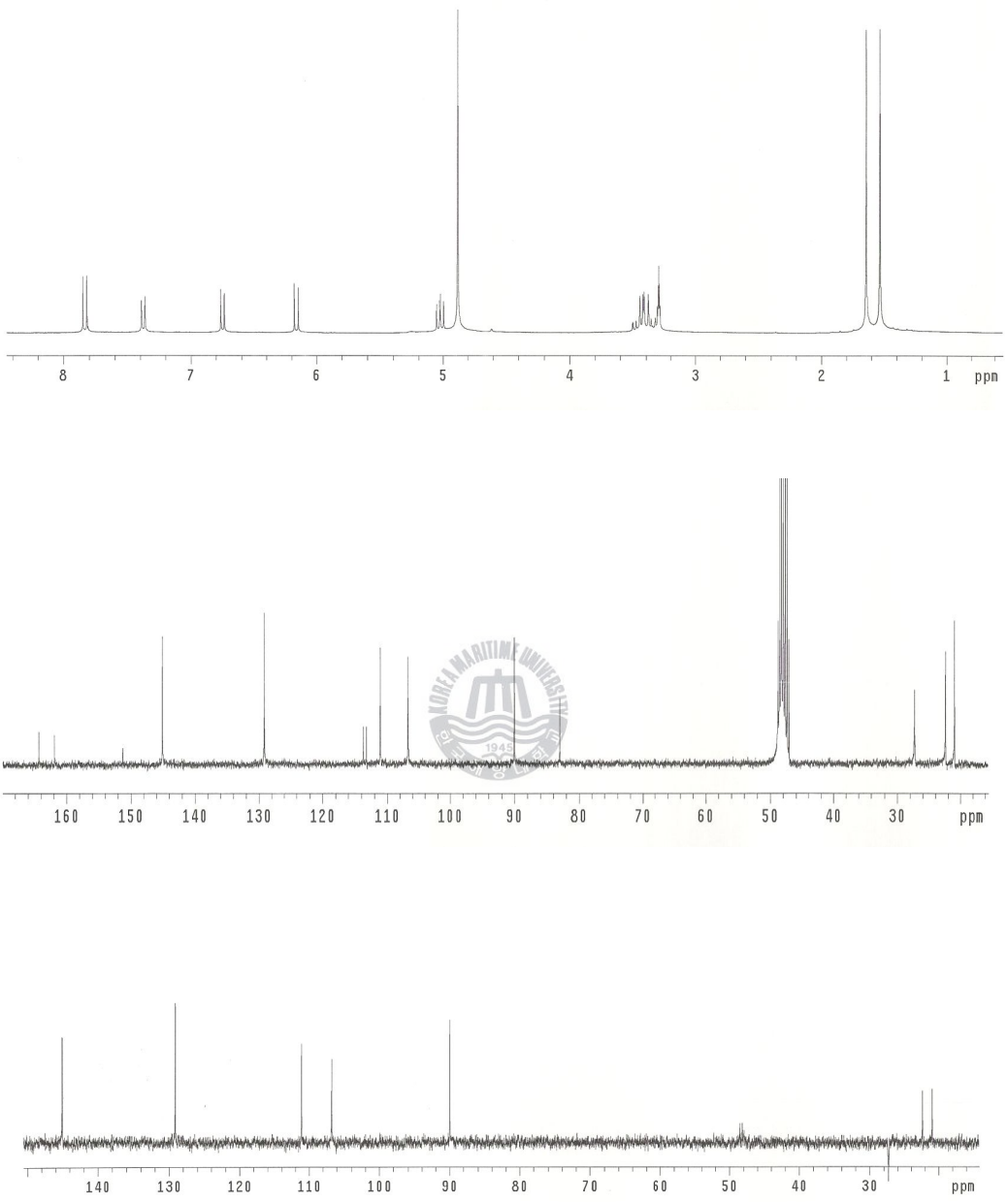

Figure 36. ^{1}H, ^{13}C NMR, and DEPT spectrum of compound **6** isolated from *Corydalis heterocarpa* in CD_3OD.

Figure 37. gDQCOSY and TOCSY spectrum of compound **6** isolated from *Corydalis heterocarpa* in CD_3OD.

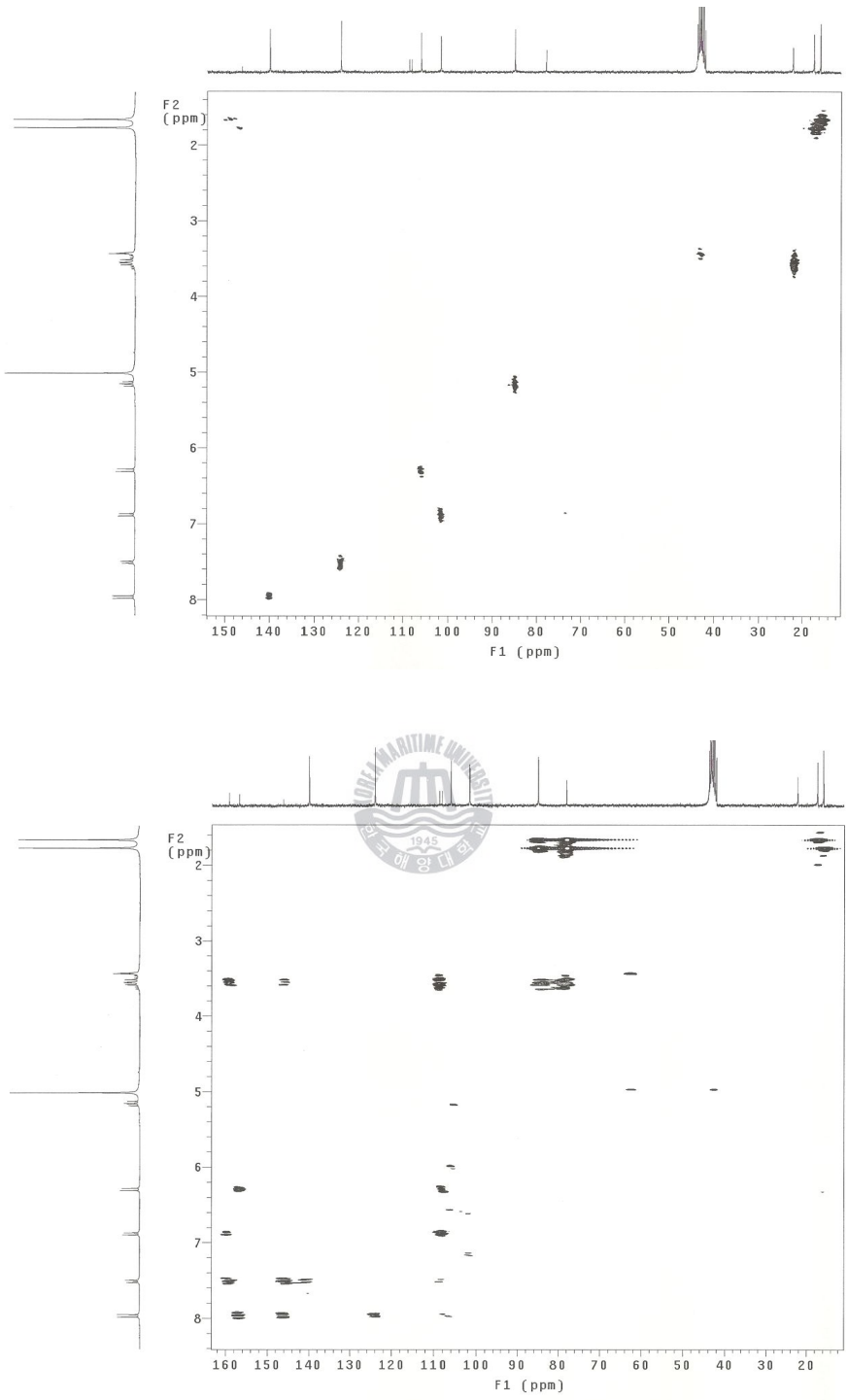

Figure 38. gHMQC and gHMBC spectrum of compound **6** isolated from *Corydalis heterocarpa* in CD_3OD.

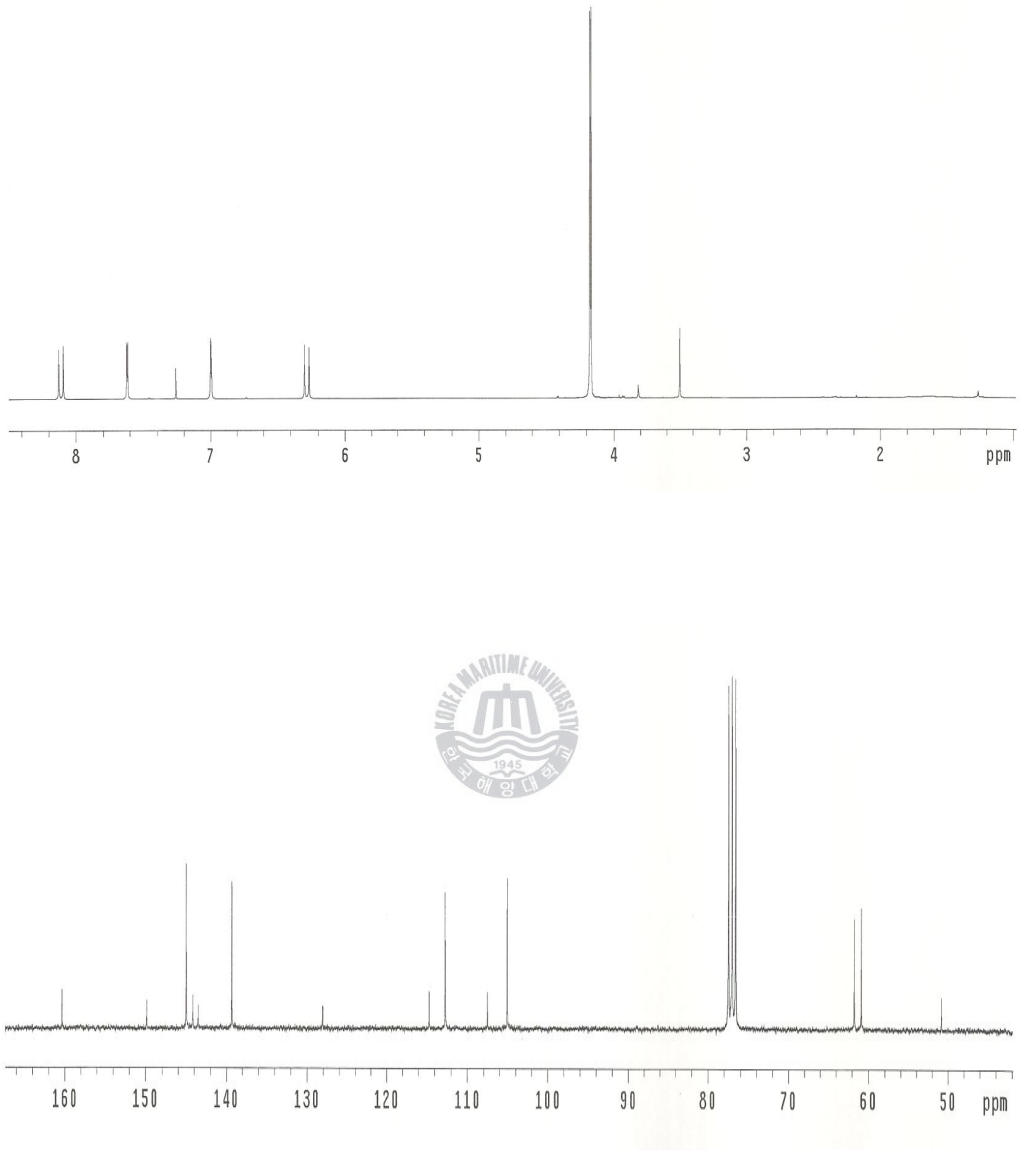

Figure 39. ^{1}H and ^{13}C NMR spectrum of compound **7** isolated from *Corydalis heterocarpa* in $CDCl_3$.

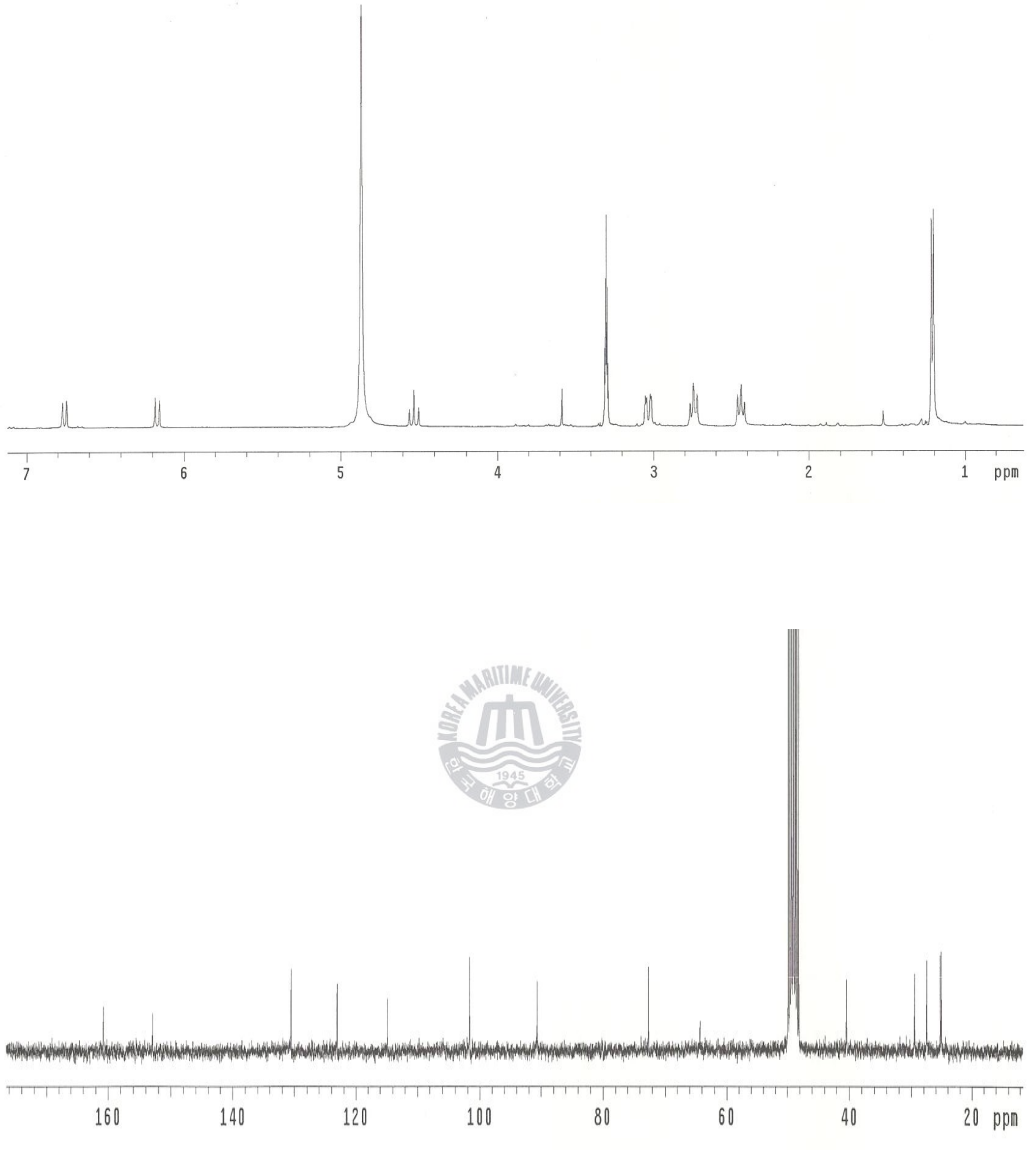

Figure 40. ^{1}H and ^{13}C NMR spectrum of compound **8** isolated from *Corydalis heterocarpa* in CD_3OD.

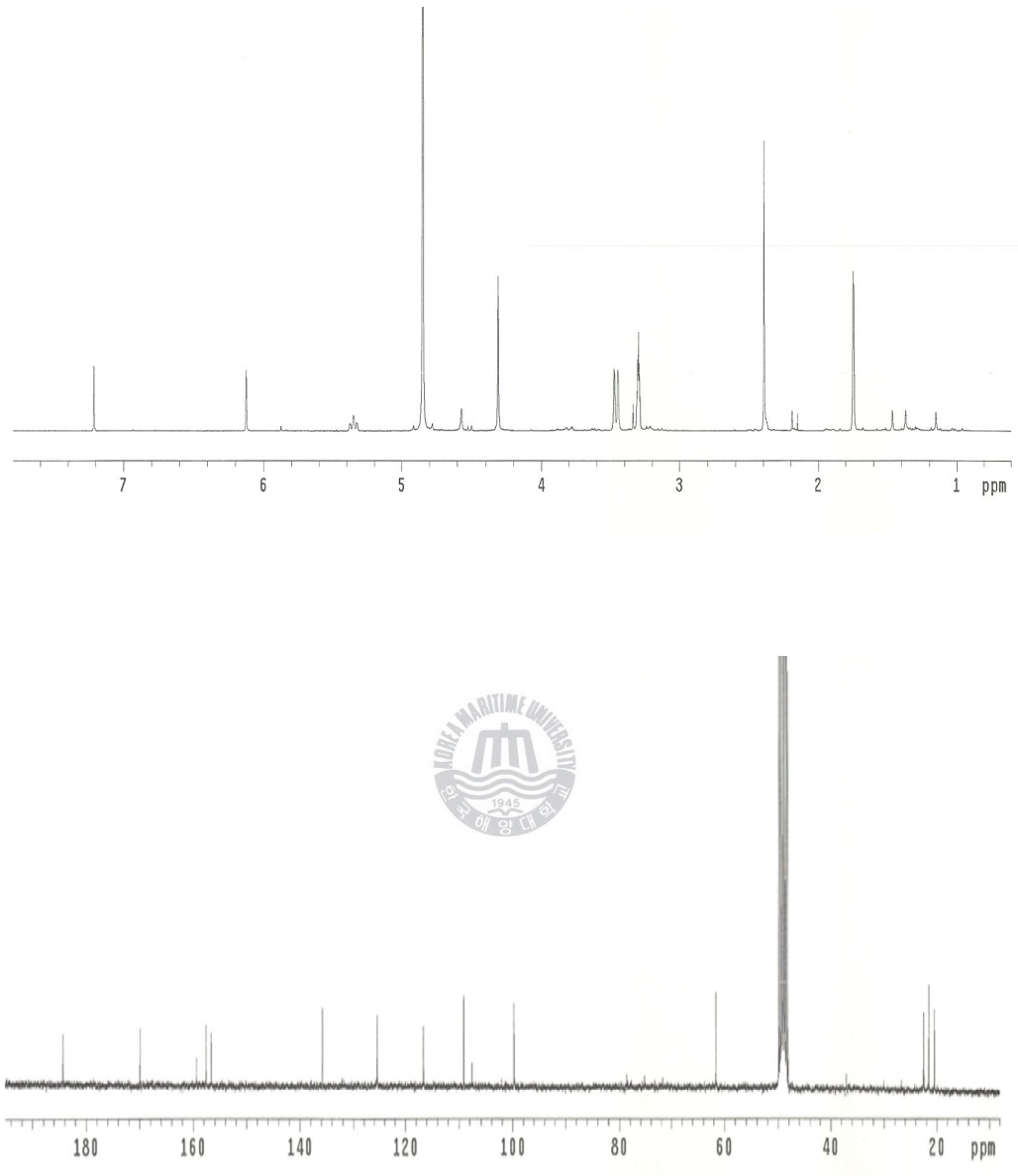

Figure 41. ^{1}H and ^{13}C NMR spectrum of compound **9** isolated from *Corydalis heterocarpa* in CD_3OD.

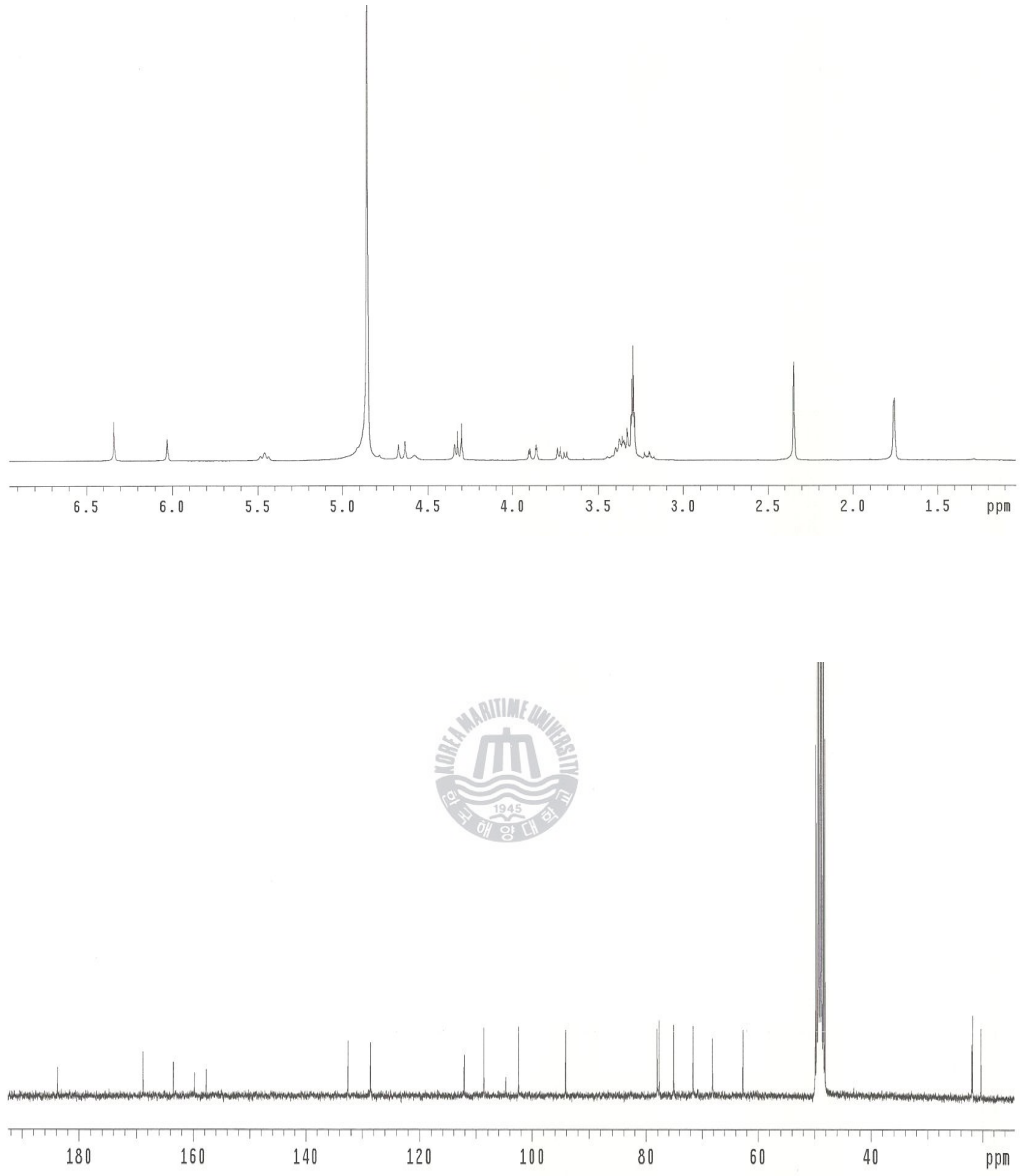

Figure 42. ^{1}H and ^{13}C NMR spectrum of compound **10** isolated from *Corydalis heterocarpa* in CD_3OD.

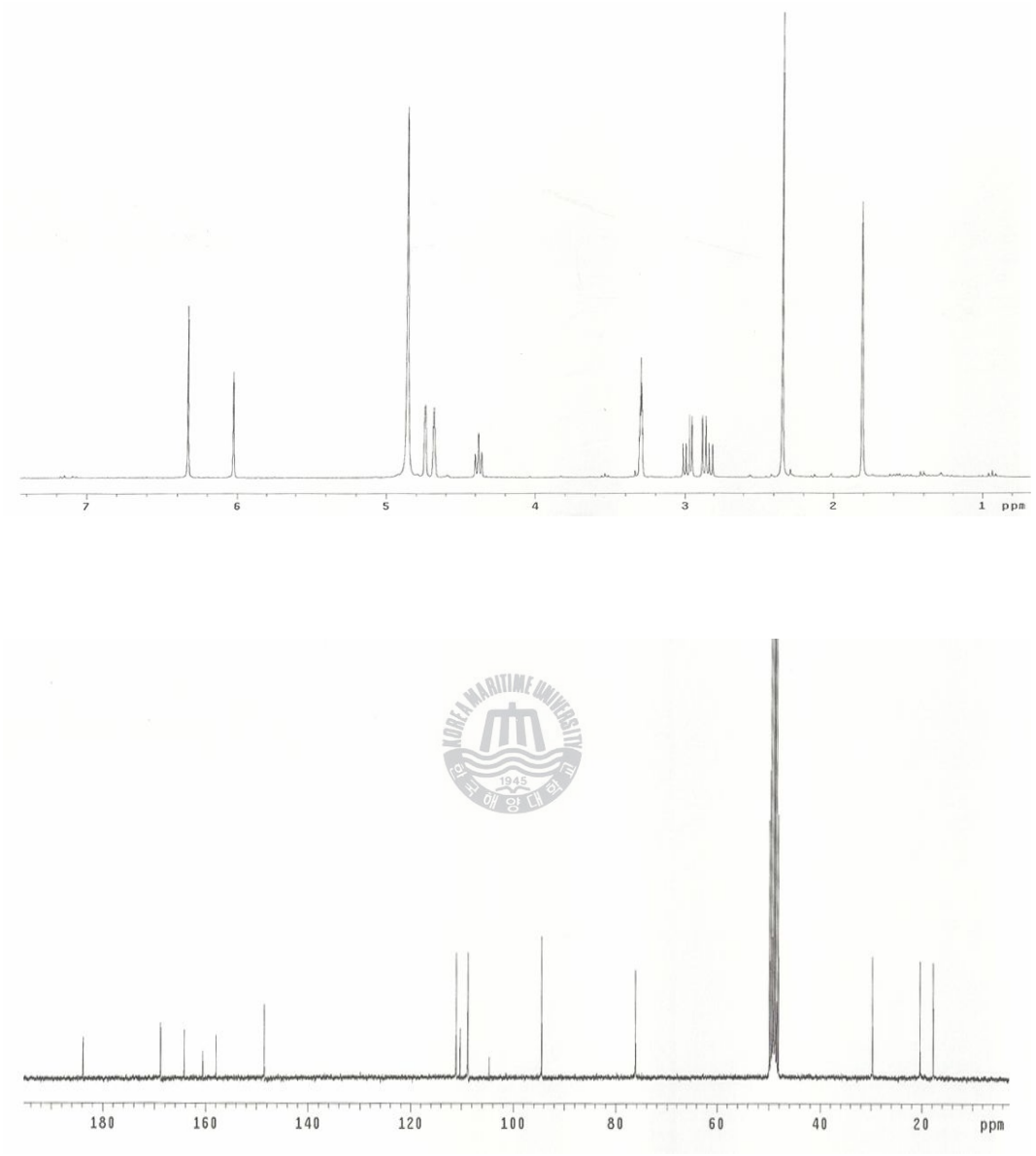

Figure 43. ^{1}H and ^{13}C NMR spectrum of compound **11** isolated from *Corydalis heterocarpa* in CD_3OD.

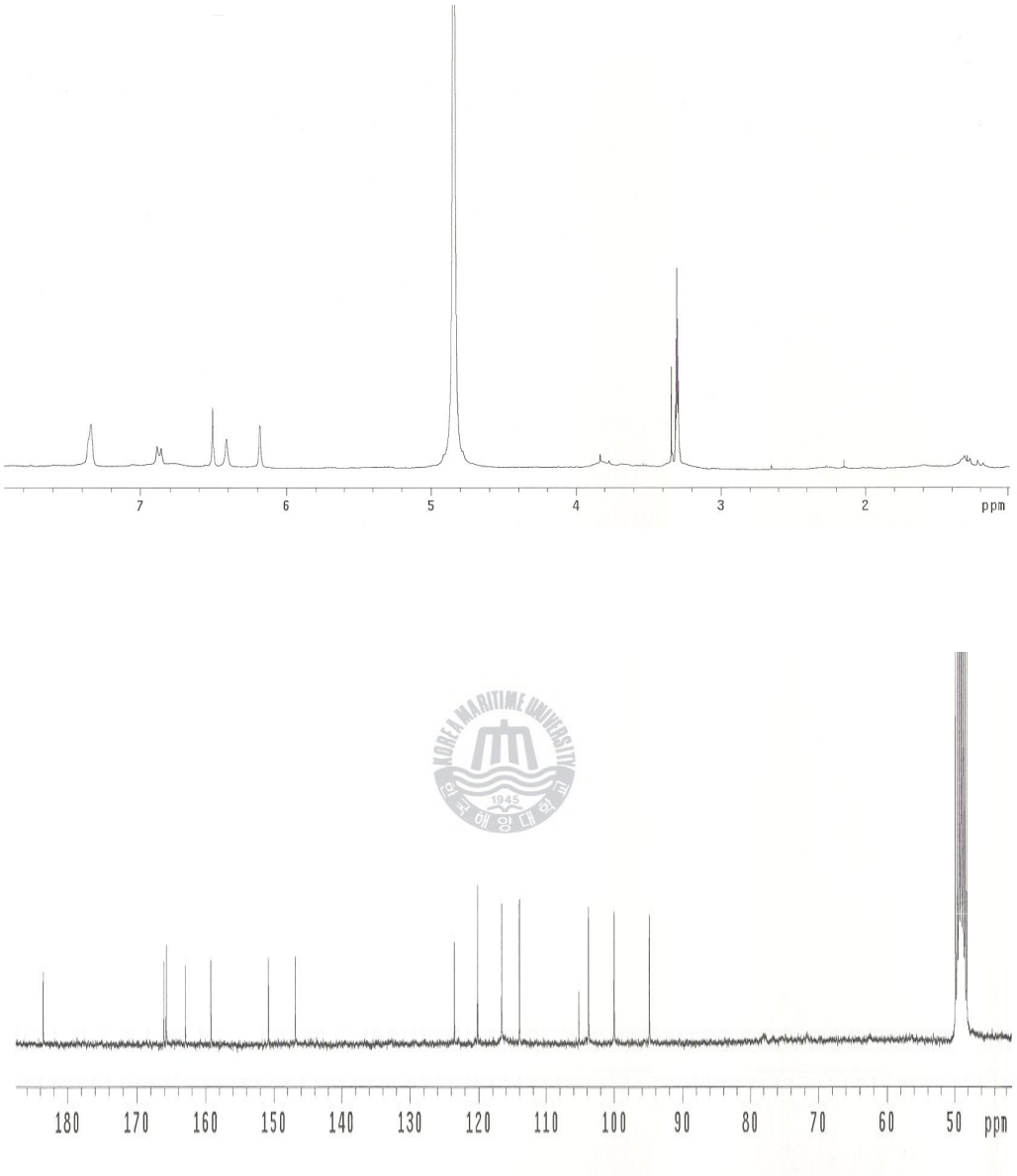

Figure 44. ^{1}H and ^{13}C NMR spectrum of compound **12** isolated from *Vitex rotundifolia* in CD_3OD.

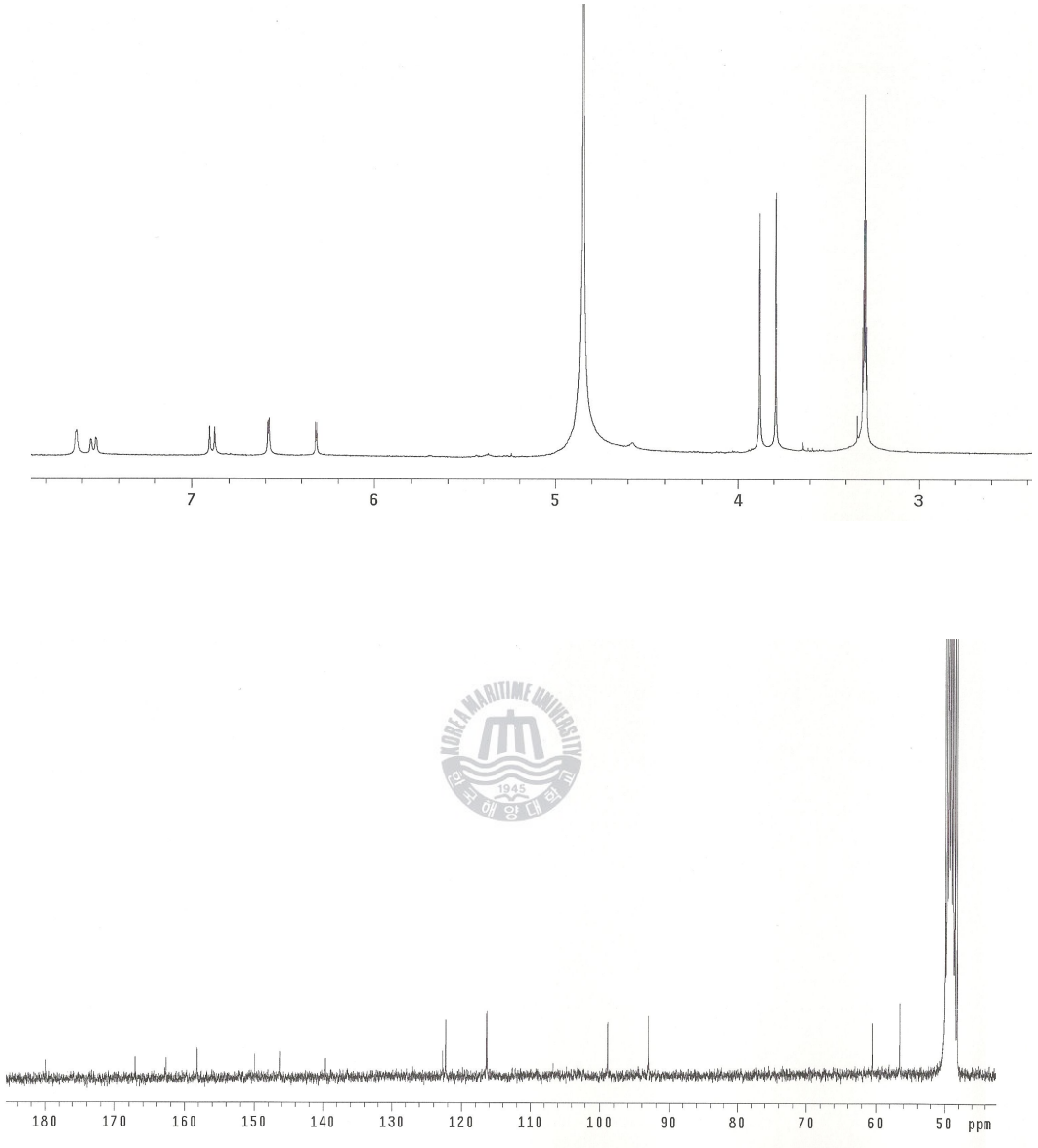

Figure 45. ^{1}H and ^{13}C NMR spectrum of compound **13** isolated from *Vitex rotundifolia* in CD_3OD.

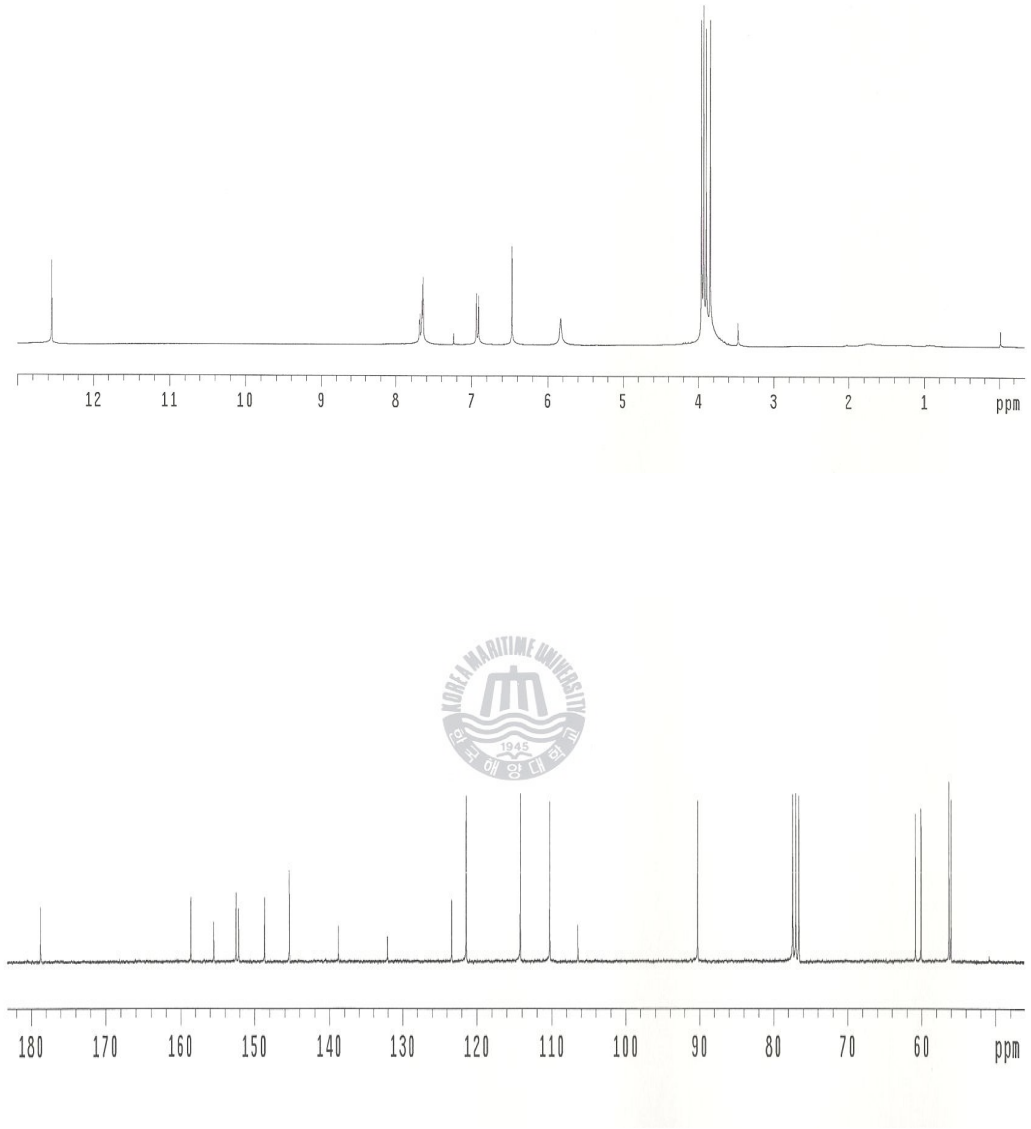

Figure 46. ^{1}H and ^{13}C NMR spectrum of compound **14** isolated from *Vitex rotundifolia* in $CDCl_3$.

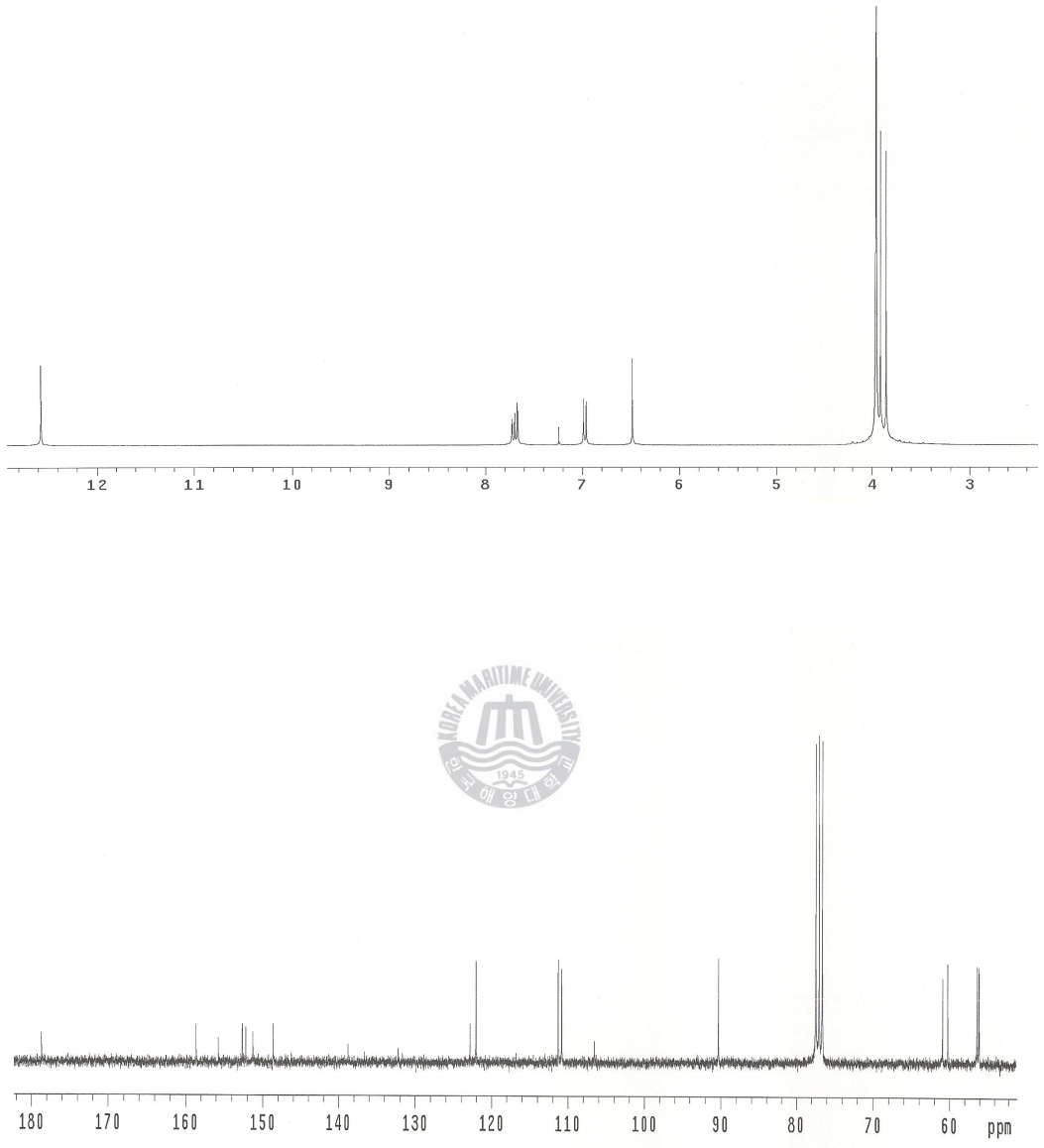

Figure 47. ^{1}H and ^{13}C NMR spectrum of compound **15** isolated from *Vitex rotundifolia* in $CDCl_3$.

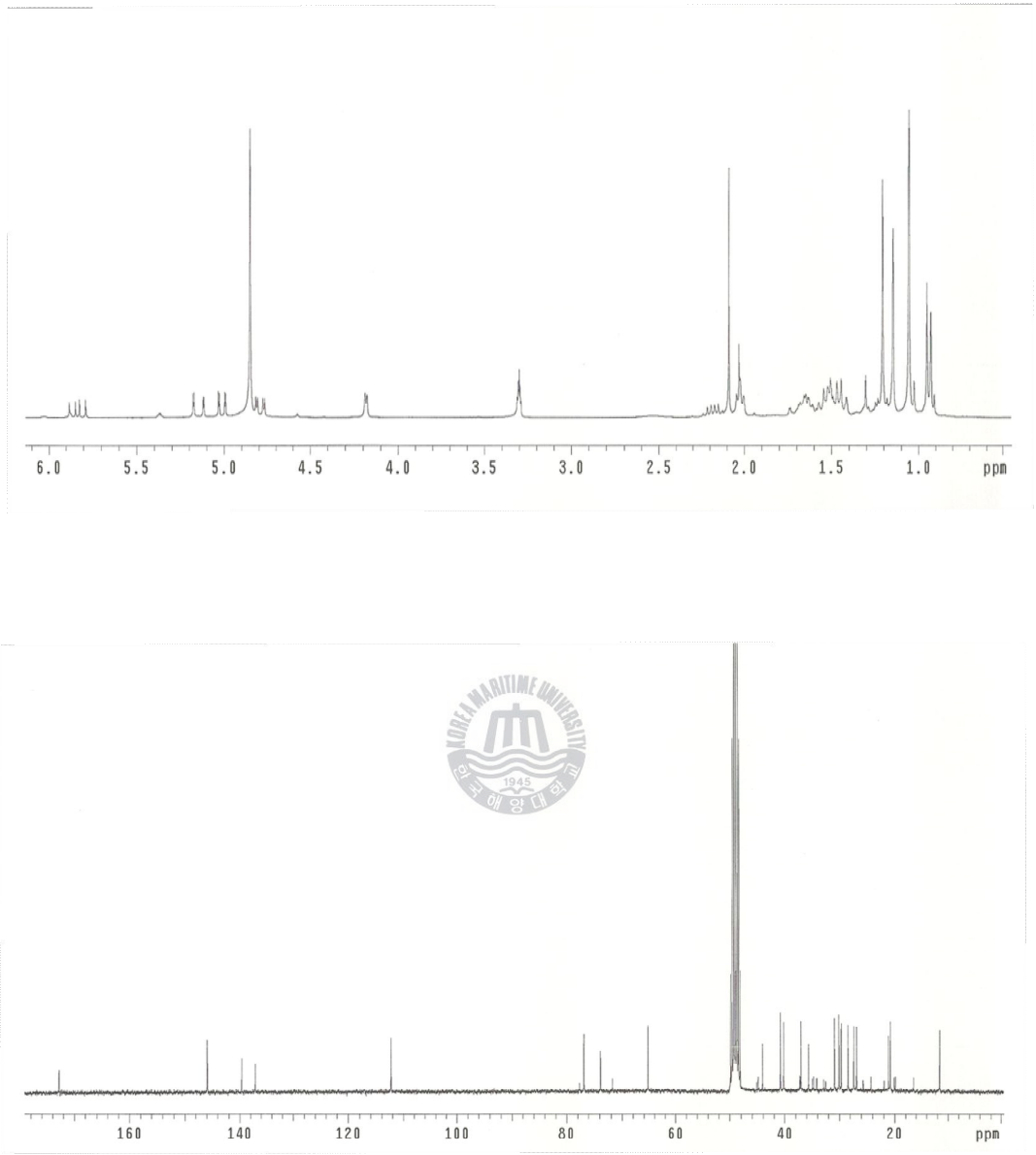

Figure 48. ^{1}H and ^{13}C NMR spectrum of compound **16** isolated from *Vitex rotundifolia* in CD_3OD.

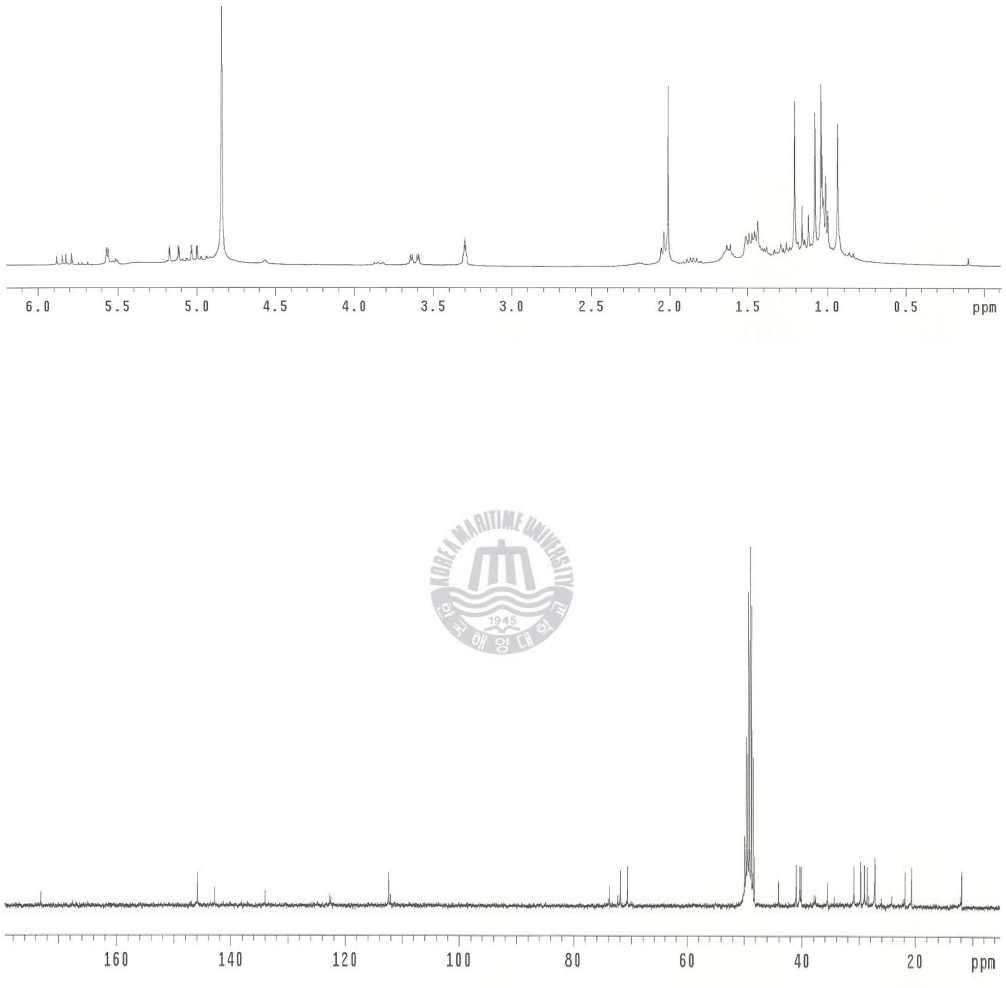

Figure 49. ^{1}H and ^{13}C NMR spectrum of compound **17** isolated from *Vitex rotundifolia* in CD_3OD.

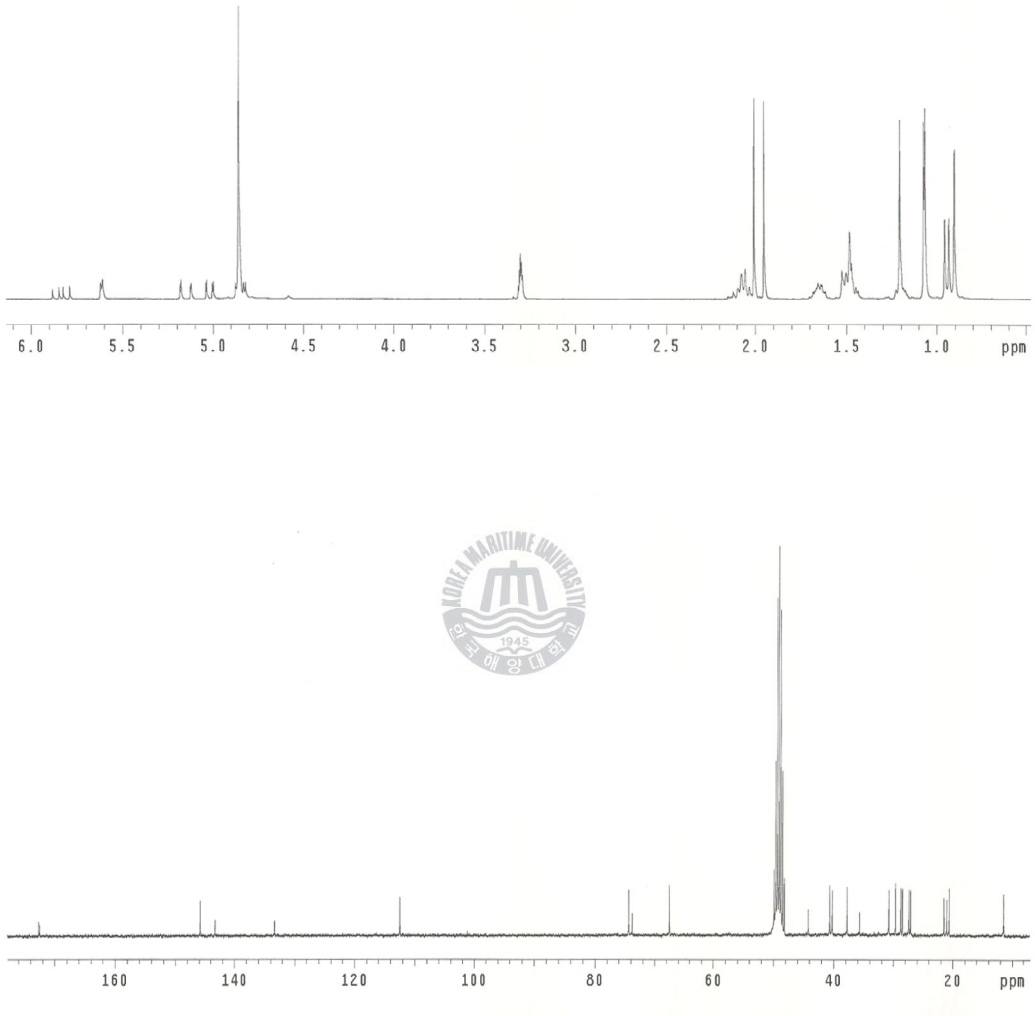

Figure 50. ^{1}H and ^{13}C NMR spectrum of compound **18** isolated from *Vitex rotundifolia* in CD_3OD.

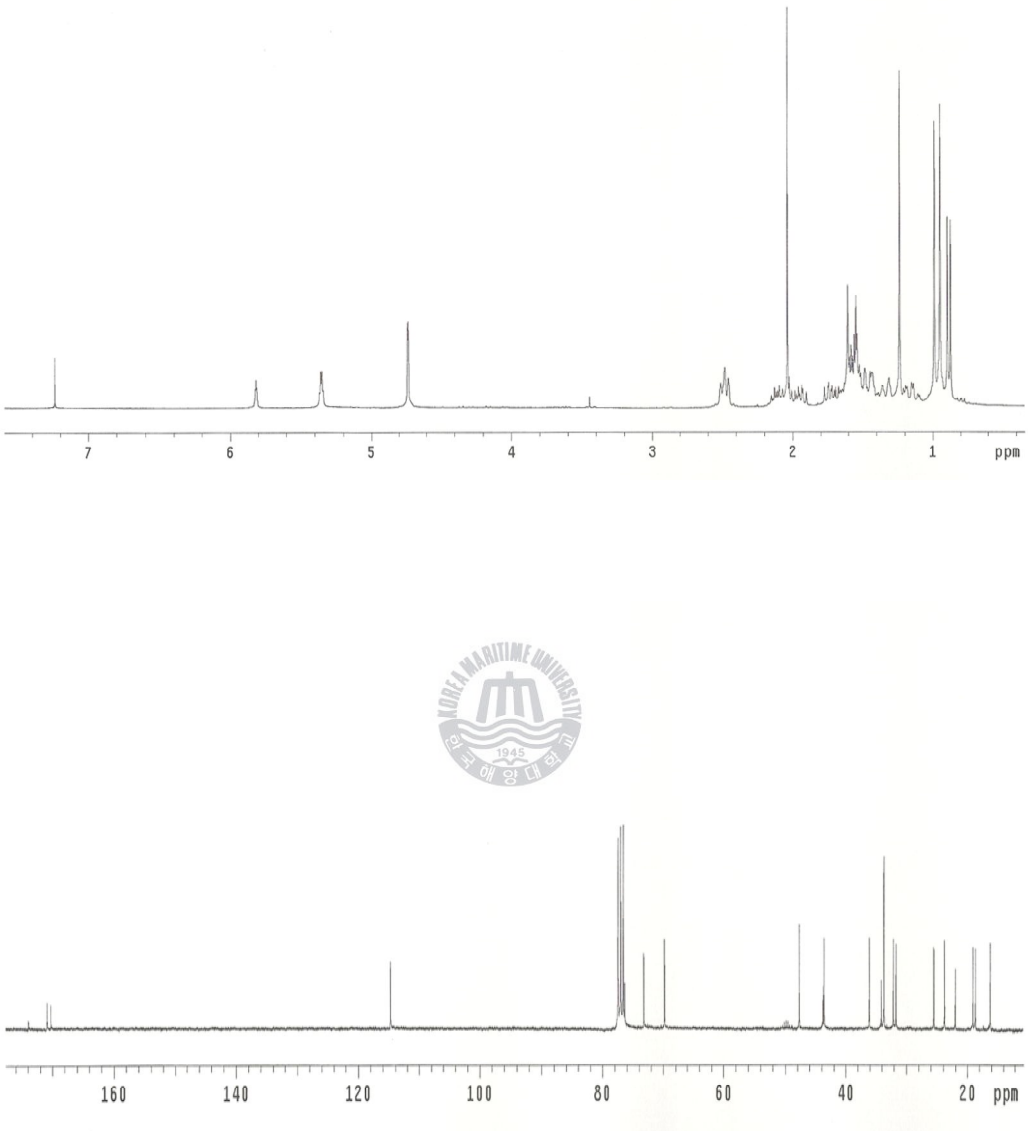

Figure 51. ^{1}H and ^{13}C NMR spectrum of compound **19** isolated from *Vitex rotundifolia* in $CDCl_3$.

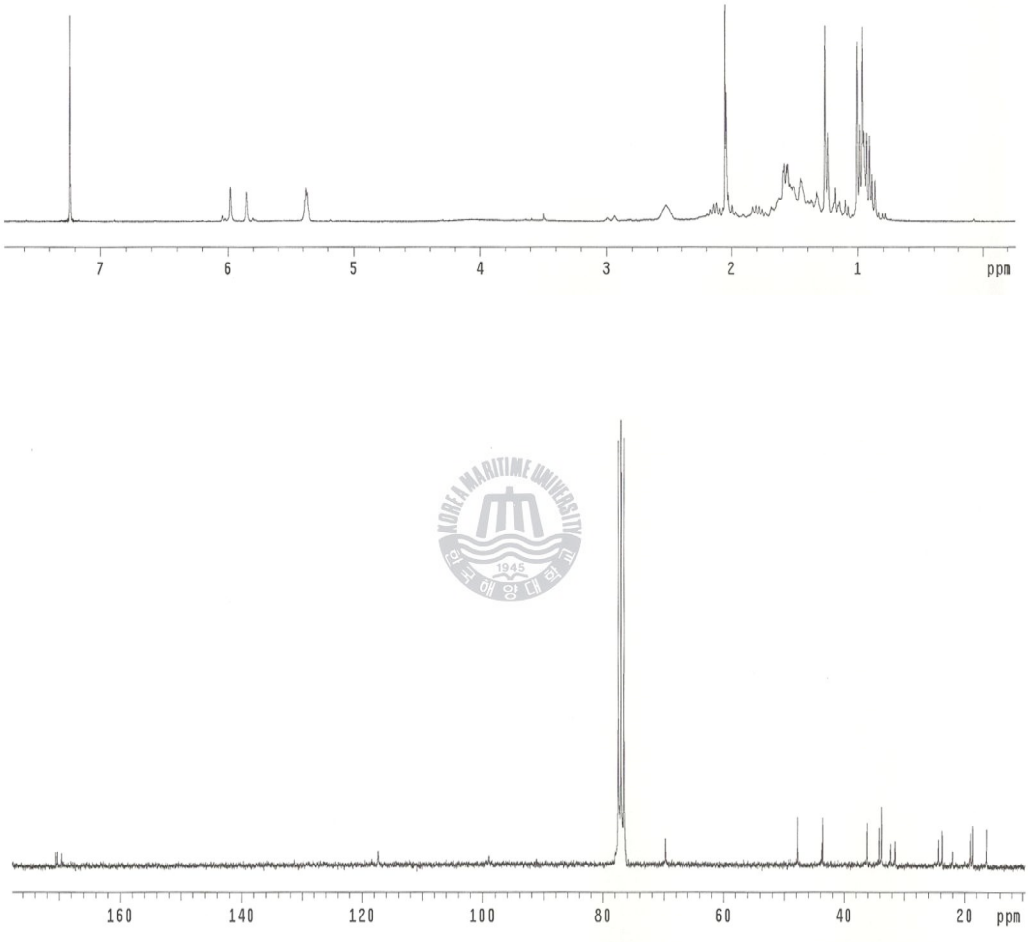

Figure 52. ^{1}H and ^{13}C NMR spectrum of compound **20** isolated from *Vitex rotundifolia* in $CDCl_3$.

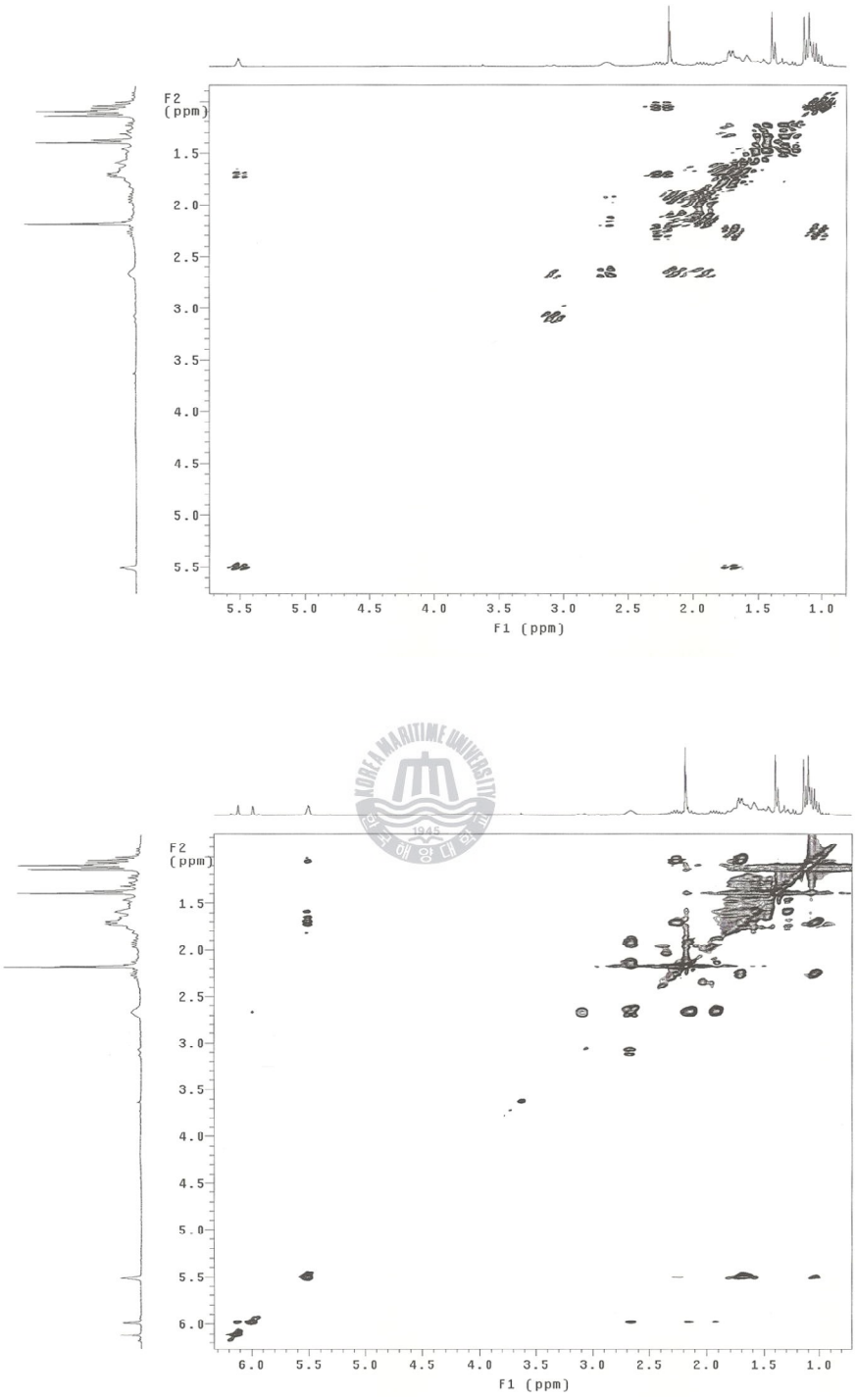

Figure 53. gDQCOSY and TOCSY spectrum of compound **20** isolated from *Vitex rotundifolia* in $CDCl_3$.

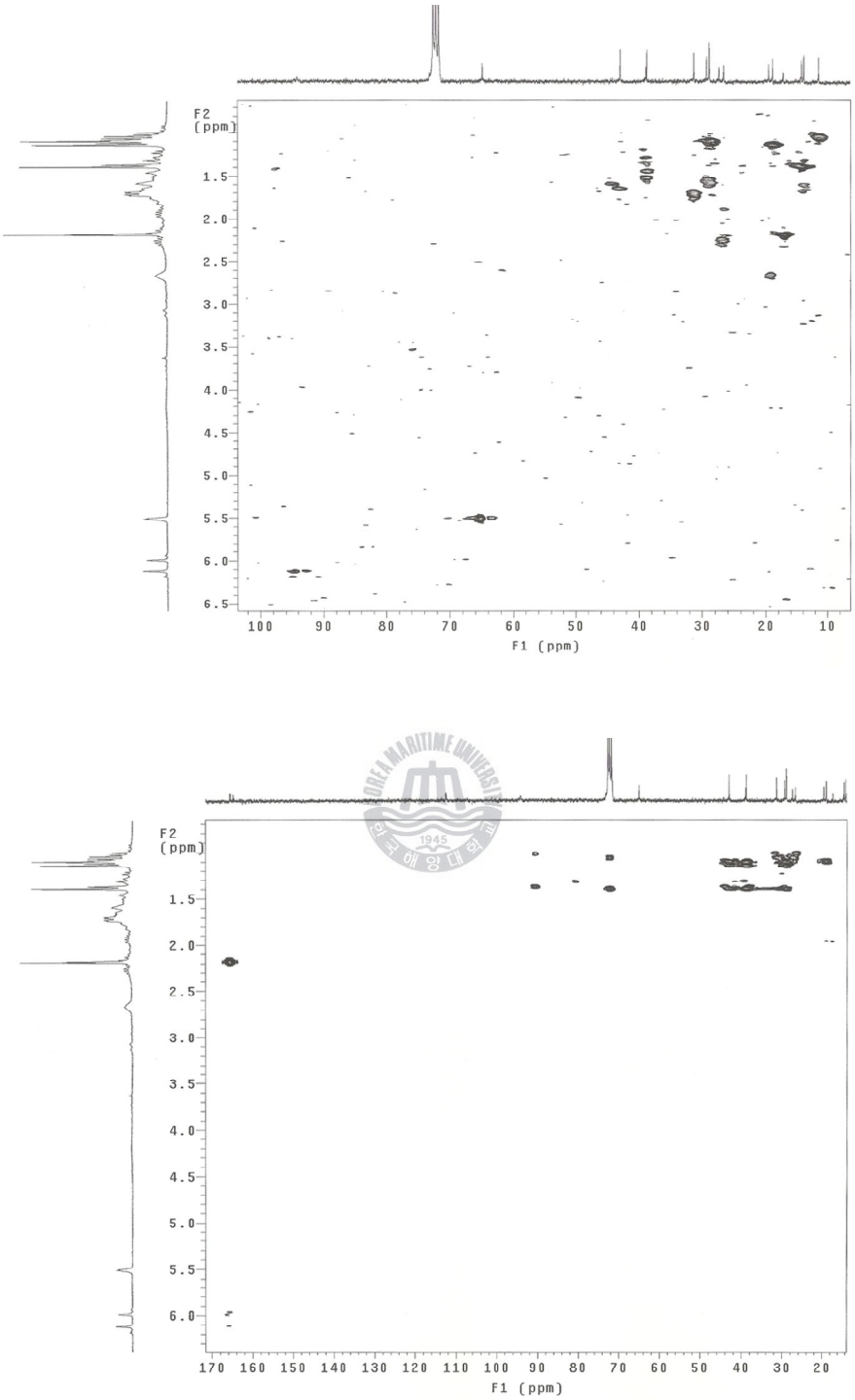

Figure 54. gHMQC and gHMBC spectrum of compound **20** isolated from *Vitex rotundifolia* in $CDCl_3$.

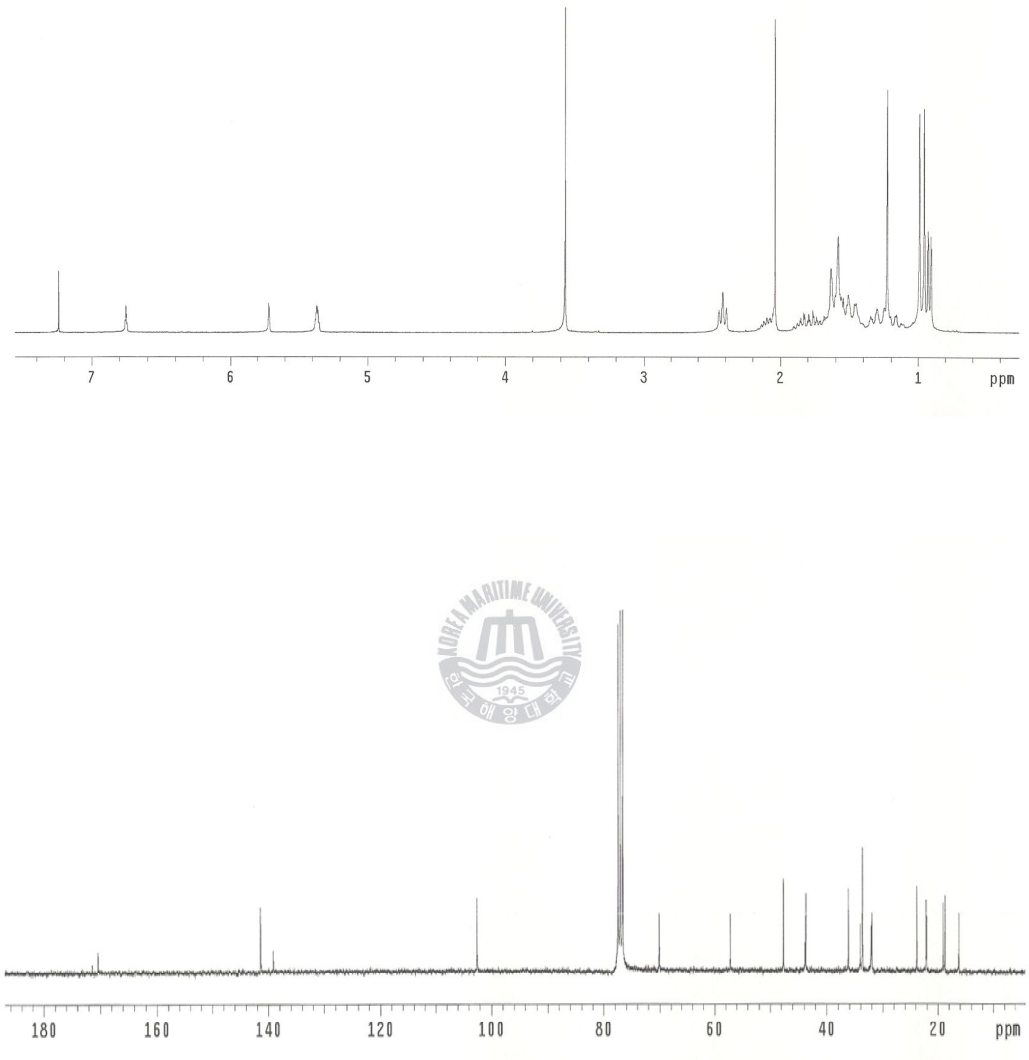

Figure 55. ^{1}H and ^{13}C NMR spectrum of compound **21** isolated from *Vitex rotundifolia* in $CDCl_3$.

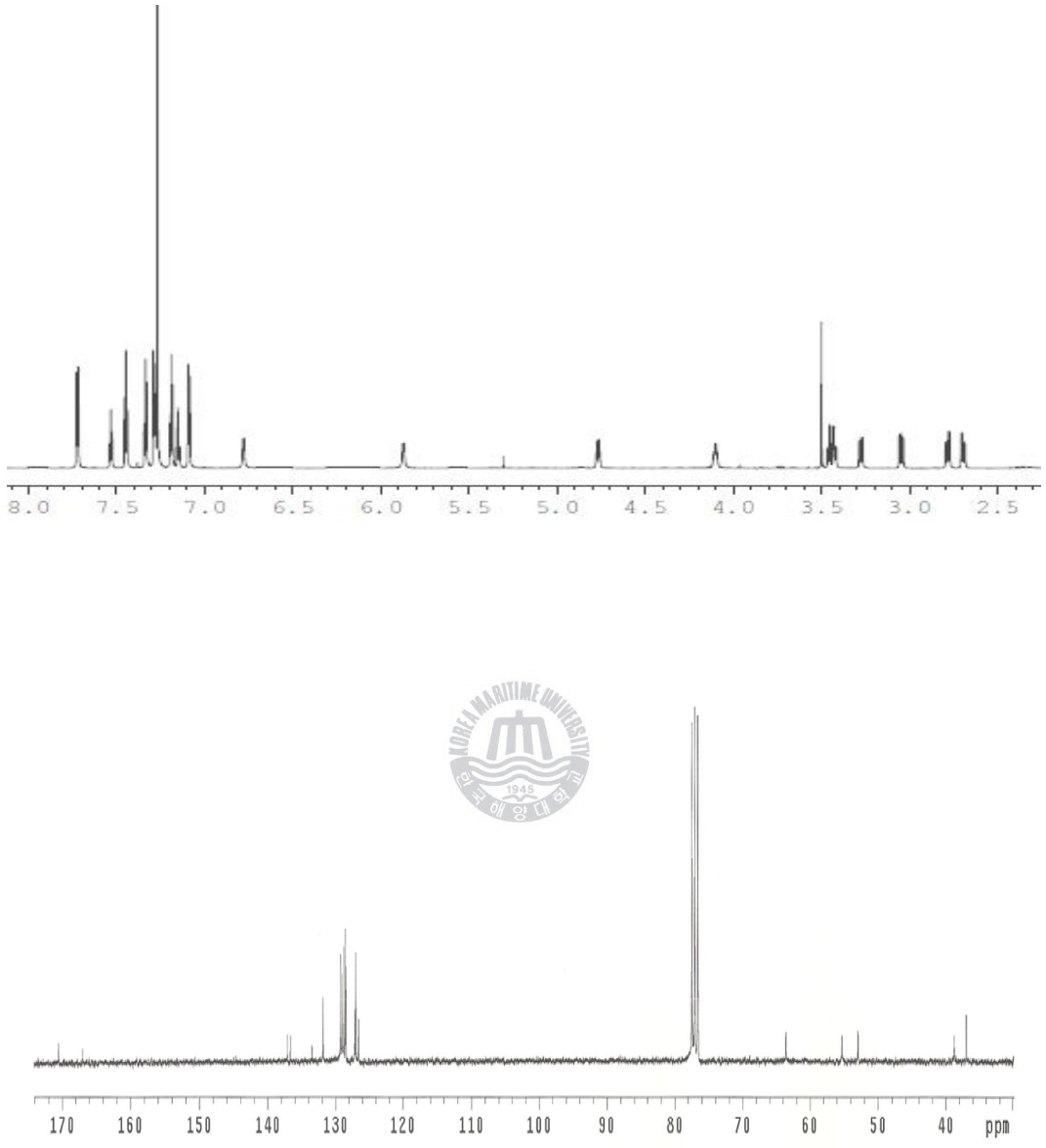

Figure 56. ^{1}H and ^{13}C NMR spectrum of compound **22** isolated from *Vitex rotundifolia* in $CDCl_3$.

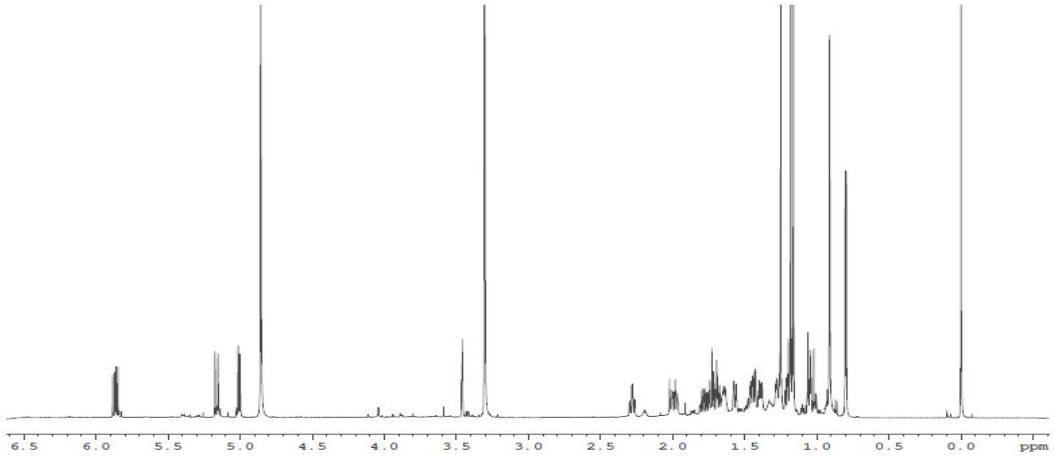

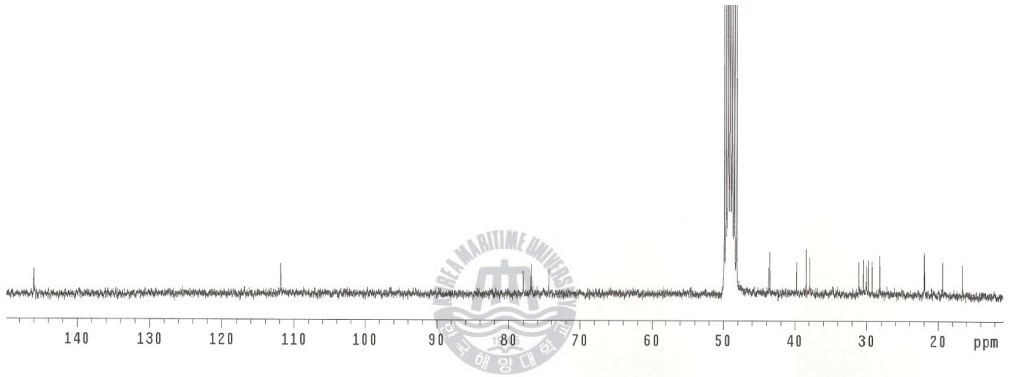

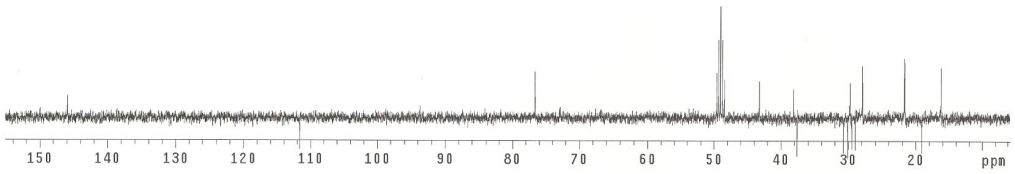

.

Figure 57. ^{1}H, ^{13}C NMR, and DEPT spectrum of compound **23** isolated from *Vitex rotundifolia* in CD_3OD.

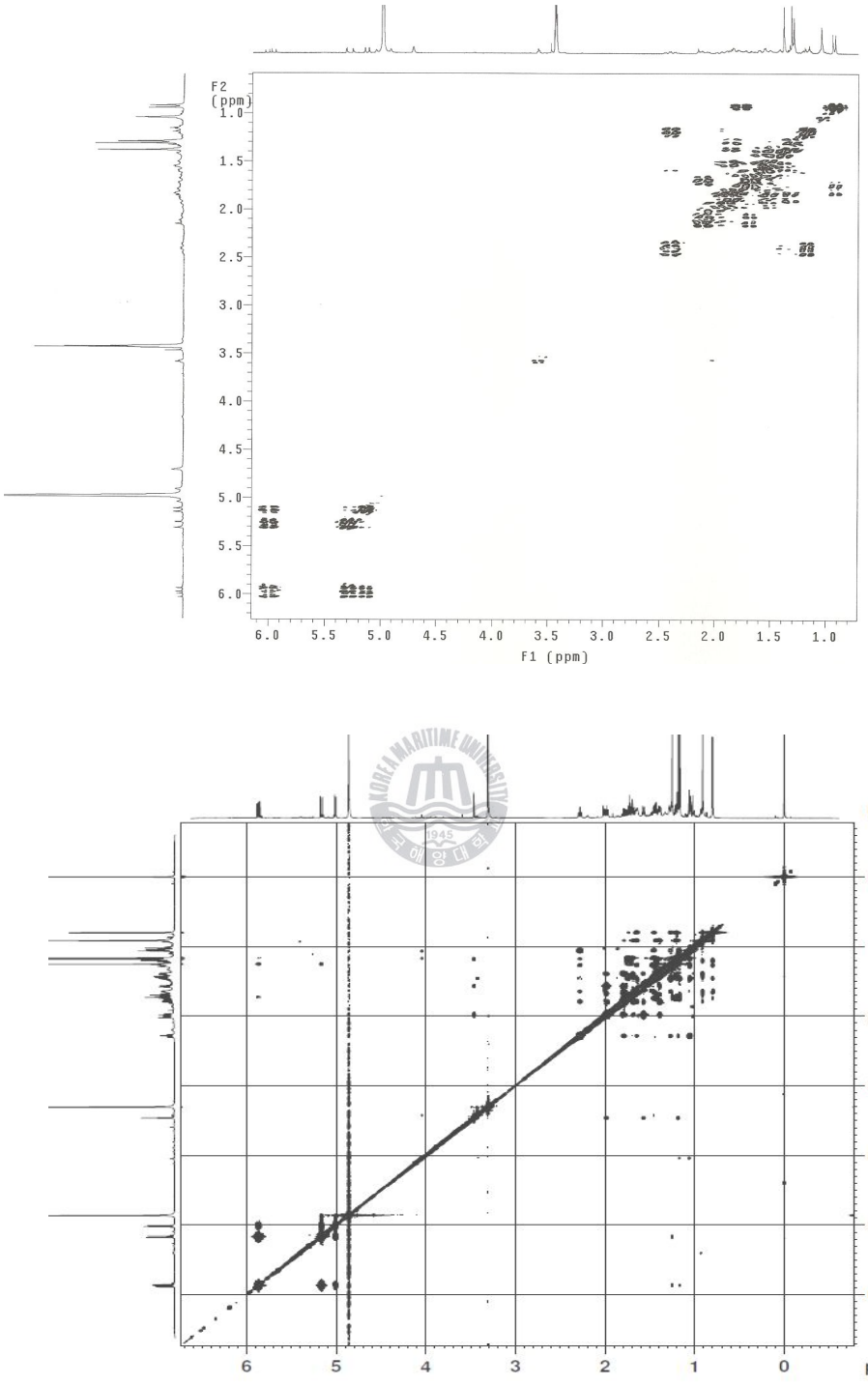

Figure 58. gDQCOSY and NOESY spectrum of compound **23** isolated from *Vitex rotundifolia* in CD_3OD.

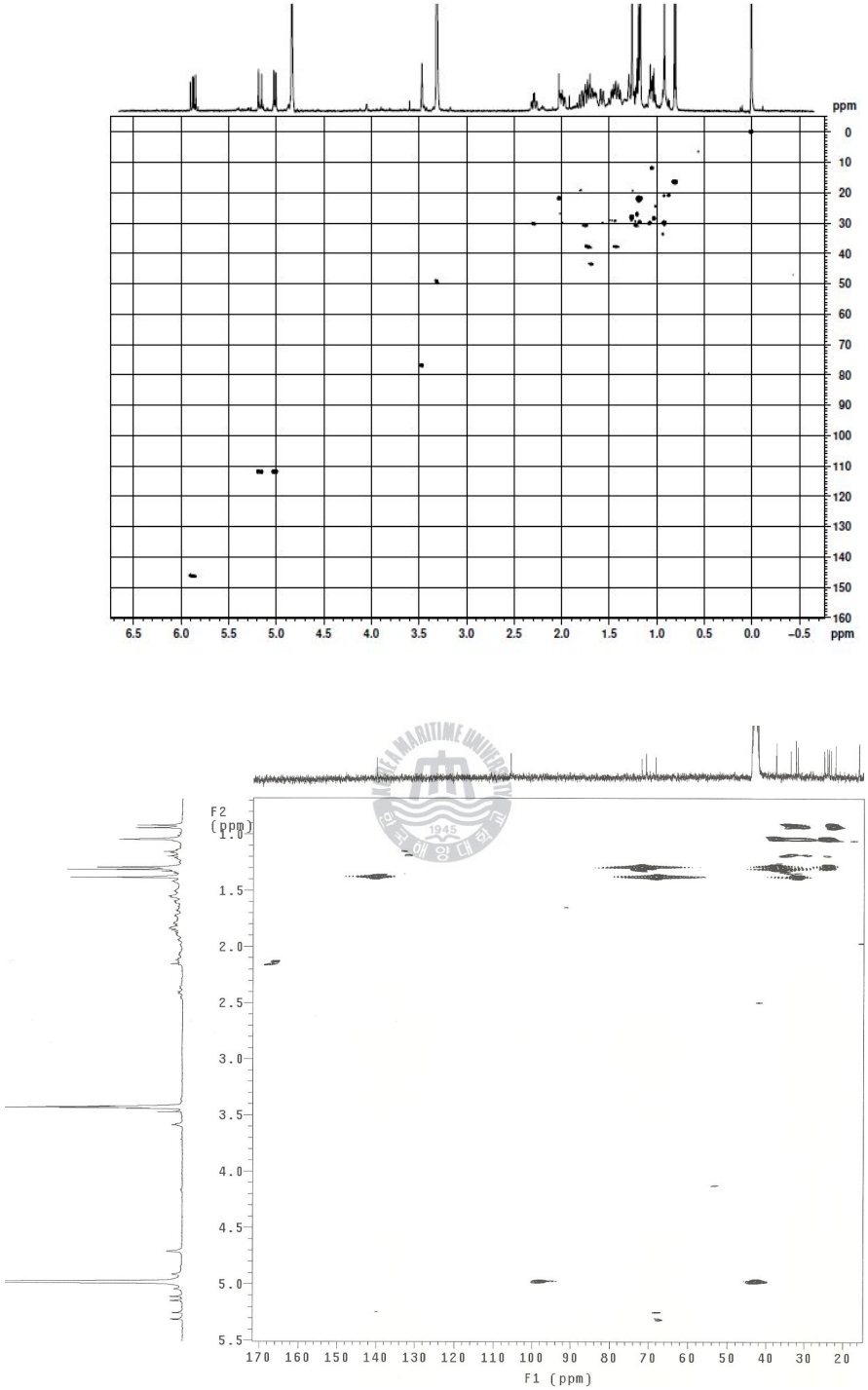

Figure 59. gHMQC and gHMBC spectrum of compound **23** isolated from *Vitex rotundifolia* in CD_3OD.

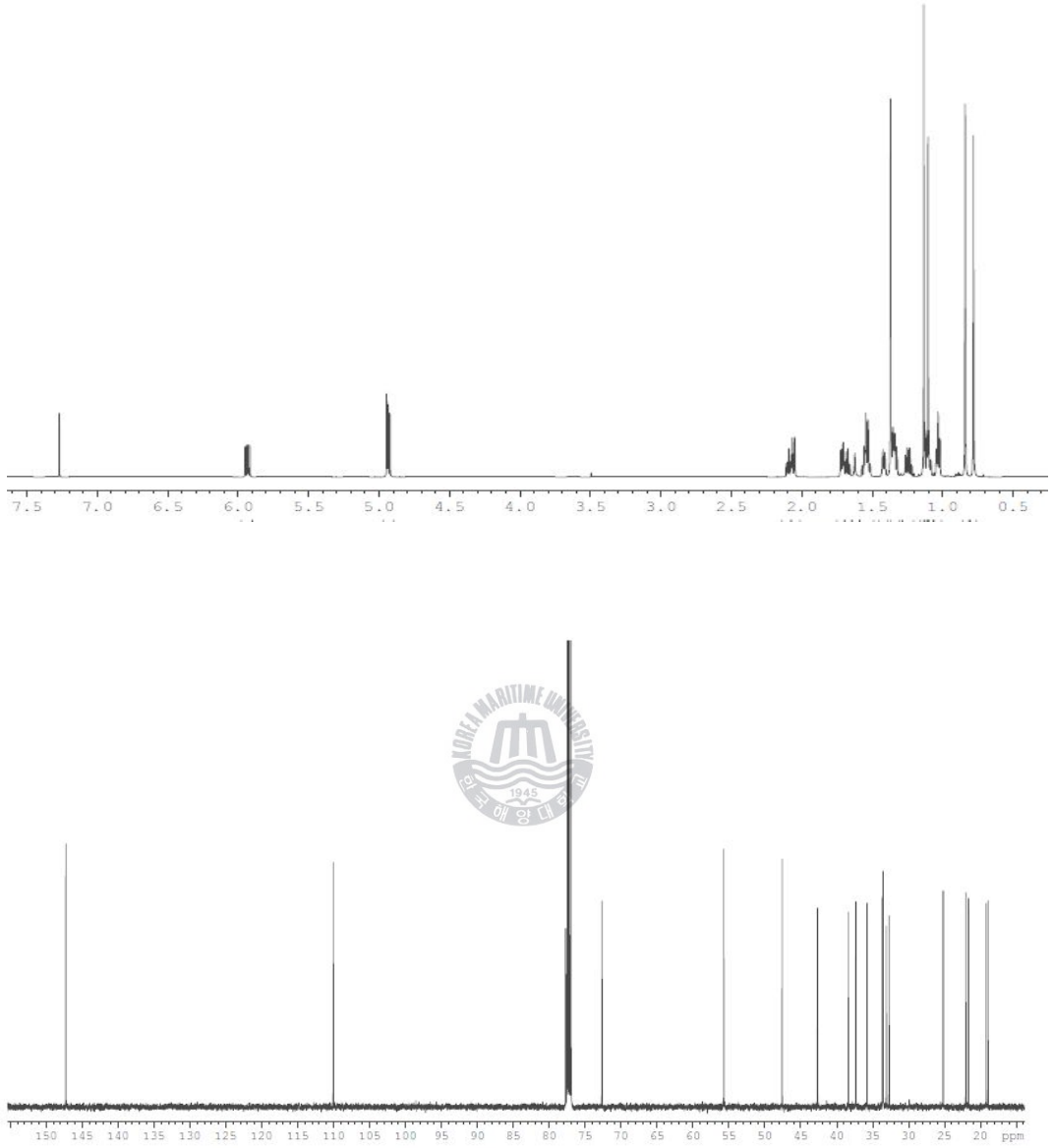

Figure 60. ^{1}H and ^{13}C NMR spectrum of compound **24** isolated from *Vitex rotundifolia* in $CDCl_3$.

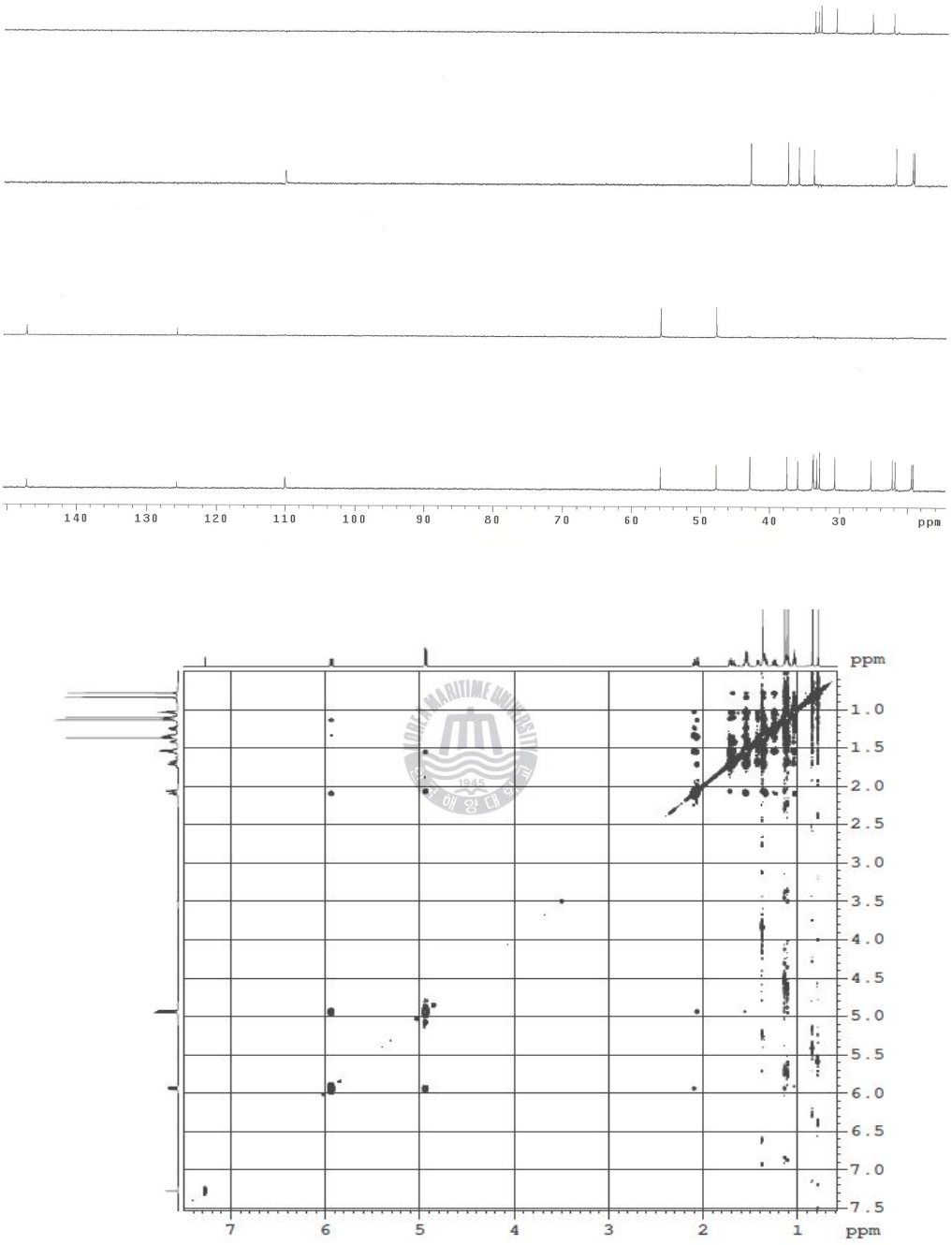

Figure 61. DEPT and NOESY spectrum of compound **24** isolated from *Vitex rotundifolia* in $CDCl_3$.

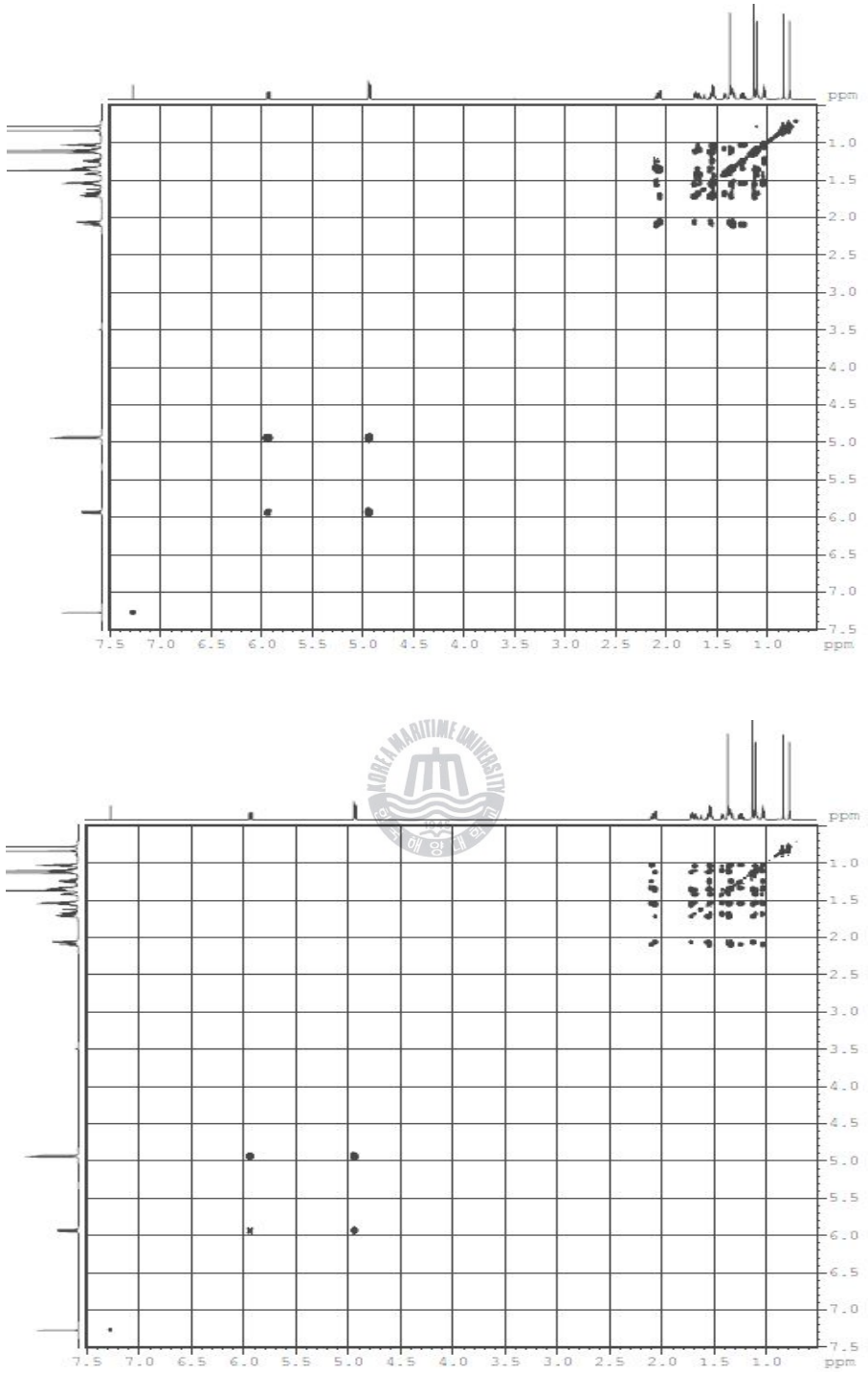

Figure 62. gDQCOSY and TOCSY spectrum of compound **24** isolated from *Vitex rotundifolia* in $CDCl_3$..

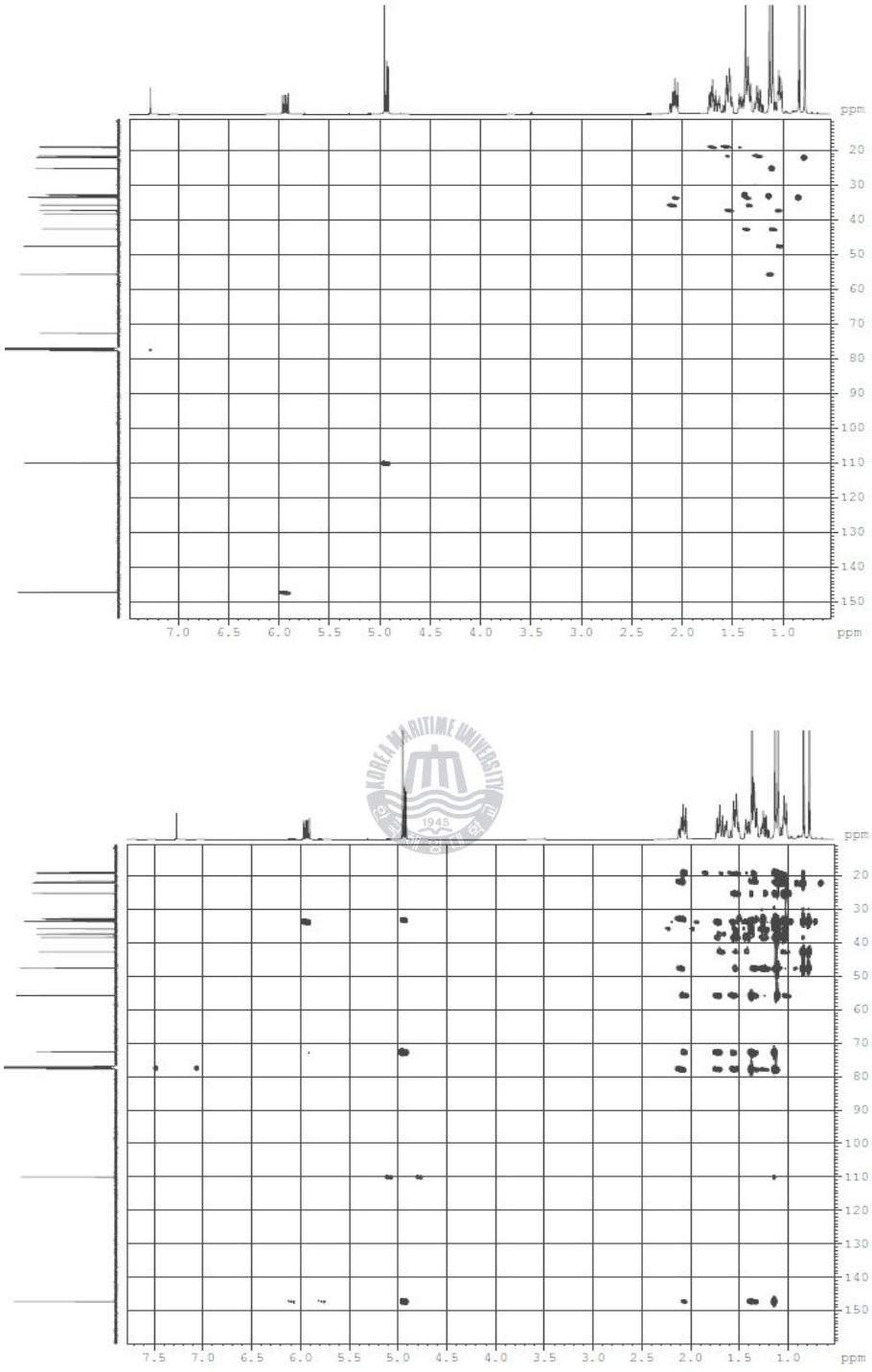

Figure 63. gHMQC and gHMBC spectrum of compound **24** isolated from *Vitex rotundifolia* in $CDCl_3$.

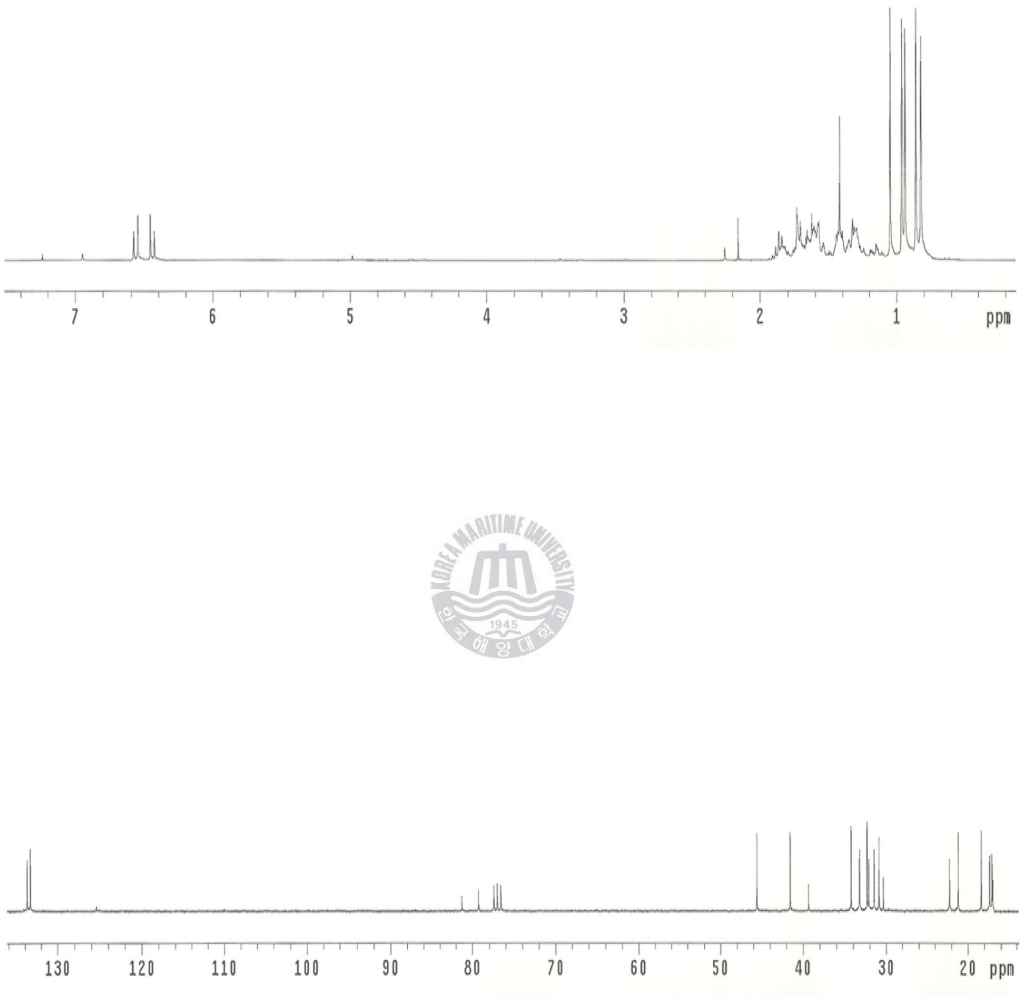

Figure 64. ^{1}H and ^{13}C NMR spectrum of compound **25** isolated from *Vitex rotundifolia* in $CDCl_3$.

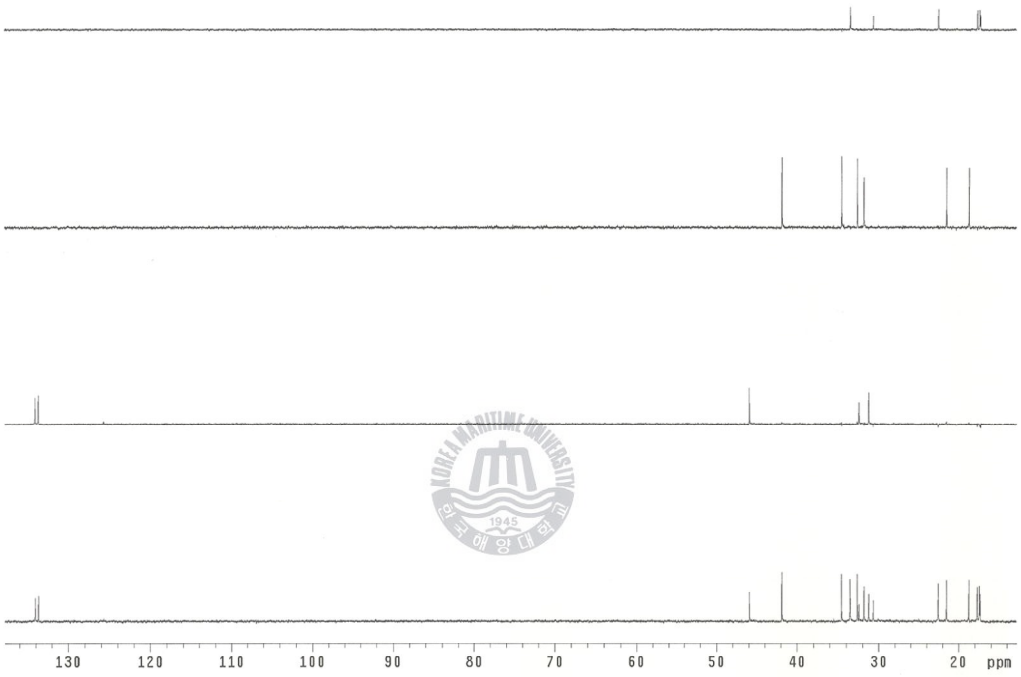

Figure 65. DEPT spectrum of compound **25** isolated from *Vitex rotundifolia* in $CDCl_3$.

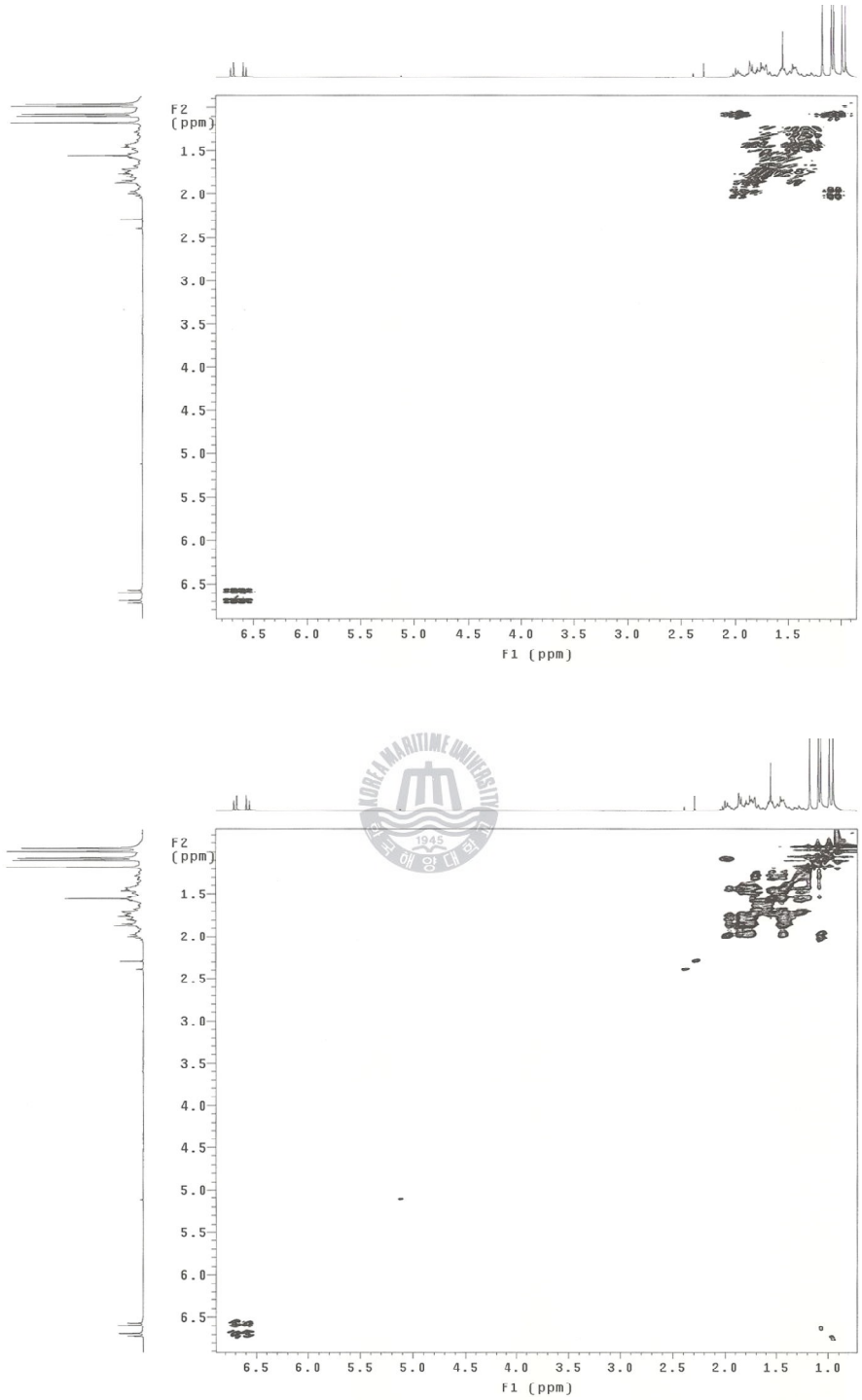

Figure 66. gDQCOSY and TOCSY spectrum of compound **25** isolated from *Vitex rotundifolia* in $CDCl_3$.

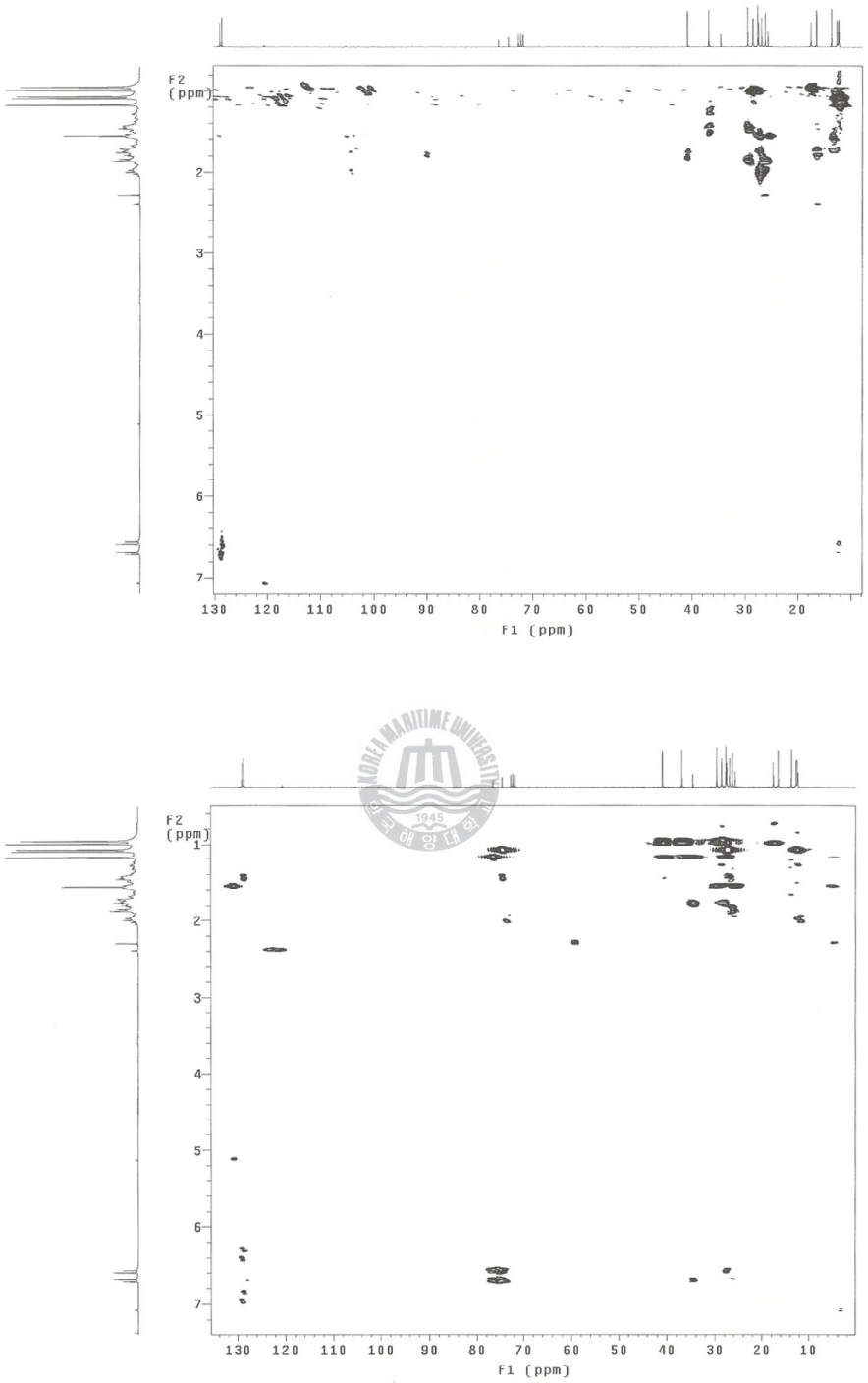

Figure 67. gHMQC and gHMBC spectrum of compound **25** isolated from *Vitex rotundifolia* in $CDCl_3$.

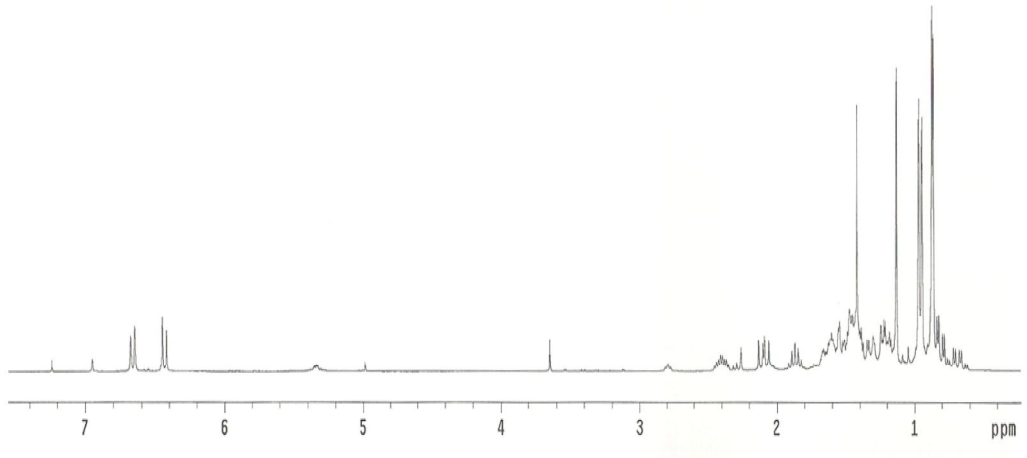

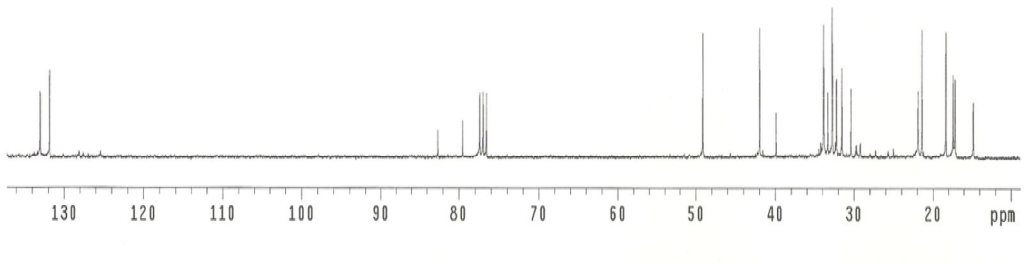

Figure 68. ^{1}H and ^{13}C NMR spectrum of compound **26** isolated from *Vitex rotundifolia* in $CDCl_3$.

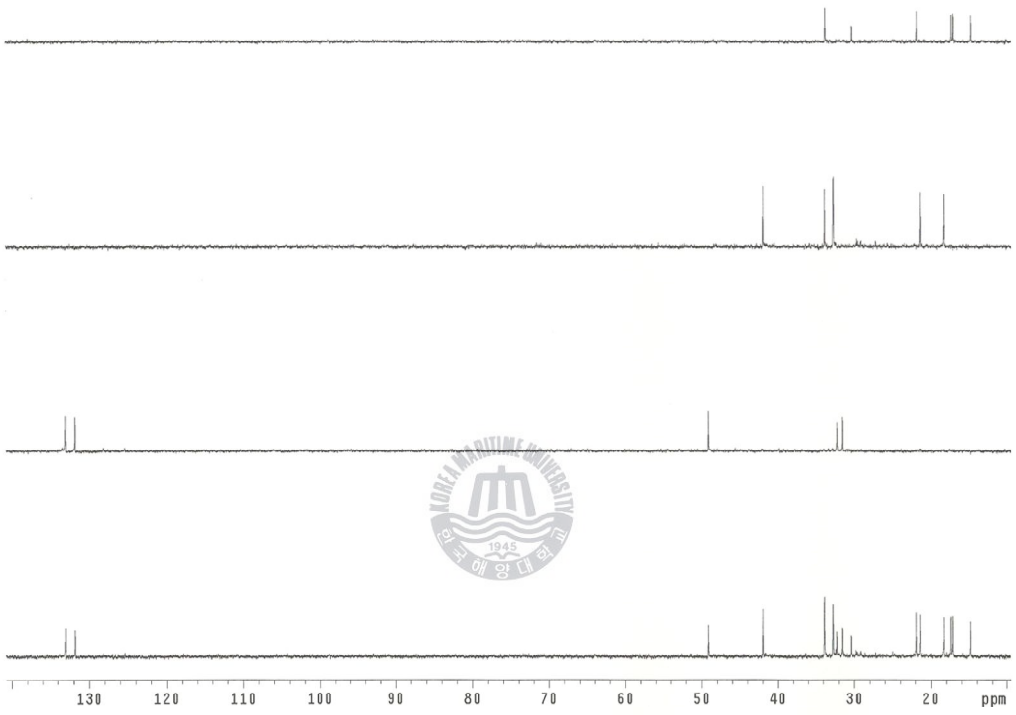

Figure 69. DEPT spectrum of compound **26** isolated from *Vitex rotundifolia* in $CDCl_3$.

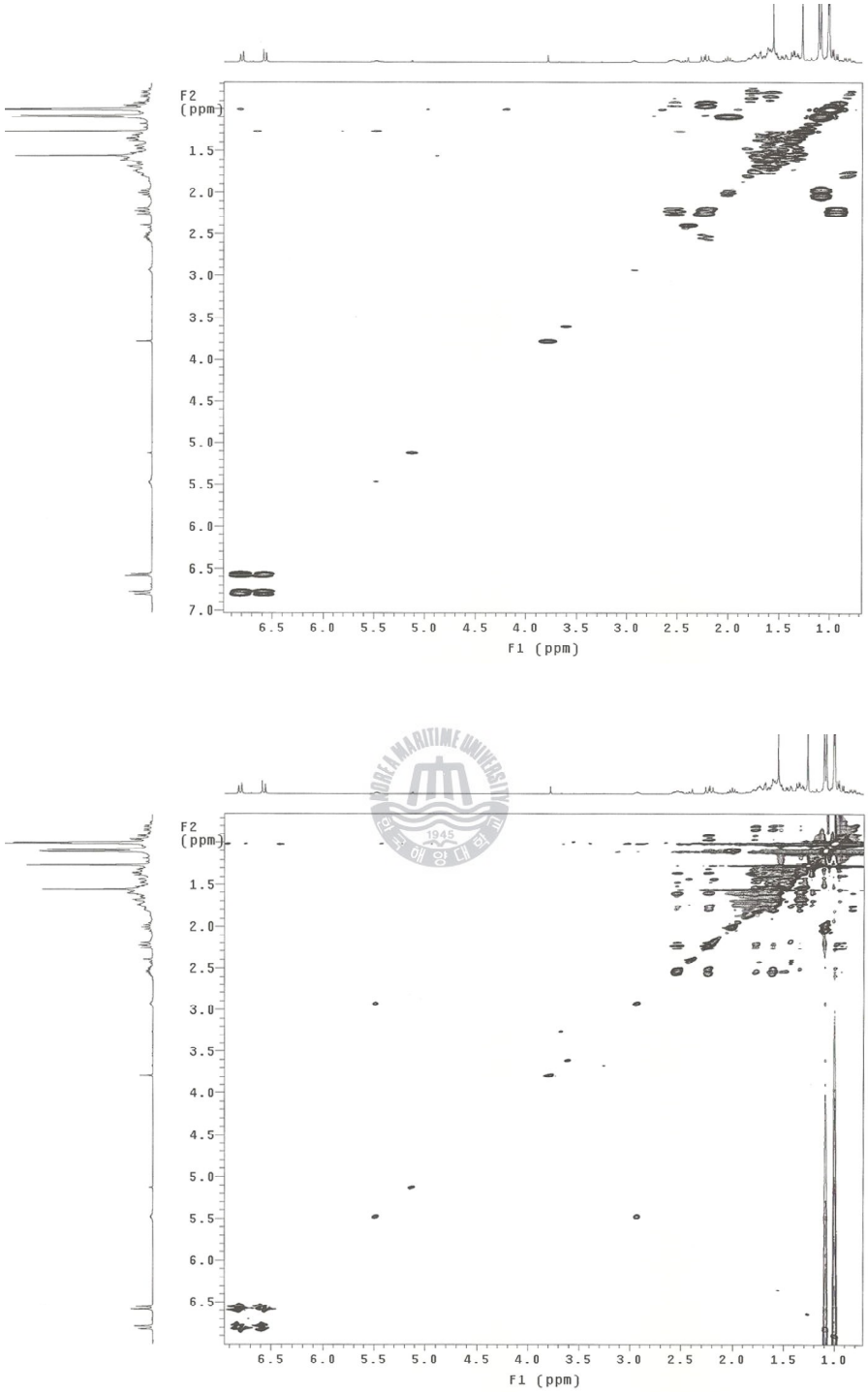

Figure 70. COSY and TOCSY spectrum of compound **26** isolated from *Vitex rotundifolia* in $CDCl_3$.

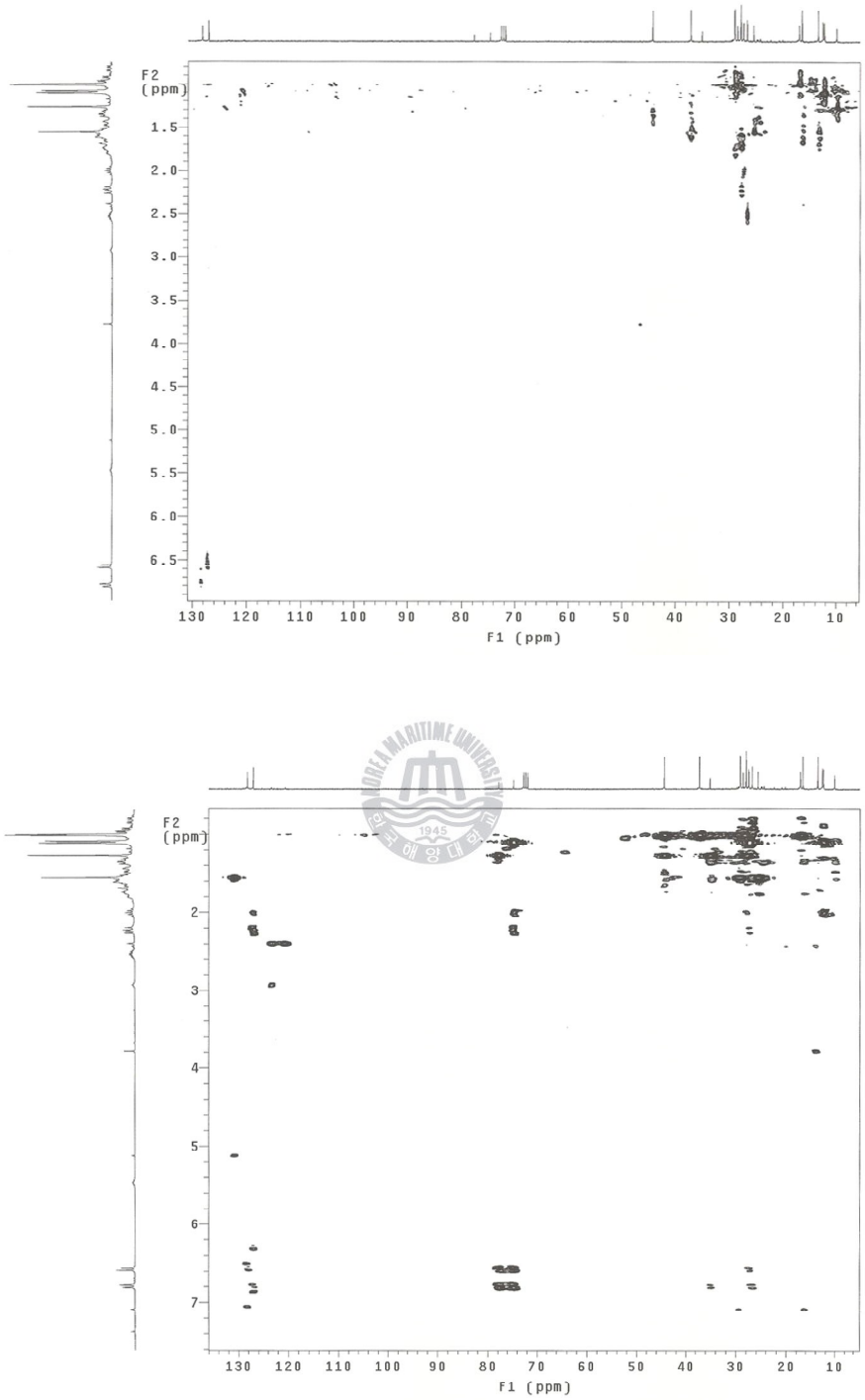

Figure 71. gHMQC and gHMBC spectrum of compound **26** isolated from *Vitex rotundifolia* in $CDCl_3$.

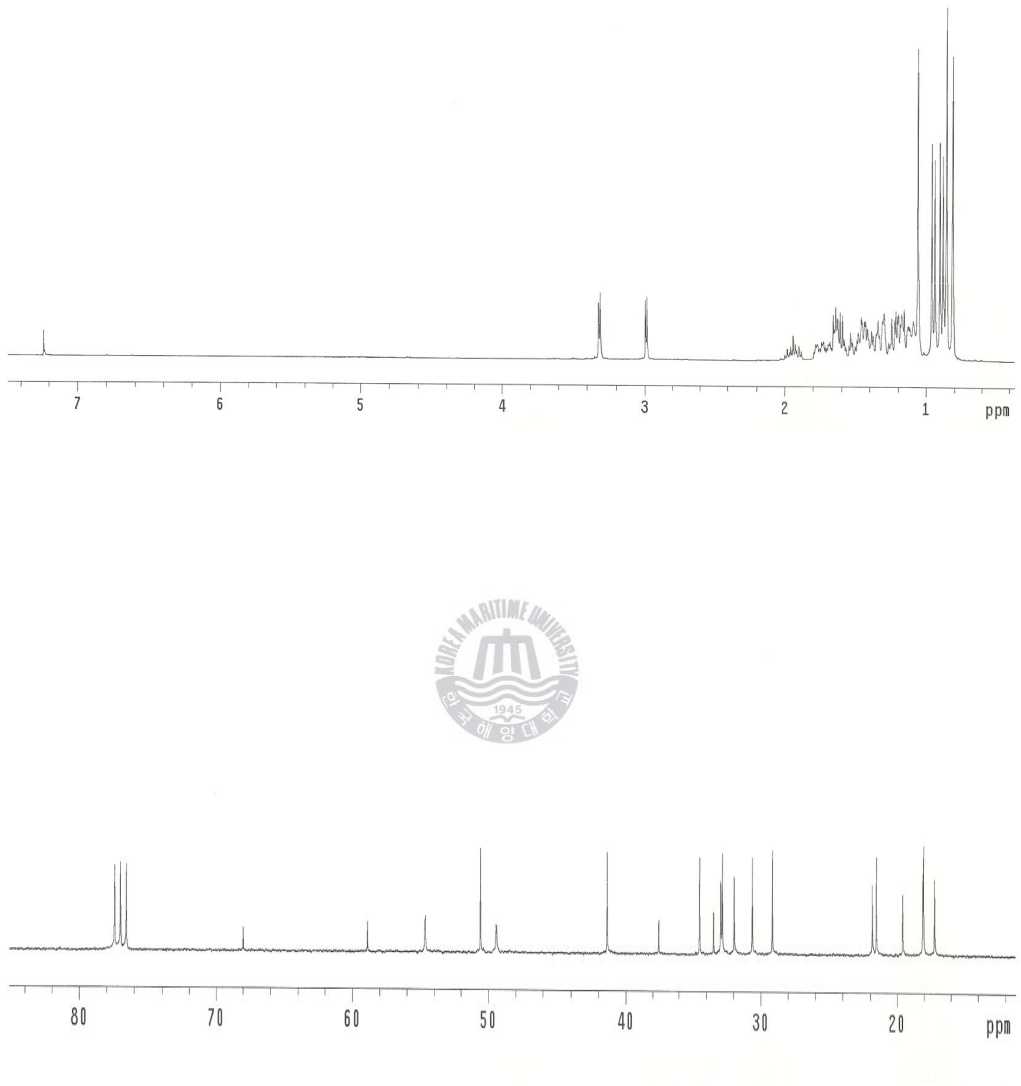

Figure 72. ^{1}H and ^{13}C NMR spectrum of compound **27** isolated from *Vitex rotundifolia* in $CDCl_3$.

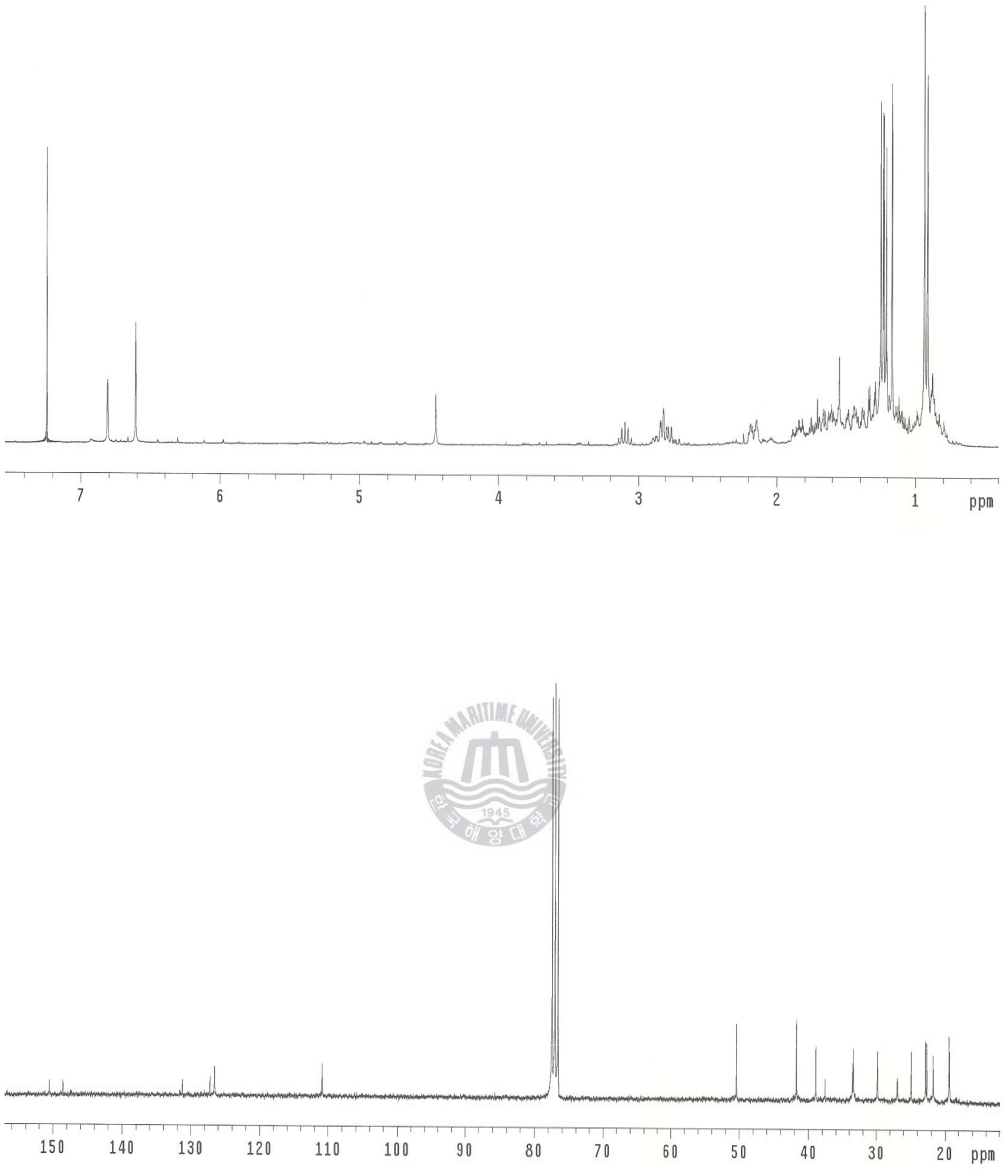

Figure 73. ^{1}H and ^{13}C NMR spectrum of compound **28** isolated from *Vitex rotundifolia* in $CDCl_3$.

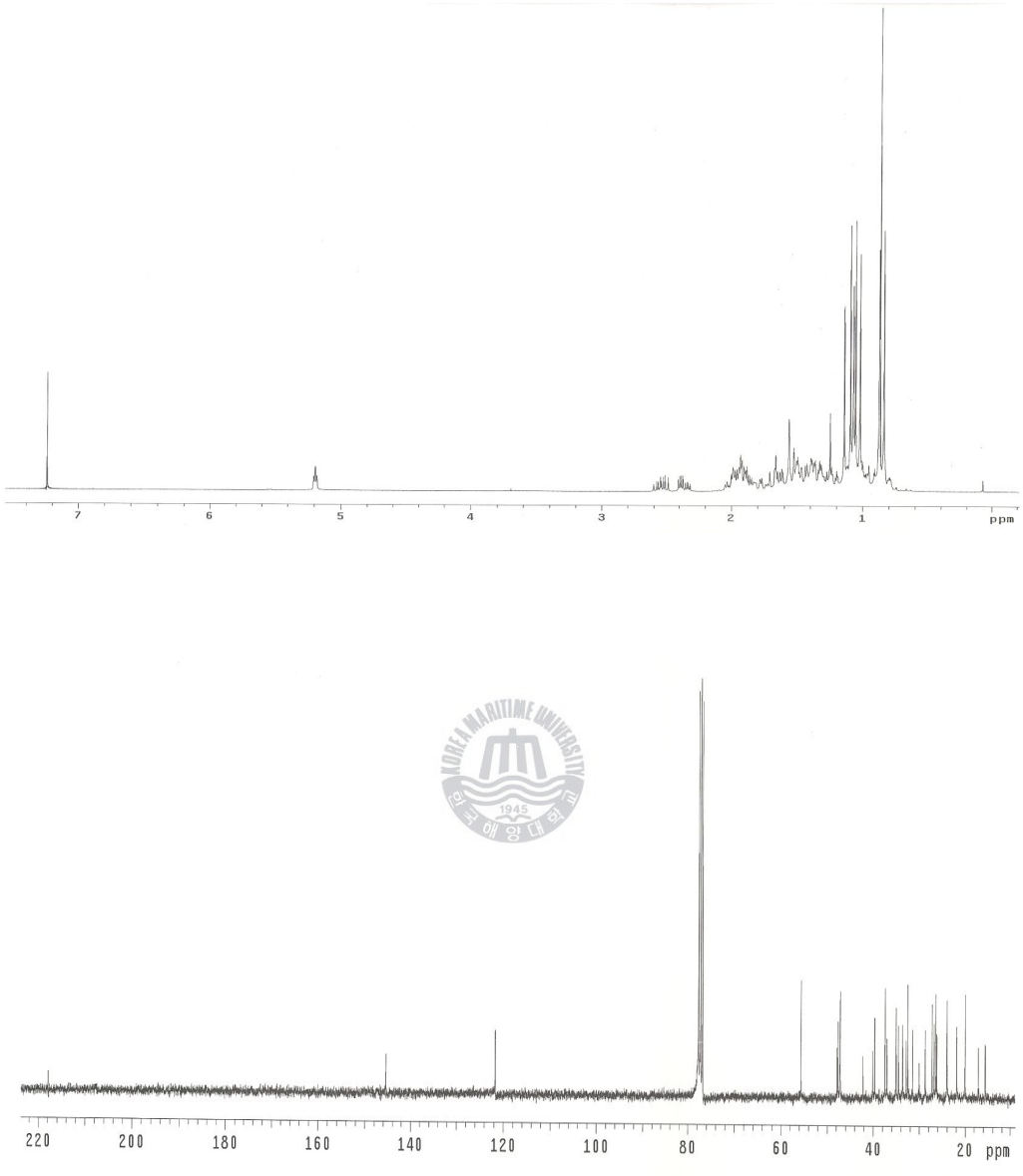

Figure 74. ^{1}H and ^{13}C NMR spectrum of compound **29** isolated from *Vitex rotundifolia* in $CDCl_3$.

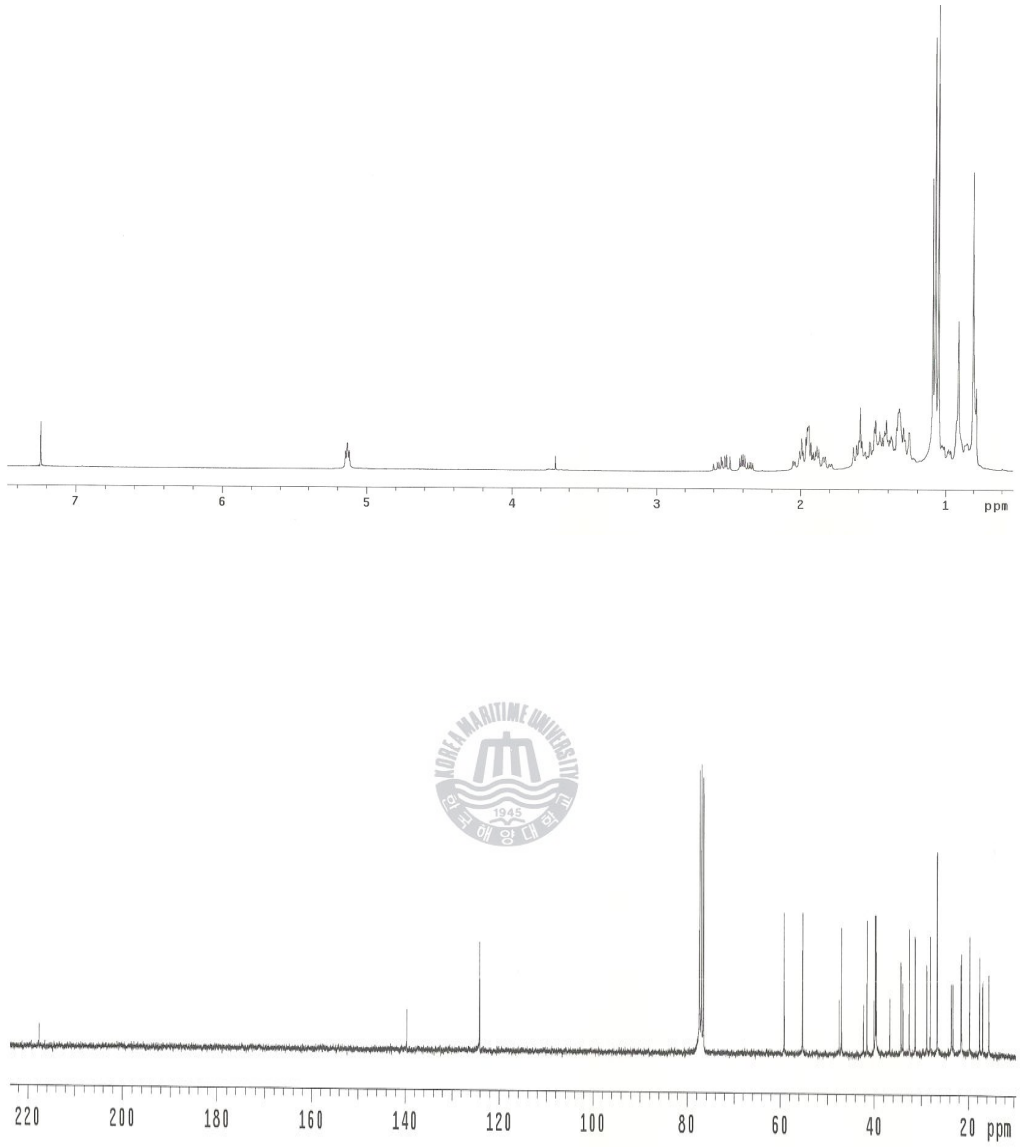

Figure 75. ^{1}H and ^{13}C NMR spectrum of compound **30** isolated from *Vitex rotundifolia* in $CDCl_3$.